Part A

Extended Abstracts of

Oral presentations

The order is chronologically as in the programme (pages *iii-ix*)

ICAM AS A REGULAR VISITOR: BACK TO GERMANY FOR THE FIFTH TIME

Gerhard Adrian[1] and Hans Volkert [2]

[1] Deutscher Wetterdienst, Forschung und Entwicklung, Offenbach, Germany
E-mail: *Gerhard.Adrian@dwd.de*

[2] Deutsches Zentrum für Luft-und Raumfahrt, Institut für Physik der Atmosphäre, Oberpfaffenhofen, Germany
Email: *Hans.Volkert@dlr.de*.

Abstract: As an introduction to the Extended-Abstract-Volume of all contributions to the 30th ICAM, the development of this long conference series is reflected in conjunction with a brief summary of current research initiatives in Germany that address aspects of weather forecasting in high spatial resolution above complex terrain.

Keywords: *Introduction, Overview*

1 ICAM BACK TO GERMANY

The *International Conference on Alpine Meteorology* comes to Germany for the fifth time in 2009 after having stayed here before in Garmisch (1958), Oberstdorf (1970), Berchtesgaden (1982) and Lindau (1994). As format, size and language(s) of communication gradually changed over more than five decades (details in Volkert, 2009), also the orographic focus became more general. The *Alps* in the centre of Europe remain to be of high interest, but studies of atmospheric phenomena around other high mountain ranges as the *Himalayas* or the *Rocky Mountains* are also presented. In addition, topographic features of lower elevation also became of significant interest, like the *Vosges* or the *Black Forest* and their intricate rôle in sparking off (occasionally also suppressing) summer convection or a small meteoritic cater in Arizona, which served as a very special natural laboratory for a measuring campaign.

The numerous contributions collected in this volume certainly provide a snapshot of the large variety of research projects which are currently undertaken to reduce uncertainties in the basic understanding of atmospheric processes, not only near mountains, as well as to enhance the spatio-temporal realism of high-resolution model simulations that are the basis of daily weather forecasts. This contribution is intended to put into perspective relevant German research initiatives, in particular those where the authors' affiliations are involved.

A larger sample of 24 more consolidated studies, which were first presented at the previous ICAM-2007 in Chambéry (France), can be found in Richard et al. (2009).

2 CURRENT RESEARCH INITIATIVES IN GERMANY

2.1 Basic research and new applications

Currently *Deutsche Forschungsgemeinschaft* (DFG) supports a six-year priority research programme *Quantitative Precipitation Forecast* (cf. Hense and Wulfmeyer, 2008), which had the *Convective and Orographically-induced Precipitation Study* (COPS; Wulfmeyer et al., 2008) as a field phase during June-August 2007. The latter received support from many countries and became endorsed as a Research and Development Programme of WMO-WWRP. A large number of oral and poster presentations during ICAM-2007 deals with episodes intensively probed obtained during COPS and general issues inspired by COPS data.

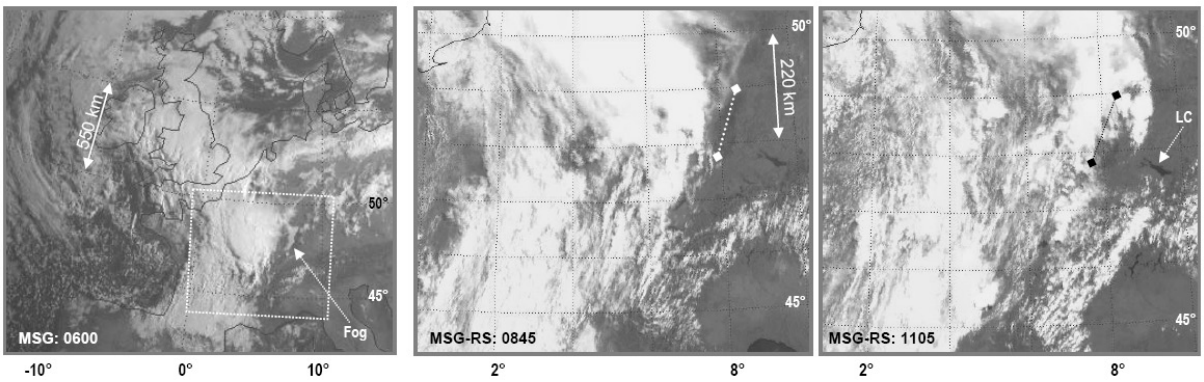

Figure 1: Cloud systems moving fast across central Europe and experiencing orographic modification on 20 July 2007 during COPS as viewed by Meteosat second generation (MSG) satellites – left: normal scan at 0600 with the cloud mass of a frontal system from Scotland to the Pyrenées approaching the upper Rhine valley covered by morning fog; middle: zoom (dotted frame in left image) into rapid scan at 0845 where cloud edge is starting to reach the Black Forest crest line (dots between diamonds); right: rapid scan at 1105 with freshly developed squall-line cloud about 100 km to the east of the Black Forest crest. LC: Lake of Constance; dotted lat./lon. grids on stereographic projections aid the orientation.

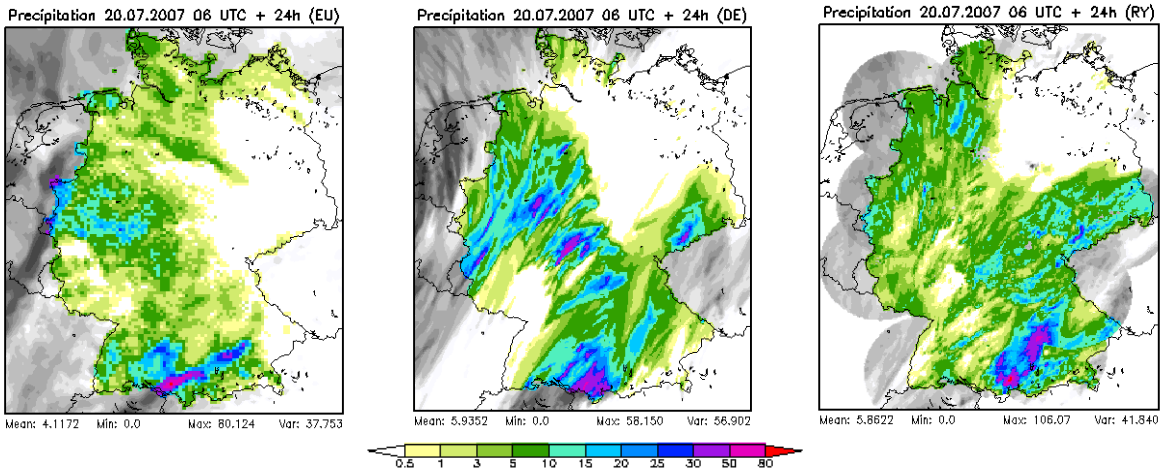

Figure 2. 24-hour accumulated precipitation (mm) on 20 July 2007, (a) predicted by COSMO-EU, (b) predicted by COSMO-DE and (c) determined from measurements obtained by the DWD radar network.

Rapid scans with 5'-intervals (normally 15') obtained from Meteosat were among the novel observing techniques during COPS. The moving frontal cloud systems of IOP-9c on 20 July are exemplified in Figure 1. The images reveal a suppression of clouds (and precipitation) at the southern end of the Black Forest, posing a severe challenge for high-resolution modelling. Display of satellite loops at variable speed can provide intuitive insights regarding the acting processes.

2.2 Orientated towards daily operations

Since 1999 DWD operates a non-hydrostatic numerical prediction model for short range weather forecasts, in close cooperation with European partners. Its version *COSMO-DE* covers Germany with a grid of 2.8 km horizontal resolution on 50 levels in a rapid update cycle of 3 h (8 runs per day over 21 h each). It is one-way nested into *COSMO-EU*, which uses a horizontal mesh size of 7 km and covers large parts of Europe.

An important difference between both model versions is that *COSMO-DE* does not use a convection parameterization and thus simulates convection cells explicitly. As a consequence, convection cells behave as a dynamical entity and move with the ambient flow field. This becomes evident from Figure 2, where accumulated precipitation fields are displayed for 20 July from *COSMO-EU* and *COSMO-DE* runs together with the corresponding estimate from radar observations. While the predominantly parameterized precipitation of *COSMO-EU* exhibits a very patchy structure, *COSMO-DE* shows clear band-like structures indicative of individual convection cells advected with the south-westerly flow. These bands are also evident in the radar-derived field, though not as pronounced as in the *COSMO-DE* forecast.

3 OUTLOOK

All contributions to this volume highlight the international collaborative spirit in meteorology. It is reassuring to note that 23 (of some 90) oral presentations and 20 (of some 100) poster presentations have lead authors working at institutions in Germany, be it at university institutes, at research laboratories of the *Helmholtz Gemeinschaft* or at *Deutscher Wetterdienst*. ICAM continues to be a vivid international forum of exchange and interaction. It is looking forward to its 31st meeting in 2011 in the United Kingdom, which recently joined the 'club' of the ICAM-countries.

Acknowledgements:
Axel Seifert and Günther Zängl provided Figure 2 and useful information. We thank them and all contributors to this volume for their cooperation on a voluntary basis as well as the ICAM-2009 sponsors for their support.

REFERENCES

Hense, A. and V. Wulfmeyer (eds.), 2008: *The Germany Priority Program SPP1167 "Quantitative Precipitation Forecast"*, special issue with 16 articles, *Meteorol. Z.* **17**, 703–948.

Richard, E., A. Buzzi, S. Mobbs, H. Volkert and M. Žagar (eds.), 2009: *Weather and Climate around Mountains: A collection of 24 papers first presented at ICAM-2007*. Special volume, *Meteorol. Atmos. Phys.* **103** , ii + 287 pp.

Volkert, H., 2009: The International Conferences on Alpine Meteorology: Characteristics and trends from a 57-year-series of scientific communication. *Meteorol. Atmos. Phys.* **103** , 5–12, DOI 10.1007/s00703-008-0312-9.

Wulfmeyer, V., A. Behrendt, H.-S. Bauer, C. Kottmeier, U. Corsmeier et *xxiii* alii, 2008: The Convective and Orographically-induced Precipitation Study: A research and development project of the world weather research program for improving quantitative precipitation forecasting in low-mountain regions. – *Bull. Amer. Meteor. Soc.* **89**, 1477–1486, DOI 10.1175/2008BAMS2367.1.

METEOROLOGY IN THE MIDDLE AGES
PART I – THERMALLY DRIVEN COASTAL WINDS

Haraldur Ólafsson[1] and Hálfdán Ágústsson[2]

[1] Háskóli Íslands, Iceland and Bergen School of Meteorology, Geophysical Institute, University of Bergen
E-mail: *haraldur68@gmail.com*
[2] Reiknistofa í veðurfræði and Háskóli Íslands, Iceland

Abstract: An investigation of Egil's Saga, written in Iceland in the early 13th century reveals a profound knowledge of local coastal wind circulations. The story-teller describes the sea breeze and the night-time returning flow, characterizing it as katabatic wind, and not land-breeze as in many modern textbooks. Numerical simulations confirm the katabatic nature of the return flow. The knowledge of these winds proved to be important for the downfall of Eric Haraldsson Bloodaxe, king of Norway.

Keywords: *Egils´ Saga, Middle Ages, Land-breeze, Sea-breeze,*

1 INTRODUCTION

In most modern textbooks, a night-time land breeze is explained as the opposite of a day-time sea breeze. This is typically illustrated by schematic figures featuring symmetric two-dimensional thermal fields and circulations, but with opposite signs, such as Fig.10.21 in Ahrens (1994) or in the internet-based Wikipedia. In this study, this concept is tested by numerical simulations. The impact of mountains on the night-time flow from land to the sea is also tested. Texts on coastal winds in Egils´s Saga Skallagrímssonar, written in the first part of the 13th century, are studied and compared to the results of the numerical simulations and modern textbooks.

2 THERMALLY DRIVEN FLOWS IN EGIL´S SAGA AND IN MODERN TIME TEXTBOOKS

Egil´s Saga Skallagrímssonar tells about the history of Egill Skallagrímsson and his family. During the reign of Haraldur Fairhair, son of Hálfdán the Blac, in the late 9th century, Egil´s father and grandfather fled from Norway to Iceland. The author of Egil´s Saga is not known, but generally considered to be Snorri Sturluson. Snorri was a well educated, wealthy and powerful personality in Iceland in the early 13th century. He wrote the history of Norway from before the settlement of Iceland, stories of the pagan gods and poetic treasures of pre-Christian times. Snorri himself was a descendant of Egill. He was fostered by the grandson of Magnus Ólafsson, king of Norway at Oddi in South-Iceland. Snorri was assassinated at his residence in Reykholt, Iceland by order from king Hákon of Norway on 23 September 1241. Egill travels to Norway to collect inheritance on behalf of his wife. In Norway, Egill does not get any money and the king, Eric Bloodaxe Haraldsson, declares Egill an outlaw. Egill is not satisfied and kills a number of the king´s men, including his son, Rögnvaldur. Perhaps more importantly, Egill raises a curse-pole with the head of a horse on top of it on the island of Herdla at the west coast of Norway. In short, the curse was that king Eric and Gunnhildur would lose their kingdom. Soon after, the curse came true. As Egill prepares the plundering and killings of the king´s men (Bergonund and others), he sails at the west coast of Norway, close to Alrekstead (now the city of Bergen):

The weather was calm, a fell-wind blew by night, a sea breeze by day. *One evening Egil sailed out to sea, but the fishermen were then rowing in to land, those, to wit, who had been set as spies on Egil's movements. They had this to tell, that Egil had put out and sailed to sea, and was gone. This news they carried to Bergonund. And when he knew these tidings, then he sent away all those men that he had had before for protection. Thereafter he rowed in to Alrekstead, and bade Frodi to his house, for he had a great ale-drinking there. (Egil´s Saga, Ch.59)…….Egil sailed out to sea for the night, as was written above. And when morning came the wind fell and there was a calm. They then lay drifting, letting the ship ride free for some nights. (Egil´s Saga, Ch.60)*

This text contains a description of the diurnal circulation of the winds during "calm" weather. Interestingly, the nocturnal wind is called "fell-wind", a translation of "fjallvindr" – mountain wind. The author attributes, in other words, the nocturnal wind to the mountains.

Most modern time meteorological textbooks present sea-breeze and land-breeze in the same context (e.g. Ahrens, 1994; Wikipedia at *http://en.wikipedia.org/wiki/Sea_breeze#Land_breezes*), and not necessarily together with slope-driven circulations, such as katabatic winds. The dynamics of the coastal nocturnal winds are thus explained in exactly the same way as the dynamics of the sea-breeze.

3 NUMERICAL SIMULATIONS

The diurnal circulation in June has been simulated with the numerical model MM5 (see Ágústsson & Ólafsson; Ólafsson & Ágústsson, 2008). Figure 1 shows the simulated sea-breeze in the afternoon and the late – night flow, with and without mountains. The simulated set-up is North-Iceland, a region well known by Snorri Sturluson and resembling West-Norway in terms of topography and fjords.

The simulations reveal firstly that there is no symmetry between the nocturnal flow and the sea-breeze. The sea-breeze is much stronger than the flow in the late night. Secondly, and most importantly in this context, there is no nocturnal flow if the land is flat, but winds of several m/s where the mountains are present.

4 DISCUSSION

The simulations show that the nocturnal wind in N-Iceland is of a katabatic nature, not a land-breeze. Consequently, many textbook descriptions of thermally driven nocturnal circulations may be characterized as misleading, at least for this part of the world. The dynamics are on the other hand in agreement with Egils´s Saga, assuming that the thermally driven flows in W-Norway are similar as in N-Iceland.

The author of Egil´s saga, and most likely Egill himself were well informed about the diurnal circulation. This is true, not only for the dynamics of the nocturnal winds, but the offshore extent of the winds. Bergonund appears to be ignorant about this and believes that Egill is leaving Norway when he sails to the west in the katabatic flow. Egill does of course not reach any further than a very short distance, and sails in with the sea breeze a few days later. Bergonund pays for his ignorance with his life and king Eric loses his kingdom for having such an idiot on his team.

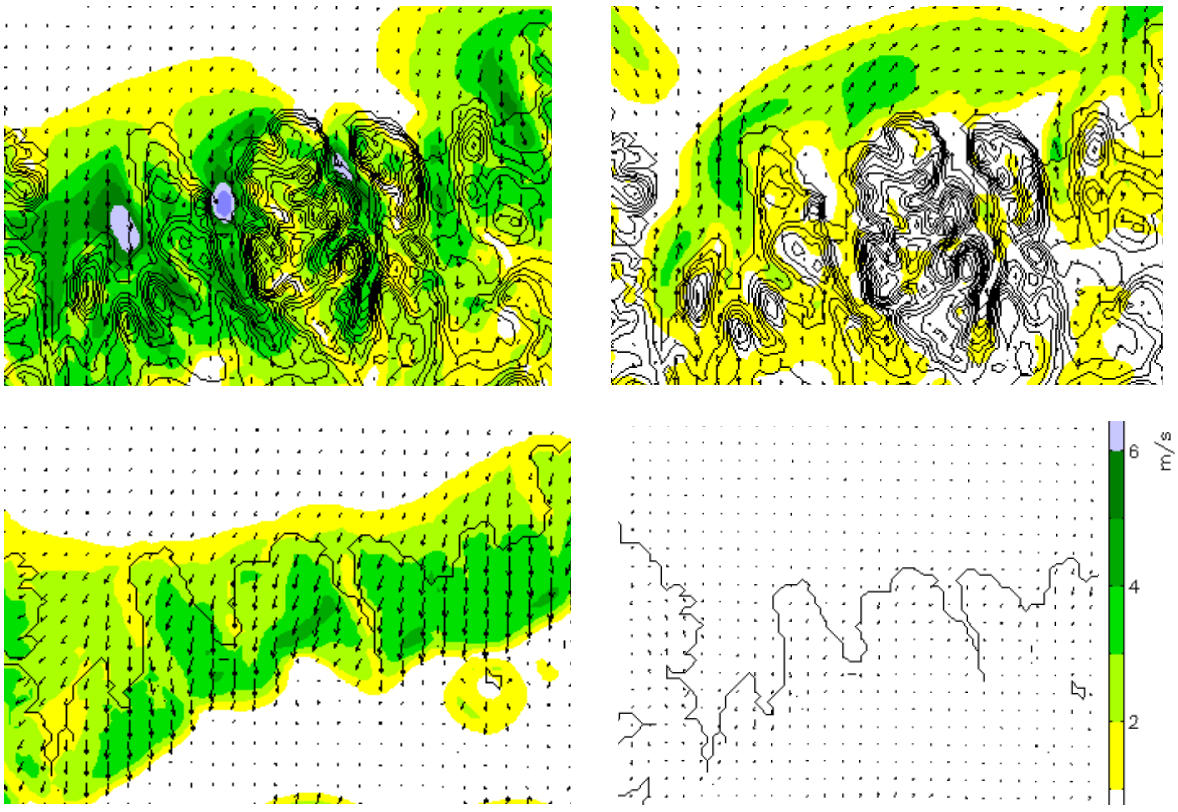

Figure 1. Simulated summer-time thermally driven surface winds at the north coast of Iceland and topographic height contours (intervals of 100 m). Top left: Afternoon. Top right: late night. Bottom left: Afternoon over flat Iceland. Bottom right: Late night over flat Iceland.

REFERENCES

Ahrens, C. D., 1994: Meteorology Today, 5th Ed., West Publishing Company, Minneapolis/St.Paul, USA. 589 p.

Ágústsson, H. and H. Ólafsson, 2008: Idealized simulations of katabatic flows in Iceland: Katabatic winds or land breeze? *Proc. Amer. Meteorol. Soc. Conf. Mountain Meteorology*, Whistler Canada. 5 p.

Egils´s Saga Skallagrímssonar, by an unknown author. Mál og menning, Reykjavík, Iceland, 1992. English translation by W.C. Green (1893) provided by the Icelandic Saga Database.

Ólafsson, H. and H. Ágústsson, 2008: Summer-time thermal winds over Iceland: Impact of topography. *Proc. Amer. Meteorol. Soc. Conf. Mountain Meteorology*, Whistler Canada. 7 p.

METEOROLOGY IN THE MIDDLE AGES
PART II – A DOWNSLOPE WINDSTORM IN LAXDÆLA SAGA

Haraldur Ólafsson[1] and Hálfdán Ágústsson[2]

[1] Háskóli Íslands, Iceland and Bergen School of Meteorology, Geophysical Institute, University of Bergen
E-mail: *haraldur68@gmail.com*
[2] Reiknistofa í veðurfræði and Háskóli Íslands, Iceland

Abstract: The texts of Laxdæla Saga, taking place in Iceland the 10th century and written in the 13th century are explored. It is argued that the saga contains a brief description of a downslope windstorm. A similar windstorm in modern times is presented to illustrate the nature of the windstorm.

Keywords: *Laxdæla Saga, Downslope windstorm, Iceland, Navigation, Middle Ages*

1 INTRODUCTION

Laxdæla Saga (Laxdale Saga) is one of the most romantic of the Icelandic Sagas, written in the middle of the 13th century. Laxdæla Saga is not signed, but its authorship has been attributed to Ólafur Þórðarson, a close relative of Snorri Sturluson, the alleged writer of Egil´s Saga Skallagrímssonar. Snorri was a celebrated scholar and a meteorologist (see Meteorology of the Middle Ages, Part I, in this publication). The story takes place in Norway, Iceland and in several other islands in the North-Atlantic, spanning from the period of the reign of Haraldur the Fairhaired in Norway and the settlement of Iceland in the late 9th century into the 11th century. This paper discusses a description of an important weather event in Laxdæla. A simulation from a similar event in modern times is presented and it is argued that we may have an example of a downslope windstorm.

2 A DOWNSLOPE WINDSTORM IN LAXDÆLA SAGA

Upon the end of the annual local parliament in Breiðafjörður at the west coast of Iceland, Þorsteinn (Thorstein) surtur sets sails for his farm Hrappsstaðir in Laxárdalur valley. This happened most likely in the month of June. Þorsteinn is hit by strong winds at the north coast of the Snæfellsnes peninsula, he wrecks the ship and everybody dies, except one person. The event is described as follows in a translation to English by M.A.C. Press, published in 1880:

Thorstein fell in with a high south-westerly gale, and they sailed up towards the roosts, and into that roost which is called Coal-chest-Roost,which is the biggest of the currents in Broadfirth. They made little way sailing, chiefly because the tide was ebbing, and the wind was not favourable, the weather being squally, with high wind when the squalls broke over, but with little wind between whiles.
(Laxdæla Saga, Ch. 18, English translation by Muriel A. C. Press, 1880)

There is intermittent rain and the strong winds that contribute to the accident are not present all the time, but they are associated with the precipitation events. This is quite usual in convective situations in south-westerly winds in the winter, but not as usual in the summer. A new translation, published in 1903 presents a different view of things:

Thorstein fell in with a fresh southwester; they sail inwards through the streams into that stream that hight Coal-kiststream; that is by far the greatest of those streams that are in Broadfirth; ill sped they with their sailing, and that was the more so, that by then was come the ebbing of the sea, but the breeze was not friendly to them; for the weather was showery and the wind was strong when it grew clear, but blew little between-whiles.
(Laxdæla Saga, Ch. 18, English translation by Robert Proctor, 1903)

Here, the strong winds are still intermittent, but they occur during clearings in between precipitation events, not during the precipitation. This must be characterized as unusual, but agrees with the original text:

Þorsteinn tók útsynning hvassan. Sigla þeir inn að straumum í þann straum er hét Kolkistustraumur. Sá er í mesta lagi þeirra strauma er á Breiðafirði eru. Þeim tekst siglingin ógreitt. Heldur það mest til

þess að þá var komið útfall sjávar en byrinn ekki vinveittur því að skúraveður var á og var hvasst veðrið þá er rauf en vindlítið þess í milli.
(Laxdæla Saga, the original in Icelandic)

Here the meaning of the text is closely linked to the interpretation of the word "rauf". The verb "rjúfa" means to open or to take apart and is commonly employed in the context of the sky clearing up. The strong winds are in other words associated with clearings in between precipitation events and we must conclude that Proctor´s translation from 1903 is more correct on this issue than the previous translation from 1880.

3 A NUMERICAL SIMULATION

The region is known for downslope windstorms, but to illustrate a windstorm similar to the one that killed Þorsteinn surtur and most of his crew, a summer windstorm is simulated and presented in Fig.1. The flow is simulated with a horizontal resolution of 3 km with the numerical model MM5 (for a detailed study of downslope windstorms in this region, see Ágústsson and Ólafsson, 2009). There is strong acceleration along the lee slopes of the mountains, and the strong winds do reach a short distance into the sea in some areas. The flow is quite non-stationary and sensitive to the representation of the topography. The exact position of the strong winds should therefore not be taken too literally.

4 DISCUSSION AND CONCLUSION

The windstorm described in Ch.18 in Laxdæla saga is associated with a clearing in the sky. This clearing is presumably being generated by downdrafts in the strong downslope flow. During period(s) of weaker winds, the downdrafts are weaker or absent and a precipitation system (a weak front) may overcome the barrier of the Snæfellsnes peninsula more easily and give precipitation on its northern side, as observed by Þorsteinn surtur. In order to generate strong downslope acceleration, a stably stratified atmosphere at low levels is required. Such a stratification is very common in winds from the southeast or south, while south-westerly winds are typically associated with an unstable atmosphere with convective precipitation. However, south-westerly flows are certainly not always unstable and they have produced many events of downslope windstorms in this region.

We conclude therefore that there is evidence that a downslope windstorm that led to a major accident at sea is being described in Laxdæla Saga, written in Iceland in the middle of the 13th century. The authors of this paper do not know of an older documentation of a downslope windstorm.

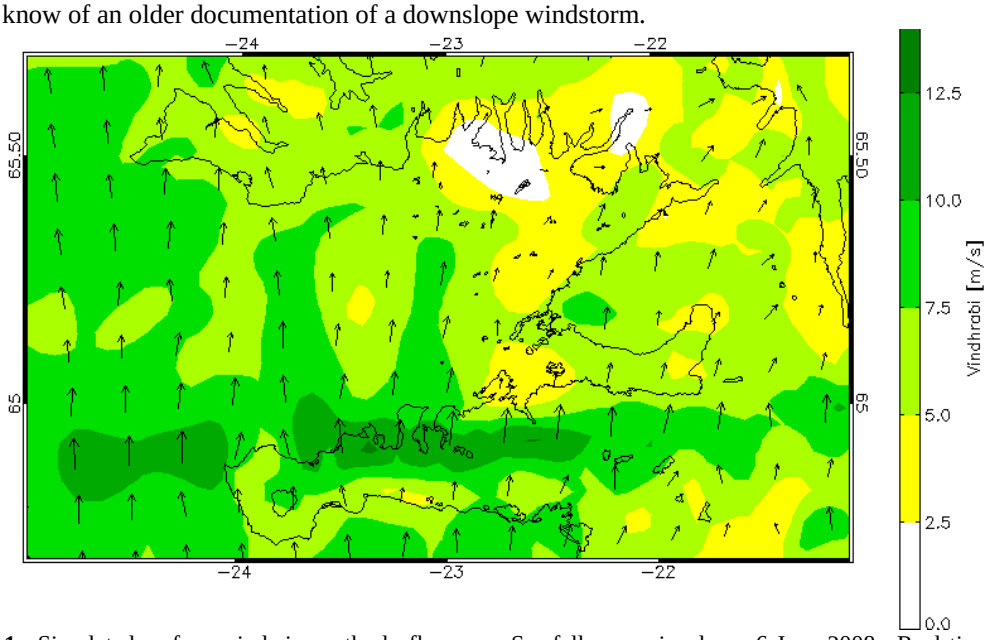

Figure 1. Simulated surface winds in southerly flow over Snæfellnes peninsula on 6 June 2008. Real-time simulations of this kind are available at http://www.belgingur.is

REFERENCES

Ágústsson, H. and H. Ólafsson, 2009: Forecasting wind gusts in complex terrain. Meteorology and Atmospheric Physics, in press

Laxdæla Saga by an unknown author. Mál og menning, Reykjavík, Iceland, 1993. English translations by Muriel A. C. Press (1880) and Robert Proctor (1903) provided by the Icelandic Saga Database.

Ólafsson, H. and H. Ágústsson, 2009: Meteorology in the Middle Ages – Part I: Thermally driven coastal winds. *Meteorologische Annalen, Proc. Int. Conf. Alpine Meteorology, Raststatt, Germany.*

THE 'MIRACULOUS' FÖHN IN BAVARIA OF JANUARY 1704

A. Tafferner[1], K.P. Hoinka[1], G. Zängl[2], L. Weber [3]

[1] Deutsches Zentrum für Luft- und Raumfahrt, Oberpfaffenhofen, Germany. (*arnold.tafferner@dlr.de)*
[2] Deutscher Wetterdienst, Offenbach, Germany;
[3] Philosophisch-Theologische Hochschule der Salesianer Don Boscos, Benediktbeuern, Germany

Abstract: According to the historic records from the monk Carolus Meichelbeck (1669–1734) the föhn of 28 January 1704 dramatically melted the frozen swamps very close to the Alpine baseline which in effect prevented the monastery of Benediktbeuern of being plundered by Tyrolian troops. In this paper we investigate whether realistic meteorological conditions during this föhn event would allow the reported strong and rapid melting of the water in the marshes. This is performed both by analytical calculation and a numerical simulation.

Keywords: *Föhn, ice melting, numerical simulation, Anastasia miracle*

1 INTRODUCTION

Before the establishment of systematic weather observations in the nineteenth century, there was a significant interest in observing the weather by individuals such as priests, writers and artists. These observations were sometimes performed unsystematically and yet there are known historical weather events which are reasonably well documented by location, date, intensity and even daily evolution. An example is the southerly föhn, one of the dominant weather phenomena in Bavaria, southern Germany. One particular event occurred on 28 January 1704, documented by the monk Meichelbeck at the Monastery Benediktbeuern. He reported that this föhn rapidly melted the frozen marshes surrounding the monastery and saved the monastery from being plundered by Tyrolean troops during the Spanish Succession War. This melting was so impressive that the chronicler praised this saving of the monastery as a divine marvel, the so-called 'Anastasia' or 'Lake Kochel' miracle.

2 TOPOGRAPHICAL BACKGROUND

The Monastery of Benediktbeuern (MB in Fig. 1) is located close to the Alpine baseline. Between Lake Kochel and Lake Walchen (LK and LW) south of the monastery there is a mountain gap (at the yellow line in Fig. 1), with nearby mountain summits reaching more than 1400 m. It is well known that mountain gaps enhance and intensify strong downslope windstorms, for example, the Chinook of Colorado. For centuries the monastery was surrounded by swamps with imbedded small swamp ponds and hamlets. These wet areas hampered approaching invaders providing a natural defence.

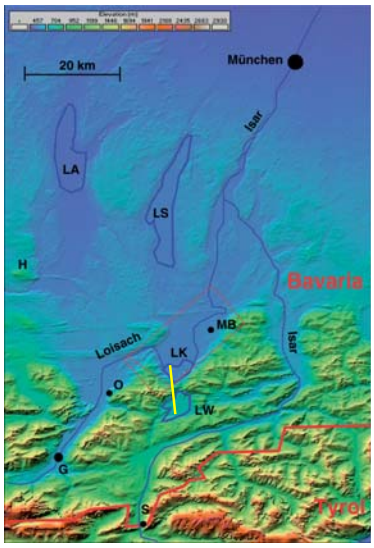

Figure 1. Map of southern Bavaria and parts of Tyrol showing the Isar and Loisach rivers. Garmisch-Partenkirchen (G), Ohlstadt (O), Hohenpeissenberg (H), Scharnitz (S), Monastery of Benediktbeuern (MB), Lake Ammer (LA), Lake Starnberg (LS), Lake Kochel (LK), Lake Walchen (LW). The scale is 1:100.000. (Elevation data, © U.S. Geological Survey.). The yellow line marks the location of the cross section of figure 2.

3 28 JANUARY 1704

In the morning of 28 January 1704, 2000 Tyrolean horsemen and soldiers started from Scharnitz (**S**, Fig. 1). They moved to Garmisch (**G**) and then along the Loisach River Valley, passing Ohlstadt (**O**) towards Großweil close to Lake Kochel. From there they planned to move along a dead-straight line over the frozen swamps and the River Loisach towards the monastery. It was hoped to arrive at the monastery in the evening. Meichelbeck pointed out that Lake Kochel was so strongly frozen that heavy load cars and 1000 men could have moved comfortably towards Benediktbeuern. When first notices of the troop's advance arrived, it was too late to organize an effective defence of the monastery. Therefore its salvation was entrusted to God. Because next day, the 29 January, was the festival day in honour of St Anastasia, the monks started to pray to Anastasia for her help in this dangerous situation. Meichelbeck reports that at 1400 h when the Tyrolean troops were about one hour away from the frozen swamps, a very warm wind appeared. Three to four hours later, the frozen swamps turned from white to black indicating that they were impassable for horses. As soon as the troops had reached the swamp areas they recognized that it was impossible for them to cross these melting surfaces because horses and men broke into the unsound ice surface. Meichelbeck mentioned also that the wind was persistently warm.

4 FÖHN AND ICE MELTING

The effect of the sudden föhn-related warming and the resulting melting of the frozen swamp must have been so impressive that for Meichelbeck the only explanation was that it was a miracle. Here a rough estimate is made to evaluate the melting effect, taking into account temporal limits and intensity reported by Meichelbeck (for details ref. to Hoinka et al., 2009). The minimum ice-layer thickness which is necessary for bearing the mean weight of a horse with horseman of about 700 kg can be estimated to between 10 and 20 cm above lakes. For the meltwater production an energy balance is considered where the available melt energy results from the radiation balance as well as sensible and latent heat fluxes. For reasons of simplicity, only the sensible heat flux is evaluated. The sensible heat flux S is calculated by a simple bulk approach $S = -\alpha (T_s - T_a)$, where $(T_s - T_\alpha)$ is the surface/air temperature difference. The heat transfer coefficient α is approximated by $\alpha = 5.7 \bullet v^{0.5}$ where v is the horizontal wind in m s^{-1}. The water-equivalent melt rate M_w is then calculated by $M_w = S\,(\rho_w \bullet r)^{-1}$. With density of water ρ_w , heat of fusion r ($3.35 \bullet 10^5$ J kg^{-1}) and S in Wm^{-2}, M_w is given in m s^{-1}. Assuming a wind of 35 m s^{-1} and a temperature difference ($T_a - T_s$) of 20 K we arrive at an ice melt rate of about 7.3 mm h^{-1}. Thus a solid lake ice-layer would be reduced by roughly 2.5 cm within 3 hours. One has to keep in mind that the solidity of lake ice and of a frozen swamp surface are quite different because the latter consists of a frozen mixture of grass, small plants, soil and water. Assuming a melting of swamp layer to be twice as effective compared to lake ice, we arrive at an estimate of about 5 cm within 3 hours. The evaluated thickness reduction is not very dramatic but sufficient to change a frozen surface from bearing to non-bearing capacity.

5 NUMERICAL SIMULATION

A numerical simulation has been set up using the MM5 model with 5 nests and highest resolution of 333m. A strong south-westerly geostrophic flow over the mountains has been initialised with linear vertical shear, with 15 m/s at 1000mb up to 33 m/s at tropopause level (for details see Zängl, 2003). As seen from the cross sections in Fig. 2 after 6 (left) and 12 (right) hours forecast time, the initial cold air pool over lake Kochel has been erased by the strong föhn flow through the mountain gap with a corresponding temperature rise of about 15 K in that area. Also strong winds spread out over the swamp area around Lake Kochel reaching 15 m/s (not shown).

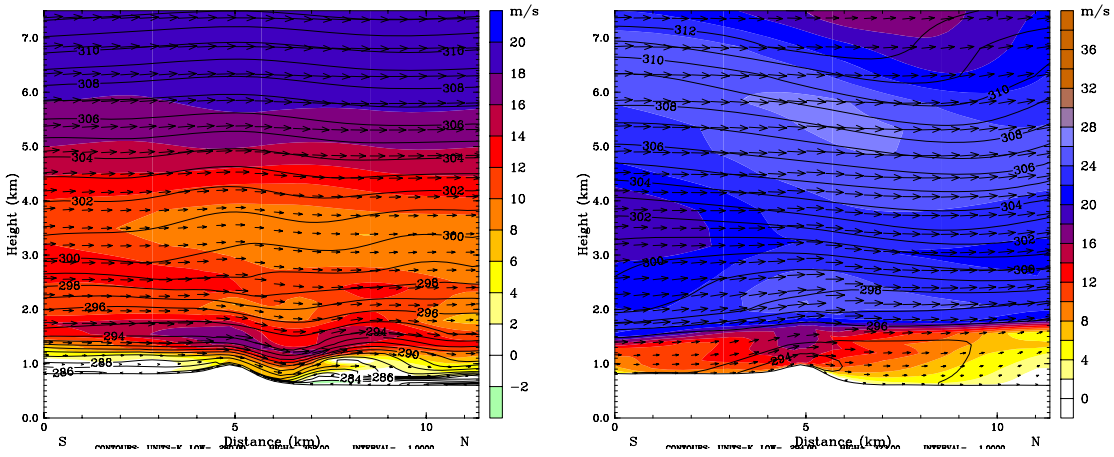

Figure 2. Cross sections of potential temperature and wind over the line indicated in fig.1 after 6 (left) and 12 (right) hours.

6 CONCLUSIONS

Inserting the wind and temperature values (15 m/s, 15 K) of the numerical föhn simulation in the equation for the melt rate M_w results in a much smaller melting rate of only about 1cm in 3 hours, or to 2 cm when taking into account the swamp surface. Meichelbeck might have dramatized the event's intensity by shortening the impact period in order to increase the 'miracle's' significance. Increasing the period up to 6 hours between the outbreak of the föhn and the recognition of the non-bearing capacity, the abovementioned values increase to 10 cm (extreme values) and 4 cm (numerical simulation). Even the smaller value would be sufficient to change a frozen surface from bearing to non-bearing capacity. Summarising one can say that no compelling evidence is indicated that a 'miracle' occurred. It suggests that the föhn of 28 January 1704 was an extraordinary event.

REFERENCES

Hoinka, K.-P., A. Tafferner, L. Weber, 2009: The 'miraculous' föhn in Bavaria of January 1704. Weather. **64** , 9-14.

Zängl, G., 2003: Deep and shallow south Foehn in the region of Innsbruck: Typical features and semi-idealized numerical simulations. Meteorol. Atmos. Phys., **83,** 237-261

AN EXAMINATION OF ATMOSPHERIC LIDS DURING COPS

Andrew Russell and Geraint Vaughan

Centre for Atmospheric Science, University of Manchester, Manchester, UK
E-mail: *andrew.russell-2@manchester.ac.uk*

Abstract: The understanding of the nature, origin and prevalence of atmospheric lids is low. There is, therefore, an opportunity to contribute significantly to this area of meteorology - this is the goal of this work. The context for this paper is the Convective and Orographically-induced Precipitation Study (COPS). The COPS observational campaign, which was undertaken in 2007, was based around the Black Forest region with the aim of improving precipitation forecasts in low mountainous regions. However, the project also represents a great data archive with which to analyse isolated features, such as atmospheric lids. In short, lids play a vital role in the development of convective storms. For example, evidence from the Convective Storm Initiation Project (CSIP), which was run in the UK in 2005, has shown that lids are important not only in determining whether a storm occurs but also when and where they develop and how intense they are – sometimes, counter-intuitively, they appear to increase the intensity. This extended abstract is intended as a brief overview of the previous literature on lids in order to place the work presented at ICAM-2009 in the wider scientific context.

Keywords: *inversions, capping, convection, convective inhibition, stability*

1 INTRODUCTION AND TERMINOLOGY

The term *lid* is often used in the context of atmospheric science. It is a useful concept, in addition to measures of lifting, when analysing or forecasting the development of convection. Therefore, it comes as little surprise that one of the first uses of the term in the scientific literature was in the description of the conditions leading to the severe storms in the Midwestern United States (Carlson and Ludlam 1968).

Why are atmospheric lids important? In the absence of the lid, the convection that develops is often widespread but shallow, unless the profile is unusually unstable. The presence of a lid can allow the lowest levels of the atmosphere to accumulate heat and moisture, creating the potential for deep convection. Release of this potential can occur at selected points along the capped region when there is sufficient boundary-layer forcing (i.e. convergence or orographic uplift). Alternatively, the lid may be weakened by large-scale uplift, or there may be a combination of the two effects. This rather complex interplay between the lid and deep convection is one reason why *convective available potential energy* (CAPE) by itself is not a good predictor of thunderstorm magnitude (McCaul and Weisman 2001).

The key feature of a lid is its *stability* (i.e. increasing potential temperature with height). Once a thermal is initiated in the atmosphere it will only remain buoyant whilst it is warmer than the air around it. Lids, or stable layers, are, therefore, very often associated with temperature *inversions* i.e. where the vertical temperature gradient changes from cooling with height to warming. Indeed, the top of the atmospheric boundary layer, which traps the turbulence that is induced at the surface, is frequently referred to as the *capping inversion* and, similarly, lids are often referred to as *caps*. However, a temperature inversion is not strictly necessary for a lid – a slowing of the lapse rate is all that is required for a previously buoyant air parcel to encounter some *convective inhibition* (CIN).

The origin of lids on the climatological has not been studied in any great depth but, given their characteristics and results from individual case studies, it is likely that the majority are derived from *residual layers* (i.e. remnants of the previous day's boundary layer) or *dry layers* that have descended from the upper-troposphere/lower-stratosphere.

2 A DEFINITION OF ATMOSPHERIC LIDS

Carlson et al. (1980) developed a Lid Strength Index (LSI) in the context of severe storm initiation in the Midwestern United States. The LSI compares buoyancy of an atmospheric profile with the lid effect thus:

$$LSI = \left(\overline{\theta}_w - \tilde{\theta}_{sw}\right) - \left(\theta_{swl} - \overline{\theta}_w\right) \tag{1}$$

Where, in the presence of a lid, $\overline{\theta}_w$ equals the mean wet-bulb potential temperature in the lowest 50 hPa, θ_{swl} equals the maximum saturation wet-bulb potential temperature and $\tilde{\theta}_{sw}$ equals the mean saturation wet-bulb potential temperature between θ_{swl} and 500 hPa. Therefore, a positive LSI means there is potential for convection without further forcing (e.g. lifting, heating) and a negative LSI implies that convection would be inhibited. However, the LSI give little indication of the thickness of the lid, whether there are multiple lids or what the relative rates of change of the lid strength and the surface layer temperature are.

3 PREVIOUS STUDIES OF ATMOSPHERIC LIDS

A number of cases from a recent UK field campaign – the Convective Storm Initiation Project (CSIP) – highlighted the importance of lids in the development of convective storms. In a summary of that project, Browning et al. (2007) discussed the role of lids in general whilst Morcrette et al. (2007), Russell et al. (2008, 2009) and Bennett et al. (2008) examined their role in individual cases in much greater detail. In particular, Russell et al. (2008) were concerned with the origin of the lid that they examined. In their case the lid had descended from the upper-troposphere but it is unclear whether the main source of lids is from descent, residual layers or differential advection, as speculated by Graziano and Carlson (1987).

Bennet et al. (2008) examined a case from the UK where multiple stable layers influenced the development of convection that led to some small showers. In particular, they consider how best to interpret radiosonde data with respect to understanding how convection develops. It would be interesting to extend their study and try to determine where these multiple stable layers came from.

Graziano and Carlson (1987) conducted an analysis of lid strength versus severe storm activity over a six month period in 1982 for the central two-thirds of the USA. Their study, representing one of the only systematic analyses of the role of lids in the initiation of convection, revealed that in order to understand the onset of severe convection both lid strength and buoyancy must be considered. For example, they found an LSI "cut-off value" above which severe convection was rarely observed. However, whilst the probability of deep convection decreases with increasing LSI, they found that when considering a given value of buoyancy the deep convection probability increased with increasing LSI.

4 SUMMARY

This extended abstract represents a short overview of the scientific literature on the subject of atmospheric lids. A suitable way to summarise this paper, therefore, is the following brief list of research questions that this review has thrown up. Here is this list:

- How important are lids in determining the strength of convective storms?
- How important are lids in determining the location of convective storms?
- How well do numerical weather prediction (NWP) models represent lids?
- Has the climatological occurrence of lids changed in recent time?
- Where do lids come from?
- Are the answers to the above questions significantly different in different geographical areas?

The data collected and the NWP models run during the COPS campaign, as summarised by Wulfmeyer et al. (2008), provide an ideal dataset to answer some of these questions.

Acknowledgements:
We would like to thank all the COPS team for the smooth running of the campaign and the high quality data that was collected. Thanks are also due to the Natural Environment Research Council (NERC) who funded UK-COPS.

REFERENCES

Bennett, L. J., A. M. Blyth, K. A. Browning, E. G. Norton, 2008: Observations of the development of convection through a series of stable layers during the Convective Storm Initiation Project. Q. J. R. Meteorol. Soc. **134**, 2079-2091.

Browning, K. A. and co-authors, 2007: The convective storm initiation project. Bull. Amer. Meteorol. Soc. **88**, 1939-1955.

Carlson, T. N. and F. H. Ludlam, 1968: Conditions for the occurrence of severe local storms. Tellus **20**, 203-226.

Carlson, T. N., R. A. Anthes, M. Schwartz, S. G. Benjamin and D. G. Baldwin, 1980: Analysis and prediction of severe storm environments. Bull. Amer. Meteorol. Soc. **61**, 1018-1032.

Graziano, T. M. and T. N. Carlson, 1987: A statistical evaluation of lid strength on deep convection. Weather Forecast. **2**, 127-139.

McCaul, E. W. and M. L. Weisman, 2001: The sensitivity of simulated supercell structure and intensity to variations in the shapes of environmental buoyancy and shear profiles. Mon. Wea. Rev. **129**, 664-687.

Morcrette, C. J., H. Lean, K. A. Browning, J. Nicol, N. Roberts, P. A. Clark, A. Russell and A. M. Blyth, 2007: Combination of mesoscale and synoptic mechanisms for triggering of an isolated thunderstorm: a case study of CSIP IOP 1. Mon. Wea. Rev. **135**, 3728-3749.

Russell, A., G. Vaughan, E. G. Norton, H. M. A. Ricketts, C. J. Morcrette, T. J. Hewison, K. A. Browning and A. M. Blyth, 2009: Convection forced by a descending dry layer and low-level moist convergence. Tellus A **61**, 250-263.

Russell, A., G. Vaughan, E. G. Norton, C. J. Morcrette, K. A. Browning, A. M. Blyth. 2008: Convective inhibition beneath an upper-level PV anomaly. Q. J. R. Meteorol. Soc. **134**, 371-383.

Wulfmeyer V. and co-authors, 2008: The Convective and Orographically Induced Precipitation Study. Bull. Amer. Meteorol. Soc. **89**, 1477–1486.

Wind measurements with lidar and cloud radar during COPS

Jan Handwerker, Katja Träumner, Jens Grenzhäuser, Andreas Wieser

Karlsruhe Institute of Technology (KIT) — Institut für Meteorology und Klimaforschung (IMK)
E-mail: *jan.handwerker@imk.fzk.de*

Abstract: The 35.5 GHz scanning cloud radar MIRA36-S and the 2 µm Doppler lidar Windtracer were collocated on the highest mountain of the Northern Black Forest (Hornisgrinde) during the COPS campaign. This study investigates wind speed data measured with these two instruments. We assume, that horizontal components should be independent of the used wavelength, delivering a unique quality check opportunity and allowing an extention of the individual measurements. Vertical components should differ in case of sedimenting particles, giving access to further physical properties of the scatterers, e.g. on the drop size distribution.

Keywords: *COPS, Radar, Lidar, Wind*

1 INTRODUCTION AND MEASUREMENT SETUP

During COPS ("Convective and Orographically-induced Precipitation Study") MIRA36-S and Windtracer were collocated on top of Hornisgrinde (1160 m asl, cf. Fig. 1). Sometimes the instruments were both vertical oriented, leading (besides further information) to direct measurements of the vertical scatterer velocity, sometimes they performed more or less complicated scan patterns, consisting of several successive PPI and RHI scans. Here, we show results from equal or comparable scan patterns for both instruments.

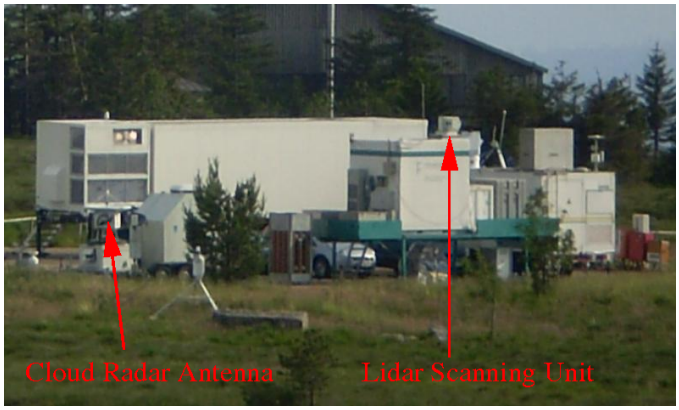

Figure 1: MIRA36-S and Windtracer at Supersite Hornisgrinde

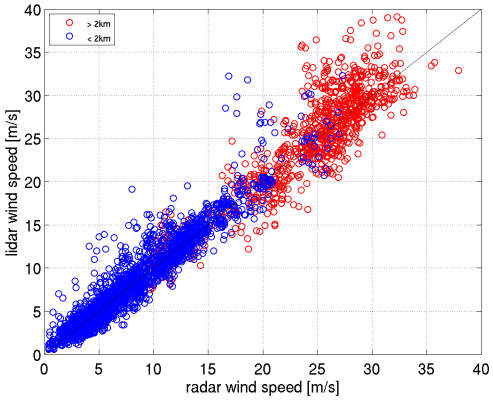

Figure 2: Intercomparison of horizontal wind speeds (radar measurements at 45°).

2 HORIZONTAL WIND SPEED

From cloud radar measurements horizontal wind speeds are derived by an improved VAD algorithm (Browning and Wexler , 1986; Tabary et al. , 2001) from PPI scans which lasted approx. 60 s. The radar performed PPI scans at 15° and 45° zenith angle, only the latter are presented here. Lidar based horizontal winds from a 10-minute scan pattern, containing two PPI scans (at 45° and 86° zenith angles) and some RHI scans. The horizontal winds are derived by a least square method, similar to the VAD algorithm. Our radar measurements are finer resolved in time and space than the lidar measurements. For comparisons we always used the nearest radar bin to a lidar measurement, i.e. there is no interpolation applied.

The scatterplot in Fig. 2 shows the correspondence of the two measurements. Blue marks measurements in the lower 2 km agl.; this height is an approximation for the maximum PBL thickness in summer on Hornisgrinde. 57 % of all measurements have a deviation of less than 1 m/s and only 3 % of more than 5 m/s.

In case of missing scatterers no horizontal wind can be derived. Radar and lidar show to be complementary. Below 2 km only 8.2 % of the possible measurements lead to simultaneously measurements of both instruments. In 16.2 % the radar could derive a horizontal wind, in 22.9 % the lidar was successful. Both instruments together provide a horizontal wind speed in 47.3 %. Above 2 km the numbers are 2.3 % (coinciding), 12.9 % (radar), 8.7 % (lidar) and 19.3 % (combined).

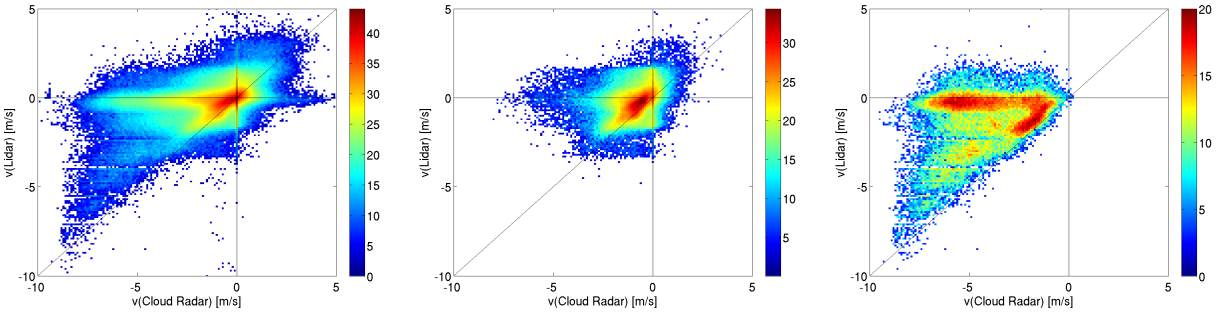

Figure 3: 2D frequency distributions of observed vertical velocities measured by radar (abscissa) and lidar (ordinate) for all measurements (left) measurements with clouds (middle) and in rain (right). Colors are coded on logarithmic scales.

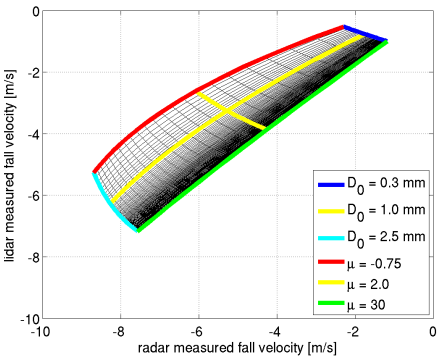

Figure 4: Expected distribution of radar and lidar measured vertical velocities for Gamma shaped drop size spectra. D_0 is varied between 0.3 mm and 2.5 mm, μ between -0.75 and 30.

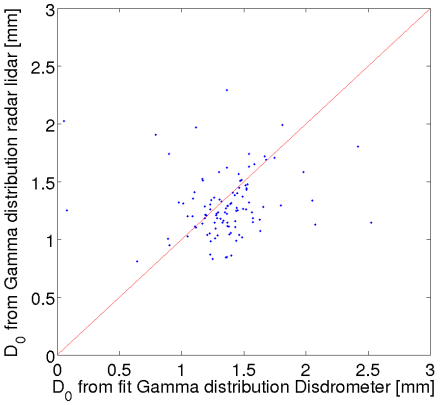

Figure 5: Reference Dropsizes measured by a Joss-Waldvogel Disdrometer compared to radar and lidar derived values.

3 VERTICAL VELOCITY COMPONENT

Due to their different wavelengths the two devices are sensitive to different scatterer sizes. Vertical wind components differ because of the size dependent sedimentation velocity of the scatterers. Scatter plots of the 2-dimensional distribution of vertical velocity measurements are shown in Fig. 3. These data are measured with vertical pointing instruments. Note, that the color codes are given in a logarithmic (dB) scale.

For all measurements (left panel of Fig. 3) upward velocities up to roughly 3 m/s are measured. In clouds (discriminated by a lidar backscatter value $\geq$ -6.8 dB, middle panel) movements are significant slower, but centered around a slow downward motion (not around 0). The fast downward motions only occur in rain events (discriminated by a radar reflectivity $\geq 0\,\mathrm{dB}_Z$ in 500 m agl).

In the latter case (rain) the different vertical velocities may be used to determine information on the drop size distribution. We (i) substract vertical wind motion (determined from lidar aerosol peak), (ii) assume a Gamma-shaped drop size distribution $N(D) = N_0 D^\mu \exp(-\lambda D)$ which has a reference drop size $D_0 = (\mu + 4)/\lambda$ and (iii) the terminal fall velocity from Atlas et al. (1973) ($v = 9.65 - 10.3\exp(-0.6D)$). With these assumptions Fig. 4 indicates the area where we expect the measured vertical velocities. The lidar software always uses the most intense peak to determine the vertical velocity. In most cases this is the aerosol peak, as can seen from Fig: 3 and by analysing the raw lidar spectra. Identifying the rain drop peak and applying the described method, leads to reference sizes (D_0) as shown in Fig. 5 in comparison to measurments of a colocated Joss-Waldvogel Disdrometer. These results are satisfactory.

4 CONCLUSIONS

Cloud radar and wind lidar are complementary in measuring horizontal winds. They allow mutual quality control. Using vertical fall velocities from both instruments yields information on microphysical parameters at least in rain.

REFERENCES

K. A. Browning and R. Wexler: A determination of kinematic properties of a wine field using doppler radar. *J. Appl. Meteor.*, **7**, 105 – 113, 1968.

P. Tabary, G. Scialom, and U. Germann: Real-time retrieval of the wind from aliased velocities measured by doppler radars. *J. Atmos. Oceanic Technol.*, **18**, 875–882, June 2001.

D. Atlas, R.C. Srivastava, and R.S. Sekhon: Doppler Radar Characteristics of Precipitation at Vertical Incidence, *Rev. Geophys. Space Phys.*, **11**, 1–35, 1973.

LIDAR AND RADAR MEASUEMENTS OF THE MELTING LAYER IN THE FRAME OF THE CONVECTIVE AND OROGRAPHICALLY-INDUCED PRECIPITATION STUDY

Paolo Di Girolamo[1], Donato Summa[1], Rohini Bhawar[1],
Tatiana Di Iorio[2], Geraint Vaughan[3], Emily Norton[3], Gerhard Peters[4]

[1] DIFA, Università degli Studi della Basilicata, Potenza, Italy
Email: digirolamo@unibas.it
[2] Dipartimento di Fisica, Università degli Studi di Roma "La Sapienza", Roma, Italy
[3] School of Earth, Atmospheric & Environmental Sciences, University of Manchester, Manchester, UK
[4] Meteorologisches Institut, Universität Hamburg, Hamburg, Germany

Abstract: During the Convective and Orographically-induced Precipitation Study (COPS), lidar dark/ bright and bands were observed by the Univ. of BASILicata Raman lidar system (*BASIL)* on several IOPs and SOPs (among others, 23 July, 15 August, 17 August). Dark/bright band signatures appear in the lidar measurements of the particle backscattering. Lidar data are supported by measurements from the University of Hamburg cloud radar *MIRA 36* (36 GHz), the University of Hamburg dual-polarization micro rain radars (24.1 GHz) and the University of Manchester Radio UHF clear air wind profiler (1.29 GHz). Results from *BASIL* and the radars will be illustrated and discussed at the Conference to support in the comprehension of the microphysical and scattering processes responsible for the appearance of the lidar dark band and radar bright band.

Keywords: *Dark and bright band, synergy of remote sensors, Raman Lidar and radars, COPS.*

1 INTRODUCTION

Changes in scattering properties of precipitating particles are found to take place during the snowflake-to-raindrop transition in the proximity of the freezing level. A maximum in radar reflectivity, known as the radar bright band, is observed in the microwave domain, while a minimum in lidar echoes appears at optical wavelengths, this phenomenon being referred as lidar dark band [1].

The radar bright band has been known and studied for more than three decades and it is presently a well understood phenomenon [2,3]. On the contrary, the lidar dark band has been poorly investigated and, to date, no systematic and coordinated observation are available. Lidar observations of the lidar dark band have been reported by Sassen and Chen [1], Demoz et al. [5] and Roy and Bissonnette [6]. Model simulations of this phenomenon have been provided by several authors [7,8]. The lidar dark band is believed to be the result of two conflicting microphysical processes: a) the structural collapse of severely melted snowflakes, leading to a decrease of lidar backscattering due to the reduced particles size and concentration and b) the completion of the melting process, leading to a sudden increase of lidar backscattering associated with spherical particle backscattering mechanisms coming into prominence [1]. The radar bright band peak occurs low in the melting region, just above (approx. 200 m) the lidar dark-band minimum. This position is close to where radar Doppler velocity reaches its plateau.

A comprehensive study of the dark and bright band phenomena has been recently published by Sassen et al. [9]. In this paper, authors report measurements performed by a single-wavelength (532 nm) backscatter lidar system and a three-wavelength Doppler radar (0.32-, 0.86-, and 10.6 cm). Unfortunately, lidar and radar depolarization data, which would have provided further information on the state of the melting particles, were not available from the instruments involved. Instead, lidar and radar depolarization measurements were performed during COPS by *BASIL* and *MIRA 36*, respectively.

2 LIDAR AND RADAR SYSTEMS

The measurements illustrated in this paper were performed in the framework of *COPS – Convective and Orographically-induced Precipitation Study* - held in the period 01 June-31 August 2007. The Univ. of BASILicata Raman lidar system (*BASIL)* was deployed throughout the duration of COPS in Supersite R (Achern, Rhine Valley, Lat: 48.64 ° N, Long: 8.06 E, Elev.: 140 m). *BASIL*, capable to provide measurements of atmospheric temperature and water vapour, particle backscatter at 355, 532 and 1064 nm, particle extinction coefficient at 355 and 532 nm and particle depolarization at 355 and 532 nm, operated between 25 May and 30 August 2007 and collected more than 500 hours of measurements, distributed over 58 measurement days.

During COPS, lidar data were supported by measurements from the University of Hamburg cloud radar MIRA 36 (36 GHz, 0.83 cm, Ka-band), the University of Hamburg dual-polarization micro rain radars (24.1 GHz, 1.24 cm, K-band) and the University of Manchester Radio clear air wind profiler (1.29 GHz, 23.24 cm,

UHF band). Additional ancillary information on the state of the atmosphere was provided by radiosondes, launched every three hours during each measurement session, as well as by a sodar and a microwave radiometer.

3 RESULTS

The time evolution of *BASIL* measurements of the particle backscatter ratio at 1064 nm (not shown) over a period of approx. 1.5 hours from 13:00 UTC to 14:35 UTC on 23 July 2007 reveal the presence of stratiform clouds, with cloud base at 3.4-3.8 km. Around 14:15 UTC melting hydrometeors start precipitating from clouds.

The left panel in figure 1 shows the vertical profile of temperature as measured by the radiosonde launched at 14:06 UTC, revealing the height of the freezing level at ~ 3.35 km. The second panel shows the vertical profile of radar reflectivity at 36 GHz, 24.1 GHz and 1.29 GHz, revealing the presence of the radar bright band at 2.95-3.0 km, i.e. 350-400 m below the freezing level at a temperature of 3.4 - 3.9 0C. The third panel shows the vertical profile of backscattering coefficient at 1064 nm, revealing the presence of the lidar dark band at 2.85-2.9 m, i.e. 450-500 m below the freezing level at a temperature of 4.4 - 4.9 0C, while the lidar bright band is approx. 200 further down at 2.7-2.75 km. The fourth panel shows the vertical profile of vertical velocity measured at 36 GHz and 1.29 GHz, with values of 2-2.5 m/s high in the melting layer and values of 3.5-4 m/s in the lower portion of the melting layer. Lidar (at 355 nm) and radar depolarization are shown in the right panel of figure 1. Enhanced radar reflectivity, increased radar depolarization and abrupt change in Doppler-derived particle velocities are found in the melting layer. Radar depolarization is most commonly increased due to the presence of wetted, asymmetric ice shapes. Lidar depolarization at 355 nm shows values of 25-30 % high in the melting layer and values of 5-10 % at the heights of the lidar dark and bright bands. These unexpectedly low values of lidar depolarization may imply that precipitating particles are almost spherical or have a more regular shapes.

Lidar measurements were stopped at 14:35 UTC because of the rain reaching surface and entering the telescope, but the lidar dark band phenomenon presumably continued for approx. 2 hours.

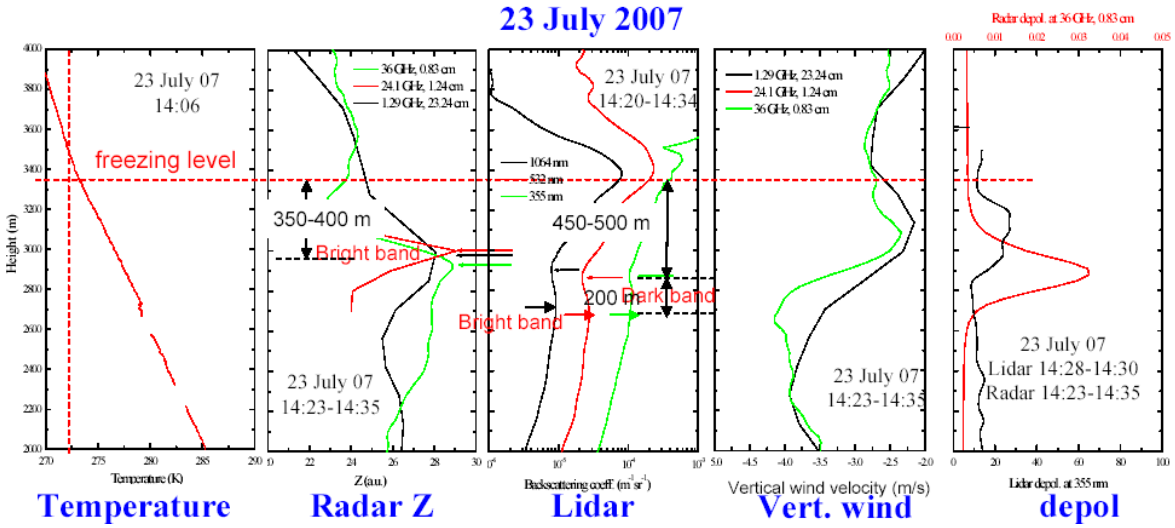

Figure 1. Vertical profile of temperature as measured by the radiosonde launched at 14:06 UTC (left panel); vertical profile of radar reflectivity at 36 GHz, 24.1 GHz and 1.29 GHz (second panel from left); vertical profile of backscattering coefficient at 1064 nm (third panel from left); vertical profile of vertical velocity measured at 36 GHz and 1.29 GHz (fourth panel from left); lidar depolarization at 355 nm (right panel).

REFERENCES

Sassen, K., and T. Chen, 1995: The lidar dark band: An oddity of the radar bright band. *Geophys. Res. Lett.*, **22**, 3505–3508.

Battan, L. J. Radar Observations of the Atmosphere, Univ. of Chicago Press, 1973, pp. 279.

Meneghini; R., and L. Liao, 2000: Effective Dielectric Constants of Mixed-Phase Hydrometeors. *J. Atm. Oceanic Tech.*, **17**, 628– 640.

Demoz, B. B., D. Starr, D. Whiteman, K. Evans, D. Hlavka, and R. Peravali, 2000: Raman LIDAR Detection of Cloud Base. *Geophys. Res. Lett.*, , **27**(13), 1899– 1902.

Roy, G., and L. R. Bissonnette,2001: Strong dependence of rain-induced lidar depolarization on the illumination angle: Experimental evidence and geometrical- optics interpretation, *Appl. Opt.*, **40**, 4770– 4780.

Di Girolamo, P., B. B. Demoz, and D. N. Whiteman, 2003: Model simulations of melting hydrometeors: A new lidar bright band from melting frozen drops, *Geophys. Res. Lett.*, 2003, **30** (12), 1626, doi:10.1029/2002GL016825.

Griaznov, V., I. Veselovskii, P. Di Girolamo, B. Demoz, D. N. Whiteman, 2004: Numerical Simulation of Light Backscattering by Spheres With Off-Center Inclusion. Application for Lidar Case. *Applied Optics*, **43**, 5512-5522.

Sassen, K., J. R. Campbell, J. Zhu, P. Kollias, M. Shupe, C. Williams, 2005: Lidar and triple-wavelength Doppler radar measurements of the melting layer: A revised model for dark and bright band phenomena, *J. Appl. Met.*, **44**, 301–312.

STUDY OF AN MCS USING RAMAN LIDAR IN THE FRAME OF THE CONVECTIVE AND OROGRAPHICALLY-INDUCED PRECIPITATION STUDY

Rohini Bhawar[a] , Paolo Di Girolamo[a], Donato Summa[a], Tatiana Di Iorio[b], Belay B. Demoz[c]

[a] *DIFA, Università degli Studi della Basilicata,Viale dell'Ateneo Lucano n. 10, 85100 Potenza, Italy*
Email: *rohinibhawar@yahoo.com*
[b] *Dipartimento di Fisica, Università degli Studi di Roma "La Sapienza", Piazzale Aldo Moro, 2, 00100 Roma, Italy*
[c] *Department of Physics and Astronomy, Howard University, 2400 Sixth Street, NW, Washington, DC , USA*

Abstract: During the *Intensive Observation Period* (IOP) 9c of the *Convective and Orographically-induced Precipitation Study* (*COPS)* on 20 July 2007 a frontal zone passed over the COPS region, with a Mesoscale Convective System (MCS) imbedded in it. The Raman lidar system *BASIL* which was deployed in Achern (Supersite R, Lat: 48.64 ° N, Long: 8.06 ^{0} E, Elev.: 140 m) in the frame of the *COPS* was operated continuously during this day. The lidar data determined the lowering of the anvil clouds, which is a signature for the approaching thunderstorm. During the time frame 10:46-11:37 UTC cloud deck is present around 2 km, which represents a mid-level outflow from the thunderstorm. Wind profiler data reveal that the wind flow at higher levels is opposite with respect to low level winds. The effect of this is to moisten that level and precipitate (mostly virga) to recycle back. Waves like structures were also seen in the data just prior to the arrival of the thunderstorm, which are due to shear between inflow or outflow regions. Thus, two primary processes stand out: the elevated outflow region above the BL (2-3.5 km) and the presence of associated shear, which helped in modifying the environment. Measurements in terms of particle backscatter and water vapour mixing ratio are discussed to illustrate the above phenomena.

1. INTRODUCTION

On 20 July 2007, an *Intensive Observation Period* (IOP) 9c of the *Convective and Orographically-induced Precipitation Study* (*COPS)* a vorticity maximum at the east side of a jet initiated over middle eastern France triggered cyclogenesis and a Mesoscale System (MCS) propagated north-eastwards. Thus, IOP 9 was particularly an experimental platform to study the development of frontal zones and their influence on the intensity of convection. The MCS reached the measurement site Archen, Rhine valley at around 09:30 UTC. Ahead of the weak cold front related to the cyclone, in which the MCS was imbedded, outflow boundaries produced a squall line with severe thunderstorm activity. The University of Basilicata Raman Lidar (*BASIL)* visualized the interaction of the MCS with the prevailing pre-storm environment and its modification. Additionally during the passage of the squall line, deep convection was triggered in the COPS region modifying the structure of the squall line and of related precipitation pattern. The cold front can also transport aerosols and trace gases from the boundary layer to the free troposphere [Cooper et al 2001, Esler et al, 2003, Stohl et al. 2001]. Water vapor is useful in studying many of the atmospheric dynamic features as it is conserved in all meteorological processes except condensation and evaporation.

The Raman Lidar system *BASIL,* deployed in Achern (Supersite R, Lat: 48.64 ° N, Long: 8.06 ^{0} E, Elev.: 140 m), operated between 25 May and 30 August 2007 and collecting more than 500 hours of measurements, distributed over 58 measurement days. The major feature of *BASIL* is represented by its capability to perform high resolution and accurate measurements of atmospheric temperature and water vapour, both in daytime and night-time, based on the application of the rotational and vibrational Raman lidar techniques in the UV. Besides temperature and water vapour, *BASIL* is capable to provide measurements of particle backscatter at 355, 532 and 1064 nm, particle extinction coefficient at 355 and 532 nm and particle depolarization at 355 and 532 nm. The Raman Lidar system *BASIL* was operated continuously during 20 July 2007 from 04:33 to 19:22 UTC. Below we present analysis of a MCS observed on 20 July 2007.

2. IMPORTANT FEATURES

Figure 1 shows the range corrected signals at 1064 nm during the total observation period from 04:33 to 19:22 UTC. There was presence of low clouds or fog in the valley till 09:30 UTC and development of convective clouds during the afternoon with different precipitation intervals throughout the day. The lidar visualized the interaction of the MCS with the prevailing pre-storm environment and also how it was modified. A signature of thunderstorm approaching is present in the 1064 nm range corrected lidar signals in figure 1, visible in the lowering of the anvil clouds up high. Low level wind below about 1km was towards the centre of the thunderstorm i.e. positive motions towards the centre within the cold air mass at an altitude range of 0.5 to 2.5 Km during the time period 10 to 12 UTC as seen in the wind profiler data from University of Manchester.

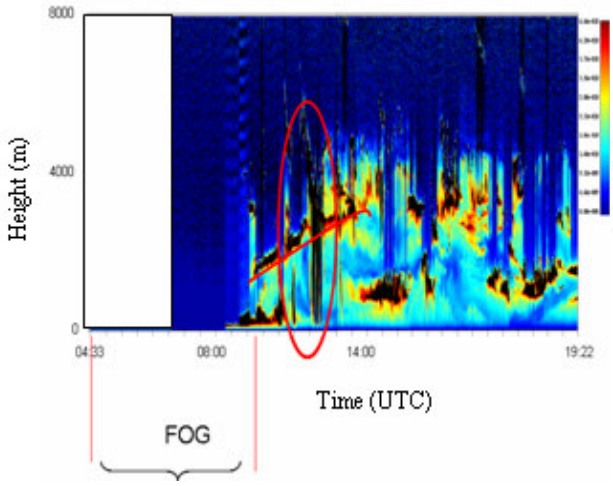

FIGURE 1. Range-corrected signals at 1064 nm during the MCS event.

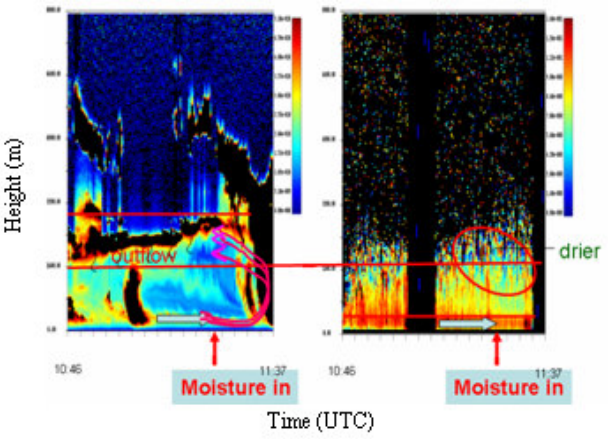

FIGURE 2. Range corrected signals at 1064 nm together with the water vapour mixing ratio data during the MCS (time frame 10:46-11:37 UTC).

The highest wind speed observed was around 15 m/s. Figure 2 shows the range corrected signals at 1064 nm together with the water vapour mixing ratio data during the MCS (time frame 10:46-11:37 UTC). An interesting fact is the cloud deck at 2km, which represents a mid-level outflow from the Thunderstorm/MCS. The wind flow at higher levels is opposite with respect to low level winds. The effect of this is to moisten that level and precipitate (mostly virga). So, we can see a conveyor belt of things here where the thunderstorm mid-level outflow spits out hydrometeor-debris and it is recycled back into it. In the water vapor mixing ratio we observe the moist layer below about 1 km and a drier layer about 2 km. This means that the MCS was modifying the environment at 1.6-2.5 km directly (outflow) and the lower levels through the virga/precipitation. In addition, the MCS can only survive by pulling in moisture from a large area (~100km radius or more) around it (below about 1km), which is somewhat modified by the virga. There is a wave like structure seen in the data just prior to the arrival of the thunderstorm present due to shear between inflow or outflow regions. Two primary and important processes which can be clearly observed are: the elevated outflow region above the BL (2-3.5km) and the presence of associated shear. Shear and mid-tropospheric moistening are important parameters to consider in convection: shear can inhibit convection, but also aid if the waves break and create self sustaining turbulence at the right level. In support of this the 09:08 UTC radiosonde showed a moist layer below about 1 km and a drier layer in the region above 1km: this was the time when the MCS entered the COPS area.

Results shown here demonstrate the excellent capability of Raman lidars in visualizing the detailed vertical and temporal structure of the atmosphere. Fine-scale structures of the boundary layer and between air masses at different altitudes detected, explaining the dynamic processes involved will be presented in the conference.

REFERENCES

1. Cooper, O.R., J.L.Moody, D.D.Parrish, M.Trainer, T.B.Ryeson, J.S. Holloway, G.Hubler, F.C.Fehsenfeld, S.J.Oltmans, and M.J.Evans, " Trace gas signatures of the airstreams within North Atlantic Cyclones:Case studies from the North Atlantic Regional Experiment (NARE'97) aircraft intensive" *J. Geophys. Res.,* **106**, 2001,5437-5456.

2. Esler, J.G., P.H.Haynes, K.S.Law, H.Barjat, K.Dewey, J.Kent, S.Schmitgen, and N.Brough, "Transport and mixing between airmasses in cold frontal regions during Dynamics and Chemistry of Frontal Zones (DCFZ), *J. Geophys. Res.,* **108**, 2003, doi:10.1029/2001JD001494.

3. Stohl, A., "A 1-year Lagrangian "climatology" of airstreams in the Northern Hemisphere troposphere and lowermost strastosphere" *J. Geophys. Res.,* **106**, 2001, 7263-7279.

INFLUENCE OF OROGRAPHY AND AEROSOLS ON THE MICROPHYSICS OF CONVECTIVE CLOUDS OBSERVED DURING COPS

Alan Blyth[1], Yahui Huang[2], Phil Brown[3], Richard Cotton[3], Hazel Jones[4], Tom Choularton[4], Gordon McFiggans[4], Martin Irwin[4], Hugh Coe[4]

[1] National Centre for Atmospheric Science, University of Leeds, Leeds LS2 9JT, UK
E-mail: blyth@*env.leeds.ac.uk*
[2] Institute for Climate and Atmospheric Science, University of Leeds, Leeds LS2 9JT, UK
[3] UK Met Office, Exeter EX1 3PB, UK
[4] School of Earth, Atmospheric and Environmental Sciences, University of Manchester, Manchester M13 9PL, UK

Abstract: Analysis is presented of microphysical data gathered on 2 days during COPS with instruments on the BAe 146 research aircraft. High concentrations of ice particles larger than 150 μm were observed in the 11 July 2007 cloud at temperatures of between -3 and -8 ˚C. In contrast, on 15 July 2007, large ice particles were barely detectable. However, the concentration of small ice particles was significantly higher than observed in the 11 July cloud. This is possibly due to the higher peak concentrations of aerosols that were observed on 15 July consistent with the model prediction of the presence of Saharan dust and the venting of aerosols from the Murg Valley.

Keywords: *COPS, aerosols, venting, convection, ice particles*

1 INTRODUCTION

The Convective Orographically-induced Precipitation Study (COPS) took place over the Black Forest mountains in the summer of 2007. The primary focus was on the formation and development of convective precipitation systems over the mountains. One goal of the project is to determine the properties of aerosol in the convective cloud inflow and to understand the formation and growth of ice and precipitation in the clouds as influenced by the aerosols.

The BAe-146 aircraft, which was equipped with state-of-art microphysics instruments such as the Cloud Particle Imager (CPI) and Small Ice Detector, penetrated developing cumulus clouds on 11 and 15 July 2007 near cloud top. Legs were also made below cloud base to investigate the properties of aerosol particles.

2 ANALYSIS OF IN SITU MEASUREMENTS

Several clouds were penetrated on 11 July as they advected across the COPS domain. It is believed that in one cloud, penetrated near the ascending top, first ice was observed with concentration of 0.04 L^{-1} at temperature of -6 ˚C. In a different cloud, which was in a mature to decaying stage, the concentration of ice particles larger than 150 μm reached to 124 L^{-1} . The high concentration of ice particles exceeds the value estimated from the Meyers formula (Meyers et al., 1992) derived from typical ice nuclei measurements for cloud tops estimated from radar. The observation of the co-existence of numerous ice particles, pristine columns, graupel particles and supercooled drops within the temperature range of -3 to -9 ˚C, suggests that the Hallett-Mossop process of splintering during riming (Hallett and Mossop, 1974) may be responsible for the ice development. Figure 1 shows the details from the penetration of Run 6.1made at a temperature of -5˚C.

Large ice particles were not measured in the clouds penetrated on 15 July. However, the concentration of ice particles smaller than about 55 μm was significantly higher than observed on 11 July. Interestingly, model results suggest that a plume of Saharan dust arrived in the COPS region early on 15 July 2007. There is a difference in the properties of the aerosol measured at the ground-based facility on Hornisgrinde on 11 and 15 July that is consistent with these model results. Higher peak concentrations of aerosols were also observed on the aircraft on 15 July. The analysis of the distributions of aerosol particles from the PCASP averaged over the legs made at similar altitudes in the two cases shows that the total concentration of aerosol and the concentration in each size range are greater on 15 July than on 11 July.

A leg was made over the Murg Valley on 15 July at an altitude of 1.7 km above MSL and below the altitude of cloud base. The track was approximately along the wind direction from SW to NE. Figure 2 shows the vertical wind and the concentrations from the PCASP and CPC. The updraft over the valley is strong with a maximum speed of 5.2 m/s. The width of the updraft is about 2.4 km (Fig. 2). In the core of the updraft the concentrations detected by the PCASP and CPC reached about 1300 cm^{-3} and 5600 cm^{-3}, respectively, while their peak values (1600 cm^{-3} and 7000 cm^{-3}, respectively) were encountered a little later. The concentration remained higher downwind of the valley than on the upwind side.

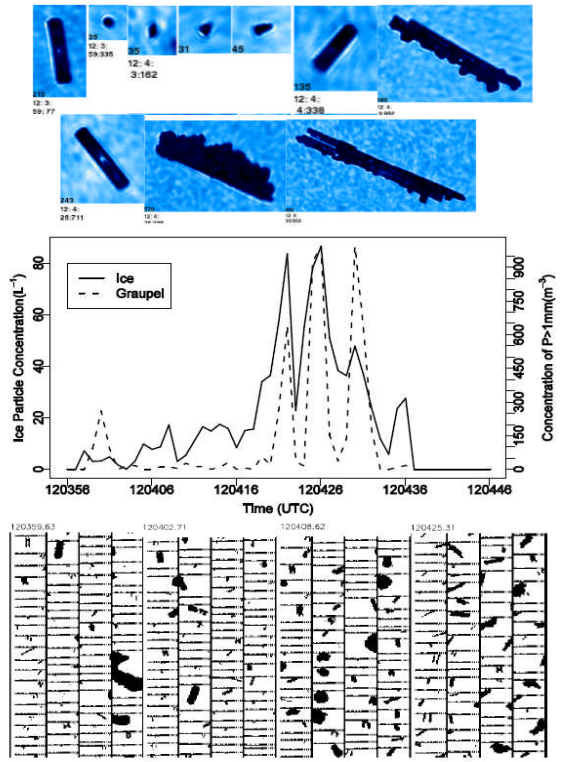

Figure 1. Ice particle concentration (solid line). Examples of particle images from CPI and 2DC are included.

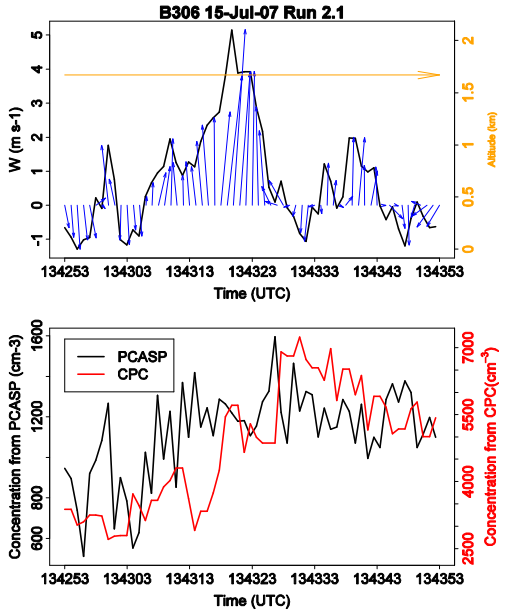

Figure 2. Wind field and aerosol concentration.

3 CONCLUSIONS

The concentration of large ice particles was greater than expected from primary ice nucleation in 11 July cloud. The observations suggest that the Hallett-Mossop process of secondary ice particle production was active and it is likely that the high concentrations could be explained with this mechanism. There are some issues to resolve however. Observations were also made near the ascending tops of some of the clouds that formed near the famous, much-photgraphed 15 July cloud. The analysis offers interesting twists to consider for modelling this cloud: mainly high concentration of aerosols probably associated with Saharan dust; and also venting of aerosols out of the Murg Valley, which likely contributes to the high concentrations. There is some support from the observations, but more modelling and data synthesis needs to be carried out. Venting from the valley was observed on a few other days during COPS suggesting that not only are the valley flows responsible for the convergence lines that help with the initiation of convection, but they may cause transport of aerosols into the clouds. Thus it is possible that the orography played a significant role in altering the microphysical behaviour of the clouds that formed or advected over the Black Forest.

Acknowledgements:
We thank the pilots of the FAAM BAe aircraft for making the flights and all the people involved in the field campaign. The COPS project is supported by the Natural Environment Research Council.

REFERENCES

Hallett, J. and S. C. Mossop, 1974: Production of secondary ice particles during the riming process. Nature, 249, 26-28.

Kalthoff, N., B. Adler, Ch. Barthlott, U. Corsmeier, S. Mobbs, S. Crewell, K. Träumner, Ch. Kottmeier, A. Wieser, and V. Smith, 2009: The impact of convergence zones on the initiation of deep convection: A case study from COPS. Atmospheric Research, doi:10.1016/j.atmosres.2009.02.010

Meyers, M. P., P. J. DeMott, and W. R. Cotton, 1992: New primary ice-nucleation parameterizatios in an explicit cloud model. J. Appl. Meteor., 31, 708-721.

Idealized Numerical Sensitivity Studies on Shallow-Convection-Triggered Storms in a Low Mountain Range

Ulrich Blahak[1]

[1] Institut für Meteorologie und Klimaforschung, Karlsruhe Institute of Technology (KIT), Karlsruhe, Germany
E-mail: *ulrich.blahak@imk.fzk.de*

Abstract: In this paper, the explicit numerical simulation of shallow convective motions and subsequent triggering of an ensemble of interacting convective cells using the COSMO-model and the newly modified Seifert-Beheng two moment bulk microphysical scheme is investigated, applying horizontal grid spacings of 100 - 500 m. Using idealized orography and initial conditions, shallow convection is forced by specifying suitable sensible and latent heat fluxes at the surface. It is shown that the used model setup and turbulence parameterization are adequate to simulate the spin-up of an ensemble of cells with, after a certain time of self-organization, take on realistic mutual distances and maximum vertical updraft speeds. In comparison with the more traditional idealized single storm simulations (triggered by, e.g., "warm bubble" or mountain wave flow) the presence of interactions with neighbouring cells leads to a (possibly) more realistic framework for sensitivity studies (microphysics, triggering mechanisms) on convective clouds.

***K*eywords:** *Shallow convection, deep convection, transition, cloud microphysics, precipitation, idealized simulations*

1 INTRODUCTION

In order to elaborate parameters crucially influencing the characteristics of convective cells, idealized high resolution cloud resolving simulations with the COSMO-model are performed using the two-moment bulk microphysical scheme of Seifert and Beheng (2006). A newly modified version is used, based on the recent extention of the scheme by considering a class of high density particles ("hail") in addition to cloud droplets, rain, cloud ice, snow and graupel.

In past idealized simulations, single convective systems have been artificially triggered either by the classical "warm bubble" approach or by wave flow over idealized orography. The numerical results often exhibited rather strong maximum updraft speeds (w > 50 m s^{-1}) and a rather quick lateral spreading of multicell/supercell type systems over the entire model domain, often accompanied by a comparatively low precipitation efficiency and low simulated radar reflectivity in the upper part of the cells.

Only a slight improvement has been obtained by changing microphysical parameters and process descriptions in the 2-moment microphysics scheme (Blahak, 2008). Therefore, we guess that another parts of the problem may be 1) the highly artificial trigger mechanism and 2) the fact that the simulated systems developed isolated and in a rather "pristine" environment, lacking interactions with neighbouring circulation patterns.

Accordingly, idealized simulations are altered by specifying an idealized daily cycle of the surface fluxes over hilly terrain (idealized hills, ridges), repesentative for a sunny summer day, such that a broad spectrum of convective structures simultaneously appears. In this way, the relevant circulation scales (shallow convection) spin up by themselves and, after removal of CIN, deep convective cells develop. To resolve the necessary spatial scales, we use model resolutions down to 100 m horizontally and approx. 50 m vertically within the PBL.

This kind of "quasi" LES simulations has been performed in the past by various authors to investigate warm shallow cumulus clouds. However, most of them did not apply such a detailed cloud microphysical parameterization and did not focus on sensitivity studies on deep convective mixed phase clouds. Balaji (1988) is one of the few who simulated the development of a deep convective cloud in a very similar fashion (but with coarser grid spacing).

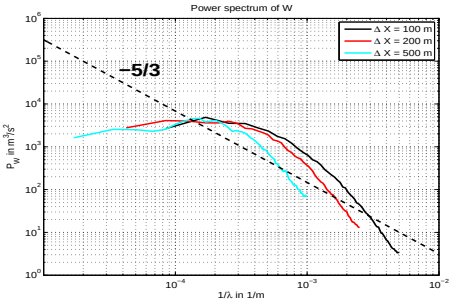

Figure 1: Mean horizontal power spectra of W in Y-direction in m^{3}s^{-2} as function of inverse wavelength in m^{-1} for simulations with ΔX = 100 m, 200 m and 500 m.

2 FROM SHALLOW TO DEEP CONVECTION

For our idealized simulations, the original soil- and radiation modules as well as any convection parameterization are turned off. The idealized daily cycle of sensible and latent heat fluxes H and E (max. H = 300 W m^{-2}) takes into account the effects of sloping terrain, slant cloud shadows and precipitation. Fully periodic lateral boundary conditions are used. Typical horizontal grid spacings for our simulations range from 100 m to 1 km. A suitable 3D turbulence closure is used which combines a Smagorinsky-type LES formulation of the turbulent lenght scale with a 1.5th order TKE closure for the turbulent diffusion coefficients (Herzog et al., 2002). The ratio of the horizontal to vertical turbulent diffusion coefficients is chosen to be 3.

Fig. 1 shows space-time-average power spectra of W in Y-direction within the planetary boundary layer (PBL) for simulations of dry shallow convection as function of the model grid spacing for a weak wind situation. Initially, the PBL is slightly stable, and shallow convection patterns develop gradually from small initial noise into a developing convective boundary layer. It is evident that, even at ΔX = 100 m, the scales of shallow convection ($\approx$ 200 – 500 m) lie within the slightly over-damped short-wave tail and not all details of this phenomenon are realistically simulated.

However, the spatial distribution of updrafts and downdrafts, updraft strengths of thermals as well as organization patterns look qualitatively ok up to $\Delta X = 300$ m, also for simulations with higher windspeed (no figures shown). Therefore, it seems that for our purpose (which is triggering of deep convective cells with realistic mutual distances), the coarsest possible grid spacing may be in the range of 300 m.

Using $\Delta X = 300$ m and activating the cloud microphysics parameterization results in an ensemble of interacting cells, like it is shown in Fig. 2 as a MAX-Cappi picture of simulated radar reflectivity. A gaussian mountain (height 500 m, half-width 20 km) in the center of the domain generated a first cell by anabatic winds (overheated south-eastern flank), and the figure captures about the time at which other cells in the surrounding area begin to develop (1:40 h after simulation start).

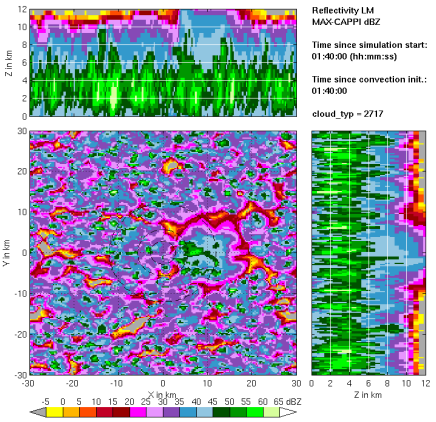

Figure 2: MAX-CAPPI of simulated radar reflectivity in dBZ after 1:40 h for the simulation with "low CCN" and "warm" environment.

3 SENSITIVITY ON TEMPERATURE REGIME AND AEROSOL CONDITIONS

In continuation of the work presented in Blahak et al. (2006), in which a single multicellular system has been initiated by pure mountain wave flow, the effect of different temperature levels in combination with low-CCN- and high-CCN-aerosol regimes on shallow-convection-triggered cells is investigated.

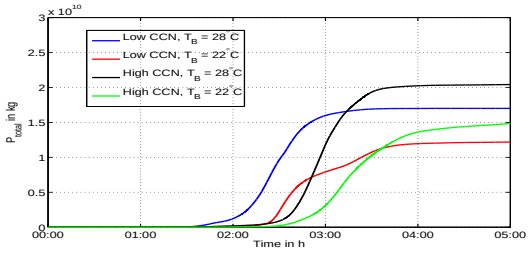

Figure 3: Time series of accum. precip. for the 4 cases. "warm" = "28°C"; "cold" = "22°C"

To this end, four simulations of the type described at the end of the last section are presented, which constitute all possible combinations of a "warm" and "cold" environment with "high-CCN" and "low-CCN" conditions, each with the same initial $CAPE \approx 1900\ \mathrm{J\,kg^{-1}}$ and at low windspeed. To summarize the results, the time series of the total accumulated precipitation (Fig. 3) show that for the simulated type of widespread "popcorn like" convection and for the specific prescribed atmospheric conditions, the effect of increased aerosol load is mainly a time delay of the precipitation, but no reduction of its amount. The "cold" environment leads to less precipitation compared to the "warm".

The simulated convection exhibits a typical life cycle of about 4 – 5 h, caused by the widespread convective vertical exchange processes and removal of $CAPE$, and maximum updraft speeds are $\approx 40\ \mathrm{m\,s^{-1}}$. Vigorous lateral spreading of cells (which has been observed the earlier study mentioned above) is hindered by interactions with neighbouring cells. Such interaction-effects will be explored in more detail in the future.

However, the sensitivities presented above strongly depend on details of the parameterizations of autoconversion, cloud nucleation and ice phase processes, which means that our results may not be generalized, and further investigations are necessary.

4 CONCLUSIONS

To study cloud microphysical sensitivities in an idealized framework using the COSMO-model and an advanced cloud microphysics parameterization, an ensemble of interacting neighbouring convective cells is triggered by (differential) surface heating and the resulting shallow convective motions. Using a simple LES 3D turbulence closure and grid spacings smaller than 300 m leads to results which seem to be "realistic enough" for this purpose. Such studies are a valuable alternative to the more traditional idealized "warm bubble" triggered single-convective-system studies and enlarge the scope to interaction effects of neighbouring cells.

REFERENCES

Balaji, V. and T. L. Clark, 1988: Scale selection in locally forced convective fields and the initiation of deep cumulus, *J. Atmos. Sci.*, **45**, 3188–3211.

Blahak, U., H. Noppel and K. D. Beheng, 2006: Influence of ambient environmental conditions and orography on the characteristics of deep convective cells as simulated with a sophisticated two-moment (bulk) microphysical scheme, 12. AMS Conference on Cloud Physics, 10. – 14.7.2006, Madison, Wisconsin, available online: http://ams.confex.com/ams/pdfpapers/113531.pdf.

Blahak, U., 2008: Towards a better representation of high density ice particles in a state-of-the-art two-moment bulk microphysical scheme, International Conference on Clouds and Precipitation, 7.7. – 11.7.2008, Cancun, Mexico.

Herzog, H.-J., G. Vogel and U. Schubert, 2002: LLM – A nonhydrostatic model applied to high-resolution simulations of turbulent fluxes over heterogeneous terrain, *Theor. Appl. Climatol.*, **73**, 67–86.

Seifert, A. and K. D. Beheng, 2006: A two-moment cloud microphysics parameterization for mixed-phase clouds. Part I: Model description, *Meteorol. Atmos. Phys.*, **92**, 45–66.

Scaling relations in warm-rain orographic precipitation

Axel Seifert, Günther Zängl

Deutscher Wetterdienst, Offenbach, Germany
E-mail: *axel.seifert@dwd.de*

Abstract: Warm rain orographic precipitation at an isolated mountain is studied by numerical experiments using the non-hydrostatic COSMO model. The simulations are analyzed in terms of precipitation amounts, precipitation efficiency and spillover factor as a function of the relevant microphysical and advective timescales and Froude numbers. For the microphysical conversion timescale a new formulation is applied based on an analysis of the stochastic collection equation. This new estimate of the warm rain microphysical timescale couples the rain formation to the forcing by condensation, i.e. updraft velocity and liquid water lapse rate, and microphysical properties like the cloud droplet number concentration. Using this microphysical timescale the scaling relations for warm-rain orographic precipitation for an isolated mountain are revisited.

***K*eywords:** *ICAM, orographic precipitation, precipitation formation, mountain flow, aerosol-cloud-precipitation effects*

1 INTRODUCTION

Understanding the warm rain formation at an isolated mountain is a classical, yet to some extent unsolved problem. The inherent difficulties arise due to the coupling of two non-linear systems, the hydrodynamic mountain flow and the rain formation by collision-coalescence. Various attempts have been made to formulate the orographic rain formation by simple scaling relations, see e.g. Jiang and Smith (2003) and the review of Smith (2006). A weak point of the previous studies is the oversimplified approach to cloud microphysics, often just described by a constant rain formation timescale. In the following a new rain formation timescale is presented which can be traced back to the stochastic collection equation itself. This timescale is then used to analyze and rationalize the results of a three-dimensional non-hydrostatic model.

2 WARM-RAIN TIMESCALE

The rain formation timescale follows the ideas of Stevens and Seifert (2008) and Seifert and Stevens (2009). They define the time τ_*, a measure for the onset of the first in-cloud rain, by a balance of production of cloud water by condensation and its depletion by the collision-coalescence process. For brevity the derivation of τ_*, which is based on the Seifert and Beheng (2001, SB2001 hereafter) warm rain scheme, is not repeated here, but the result is simply stated from Eq. (29) of Stevens and Seifert (2008):

$$\tau_* = \left[\beta_* + \sqrt{\beta_* + \frac{\tau_0^4}{(1-\epsilon_*)^4 \phi_{cc}(\epsilon_*)}} \right]^{1/2} \qquad \text{with} \qquad \beta_* = \frac{k_{cr}\, N_c^2}{2\, k_{\text{au}}} \, \frac{\epsilon_* \, \phi_{cr}(\epsilon_*)}{(1-\epsilon_*)^3 \phi_{cc}(\epsilon_*)} \tag{1}$$

and $\tau_0 = N_c^{1/2}\, \tau_{\text{cond}}^{3/4}\, k_{\text{au}}^{-1/4}$. Here N_c is the cloud droplet number concentration, τ_{cond} the condensation timescale, and ϵ_* the rain fraction at the time τ_*. The ϕ_{cc} and $\phi_{cr}(\epsilon)$ are the similarity functions of SB2001 for autoconversion and accretion. The autoconversion parameter k_{au} depends on the shape parameter ν of the cloud droplet size distribution, k_{cr} is the kernel coefficient for accretion. For further details, e.g. how to estimate ϵ_*, it is referred to Seifert and Stevens (2009). This warm-rain timescale has two advantages over previous formulations: First, it has been derived from the stochastic collection equation and includes all relevant microphysical sensitivities. Second, by including the condensation timescale τ_{cond} it is coupled to the dynamics of the cloud, since $\tau_{\text{cond}}^{-1} = w\, \Gamma_l$ with the updraft velocity w and the liquid water lapse rate Γ_l.

3 MODEL SETUP

Using the non-hydrostatic COSMO model we investigate the 3-d mountain flow across an isolated bell-shaped hill with height $h(x) = H/(1 + x/a)^{3/2}$ and a mountain half-width a. As initial condition we use a moist stable stratification, with the moisture in the lowest kilometer being close the saturation value. The simulations are performed with 1 km grid spacing on a 250×101 domain with 50 vertical levels. As microphysics scheme we use the SB2001 warm rain scheme with a fixed cloud droplet number concentration. Using a fixed initial condition for moisture and temperature we investigate the dependency of the flow and the resulting clouds and precipitation on the wind speed U_0, the mountain height H, mountain width a, and the cloud droplet number concentration N_c.

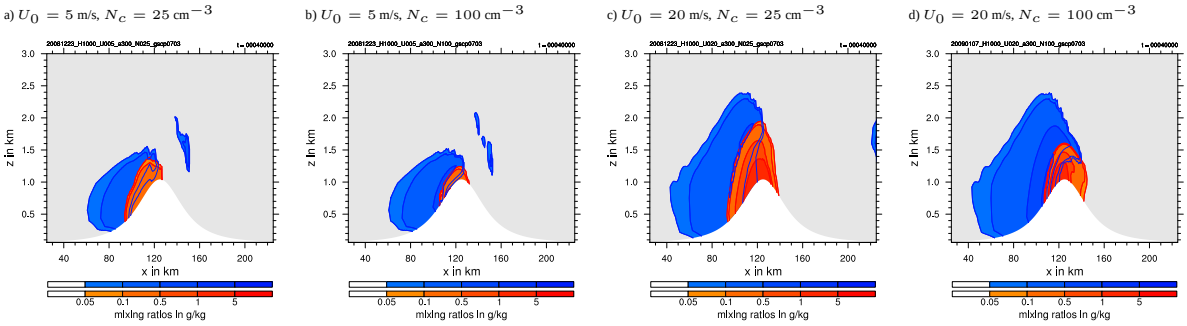

Figure 1: Vertical cross sections of cloud (blue) and rain (red) mixing ratios for different wind speeds and cloud droplet number concentrations ($H = 1000$ m, $a = 30$ km).

4 A FEW PRELIMINARY RESULTS

Figure 1 shows cross sections of the simulated orographic cloud for 4 different configurations. As expected, increasing the cloud droplet number concentration from 25 cm^{-3} to 100 cm^{-3} slows down the rain formation in the cloud resulting in less rain that is shifted to the mountain top. Increasing the wind speed leads to a bigger and thicker cloud which produces more rain, but is also susceptible to variations in the cloud droplet number concentration. Overall more than 1000 simulations of this type have been performed.

Figure 2 shows a result for the precipitation efficiency E_c, defined as surface precipitation amount over total condensate in the volume, for various simulations varying U_0 and N_c only. E_c is plotted as a function of the ratio of the advective timescale $\tau_{\text{adv}} = a/U_0$ and the microphysical timescale $\tau_*(N_c)$. For each U_0 there is a certain ratio τ_{adv}/τ_*, i.e. a certain N_c, at which surface precipitation starts. For large τ_* (higher N_c) no surface rain occurs, for smaller τ_* (lower N_c) we find first a linear increase of the precipitation efficiency with τ_{adv}/τ_*, and then the system goes into saturation when an efficiency of about 40-50 % is reached. Unfortunately, the curves for different U_0 do not fall onto each other. We argue that this is due to the oversimplified formulation of the advective timescale $\tau_{\text{adv}} = a/U_0$. There are probably two modifications necessary: (1) For larger U_0, or U_0/N with Brunt-Vaisala frequency N, the mountain wave becomes larger and therefore the advective timescale decreases more slowly than U_0^{-1}. (2) For small Froude numbers $U_0/(N\ H)$ the flow will prefer flow-around instead of flow-across the mountain resulting in a larger advective timescale.

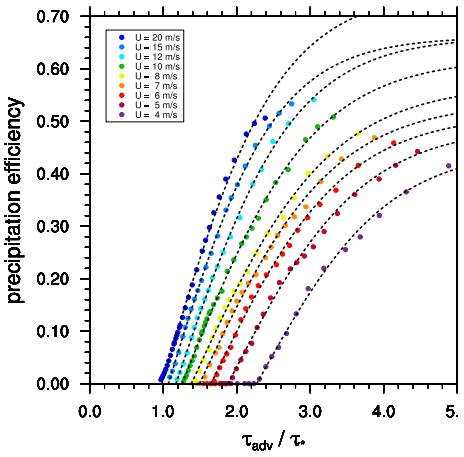

Figure 2: Precipitation efficiency for various simulations with $U_0 \in [4-20]$ m/s and $N_c \in [20-700]$ cm^{-3} as a function of the ratio of the advective timescale $\tau_{\text{adv}} = a/U_0$ and the microphysical timescale τ_* ($H = 1000$ m, $a = 30$ km).

5 CONCLUSIONS AND OUTLOOK

We presented a refined approach to rationalize the warm-rain orographic precipitation problem. The basic idea follow previous work of Jiang and Smith (2003) an others, but is now extended to a more sophisticated microphysical timescale. We argue that a more detailed formulation of the advective time scale is also necessary that includes the linear mountain wave effect as well as non-linear Froude number effects.

REFERENCES

[1] Jiang, Q., and Smith, R.B., 2003: Cloud timescale and orographic precipitation. *J. Atmos. Sci.*, **60**, 1543–1559.

[2] Stevens, B. and Seifert, A., 2008: On the sensitivity of simulations of shallow cumulus convection to their microphysical representation. *J. Meteorol. Soc. Jap.*, **86**, 143–162.

[3] Smith R.B., 2006: Progress on the theory of orographic precipitation. *in Willett, S.D. et al. Tectonics, Climate and Landscape evolution*, Geological Society of America Special Paper 298.

[4] Seifert, A. and Beheng, K.D., 2001: A double-moment parameterization for simulating autoconversion, accretion and selfcollection. *Atmos. Res.*, **59-60**, 265–281.

[5] Seifert, A. and Stevens, B., 2009: Microphysical scaling relations in a kinematic model of isolated shallow cumulus clouds, *J. Atmos. Sci.*, submitted.

THE INFLUENCE OF THE FREEZING LEVEL ON OROGRAPHIC PRECIPITATION PATTERNS AT SMALL SCALES

Günther Zängl

Deutscher Wetterdienst, Offenbach, Germany
E-mail: *Guenther.Zaengl@dwd.de*

Abstract: Idealized numerical simulations have been conducted to investigate the influence of the freezing level on precipitation patterns over narrow mountain ridges. The focus is on precipitation enhancement via the seeder-feeder mechanism, implying that widespread precipitation is locally enhanced by orographic lifting. The results indicate a marked sensitivity to the location of the freezing level with respect to the mountain peak height. For freezing levels significantly below or above the peak height, a single precipitation maximum near the mountain peak dominates, whereas for a freezing level near the peak height, the precipitation maximum tends to be shifted towards the lee slope. Analysis of the model results indicates that this is partly related to the fall-speed-difference between snow and rain and partly to the higher accretion efficiency of snow than of rain.

***K*eywords:** *Orographic precipitation, seeder-feeder mechanism*

1 INTRODUCTION

It has been known for quite a long time that mountainous orography can induce marked small-scale variability of precipitation, not only for single events but also on climatological time scales. This variability is related to various mechanisms of orographic precipitation enhancement, the most important of which being orographic triggering of convection and local intensification of stratiform precipitation via the seeder-feeder mechanism. A systematic spatial variability in climatological rainfall amounts appears in the first case if there are preferred triggering locations of convection, whereas in the second case the largest effect arises when precipitation predominantly falls in a narrow range of wind directions. At small scales, precipitation enhancement through the seeder-feeder mechanism usually leads to local precipitation maxima somewhere over the lee slopes of individual mountain ridges because of hydrometeor advection (e.g. Carruthers and Choularton, 1983). A more subtle aspect of seeder-feeder-induced precipitation enhancement, which was recently discovered by Zängl (2008) and Zängl et al. (2008), is an apparent temperature dependence of the enhancement intensity. Specifically, data analysis suggested that climatological precipitation enhancement over the lower lee slope of individual mountain ridges exhibits a correlation between ridge height and the height of the freezing level, in the sense that higher (lower) mountains induce larger precipitation enhancement for higher (lower) freezing levels. To gather more insight into this phenomenon, particularly into the underlying physical processes, idealized numerical simulations with the Penn State/NCAR mesoscale model MM5 have been conducted.

2 MODEL SETUP

The simulations discussed in the following have been conducted with four interactively nested model domains, having a finest horizontal mesh size of 750 m. The model topography is composed of a wide plateau-like elongated ridge with a height of 1000 m, and four small-scale mountains located on the upper windward slope of the basic ridge with an excess height of 400 m, 800 m, 1200 m and 1600 m, respectively (see Fig. 1a). The purpose of the basic ridge is to generate large-scale atmospheric lifting and thereby widespread moderate precipitation, providing the basis for seeder-feeder-induced enhancement over the small-scale mountains. The atmospheric conditions assumed in the simulations involve a ridge-normal flow with positive shear from 12.5 m s^{-1} at sea level to 25 m s^{-1} at tropopause level, and constant wind speed higher above, and a nearly saturated moisture field up to a pressure of 400 hPa. Seven different temperature profiles are considered with freezing levels ranging from 2800 m (T1) to 400 m (T7) at nearly equal steps, each having a lower-tropospheric moist Brunt-Väisälä-frequency of about 5×10^{-3} s^{-1}. The simulations use a PBL parameterization to account for surface friction and a sophisticated mixed-phase microphysics scheme including graupel (Tao and Simpson, 1993). For further details see Zängl (2008).

3 RESULTS

Simulated precipitation amounts are displayed in Fig. 1b,c along cross-sections through the 800-m and 1600-m mountains (lines AA' and BB' in Fig. 1a). They refer to an accumulation period of 6 hours, starting at a simulation time of 9 h. Inspecting the results for the different temperature profiles, one notices that the warmest (T1) and the two coldest (T6, T7) profiles produce a single precipitation maximum near the mountain top (dashed line). However, substantially different precipitation patterns are found for the intermediate temperature profiles: For the

800-m mountain (Fig. 1b), T2 still has a single maximum near the peak but a slower precipitation decay in the lee than T1. Continuing this trend, T3 exhibits a secondary maximum over the lower lee slope ($x \approx 5$ km), turning into the primary maximum for T4. With further decreasing temperatures (T5), the leeside precipitation maximum starts to shift back to the mountain peak. A qualitatively similar behaviour is found for the 1600-m mountain (Fig. 1c), but the pattern sequence is shifted towards higher temperatures. Now, the T2 run already features a marked secondary precipitation maximum over the lee slope, turning into the primary one for T3. The T4 run now shows a single maximum over the lee slope as the T5 run did for the lower mountain, whereas for the T5 run, the precipitation maximum has almost retreated to the mountain top. Obviously, these model results are consistent with the above-mentioned temperature-dependence of observed precipitation enhancement in the immediate lee of small-scale mountains.

Further inspection of the results suggested that a complex interaction between cloud microphysics and hydrometeor transport is responsible for the apparent temperature-dependence of the precipitation patterns. The first factor arises from the fact that the accretion efficiency of snow and graupel is higher than that of rain because of their slower fall speed and larger surface area. Thus, hydrometeor growth attains a maximum right above the freezing level when the freezing level intersects the mountain or lies close to the mountain top (otherwise, the vertical decrease of lifting compensates for this effect). This favours a leeside precipitation maximum when the freezing level is close to the mountain peak height. The second factor is related to the fall-speed difference between snow/graupel and rain. In case of strong winds following the topography and the freezing level crossing the topography, this fall-speed difference induces a local minimum (maximum) of the surface precipitation rate on the windward (lee) side above (below) the freezing level due to a local divergence (convergence) of hydrometeor trajectories. For a freezing level close to the mountain peak height, this again favours a precipitation maximum over the lee slope.

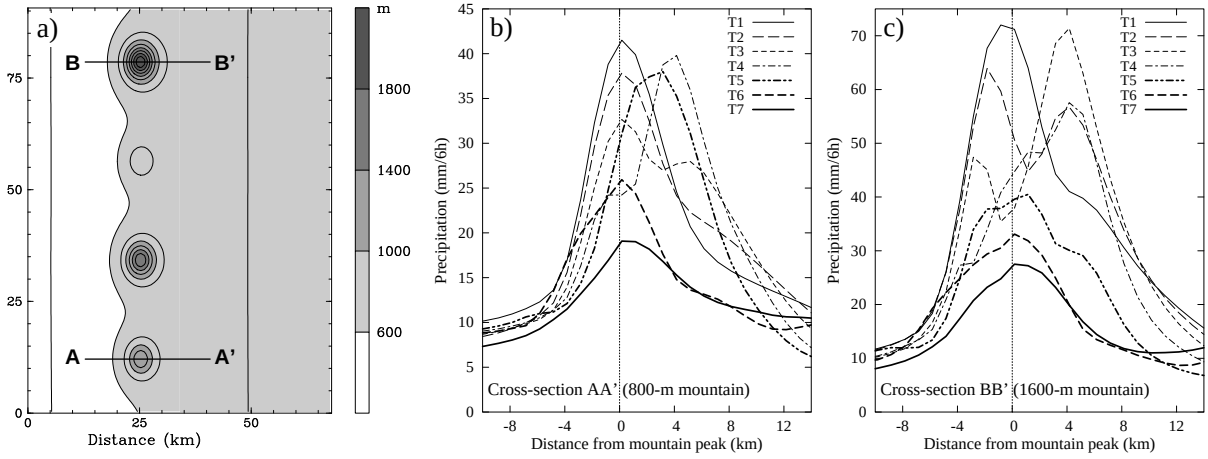

Figure 1: (a) Topography of the finest model domain, contour interval 200 m with additional shading increments every 400 m. Bold lines denote the cross-sections shown in (b,c). (b,c) Accumulated precipitation (mm/6h; accumulation period 9h–15h) for the 800-m and 1600-m mountains, respectively. See text for further explanation.

4 CONCLUSIONS

Based on these results, it can be concluded that the idealized simulations presented here qualitatively reproduce the observed phenomenon and provide plausible hypotheses about the underlying physical mechanisms

REFERENCES

Carruthers, D. J., and T. W. Choularton, 1983: A model of the feeder-seeder mechanism of orographic rain including stratification and wind-drift effects. *Quart. J. Roy. Met. Soc.*, **109,** 575–588.

Tao, W-K, and J. Simpson, 1993: Goddard cumulus ensemble model. Part I: Model description. *Terr., Atm. Ocean. Sci.*, **4,** 35–72.

Zängl, G., 2008: The temperature dependence of small-scale orographic precipitation enhancement. *Quart. J. Roy. Met. Soc.*, **134**, 1167–1181.

Zängl, G., D. Aulehner, C. Wastl, and A. Pfeiffer, 2008: Small-scale precipitation variability in the Alps: Climatology in comparison with semi-idealized numerical simulations. *Quart. J. Roy. Met. Soc.*, **134**, 1865–1880.

DRIVING PROCESSES FOR DEEP CONVECTION OVER CONPLEX TERRAIN: COPS OBSERVATIONS AND RESPECTIVE COSMO SIMULATIONS

Ulrich Corsmeier[1], Christian Barthlott[1], Norbert Kalthoff[1], Heike Konow[1], Christoph Kottmeier[1], Volker Wulfmeyer[2], Andreas Behrendt[2], and the COPS Team

[1] Institute for Meteorology and Climate Research, Karlsruhe Institute of Technology, Karlsruhe, Germany
E-mail: *ulrich.corsmeier@imk.fzk.de*
[2] Institute of Physics and Meteorology, University of Hohenheim, Stuttgart, Germany

Abstract: Data of COPS IOP 9c measured at July 20, 2007 were used to analyse the interaction of convection initiating processes of different scales. A weak cold front passing the COPS area in the morning from west to east was further weakened over the Rhine valley and partly strengthened by a gust front resulting from a MCS behind the front. Further convection initiation appears from a thermally driven convergence zone east of the Black Forest and valley and slope winds over the low mountain range. This leads to a series of severe convective systems in front of the former cold front. Model simulations with COSMO-DE show a not sufficient representation of the sub synoptic scale convection driving processes. Although moisture convergence and CAPE are simulated roughly at the right location, they are not strong enough to initiate deep convection und subsequent precipitation.

Keywords: *COPS, convection initiation, observation, modelling, scale interaction, moisture convergence, ICAM*

1 INTRODUCTION

The "Convective and Orographically induced Precipitation Study" (COPS), aims on the forecast improvement of convectively driven precipitation by mesoscale models. COPS was mainly funded by the DFG and took place from June to August 2007 in southwestern Germany and eastern France over the low mountain ranges of the Black Forest and the Vosges mountains.

2 MEASUREMENTS

During IOP 9c a mesoscale convective system (MCS), visible by a distinct surface low over eastern France, propagated north-eastward and a gust front of the MCS reached the COPS region in the morning. During the passage of the gust front from west to east through the Rhine valley, the convective weather activity was significantly reduced. When the air reached the western slope of the Black Forest, the air has been lifted to propagate over the mountain range. More to the east the sky was still free of clouds and radiation led to a high air temperature of up to 30 °C, to the formation of local slope and valley circulations, and on larger scale to the development of a north – south orientated convergence line over the northern Black Forest. The interaction of local scale orographic winds, the regional scale gust front, the mesoscale convergence line and the cold front led to organized deep convection over the eastern Black Forest and the Swabian Jura.

The transformation of stable air masses passing the Rhine Valley into air masses of high instability when passing the Black Forest is studied by analysis of airborne measurements and data of ground based in situ and remote sensing instruments. Upper tropospheric forcing and ground based lifting processes are discussed with special emphasis of the high spatial and temporal variability of the atmospheric stability and the humidity within the boundary layer.

3 COSMO-DE MODELLING

Model simulations of COSMO-DE without convection parameterisation are compared with the measurements. It is shown that larger scale features with horizontal scales far above the model resolution of 2.8 km like the cold front of the MCS and partly the convergence line with the resulting moisture convergence and CAPE over the Black Forest are reasonably represented in the model. The amplification of the convergent flow especially over the northern Black Forest by small scale forces (gust front and orographic winds) are suboptimal resolved in COSMO-DE. This results in missing deep convection and subsequent precipitation along the convergence line in the model and leads to insufficient precipitation forecast.

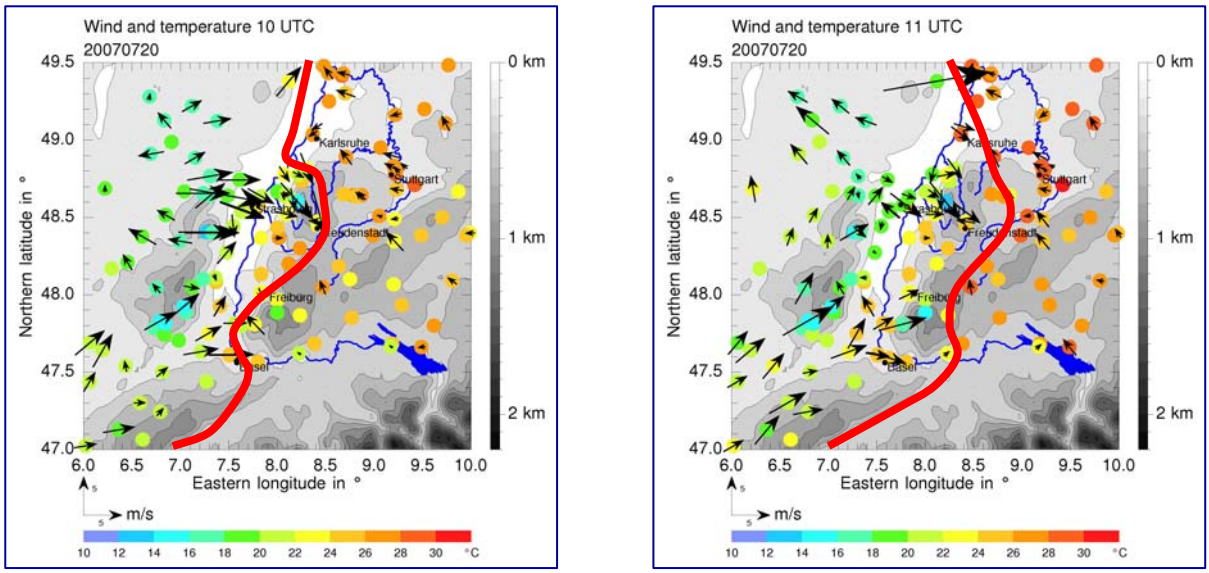

Fig. 1: A gust front is reaching the northern Black Forest. There are still easterly winds in the East. The temperature gradient is increasing (14 K). There is high cloud coverage in the West (10 UTC, left). A convergence line is developing east of Black Forest. Wind increases up to 6 ms^{-1} from opposite directions. The gust front is locally enhanced by orography. The temperature gradient is increasing. Convection is initiated (11UTC, right).

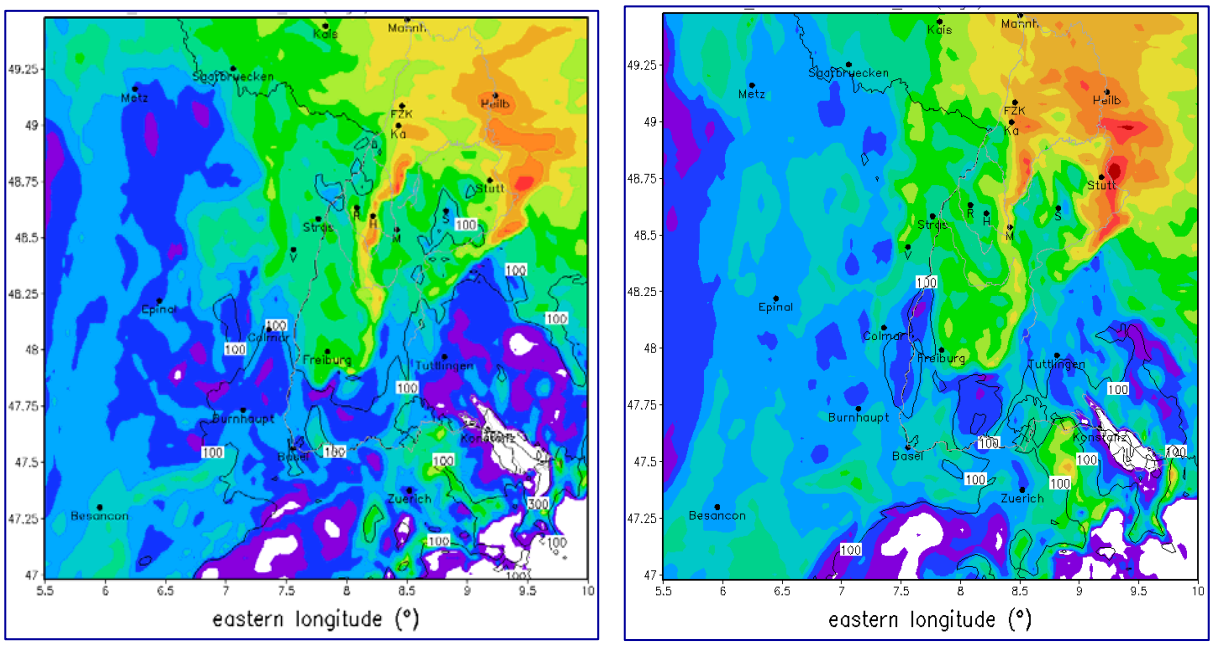

Fig. 2: Simulated CAPE increasing along simulated moisture convergence and observed gust front (~2500 J kg-1). CI is detected by radar along the high CAPE line (10 UTC, left). Weak convergence causes CAPE line moving east and CAPE maximum near Stuttgart moving west and increasing. CI observed in reality but not in the model (11 UTC, right).

REFERENCES

Kalthoff, N., B. Adler, Ch. Barthlott, U. Corsmeier, S. Mobbs, S. Crewell, K. Träumner, Ch. Kottmeier, A. Wieser, V. Smith, P. Di Girolamo, 2009: The impact of convergence zones on the initiation of deep convection: A case study from COPS, Atmos. Research, in press.

Kottmeier, Ch., N. Kalthoff, U. Corsmeier, Ch. Barthlott, J. Van Baelen, A., Behrendt, R. Behrendt, A. Blyth, R. Coulter, S. Crewell, M. Dorninger, C., Flamant, Th. Foken, M. Hagen, C. Hauck, H. Höller, H. Konow, M. Kunz, H., Mahlke, S. Mobbs, E. Richard, R. Steinacker, T. Weckwerth, A. Wieser, and V. Wulfmeyer, 2008: Mechanismus initiating deep convection over complex terrain during COPS, Meteorol. Z., **17** (6), 931-948, DOI 10.1127/0941-2948/2008/0348.

Wulfmeyer, V., Behrendt, A., Kottmeier, Ch., Corsmeier, U., et. al., 2008: The Convective and Orographically-induced Precipitation Study: A Research and Development Project of the World Weather Research Program for Improving Quantitative Precipitation Forecasting in Low-mountain Regions Bull. Amer. Meteor. Soc., **89** (10), 1477-1486.

FORECASTING SUMMER CONVECTION OVER THE BLACK FOREST: A CASE STUDY FROM THE COPS EXPERIMENT

Evelyne Richard[1], Jean-Pierre Chaboureau[1], Cyrille Flamant[2], Cédric Champollion[3]

[1] Laboratoire d'Aérologie, CNRS and Université Paul Sabatier, Toulouse, France
E-mail: *Evelyne.Richard@aero.obs-mip.fr*

[2] LATMOS, CNRS and Université Pierre et Marie Curie, Paris, France
[3] Géosciences Montpellier, France

Abstract: On 15 July 2007, in a very warm but also very dry environment, an isolated short-lived deep convective storm developed over the Black Forest in the late afternoon. Very few of the high-resolution models involved in COPS were able to capture this event. Based on various Meso-NH simulations, the conditions leading to the development of the storm have been investigated and carefully checked against a variety of observations. Although the modelled storm tends to appear a few kilometres south of the observed one, it is clear that the triggering and propagation of the storm are strongly controlled by the presence of a low-level convergence line, roughly north-south oriented, located along the crest line of the Black Forest massif and propagating eastwards.

Keywords: *ICAM, convection, mountainous area, COPS*

1 INTRODUCTION

On 15 July 2007, the COPS area is located in the transition zone between an eastern European ridge, stretching from the Mediterranean Sea to Poland and a high amplitude eastern Atlantic trough. The associated large scale forcing is very weak (Kottmeier et al. 2008). The different soundings performed in the COPS area exhibit only moderate values of Convective Available Potential Energy (CAPE) and relatively high values of Convective Inhibition (CIN, Adler et al. 2009). Under such conditions, convection triggering is unlikely. However a line of deep convective clouds reaching 12 km develop over the southern Black-Forest during the early afternoon.

2 MODEL RESULTS

The numerical simulations are performed with the French non-hydrostatic mesoscale model Meso-NH. During the COPS field experiment the model is run on three interactive 2-way nested domains with horizontal mesh sizes of 32, 8, and 2 km. The convection scheme is activated for the coarser grids while convection is assumed to be explicitly resolved for the 2-km grid. The bulk explicit microphysical scheme accounts for seven water species (vapor, cloud water, liquid water, pristine ice, snow, graupel, and hail). The initial conditions are obtained from the ECMWF analysis of 15 July 00:00 UTC and the boundary conditions for the outermost domain are interpolated in time from the 6-hourly ECMWF forecasts.

Model results are first assessed in terms of satellite and radar pseudo-observations. The brightness temperature as measured in the METEOSAT 10.8 μm channel is compared with the brightness temperature as reconstructed from the model fields. The time evolution of the 280 K contour, representative of mid- to high-level clouds, is used to monitor the convective activity. Model results are in good agreement with observations: convection starts to develop around 13:00 UTC and only lasts for a couple of hours. The triggering occurs on the eastern slope of the North tip of the southern Black Forest (48N, 8.35E) and the storm propagates towards the north-east. The main departure from the observations is a slower propagation and thus a shorter trajectory of the storm. However this effect might also be artificially amplified due to the parallax error of the satellite observations.

A similar comparison is performed using the time evolution of the 1dBZ reflectivity contour measured by the Montancy radar every 15 minutes during its 1° elevation scan. At the location of the storm, this elevation roughly corresponds to 1000m ASL. The agreement between the observations and the simulation is remarkable. Initiation time, duration, and trajectory of storm are quite well captured by the model. Taking into account the weak likelihood for convective development on this particular day as well as the great difficulty of accurately predicting isolated storms, the Meso-NH forecast can be considered as very successful but the question is whether it was obtained for the good reasons?

3 TRIGGERING PARAMETERS

In the absence of large scale forcing, the triggering of convection essentially depends on three parameters: the moisture supply in the low levels of the atmosphere, the potential instability of the air-mass and a vertical ascending motion resulting from either orographic lifting or diurnal thermal heating of the ground.

At 14 UTC, the CIN is very weak in the mountainous areas but only the Black Forest region exhibits significant amounts of CAPE. Two spots with CAPE exceeding 3000 J/kg are present in the model domain: one over the western slope of the southern Black Forest (corresponding to the steepest orography of the domain) and a second one, less intense but spatially wider, over the area where the convection is triggered. According to the model, high CAPE appears to be necessary but not sufficient. The comparison with the observed soundings does not show any inconsistency but unfortunately no soundings are located sufficiently close to the area of interest.

A real achievement of the COPS experiment is the fairly exhaustive documentation of the water vapor field which was sampled by several in situ and remote, ground based and airborne instruments. Model results were carefully checked against this very dense and unique data set. The main conclusions are i) the model results tend to have a moist bias in the layer 1km-3km – this bias is quite moderate in the morning but reaches 2g/kg in the afternoon, and ii) the model results depict very well the spatial variability of the moisture field including the observed accumulation of moisture above and in the lee of the two massifs.

This accumulation directly results from the presence of convergence lines generated in response to the diurnal heating and located along the crest lines of the two massifs. Patchy in the morning, these lines becomes more organized in the afternoon especially over the Black Forest (see Fig.1). Furthermore, at the northern tip of the southern Black Forest, the vertical motion is significantly reinforced by the lee-side convergence. The Doppler velocity observations from the Feldberg radar support the model results regarding the occurrence and location of such convergence. This mechanism plays a crucial role in the triggering of the convection.

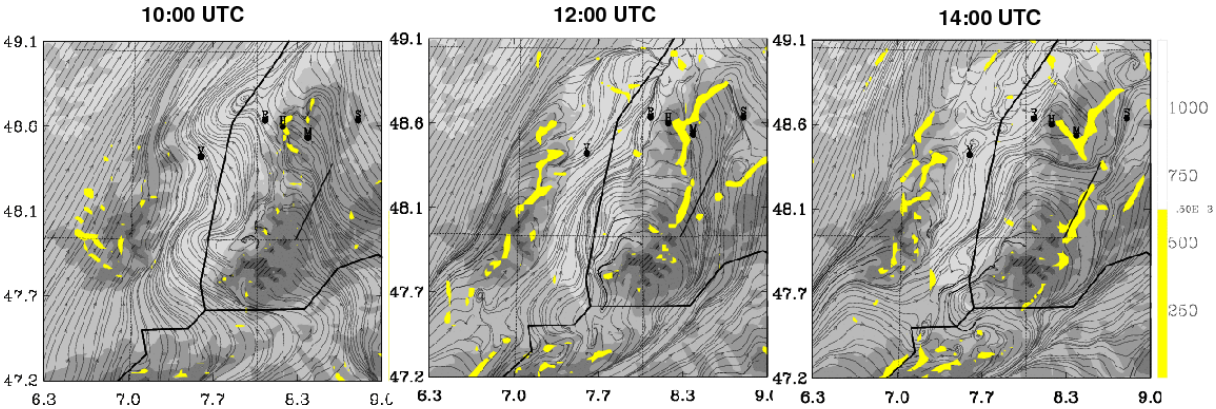

Figure 1: Streamlines and convergence in excess of 0.5 10^{-3} s^{-1} at 1000 m ASL. The thick black line indicates the trajectory of the storm.

4 CONCLUSIONS

The Meso-NH forecast of July 15 storm appears fairly realistic. The initiation time, duration, and trajectory of the storm are quite well captured. According to the model, convection is mainly triggered by the convergence which developed in the lee of the southern Black Forest. Despite these good results, the positive bias found in the humidity fields has to be further investigated. The envisaged model intercomparison exercise on this case will help to clarify this issue and to understand why others models (see for instance Barthlott et al., 2009) were not as successful.

REFERENCES

Adler, B., et al.., 2009: The impact of convergence zones on the initiation of deep convection: A case study from the COPS campaign. Atmos. Res., submitted.

Barthlott, Ch., Schipper, J.W., Kalthoff, N., Adler, B. and Kottmeier, Ch., 2009 : Model representation of boundary-layer convergence triggering deep convection over complex terrain: A case study from COPS, Atmos. Res., submitted.

Kottmeier, C. et al., 2008: Mechanisms initiating convection during the COPS experiment. Meteor. Z., 17, 931-948.

COSMO MODEL SIMULATION OF CONVERGENCE ZONES IN COMPLEX TERRAIN: A CASE STUDY FROM COPS

Christian Barthlott, Janus Willem Schipper, Norbert Kalthoff, Bianca Adler, Christoph Kottmeier

Institute for Meteorology and Climate Research, Karlsruhe Institute of Technology (KIT), Karlsruhe, Germany
E-mail: *christian.barthlott@imk.fzk.de*

Abstract: An isolated thunderstorm from the Convective and Orographically-induced Precipitation Study in southwest Germany and east France in 2007 is analysed. On July 15, deep convection developed east of the Black Forest crest, although convective available potential energy (CAPE) was only moderate and convective inhibition (CIN) was high. Data analysis revealed that convection was triggered by updrafts penetrating the capping inversion of the planetary boundary layer as a result of low-level convergence. Although the numerical weather prediction model COSMO-DE of the German Weather Service (2.8 km grid resolution) simulated a convergence line and the evolution of a line of low clouds in good agreement with radar and satellite observations, no precipitating deep convection developed from this line of clouds. For an improved representation of orographic effects, simulations with a finer grid resolution of 1 km were performed. Despite almost optimal conditions, i. e. moderate amount of CAPE and almost vanishing CIN, the updrafts required to overcome CIN were not reached in both model configurations. Although both simulations did not initiate deep convection, the results suggest that in an air mass convection situation without mid-tropospheric forcing, the simulated location and timing of convergence lines with coexistent large values of CAPE and low values of CIN can be used as diagnostic parameters for deep convection nowcasting.
Keywords: *Moist convection, Convergence zones, COSMO model, Black Forest*

1 INTRODUCTION

Quantitative Precipitation Forecasting (QPF) still is a challenge for state-of-the-art numerical weather prediction (NWP) models. The existing QPF deficiencies are determined mainly by the model's capacity to forecast the initiation of convection at the right location and time. The international field campaign COPS (Convective and Orographically-induced Precipitation Study) took place in southwest Germany and east France in summer 2007 with the overall goal to advance the quality of forecasts of orographically-induced convective precipitation by four-dimensional observations and modeling of its life cycle (Wulfmeyer et al., 2008).

During the intensive observation period (IOP) 8b on July 15, a single convective cell developed east of the Black Forest crest (Fig. 1), although convective available potential energy (CAPE) was only moderate and convective inhibition (CIN) was high. The break-out of deep convection and subsequent precipitation had not been predicted by the convection-resolving model COSMO-DE used by the German Weather Service (DWD) for operational forecasting. Data analysis by Kottmeier et al. (2008) and Kalthoff et al. (2009) revealed that convection was triggered by low-level convergence zones. As a result of the convergent flow, strong updrafts were observed above the mountains which penetrated the PBL-capping inversion and reached the level of free convection (LFC).

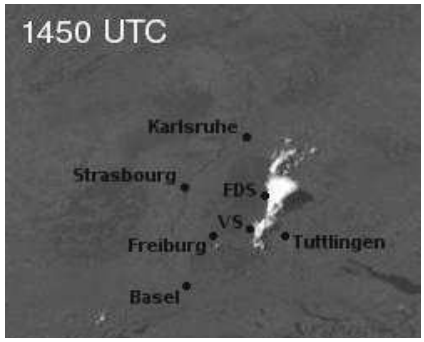

Figure 1: MSG visible image on 15 July 2007.

2 NUMERICAL SIMULATIONS

The non-hydrostatic limited-area atmospheric prediction model COSMO-DE (version 4.0) of the German Weather Service was used for simulations with 2.8 and 1 km horizontal grid resolution (hereinafter referred to as COSMO_2.8 and COSMO_1, respectively). Initial and hourly boundary data come from the COSMO-EU forecast, initial time was 0000 UTC.

COSMO_2.8 succeeds well in reproducing the observed mesoscale convergence line, i. e. its location and timing and the subsequent formation of shallow clouds (Fig. 2). The absence of deep convection in the model despite almost optimal conditions (CAPE $> 2000\ \mathrm{J\,kg^{-1}}$, CIN $< 5\ \mathrm{J\,kg^{-1}}$) may possibly be explained by the vertical extent of the updrafts caused by low-level convergence. In the COSMO_2.8 simulations (Fig. 3, left), the convergence zone extends up to 1400 m amsl with maximum vertical wind speeds of $0.07\ \mathrm{m\,s^{-1}}$. It is obvious that the rising air does not reach the LFC which has a height of around 3100 m amsl. The results with COSMO_1, (Fig. 3, right) show a thinner convergence zone, whereas its vertical extent at the position of maximum convergence is comparable to that of the COSMO_2.8 simulation. Horizontal convergence itself is higher by a factor of 5, thus inducing maximum vertical wind speeds of $0.6\ \mathrm{m\,s^{-1}}$. Despite the higher vertical wind speeds, the rising air reaches a level of 2200 m amsl only, which equals the level in the COSMO_2.8 simulation. As a consequence, CAPE cannot be released, since the LFC is not reached by ascending parcels.

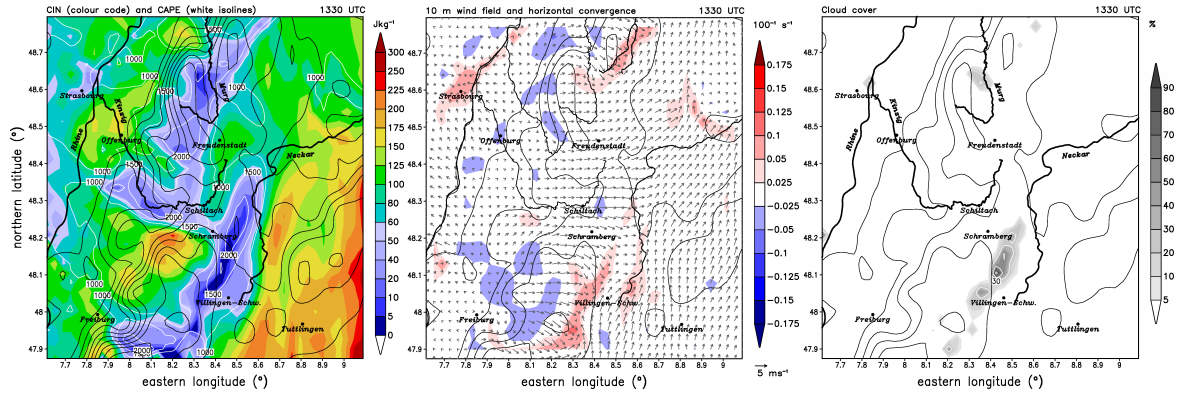

Figure 2: CIN and CAPE (left), 10 m horizontal wind field and convergence (middle), and cloud cover (right) at 1330 UTC as simulated by COSMO_2.8. Black isolines indicate model topography.

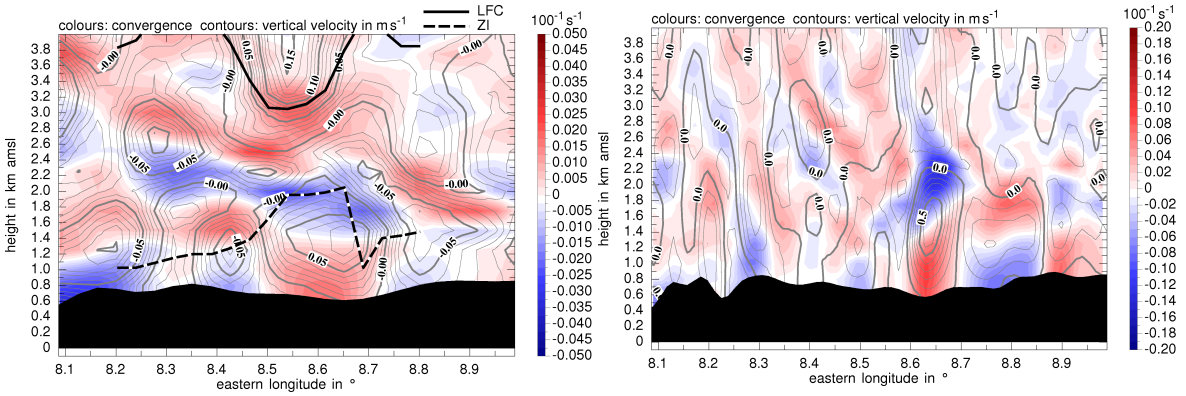

Figure 3: Vertical cross-section of horizontal convergence and vertical wind speed at 1400 UTC along the northern latitude of 48.19° N simulated with COSMO_2.8 (left) and COSMO_1 (right).

3 CONCLUSIONS

COSMO_2.8 succeeds well in reproducing the location and timing of the observed mesoscale convergence line and the subsequent formation of shallow clouds but generates no deep convection. Although the increase of horizontal grid resolution from 2.8 to 1 km increases the strength of the convergence zone and the vertical wind speeds, the vertical extent of the updrafts remains the same and the capping inversion inhibits the breakout of deep convection in the simulation. In comparison to the measured vertical wind speeds, the simulated ones are considerably smaller and, hence, considered to be decisive for the missing initiation of deep convection.

Besides an accurate specification of the thermodynamic and kinematic fields, the results highlight the role of boundary layer convergence features for QPF. It is hypothesized that the lifting depth of a convergence line must be simulated well enough to correctly account for its triggering effect on deep moist convection. Although both simulations did not initiate deep convection, the results suggest that in an air mass convection situation without mid-tropospheric forcing, the simulated location and timing of convergence lines with coexistent large values of CAPE and low values of CIN can be used as diagnostic parameters for deep convection nowcasting.

REFERENCES

Kalthoff, N., B. Adler, C. Barthlott, U. Corsmeier, S. Mobbs, S. Crewell, K. Träumner, C. Kottmeier, A. Wieser, and V. Smith, 2009: The impact of convergence zones on the initiation of deep convection: A case study from COPS. *Atmos. Res.*, doi:10.1016/j.atmosres.2009.02.010.

Kottmeier, C., N. Kalthoff, C. Barthlott, U. Corsmeier, J. Van Baelen, A. Behrendt, R. Behrendt, A. Blyth, R. Coulter, S. Crewell, P. D. Girolamo, M. Dorninger, C. Flamant, T. Foken, M. Hagen, C. Hauck, H. Höller, H. Konow, M. Kunz, H. Mahlke, S. Mobbs, E. Richard, R. Steinacker, T. Weckwerth, A. Wieser, and V. Wulfmeyer, 2008: Mechanisms initiating deep convection over complex terrain during COPS. *Meteorol. Z.*, **17**, 931–948.

Wulfmeyer et al., 2008: The Convective and Orographically-induced Precipitation Study: A Research and Development Project of the World Weather Research Program for improving quantitative precipitation forecasting in low-mountain regions. *Bull. Amer. Meteor. Soc.*, **89**, 1477–1486, doi:10.1175/2008BAMS2367.1.

INFLUENCE OF THE WIND PROFILE ON THE LOCATION OF HOTSPOTS OF CONVECTION IN MOUNTAINOUS TERRAIN

Martin Hagen[1], Joël Van Baelen [2], Evelyne Richard [3]

[1] Deutsches Zentrum für Luft- und Raumfahrt (DLR), Oberpfaffenhofen, Germany
E-mail: *martin.hagen@dlr.de*
[2] Université de Clermont-Ferrand, France
[3] Observatoire Midi-Pyrénées, Toulouse, France

Abstract: Radar observation of the initiation and life cycle of small convective cells during the COPS field campaign in south-western Germany and eastern France show a dependence on the prevailing wind profile. Several hotspots for convective initiation were identified. Orographic features favour convergent flow. On the days when weak winds were prevailing cells developed over the crest line, whereas on days when strong westerly wind were observed the initiation of convection took place in the lee of the mountains within convergent flow.

Keywords: *convection, mountainous area, radar observations*

1 INTRODUCTION

COPS (Convective and Orographically-induced Precipitation Study, Wulfmeyer et al., 2008) was an international field campaign that took place in the Upper Rhine Valley, the Black Forest and the Vosges Mountains during summer 2007. The aim of COPS was to study the orographic influence on the initiation and life cycle of convection, mainly by investigating the humidity structure. Observations with advanced instruments should help to improve the forecast skill of mesoscale numerical models, especially precipitation forecasts. Among the large number of observed convective systems we will concentrate on the observations of isolated small convective rain showers which developed in the Vosges Mountains on two consecutive days. While on one day the cells were initiated at the crest line of the mountain range, on the second day the cells developed on the lee side of the Vosges Mountains in the Rhine Valley.

2 THE COPS FIELD CAMPAIGN

For the COPS field campaign the polarimetric C-band Doppler radar POLDIRAD was deployed for 3 month in the foothills of the Vosges Mountains about 20 north-west of Strasbourg (Fig. 1) and about 100 m above the floor of the Rhine Valley. Volume scans were performed up to 120 km range every 10 minutes. A large set of instruments were set up at the super sites Aachern, Hornisgrinde, Deckenpfronn, and Bischenberg/ Meistratzheim. Additionally the ARM mobile facility was installed in the Murg Valley. At the French super site Bischenberg a high resolution (temporal 30 sec., radial 60 m) scanning X-band radar was installed. The maximum range was 20 km.

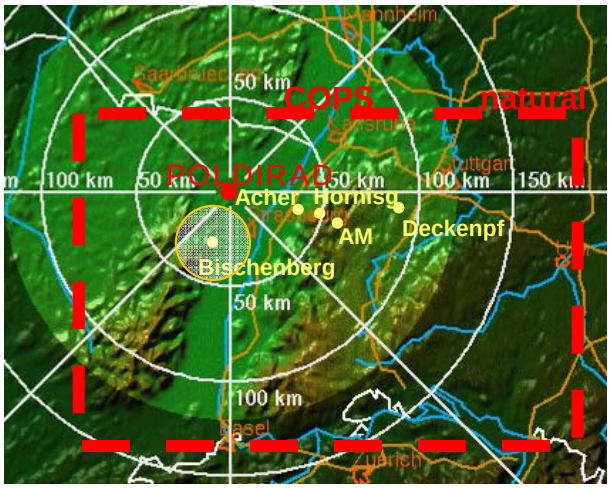

Fig. 1 The COPS region in South-Western Germany and North-Eastern France. Range rings are from POLDIRAD, yellow dots show locations of super sites. The highlighted circle around Bischenberg indicates the 20 km range of the X-band radar.

In addition to the observations several meso-scale numerical models were used to provide forecasts for the field campaign and to perform studies with different microphysics schemes. For the present study we used the simulations with the French MesoNH model.

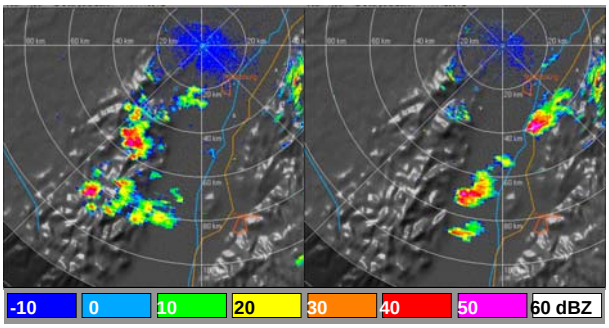

Fig. 2 PPI of reflectivity on 12 Aug. 2007 1440 UTC (left) and 13 Aug. 2007 1120 UTC (right).

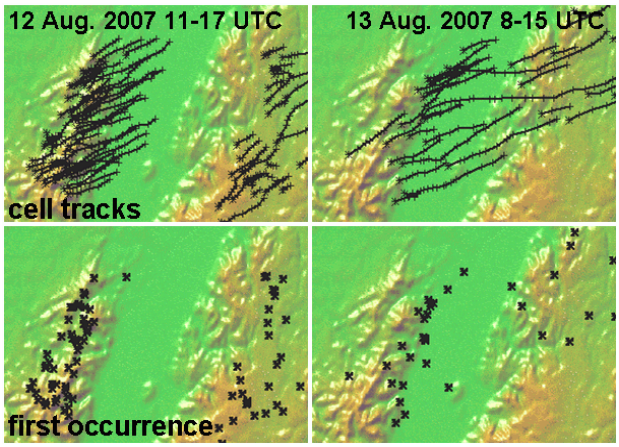

Fig. 3 Tracks of cells (top row) and location of first occurrence (bottom row) for 12 August and 13 August 2007.

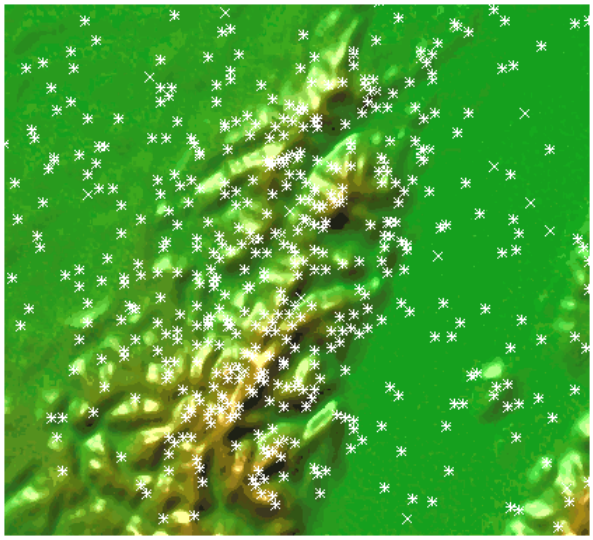

Fig. 4 Location of first occurrence of convective cells observed by POLDIRAD over the Vosges Mountains on 15 days during COPS.

3 OBSERVATIONS OF ISOLATED CELLS

In addition to stratification and the moisture field, topographic features have a strong influence on the initiation and development of convection. Mountains provide elevated heat surfaces which can destabilize the stratification in the boundary layer. Also, mountains can initiate flow convergence along the crest line providing a source for convection initiation. On a larger scale mountains can distort the flow generating convergence in relation the orography. During COPS on several days only small isolated shower or thunderstorm cells developed in the COPS region. A distinct situation was observed on August 12 and 13, 2007. On both days isolated cells developed in relation to the Vosges Mountains. Fig. 2 shows two sample PPI images of reflectivity for the two days. On 12 August cells developed over the Vosges and travelled afterwards with the mean south-westerly flow into the Rhine Valley while decaying there. On 13 August the cells developed in the lee of the Vosges, travelling across the Rhine Valley and some of them where enhanced again at the windward slopes of the Black Forest. Fig. 3 shows the cell tracks and location of first radar echo for the two days. In total 80 and 38 cells were tracked on 12 and 13 August, respectively. 51 (22) of them have been initiated in relation to the Vosges Mountains. On both days the life time was in the order of 0.5 to 2 hours, with some cells being active for even a longer time. This was mainly for 13 August.

Simulations with the mesoscale model MesoNH have been able to reproduce the diverse life cycle of the cells. The quite realistic simulations are also of great value to access atmospheric parameters which have not been observed in 3 dimensions, like the moisture structure and the wind field. While on 12 Aug. weak south-westerly winds are prevailing, strong westerly winds are simulated and observed on 13 Aug. The simulated cells correspond to the observed ones, not exactly in time and location, but with similar life time and cell initiation.

Fig. 4 shows the convective initiation over the Vosges Mountains on 15 days in 2007 (June 4+5, 8-12, July 17, Aug. 3, 6, 12, 13, 17, 23, 24). Wind direction and profile were varying and radar observations were available only every 10 minutes. Despite the large variability of the initiation points common features can be identified: (i) initiation tends to be located along mountain ridges; (ii) initiation is concentrated along mountain peaks; (iii) initiation occurs along the edge of ridges towards the Rhine Valley (right side); (iv) there is a gap region between the crest line and the edge towards the Rhine Valley.

4 CONCLUSIONS

Observations with radar during the COPS field campaign in Central Europe of isolated shower cells show a strong dependence on the orography and the prevailing wind field. The simulations with MesoNH were able to reproduce the observations in a quite realistic manner, even reproducing “hot spots” of cell initiation in relation to orography. The X-band radar at Bischenberg allowed for observations with high temporal resolution at one of the north-eastern hot spots. Convergences along ridges favours the initiation of convection.

REFERENCES

Wulfmeyer, V., et al., 2008: The Convective and Orographically-induced Precipitation Study. *Bull. Amer. Meteor. Soc.*, **89**, 1477-1486.

GENERALIZING THE LOCAL MIXING LENGTH-SCALE FOR STABLE ATMOSPHERIC BOUNDARY LAYERS

Branko Grisogono

Dept. of Geophysics, University of Zagreb, Zagreb, Croatia
Email: *bgrisog@gfz.hr*

Abstract: Excessively diffusive and much-too-deep modeled stable ABL flow is remedied by using a new generalized „z-less" mixing length-scale, Λ, including the vertical wind shear, S explicitly. This generalization of Λ is based on a simplified turbulent kinetic energy (*TKE*) eqn. yielding $\Lambda \sim (TKE)^{1/2}/|S|$, almost regardless of other parameterization details. The proportionality depends on known model constants and a function of Ri and turbulent Prandtl number, Pr; Λ approaches Ozmidov scale (determined by the turbulent dissipation and buoyancy frequency) in the limit $Ri >> 1$. Tests with mesoscale MIUU model and a calibrated 1D semi-analytic Prandtl model prove this generalization of Λ correct and useful.

***Keywords**: ICAM, katabatic flow, modeling, parameterization, Prandtl, Richardson number, strongly stratified turbulence*

1 INTRODUCTION

Recent research suggests that the evolution of the stable atmospheric boundary layers (SABL) is poorly understood, especially so over inclined (mountainous) areas. The emphasis is on parameterizing turbulent effects in the SABL. The "classical" SABL is always stratified weakly (i.e. the gradient Richardson number, $Ri << \infty$, usually, $0 < Ri \leq 1$) and modeled reasonably well during past decades; however, the strongly- or very stably-stratified SABL (VSABL, typically $Ri >> 1$) is not understood well. Various problems with current turbulence parameterization schemes become more apparent as the refining model resolution is used over complex terrain (e.g. Gohm et al. 2008, Grisogono and Belušić 2009); these problems include over-diffusion, frictional decoupling, etc. Excessively diffusive, much-too-deep SABL flows, as often modeled numerically, are assessed in the light of a recently proposed alleviation of this problem, using a calibrated Prandtl model (Grisogono and Belušić 2008, later GB08) and extended to other SABL flows. The latter demanded an explicit inclusion of the vertical shear of quasi-horizontal wind, S, in the local, so called „z-less" mixing length. A potential weakness of the mixing length in GB08 was the lack of its smoothness (it used min-max option).

A generalization of this proposal is given via simplified turbulent kinetic energy (*TKE*) eqn. and a set of related parameterizations for the eddy diffusivity and conductivity with respect to "z-less" mixing length, Λ. It will be shown that $\Lambda \sim \Lambda_0 = (TKE)^{1/2}/|S|$, almost regardless of other closure details. The dimensionless factor of proportionality in Λ is a simple function of Ri and turbulent Prandtl number, Pr, derived from a particular parameterization chosen and the model's known details. This new Λ mitigates over-diffusive SABL in models. For example, Λ proposed here may improve forecasting the minimum near-surface temperature and the low-level wind in mountainous areas (e.g. katabatic wind) since the VSABL is now simulated more reliably.

2 GENERALIZED „Z-LESS" MIXING LENGTH-SCALE

Begin with the *TKE* eqn. under the usual simplifications: horizontal homogeneity, the x-axis mean flow alignment, Boussinesq and the absence of mean vertical motions; thus:

$$\frac{\partial (TKE)}{\partial t} = -\overline{u'w'}\frac{\partial \bar{u}}{\partial z} + \frac{g}{\theta}\overline{w'\theta'} - \frac{\partial}{\partial z}\left[\overline{w'\left(\frac{p'}{\rho_0} + TKE\right)}\right] - \varepsilon \qquad (1)$$

where the terms have their very typical meaning. The change of *TKE* is balanced by the shear production, buoyant destruction (in the SABL), transport due to pressure- and turbulence-correlations and dissipation, respectively. Assuming steadiness, and neglecting transport terms, we parameterize the momentum and heat fluxes in (1) as $K_m\$$, $K_h\$$, where K_m, K_h are eddy diffusivity and conductivity and $\$ \equiv |S|$. Also in (1) we use $\varepsilon = b(TKE)^{3/2}/\Lambda$, where b is a model constant and Λ is a new mixing length. Hence, (1) yields:

$$0 = K_m \$^2 - K_h N^2 - \frac{b}{\Lambda}(TKE)^{3/2}. \qquad (2)$$

This gives a simple eqn. for Λ. A 1st order closure assumes $K_m = a_1\Lambda^2\$$, $K_h = a_1\Lambda^2\$/Pr$, a_1 is a model constant; moreover, typically $Pr \geq 1$ and $Pr > Ri$ in the SABL (e.g. Zilitinkevich et al. 2008). An advanced parameterization, i.e. a higher-order closure, may take a form $K_m = a_2\Lambda(TKE)^{1/2}$, $K_h = a_2\Lambda(TKE)^{1/2}/Pr$. When either closure type is plugged in (2), expanding it in $Ri/Pr << 1$, the corresponding Λ ensues, Table 1.

K_m	$\Lambda(\Lambda_0)$	$\Lambda(\Lambda_N)$
$a_1\Lambda^2\|S\|$	$\Lambda_0(b/a_1)^{1/3}[1+Ri/(3Pr)]$	$\Lambda_N\,(b/a_1)^{1/3}\,Ri^{1/2}[1+Ri/(3Pr)]$
$a_2\Lambda(TKE)^{1/2}$	$\Lambda_0(b/a_2)^{1/2}[1+Ri/(2Pr)]$	$\Lambda_N(b/a_2)^{1/2}Ri^{1/2}[1+Ri/(2Pr)]$
$a_3(TKE)/N$	$\Lambda_0(b/a_3)Ri^{1/2}[1+Ri/Pr]$	$\Lambda_N(b/a_3)Ri[1+Ri/Pr]$

Table 1. Generalized mixing length, Λ. For three typical types of eddy diffusivity, K_m, $K_h = K_m/Pr$, Λ is derived in terms of either Λ_0 or Λ_N, (Ozmidov length) including explicity shear or buoyancy frequency, i.e. $\Lambda_0=(TKE)^{1/2}/|S|$ or $\Lambda_N=(TKE)^{1/2}/N$. Richardson gradient and turbulent Prandtl numbers are Ri and Pr; $0 < a_i < 1$, $0 < b < 0.1$ are constants ($Pr >> Ri$).

Next, the MIUU model is used, as in GB08, where the same run as here was compared to Prandtl model. The default run with only Λ_N produces an over-diffusive and too deep SABL, Fig. 1, upper panels; the middle panels show the correct SABL, i.e. VSABL, corresponding to Prandtl model; the lower panels show the new result with generalized Λ, which is almost the same as in the middle panel (from GB08). This gives credit to our new Λ.

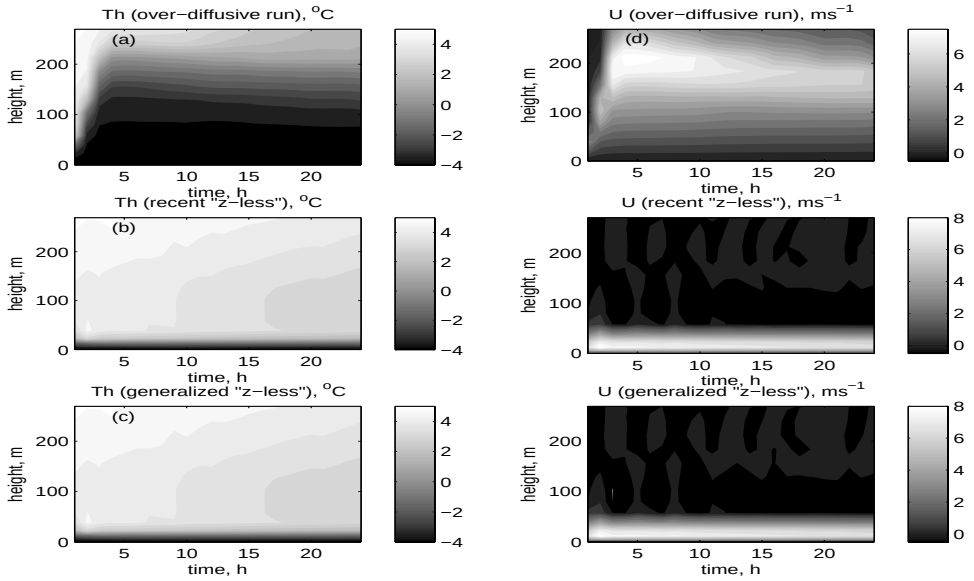

Figure 1. Left (a,b,c): potential temperature Th and right (d,e,f): downslope wind component U vs. time and height simulated using MIUU model. Upper two panels (a,d) show an over-diffusive SABL; middle: recent (b,e), correct results concuring to Prandtl model (GB08); lowest (c,f) use Λ_2 from Table 1; note that (c,f) are almost the same as (b,d), giving approval to the derivation of the generalized "z-less" mixing length Λ. The simulated flow assumes a constant slope -2.2°, windless background atmosphere, $\Delta\theta/\Delta z$ = 5K/km, and the surface potential temperature deficit 6.5 K, the low-level jet is at ~ 20 m.

3 CONCLUSION

A thin and „sharp" VSABL flow is obtained using the generalized mixing length, Λ, Table 1 and Fig. 1, giving the same result as recently recommended by GB08, where the low-level jet is imbedded in a sharp near-surface inversion. The strength of this approach is that Λ is not given but derived from the simplified *TKE* eqn.

Acknowledgements:
Danijel Belušić is thanked for his comments. The study is supported by the Croatian Ministry of Science, Education & Sports, project BORA, No. 119-1193086-1311 and by EMEP4HR, No. 175183/S30 provided by the Research Council of Norway.

REFERENCES

Gohm, A., G.J. Mayr, A. Fix and A. Giez, 2008: On the onset of bora and the formation of rotors and jumps near a mountain gap. Quart. J. Roy. Meteorol. Soc. **134**, 21-46.

Grisogono, B., and D. Belušić, 2008: Improving mixing length-scale for stable boundary layers. Quart. J. Roy. Meteorol. Soc. **134**, 2185-2192 (GB08).

Grisogono, B. and D. Belušić, 2009: A review of recent advances in understanding the meso- and micro-scale properties of the severe Bora wind. Tellus **61A**, 1-16.

Zilitinkevich, S.S., T. Elperin, N. Kleeorin, I. Rogachevskii, I. Essau, T. Mauritsen and M. W. Miles, 2008: Turbulence energetics in stably stratified geophysical flows: strong and weak mixing regimes. Quart. J. Roy. Meteorol. Soc. **134**, 793-799.

CHARASTERISTICS OF THE NEAR-SURFACE TURBULENCE DURING A BORA EVENT

Željko Večenaj, Danijel Belušić and Branko Grisogono

Department of Geophysics, Faculty of Science, Zagreb, Croatia
E-mail: *zvecenaj@gfz.hr*

Abstract: Wind velocity at the town of Senj was measured at 13 m above the ground with a 3D ultrasonic anemometer operating at 4 Hz sampling frequency. The severe bora case that occurred on 07 January and lasted to 11 January 2006 is analyzed here. This data set is used for evaluation of the turbulent kinetic energy, *TKE*, and its dissipation rate, ε. Some considerations about defining turbulent perturbations of the bora wind speed are pointed out. The inertial dissipation method for estimation of ε is used. The empirical length scale parameter for this event is estimated with respect to ε and *TKE*.

Keywords: bora wind, inertial dissipation technique, turbulent kinetic energy, dissipation rate, mixing length-scale

1 INTRODUCTION

Bora (locally *bura*) is a downslope windstorm that blows from the northeastern quadrant in the lee of the coastal mountains when the relatively cold northeasterly flow impinges on the Dinaric Alps (e.g. Yoshino, 1976; Grisogono and Belušić, 2009). Belušić and Klaić (2006) analyzed bora case with gusts speed maxima > 60 m s^{-1}. They found that the values of turbulent kinetic energy (*TKE*) can surpass 30 J kg^{-1}.

TKE dissipation rate (ε) describes dissipation of *TKE* by molecular viscosity into the heat. Improvements needed for a more faithful turbulence parameterization in e.g. air-pollution and dispersion calculations during bora events require a more detailed understanding of bora turbulence (e.g. Baklanov and Grisogono, 2007). This is impossible without a more complete knowledge of *TKE* and ε. Piper and Lundquist (2004) evaluated ε related to the cold front. Their results are compared with those derived here with the respect to the mean streamwise velocity component, giving also credibility to this study.

2 DATA AND METHODS

The 3D wind speed measurements were performed in the town of Senj (44.99°N, 14.90°E, 2 m above MSL) at a height of 13 m above the ground with the WindMaster ultrasonic anemometer (Gill Instruments). The anemometer records the data with a sampling frequency f = 4 Hz. The observed bora episode extends from 07 to 11 January 2006 (4 day time series). The coordinate system is rotated in the mean wind direction (55°). Figure 1 depicts the measured 4 day time series of the streamwise velocity component with 1 hr mean superimposed.

We used the inertial dissipation method (IDM) for evaluation of ε (e.g. Večenaj et al., 2007). Using Taylor's hypotheses of frozen turbulence (e.g. Stull, 1988), ε can be evaluated from:

$$\varepsilon = \frac{2\pi}{\overline{U}}\left[\frac{f^{5/3}S_u(f)}{\alpha}\right]^{3/2} \qquad (1)$$

where $\overline{U}$ is a mean streamwise velocity component, $S_u(f)$ is the spectrum and α is the Kolmogorov constant.

Starting from the local one-and-a-half-order closure, ε can be parameterized in numerical models using the mean value of *TKE* (e.g. Mellor and Yamada, 1974):

$$\varepsilon = \frac{TKE^{3/2}}{\Lambda} \qquad (2)$$

where $TKE = \frac{1}{2}\left(\overline{u'^2} + \overline{v'^2} + \overline{w'^2}\right)$ and u', v' and w' are turbulent perturbations of the streamwise, transverse and vertical velocity components, respectively, while bars represent a suitable averaging. The parameter Λ is the empirical length scale that is closely related to the size of dissipating turbulent eddies.

3 RESULTS

The relationship between the standard deviation of the streamwise velocity component (σ_u), and $\overline{U}$ in the surface layer is usually linear (e.g. Stull, 1988), which was shown by Belušić et al. (2006) to be valid for the local bora turbulence. Moving averages with lengths from 1 min to 1 h are subtracted from the entire 4 day bora episode to determine the perturbations. Then a power law of the form (3a) is fitted to the scatter diagrams of σ_u

vs. $\overline{U}$ for different moving averages. Expecting b to be 1, Fig. 2 shows that the closest value for $b \approx 1$ is achieved for the 1 min moving average. Therefore, we use the 1 min moving average for determination of the local turbulence perturbations in this bora episode. From (2) it follows that $\varepsilon \propto TKE^{1.5}$. This relation is tested by fitting the (3b) power law to the ε vs. *TKE* scatter diagram of 1 h mean values for the entire bora episode. This fit gives coefficient d and parameter $\Lambda = (c)^{-1}$ to be 1.3 and 60 m, respectively.

$$\sigma_u = a\left(\overline{U}\right)^b \quad \text{(3a)}; \qquad \varepsilon = c(TKE)^d \quad \text{(3b)}$$

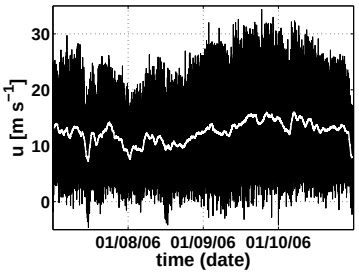

Figure 1. A 4 day raw 4 Hz data time series (07 to 11 January 2006) of the streamwise-wind component measured in Senj, with the 1 h mean superimposed.

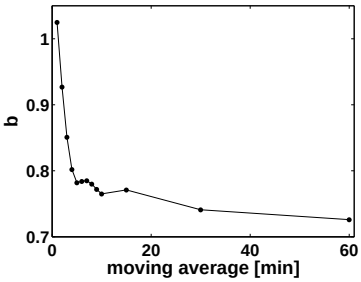

Figure2. The power coefficients b from (3a) for different moving averages subtracted from the entire bora episode.

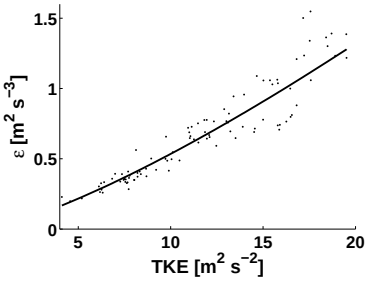

Figure3. Scatter plot ε vs. *TKE* for the entire bora episode. Solid line is the fit with the *a priori* unknown coefficients c and d from (3b).

4 CONCLUSIONS

Our data suggest that the 1 min moving average may be recommended for determination of the local turbulence perturbations for bora. Estimations of ε using IDM agree well with those of Piper and Lundquist (2004) with respect to the mean streamwise velocity component. In this bora episode ε is proportional to $TKE^{1.303}$. This model explains 91 % of ε vs. *TKE* variance. From (3b) it follows that $\Lambda \approx 60$ m.

Many current state-of-the-art models use Blackadar length-scale parameterization which would for this situation give $\Lambda \approx 25$ m. This is derived on the basis of the vertical *TKE* profiles from Belušić and Klaić (2004), using MEMO 6 mesoscale model to simulate several bora events. The same result is obtained using the WRF-ARW model with Mellor-Yamada-Janjic turbulence parameterization scheme. The model-based Λ obviously underestimates Λ derived here from *TKE* and ε values. This may imply the inadequacy of the Blackadar type of parameterizations for the bora related turbulence.

Future work related to the near-surface bora turbulence will include the 4 Hz data analysis of a variety of the bora episodes, categorized by their nature (type), severity (strength) and seasonal period. In this way, a comprehensive picture of the bora related near surface turbulence will be revealed.

Acknowledgements:
This study is supported by the Croatian Ministry of Science, Education & Sports, projects BORA No. 119-1193086-1311 and by EMEP4HR project number 175183/S30 provided by the Research Council of Norway.

REFERENCES

Baklanov, A. and B. Grisogono (Eds), 2007: Atmospheric Boundary Layers: Nature, Theory and Applications to Environmental Modelling and Security, Springer, New York, 241 pp.

Belušić, D. and Z.B. Klaić, 2006: Mesoscale dynamics, structure and predictability of a severe Adriatic bora case. Meteorol. Z. **15**, 157-168.

Belušić, D., M. Pasarić, Z. Pasarić, M. Orlić, and B. Grisogono, 2006: A note on local and non-local properties of turbulence in the bora flow. Meteorol. Z. **15**, 301-306.

Grisogono, B. and D. Belušić, 2009: A review of recent advances in understanding the meso- and micro-scale properties of the severe Bora wind. Tellus A **61**, 1-16.

Mellor, G.L. and T. Yamada, 1974: A hierarchy of turbulence closure models for planetary boundary layers. J. Atmos. Sci. **31**, 1791-1806.

Piper, M. and J.K. Lundquist, 2004: Surface layer turbulence measurements during a frontal passage. J. Atmos. Sci. **61**, 1768-1780.

Stull, R.B., 1988: An Introduction to Boundary Layer Meteorology, Kluwer Academic, 666 pp.

Večenaj, Ž., D. Belušić, and B. Grisogono, 2007: Estimation of turbulence kinetic energy dissipation rate in a bora event. *Proc. 29th Intern. Conf.on Alpine Meteorology*, Chambery, France, 745-748.

Yoshino, M.M., 1976: Local wind bora: a research summary. *Yoshino, M.M. (Ed.), Local wind bora*, University of Tokio Press, 277-282.

AN INVESTIGATION INTO RIDGE-TOP TURBULENCE CHARACTERISTICS: A CASE STUDY OF IN SITU MEASUREMENTS AND LARGE EDDY SIMULATION

Marwan Katurji, Peyman Zawar-Reza, Andrew Sturman

Centre for Atmospheric Research, University of Canterbury, Christchurch, New Zealand
E-mail: *mka94@student.canterbury.ac.nz*

Abstract: High Reynolds number turbulent flow over a ridge top in New Zealand is investigated through in situ measurements and large eddy simulations. Spectral analysis was performed for observed stream-wise and lateral velocity components for two different locations along the ridge. Multi-scale turbulent interactions are examined and the 3-dimensional isotropy assumption in the inertial sub-range of the spectrum assessed. Turbulent eddy length scales were derived showing increased dissipative length scales during day time. The Advanced Regional Prediction System (ARPS) large eddy simulation (LES) model was used in 2-D simulations over the experimental site to examine the sensitivity of surface layer turbulence to soil moisture initialization. Results for the dry soil runs showed a relative increase in daily averaged turbulent kinetic energy by 25 % and 23 % for two different locations in the domain. The nature of turbulent eddy evolution, structure and interaction over a complex ridge is examined.

Keywords: *Turbulence, velocity spectra, mountain ridge top, large eddy simulation.*

1 BACKGROUND AND INTRODUCTION

Atmospheric surface layer turbulence over flat terrain is well understood under different stability conditions. Turbulence over hill tops has also attracted interest in the research community, but there is still much knowledge to be gained. Large scale eddies having length scales larger than the hill length scale are transported over hills within a time period less than their own turnover time following the rapid distortion theory discussed by Townsend (1972). Panofsky et al. (1982) showed through observations of spectra over different fetch distances in complex terrain that the response rate differs for small and large eddies. They suggested that while the small high frequency turbulent eddies adjust to new terrain quickly the large low frequency ones still hold memory of the terrain upstream of the flow. More recent theories of turbulence structure and processes in the atmospheric surface layer have negated Monin-Obukhov similarity theory (Hunt and Morrison 2000), while McNaughton and Brunet (2002) have shown the existence of two interacting scales of turbulence initiated from the surface upward by rising unstable thermal eddies that interact with the mean flow. The current work provides an insight into turbulence in high Reynolds number ($\sim 10^9$) flow over a ridge top through in situ measurements and large eddy simulations in an attempt to critically assess previous theories. The main objective of this paper is to understand the turbulent structure and mechanisms of flow over a mountain ridge top in the South Island that is a potential site for wind turbines.

2 METHODOLOGY AND RESULTS

Two ultra-sonic anemometers were mounted on 20 metre towers 3 km apart along a ridge top. Sampling rate was 60 Hz, block averaged to 20 Hz. The p-welch fourier transform routine was used to produce spectral plots after de-trending and windowing the discrete data. Daytime and night time datasets were analyzed from the two towers, and spectral data were carefully examined to ensure that the time period represented the complete spectrum of energy production and dissipation. Dissipative eddy sizes were derived from spectral plots of eddy dissipation rate using the spectral model equation in the inertial sub-range after Kolmogorov (1941a & b) and Obukhov (1941). The power spectra were scaled by the variance of the wind speed and the frequency was scaled by z/L (Figure 1 a & d). Power ratios of cross-wise and vertical spectra to stream-wise spectra were derived to investigate the isotropic assumption of turbulence (Figures 1 b, c, e & f). Site 2 was more turbulent and had higher wind speeds than site 1 for both day and night time conditions, which relates to their relative exposure. The entire range of the energy spectrum was captured, from the large and low frequency eddies to the small and high frequency eddies. Day and night spectra differ slightly for the two sites and show a drop of energy for the night time period, which is evidence that the increase in energy during daytime was from thermally induced turbulence production. An interesting feature in the normalized spectral plots is the double peak depicted in the spectra of site 2.

The Advanced Regional Prediction System model (ARPS) was used to undertake 2-D sensitivity experiments, as it is capable of resolving atmospheric phenomena to a high degree of accuracy using large eddy simulation techniques. A north-west/south-east section was chosen since this direction represents the prevailing wind direction. Terrain data were selected from 25 m resolution digital elevation model output and was smoothed using a robust locally weighted scatter plot model. A silty-clay soil type and grassland with shrub

cover were selected to represent surface conditions. The main focus of this modelling exercise is to study the effect of homogenous soil moisture initialization on the turbulent kinetic energy and wind speeds, so two runs were performed – a wet soil run (65 % saturation) and a dry soil run (40 % saturation). The 2-D large eddy simulation soil moisture sensitivity experiments clearly show increase in turbulent activity during daytime for both moist and dry soil conditions with the dry soil simulation contributing more to the turbulent kinetic energy. Average daily values of turbulent kinetic energy show an increase of 23 % and 25 % relative to the wet soil run for the two locations.

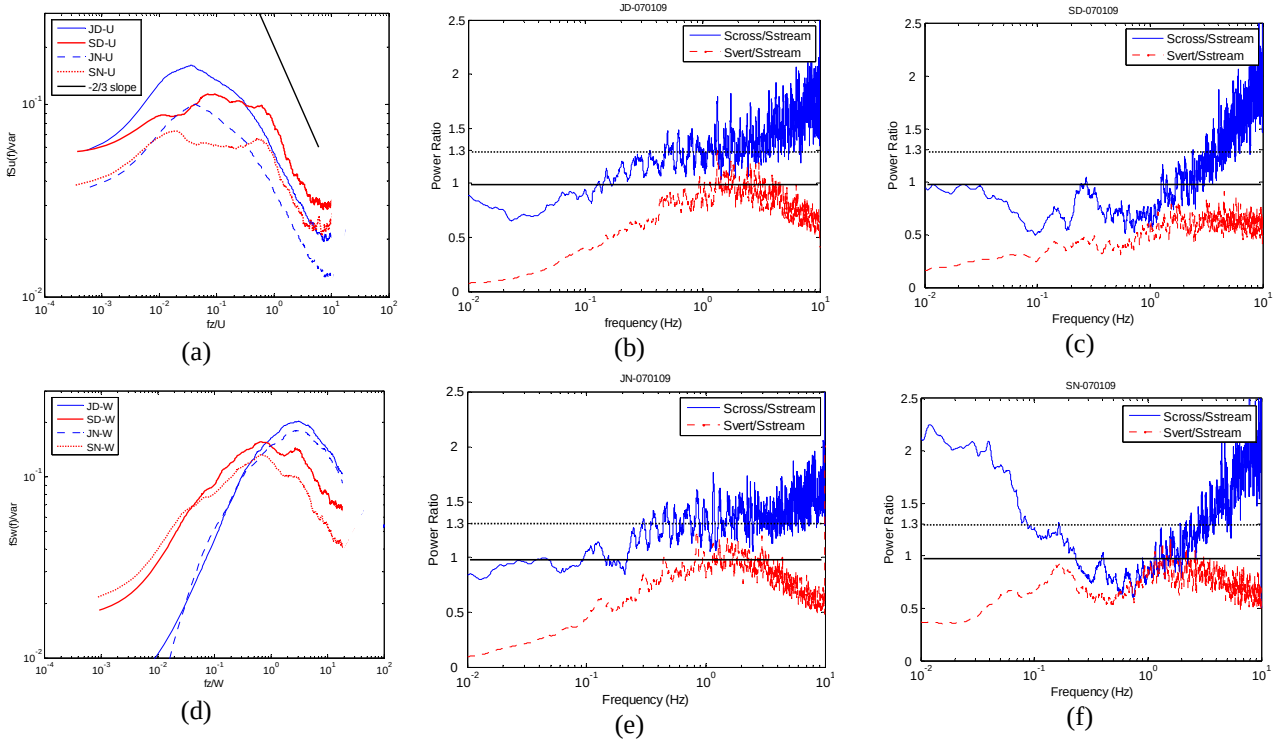

Figure 1. (a, b): Normalized power spectra for the day and night periods at the two sites for the stream-wise (U) and vertical (W) velocity component. (b, c, e, f): Spectral ratios of the lateral (or cross-wise) and vertical power to the longitudinal (or stream-wise) power for cases JD (site 1 day), SD (site 2 day), JN (site 1 night), and SN (site 2 night).

CONCLUSION

The value of high resolution meteorological data along ridge tops in complex terrain under high wind speed conditions is evident. Spectral data analysis for daytime and night time provided evidence about turbulent eddy sizes and structures in the atmospheric surface layer. The double peak in the spectrum occurred both during unstable and near neutral conditions and during night time, implying that the terrain upwind of the sensor and in the vicinity of the flux footprint can have an important influence on the turbulence spectra. The isotropic hypothesis held true during a night time case when turbulence was dominated by shear rather than thermal buoyancy. Model simulations showed that soil moisture can be an important factor in surface layer turbulence.

REFERENCES

Hunt, J.C.R, Morrison, J.F. (2000). Eddy structure in turbulent boundary layers. Euro J. Mech. B. Fluids, 19, 673-694.

Kolmogorov, A. N. (1941a). Energy dissipation in locally isotropic turbulence. Quarterly Journal of the Royal Meteorological Society, 32(1), 19-21.

Kolmogorov, A. N. (1941b). The Local Structure of Turbulence in Incompressible Viscous Fluid for Very Large Reynolds Numbers. Proceedings: Mathematical and Physical Sciences, 434(1890), 9-13.

McNaughton, K. G., & Brunet, Y. (2002). Townsend's hypothesis, coherent structures and Monin-Obukhov similarity. Boundary-Layer Meteorology, 102(2), 161-175.

Obukhov, A.M. (1941). Energy distribution in the spectrum of a turbulent flow. Ser. Geogr. Geofiz., 4-5, 453-466.

Panofsky, H. A., Larko, D., Lipschutz, R., & Stone, G. (1982). Spectra of velocity components over complex terrain. Quarterly Journal of the Royal Meteorological Society, 108, 215-230.

Townsend, A. A. (1972). Flow in a deep turbulent boundary layer over a surface distorted by water waves. Journal of Fluid Mechanics Digital Archive, 55(04), 719-735.

The application of microscale airflow simulations for quantifying snow drift processes over complex terrain

Rebecca Mott and Michael Lehning
Email: mott@slf.ch

WSL-Institute for Snow and Avalanche Research (SLF), Davos, Switzerland

Abstract:
The inhomogeneous snow distribution found in alpine terrain is the result of wind and precipitation interacting with the snow cover. In this study we compute high resolution wind fields for a specific snow fall event in October 2003 in order to explain zones of snow deposition/erosion and to investigate length scales of relevant snow transport and deposition processes. We use the wind fields as input for Alpine3D in order to quantify the redistribution of snow via saltation, suspension and the preferential deposition of precipitation. The results obtained with Alpine3D confirm the hypothesis that preferential deposition is active at the ridge scale and true redistribution, mainly via saltation, forms smaller scale deposition patterns such as dunes and cornices. A sensitivity analysis is presented using diverse numerical resolutions to separate numerical from physical effects concerning local erosion and deposition.

Keywords: *preferential deposition, snow drift processes, small scale windfields*

INTRODUCTION

In complex terrain, characteristic local wind flow patterns are induced by the topography. During snow fall events the modification of the near surface wind field results in a spatially varying preferential deposition of precipitation and in transport of already deposited snow. In high alpine terrain it is especially apparent that drift processes are active on many different scales.

The aim of our work is to explain zones of snow deposition/erosion which can be attributed to wind driven processes and to investigate length scales of relevant snow transport and deposition processes. Previous studies show that a horizontal resolution of 25m is sufficient to represent general deposition features (Mott et al., 2008, Dadic et al., submitted), especially on glaciers. However, recent investigations (Raderschall et al., 2008, Lehning et al., 2008) also suggest that preferential deposition is only active at the ridge scale and redistribution of snow by saltation and suspension is active on smaller scales.

In this study we discuss windfields and respective flow patterns on different scales. The effect of the representation of specific flow patterns on preferential deposition and pure snow drift processes is discussed. The relative contribution of the individual transport processes are presented. Finally we compare model simulation of snow distribution to observed snow variability at different numerical resolutions.

DATA AND METHODS

A steep mountain ridge, the Gaudergrat (Davos, Switzerland), was used as a test site for wind and snow drift experiments. Three automatic meteorological stations, located in the luff, top and lee of the mountain ridge, provide a long series of wind data. In summer 2003 the GAUDEX experiment was conducted at Gaudergrat with a total number of 33 measurement stations, consisting of 27 automatic weather stations and 6 turbulence stations (Lewis et al., 2008). This unique set of wind and turbulence data provides detailed insight into the mean flow patterns of this specific area. In this study we use this knowledge to compute high resolution wind fields for a specific snow fall event in October 2003.

Wind fields were computed with the non-hydrostatic and compressible weather model, Advanced Regional Prediction System (ARPS) and compared to the detailed data set available. The snow distribution after the snow fall event was measured by manual snow probing. We used the wind fields as an input for Alpine3D (Lehning et al., 2008) in order to quantify the redistribution of snow via saltation and suspension and the preferential deposition of precipitation.

A sensitivity analysis is presented using a number of numerical resolutions to separate numerical from physical effects with respect to local erosion and deposition. The sensitivity analysis is carried out by resampling the grid with the smallest scale (10m) to coarser grid resolutions. All sensitivity analysis runs were carried out with the same initial and boundary conditions. In order to discuss the individual transport processes a time series of precipitation and the total deposition is analyzed. The relative contribution of saltation/suspension versus preferential deposition has been evaluated by switching off saltation/suspension in the corresponding sensitivity cases as described by (Lehning et al., 2008).

RESULTS AND CONCLUSION

The results of drift simulations show two characteristic patterns of snow deposition. At ridge scale, strong snow loading is simulated in the lee-slope of the ridge, which is attributed to the cross-ridge flow and the associated strong wind gradient behind the ridge often leading to flow resolution. If the horizontal resolution is 10m, the maximum snow loading is found directly behind the ridge, whereas at 25m resolution the snow loading is distributed further down the lee slope. Secondary deposition features are found in the lee of smaller scale cross

slope ridges, and are caused by flow parallel to the main ridge. These deposition features, small scale snow dunes, were formed mainly due to pure drift-processes without the contribution of preferential deposition. Therefore these patterns are best represented in simulations with a horizontal resolution of 10m or less.

The results obtained with Alpine3D confirm the hypothesis that preferential deposition is active at the ridge scale and true redistribution mainly via saltation forms smaller scale deposition patterns such as dunes and cornices. The sensitivity analysis shows that a resolution of 10m or less is necessary to capture smaller scale deposition features observed, as suggested earlier by Lehning et al. (2008). With an increase of grid resolution the speed-up effect at the mountain ridge increases dramatically. This leads to stronger wind velocity gradients in the direction of the mean flow (see Figure 2 and Figure 3). The effect of the gradient (see Figure 3) is clearly represented by a maximum snow deposition where the velocity gradient becomes strongest, directly behind the ridge.

Overall the snow drift modelling shows that the mean flow characteristics observed and modelled at Gaudergrat explain the major drift zones observed after the snow fall event in October 2003. The choice of the numerical grid is shown to be crucial when explaining different drift zones on different scales.

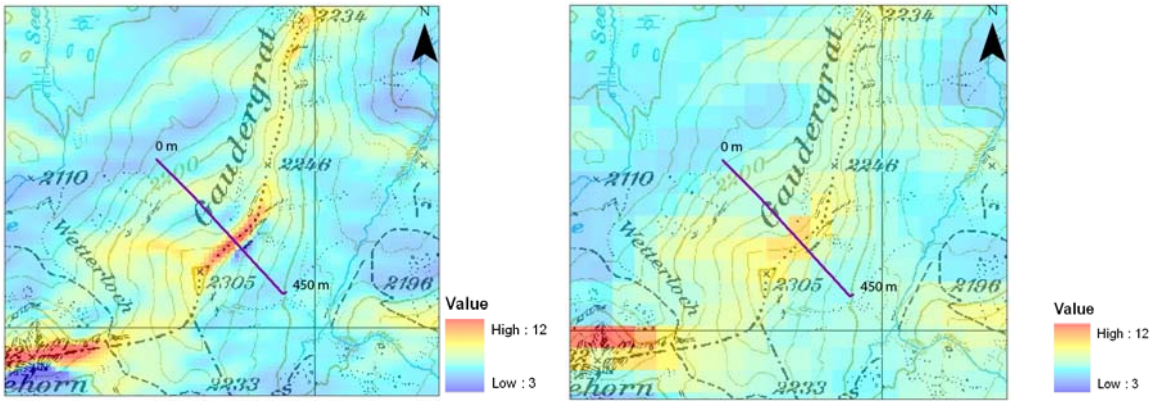

a) b)

Figure 1: Wind velocity [m/s] with resolutions of a) 10m and b) 50m under northwesterly wind condition. The line indicates the transect (see Fig. 2 and Fig. 3)

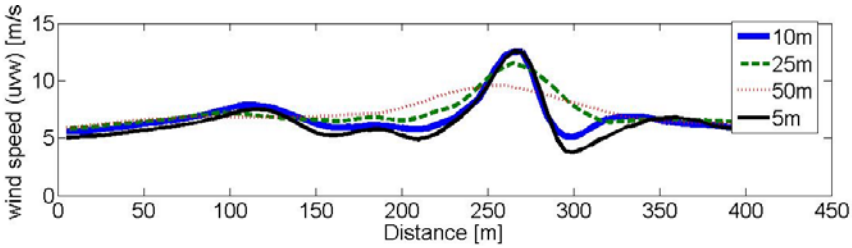

Figure 2: Transect of wind speed of different numerical resolutions (5, 10, 25, 50)

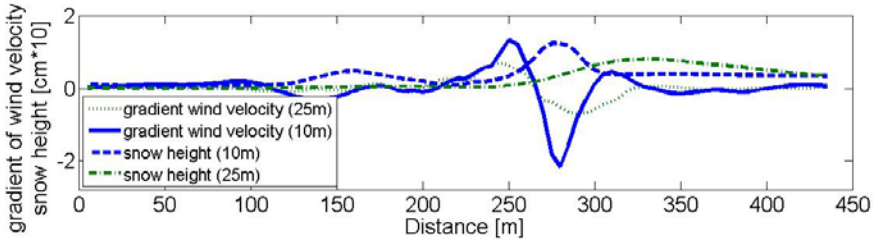

Figure 3: Transect of the gradient of wind speed and respective snow height simulation for dx, dy 10m and 25m

REFERENCES

Mott R., Faure F., Lehning M., Löwe H., Hynek B., Michlmayr G., Prokop A., Schöner W. 2008: Simulation of seasonal snow-cover distribution for glacierized sites on Sonnblick, Austria, with the Alpine3D model. Annals of Glaciology **49**. 155 -160.

Lehning, M., H. Löwe, M. Ryser, and N. Raderschall (2008), Inhomogeneous precipitation distribution and snow transport in steep terrain, Water Resour. Res., **44**, W07404, doi:10.1029/2007WR006545.

Raderschall N., M. Lehning, C. Schär (2008), Fine-scale modeling of the boundary layer wind field over steep topography, Water Resour. Res., **44**, W09425, doi:10.1029/2007WR006544.

Dadic R., Mott R., Lehning M., Burlando P., submitted: Wind Influence on Snow Distribution and Accumulation over Glaciers. Submitted to Journal of Geophysical Research. Doi:10.1029.

Lewis, H.W., Mobbs, S.D., Lehning M., 2008. Observations of cross-ridge flows across steep terrain, Q.J.R.Meteorol.Soc., 134, 801–816, doi: 10.1002/qj.259.

MECHANISMS OF ALONG-VALLEY WINDS

Juerg Schmidli[1], Richard Rotunno[2]

[1] Institute for Atmospheric and Climate Science, ETH, Zurich, Switzerland
[2] National Center for Atmospheric Research, Boulder, USA
E-mail: *jschmidli@env.ethz.ch*

Abstract: The physical mechanisms leading to the formation of along-valley winds are investigated. A diagnostic equation for the along-valley pressure gradient is developed and used in combination with numerical model simulations to clarify the relative role of various mechanisms such as the valley volume effect (TAF) and subsidence heating in the formation of along-valley winds. The setup for the numerical simulations consists of an idealized three-dimensional topography and two sets of thermal forcings: A simplified sinusoidal forcing in the first case, and a realistic forcing in the second case. The present analysis confirms the importance of the valley volume effect for the formation of along-valley winds, but also clarifies the role of subsidence heating and the limitations of the TAF argument.

***K*eywords:** *ICAM, valley winds, volume effect, topographic amplification factor, TAF, subsidence heating*

1 INTRODUCTION

Thermally driven slope and valley winds are an essential component of the fair-weather boundary layer over mountainous terrain. Together with turbulent processes they control the exchange of energy, momentum, moisture and pollutants between the land surface and the free atmosphere. Despite their importance there is still debate about the mechanisms driving the along-valley wind and their relative importance. Is the valley volume effect or topographic amplification factor (TAF; Steinacker , 1984) sufficient to explain the formation of the up-valley wind? How important is subsidence heating (Rampanelli et al., 2004; Weigel et al., 2006)? In order to clarify the relative role of the different mechanisms in the formation of the along-valley wind, a diagnostic equation for the along-valley pressure gradient is developed and used in combination with numerical model simulations.

2 METHOD OUTLINE

Starting from the along-valley momentum equation, and using the thermodynamic equation and the hydrostatic approximation, it is shown that the along-valley pressure gradient ΔP can be expressed by

$$\Delta P|_{x,z=0} = -\frac{gQ_p^n}{\theta_0}(\tau - 1) + \Delta P_h \tag{1}$$

where Q_p^n represents the net heat input into the control volume over the plain, ΔP_h represents the upper-level large-scale forcing, and the total amplification factor τ is given by

$$\tau = \tau_a \cdot \tau_v \cdot \tau_q \cdot \tau_e = \tau_a \cdot \tau_h. \tag{2}$$

Here τ_a is related to the geometry of the valley cross-section, τ_v is the topographic amplification factor, τ_q is the ratio of the valley to the plain surface sensible heat flux, and τ_e is related to the heat exchange of the valley with the free atmosphere. In summary, the diagnostic relation relates the along-valley pressure gradient to the topographic amplification factor (τ_v), the time evolution of the valley heat budget (τ_e, τ_q), and the large-scale forcing (ΔP_h).

3 MODEL SETUP

The setup for the numerical simulation of the thermally driven flows using the Advanced Regional Prediction System (ARPS) consists of an idealized three-dimensional topography and two sets of thermal forcing: A *simple forcing* assuming a spatially uniform sensible heat flux with sinusoidal variation in time (diurnal cycle) in the first case, and a *realistic forcing* determined by the full physics including radiation transfer, land surface processes and turbulence in the second case.

4 RESULTS

Fig. 1 shows a snap-shot of the simulated cross-valley and along-valley flow at 1200 local time (LT) at a location 20 km up-valley from the valley entrance for the two sets of thermal forcing. The stronger along-valley

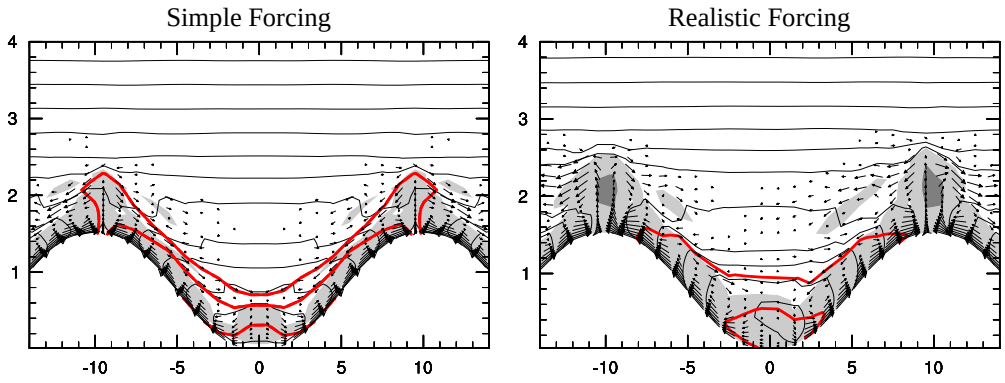

Figure 1: Simulated cross-valley wind vectors and along-valley flow (bold contours) 20 km up-valley from the valley mouth at 1200 LT for the two sets of thermal forcing. The thin lines indicate potential temperature and the shading indicates the vertical eddy diffusivity.

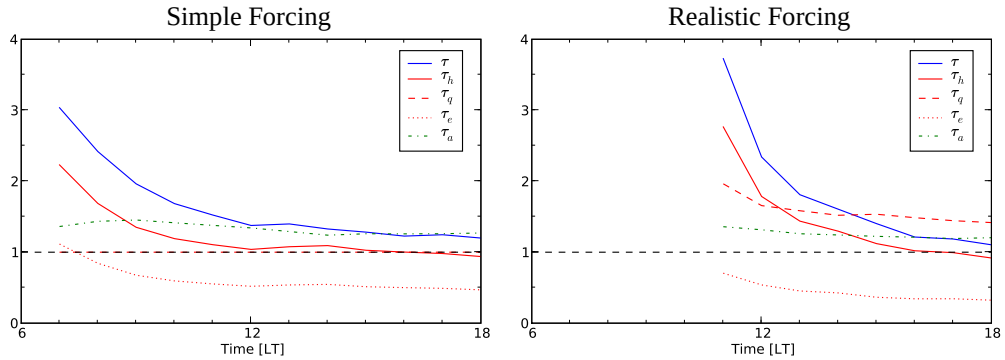

Figure 2: Time evolution of the valley wind forcing factors 20 km up-valley from the valley entrance. For the realistic forcing case, the factors can not be calculated prior to 1100 LT due to cooling instead of heating over the plain during the first few hours.

wind in the simple forcing case can be explained by the larger sensible heat flux during the first few hours in the simple forcing run. The deeper boundary layer in the realistic forcing run is the result of a larger sensible heat flux in the hour prior to the snap-shot (314 W m^{-2} versus 197 W m^{-2}). Note that the integrated forcing in the period 0600 – 1200 LT is very similar for the two cases. Fig. 2 portrays the temporal evolution of the different forcing factors introduced in Eq. (2). Note that $\tau_v = 2$ for the chosen valley geometry. It can be seen that the total amplification factor τ decreases rapidly with time due to significant and increasing heat exchange of the valley with the atmosphere above (τ_e). For the realistic forcing run there is an additional contribution to the forcing due to a larger sensible heat flux in the valley in comparison to the plain (τ_q).

5 CONCLUSIONS

The study finds that the underlying assumption of the valley volume argument, that there is no heat exchange with the free atmosphere, is not fulfilled for the case examined. The heat exchange is small during the first few hours, but rapidly increases thereafter. In the afternoon it is comparable in magnitude to the sensible heat input into the valley atmosphere. The present study confirms the importance of the valley volume effect for the formation of the along-valley wind, but also clarifies the role of subsidence heating and the limitations of the TAF argument. In summary, the analysis brings together different ideas of the valley wind into a unified picture.

REFERENCES

Steinacker, R., 1984: Area-height distribution of a valley and its relation to the valley wind. *Beitr. Phys. Atmosph.*, **57**, 64–71.

Weigel, A.P., F.K. Chow, M.W. Rotach, R.L. Street, and M. Xue, 2006: High-resolution large-eddy simulations of flow in a steep alpine valley. Part II: Flow structures and heat budgets. *J. Appl. Meteor. Climatol.*, **45**, 87–107.

Rampanelli, G., D. Zardi, and R. Rotunno, 2004: Mechanisms of up-valley winds. *J. Atmos. Sci.*, **61**, 3097–3111.

A CONCEPTUAL MODEL FOR THE DAYTIME EVOLUTION OF THE THERMAL STRUCTURE IN A MOUNTAIN VALLEY UNDER FAIR WEATHER CONDITIONS

Dino Zardi
Gruppo di Fisica dell'Atmosfera,
Dipartimento di Ingegneria Civile e Ambientale, Università di Trento, Trento, Italy
E-mail: *Dino.Zardi@ing.unitn.it*

Abstract: A simplified model is proposed to reproduce the essential features of the diurnal evolution of a convective boundary layer (CBL) in a mountain valley. A zero-order order mixed layer (ML) scheme is adopted for the thermal structure above the valley floor, while up-slope mass and heat flows are estimated by means of a Prandtl-like solution. The effects of compensating subsidence are evaluated by estimating the downward motion from mass conservation and assuming a linearly stratified free atmosphere. The resulting evolution equation for the ML height incorporates all the parameters controlling the diurnal evolution of the layer. Thus the model allows to compare CBL growth in the valley and over a plain and to estimate how various factors concur to determine the observed amplification of the diurnal temperature cycle in mountain valleys.

Keywords: *valley, slope, heat flux, convective boundary layer, subsidence, topographic amplification factor (TAF).*

1 INTRODUCTION

Under fair weather conditions in mountain valleys typical winds develop, driven by the along-valley pressure gradients determined by the enhanced heating of the valley atmosphere with respect to the adjacent plains. The factors producing such an amplified temperature range have been extensively explored (Steinacker, 1984, Whiteman, 2000, Rampanelli, et al. 2004). Recent contributions suggest that this effect cannot be explained in terms of geometric factors only (Serafin, 2006). Indeed the processes heating the valley atmosphere are: (a) the subsidence of potentially warmer air in the valley core compensating the development of up-slope flows along the sunny sidewalls; (b) the turbulent heat flux over the valley floor originated from solar radiation and driving the development of a Convective Boundary Layer (CBL). The latter typically displays a vertical structure significantly different than over flat terrain: in particular the mixed layer is usually shallower, whereas the stably stratified capping inversion layer is usually deeper, as a consequence of the core subsidence (Figures 1 and 2).

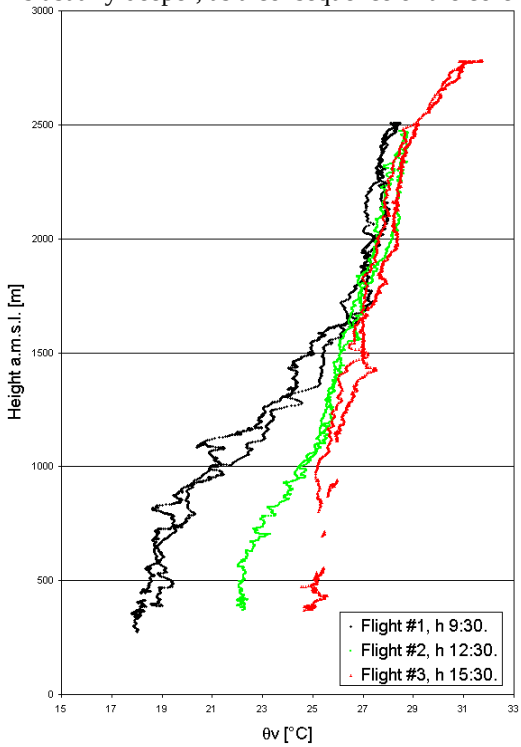

Figure 1: Profiles of virtual potential temperature θ_v during flights subsequently performed in the Adige Valley over Besenello on 1 October 1999 at times reported in the figure legend (adapted from de Franceschi et al., 2003).

2 OUTLINE THE MODEL

The proposed conceptual model assumes a simplified trapezoidal valley cross-section and adopts a zero-order mixed layer (ML) scheme to reproduce the thermal structure of the atmosphere up to the ML height above the valley floor, whereas the initial state of the atmosphere is given by $\theta(z)=\theta_0+\gamma z$.

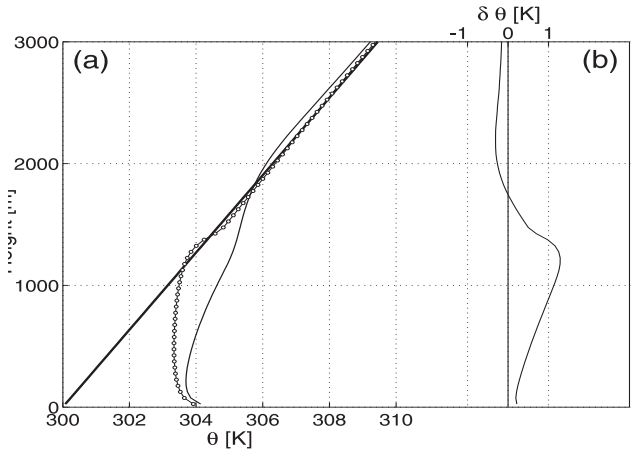

Figure 2: (a) Vertical profiles of potential temperature along the valley axis (thin solid line) and over the plain (bullets) at *t = 6h* after sunrise (the dark solid line shows the initial profile). (b) Difference between the two profiles at various heights (adapted from Rampanelli et al. 2004).

The up-slope mass and heat flow is estimated by means of a Prandtl-like scheme. Accordingly the effect of the subsidence warming is evaluated by estimating the compensating downward motion from mass conservation and evaluating the potential temperature of air parcels entering the top of the ML at any time after sunrise. By combining all these equations and related constraints deriving from continuity and consistency conditions, an evolution equation for the mixed layer height is obtained, which incorporates all the parameters concurring to control the diurnal evolution of the layer. As a result the model allows to evaluate how the air in the valley mixed layer gets warmed more than over the adjacent plain (Figure 3) . This also allows a first estimate of various factors determining the observed amplification of the diurnal temperature cycle in mountain valleys.

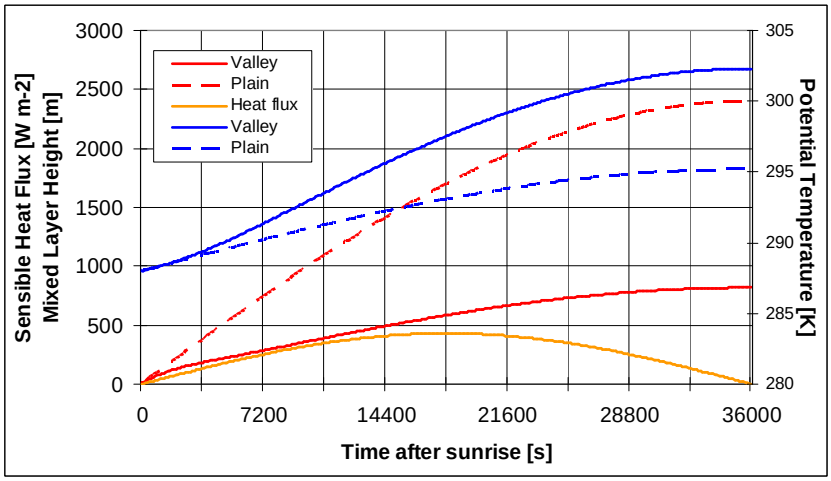

Figure 3: Simulated diurnal evolution of potential temperature (blue lines) and mixed layer height (red lines) respectively in the valley (solid lines) and over the plain (dashed lines) under the same sensible heat flux at ground (orange line) for a valley displaying a floor width of 3 km, a crest height of 3.5 km, a sidewall slope angle α=45° (θ_0 = 288 K, γ = 0.003 K km^{-1}).

Acknowledgements:
I am greatly indebted with Max de Franceschi, Gabriele Rampanelli, Stefano Serafin, Mathias Rotach, Richard Rotunno and Dave Whiteman for many fruitful discussions in these years. I am also very grateful to the late lamented prof. Ignaz Vergeiner for his warm encouragement to pursue my work on conceptual modeling at an early stage of my research activity.

REFERENCES

de Franceschi, M., G. Rampanelli, D. Sguerso, D. Zardi, and P. Zatelli: 2003, Development of a measurement platform on a light airplane and analysis of airborne measurements in the atmospheric boundary layer, Ann. of Geophys. **46**, 269-283.

Rampanelli, G. and D. Zardi: 2004, `A method to determine the capping inversion of the convective boundary layer'. J. Appl. Meteor. **43**, 925-933.

Rampanelli, G., Zardi, D., Rotunno, R., 2004, Mechanisms of Up-Valley Winds , J. Atmos. Sci., **61**, 3097-3111.

Serafin, S., 2006, Boundary-layer processes and thermally driven flows over complex terrain. Ph.D. thesis in Environmental Engineering, Univesity of Trento, Italy, 200 pp.

Steinacker, R., 1984: Area-height distribution of a valley and its relation to the valley wind. Contrib. Atmos. Phys., **57**, 64-71

Whiteman, C. D., 2000: Mountain Meteorology: Fundamentals and Applications. Oxford Univ. Press, New York, 355pp.

OBSERVATIONS AND NUMERICAL SIMULATIONS OF THE INTERACTION BETWEEN THE THERMALLY-FORCED OROGRAPHIC CIRCULATION IN THE CONVECTIVE BOUNDARY LAYER AND DEEP CONVECTION

Bart Geerts and Joshua C. Demko

University of Wyoming, Laramie, Wyoming
E-mail: *geerts@uwyo.edu*

Abstract: Surface and upper-air data, collected as part of the Cumulus Photogrammetric, In situ and Doppler Observations (CuPIDO) experiment during the 2006 monsoon season around the Santa Catalina Mountains in southeast Arizona, are used to study the development of the mountain-scale surface convergence and its interaction with deep convection, which develops very regularly in the afternoon over this mountain. High-resolution multi-nest WRF simulations are being conducted for several days to examine WRF's ability to reproduce the observed convective evolution. The model is validated with observed mountain-scale surface convergence and cloud top height.

Keywords: *ICAM, convection, mountainous area (9 pt in italics)*

1 INTRODUCTION

During the summer, cumulus convection erupts almost daily close to solar noon over the ranges of the interior Mountain West of the United States. The lower troposphere is marked by a deep convective boundary layer (CBL) and weak winds. The moist convection is essential to warm-season precipitation and to surface-troposphere exchange of water and heat in the region. Even relatively simple numerical simulations have shown that under sufficient solar radiation, weak stratification, and weak wind, a thermally-direct circulation develops over a mountain, with anabatic flow converging over a mountain [e.g., Fig. 1 in Demko et al. (2009)]. It is generally believed that the low-level convergence associated with this toroidal circulation, combined with heating over elevated terrain, is responsible for the initiation and maintenance of cumulus convection over or near the mountain [e.g., Fig. 8.15 in Whiteman (2000)].

Few observational studies have documented the thermally forced toroidal circulation over mountains, and they generally only describe the surface component (e.g., Garrett 1980; Banta 1984; Vergeiner and Dreiseitl 1987). Demko et al. (2009) used both aircraft and surface measurements to characterize this circulation around the relatively isolated Santa Catalina Mountains (SCM) in Arizona, a mountain peaking ~2000 m above the plains with a diameter of ~30 km. The surface measurements around the mountain clearly reveal the diurnal evolution of mountain-scale convergence (MSC), which tends to peak around solar noon. The divergent component of the toroidal circulation near the CBL top proved more difficult to capture, even with ~50 flight loops around the SCM. Surface measurements around and on top of the SCM show that the MSC was forced by a diurnally-varying pressure difference between the high terrain and the surrounding plains (Geerts et al. 2008). The diurnal signal of this perturbation pressure difference suggests that is due to heating of the CBL over elevated terrain.

Because the mountains that drive the CBL convergence and deep convection are generally small compared to model resolution, the resulting cloudiness and precipitation are poorly predicted by current numerical weather prediction (NWP) models. Even NWP models of sufficient resolution to resolve the thermally-direct orographic circulations are challenged in their ability to simulate the surface fluxes and CBL growth over complex terrain, and thus accurately predict the timing and intensity of ensuing thunderstorms. Several modeling studies have depicted the development of the CBL and of thermally-forced circulations, but most studies assumed an idealized vertical profile and an idealized mountain. Our study employs real cases to simulate CBL development of a real mountain range, i.e. the SCM. The selected cases occurred during the CuPIDO field campaign (Damiani et al. 2008), therefore detailed observations are available for some basic model validation. This study first verifies whether the model captures the observed MSC and its forcing. The objective then is to use the spatially and temporally continuous, dynamically consistent model output to shed light upon the nature and dynamics of CBL growth and orographic circulations. The first part focuses on cases with little cumulus convection over the SCM, of insufficient depth to produce precipitation and a cold pool. The second part examines the interaction between CBL flow and orographic deep convection.

2 RESULTS

Key observations are summarized in Demko et al. (2009) and Geerts et al. (2008). The WRF v.3.0.1 non-hydrostatic mesoscale model was run with an inner next resolution of 1 km for five days in CuPIDO, two with only Cu congestus, and three others with cumulonimbus development over the SCM. In general the model

captures the MSC (**Fig. 1**, for one of the 5 cases) and convective evolution (as measured by cloud top chronology, not shown) remarkably well. The model is then used to study the diurnal evolution of MSC, CBL depth, and deep convection (Fig. 2). On 9 July deep convection broke out around sunset (02:15 UTC).

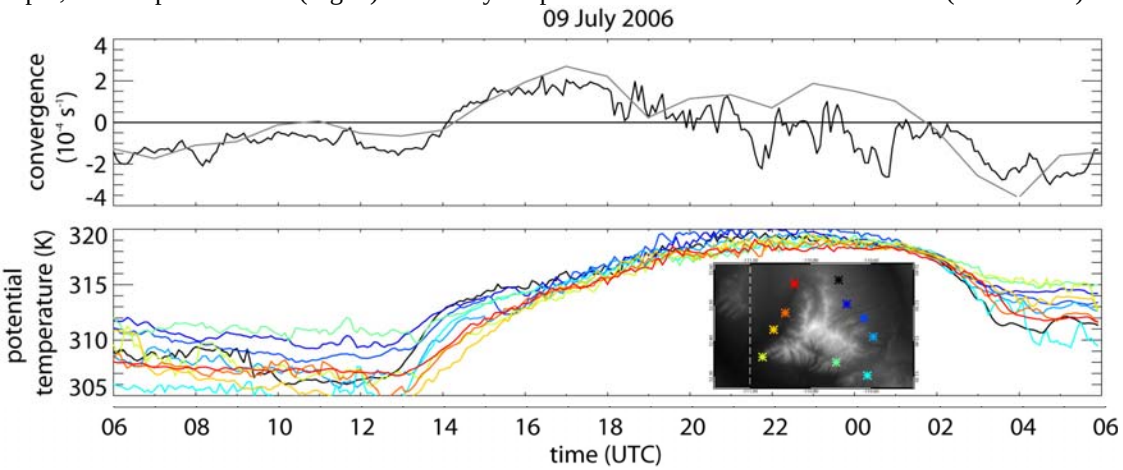

Figure 1: (top) Observed (black) and WRF-modeled (grey) MSC calculated from the 10 ISFF stations and WRF's closest grid point; (bottom) observed potential temperature at the ISFF stations color-coded as shown in the insert terrain map. Solar noon is at 19:30 UTC.

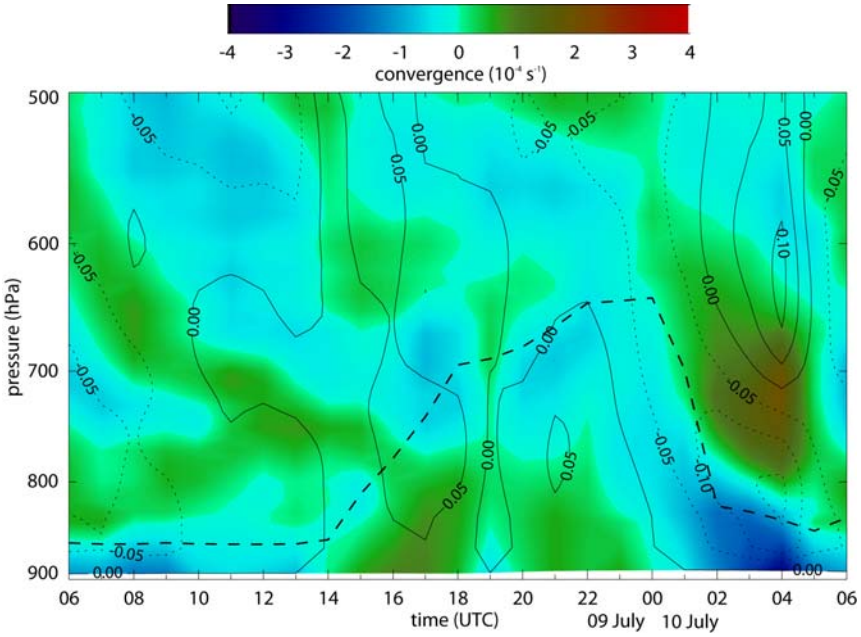

Figure 2: Time-height plot of MSC for the 900 km^2 box (color shaded), mean vertical velocity within this box inferred from mass continuity (solid lines for updrafts, dotted lines for downdrafts, contour interval 0.05 ms^{-1}), and mean CBL height (bold dashed line), for the 9 July case.

Acknowledgements: *This work is funded by National Science Foundation grant ATM-0444254.*

REFERENCES

Banta, R. M., 1984: Daytime boundary-layer evolution over mountainous terrain. Part I: Observations of the dry circulations. *Mon. Wea. Rev.*, **112**, 340-356.

Damiani, R., J. Zehnder, B. Geerts, J. Demko, S. Haimov, J. Petti, G.S. Poulos, A. Razdan, J. Hu, M. Leuthold, and J. French, 2008: Cumulus Photogrammetric, In-situ and Doppler Observations: the CuPIDO 2006 experiment. *Bull. Amer. Meteor. Soc.*, **89**, 57–73.

Demko, J. C., B. Geerts, Q. Miao, and J. Zehnder, 2009: Boundary-layer energy transport and cumulus development over a heated mountain: an observational study. *Mon. Wea. Rev.* , **137**, 447–468.

Garrett, A.J., 1980: Orographic cloud over the eastern slopes of Mauna Loa Volcano, Hawaii, related to insolation and wind. *Mon. Wea. Rev.*, **108**, 931–941.

Geerts, B., Q. Miao, and J.C. Demko, 2008: Pressure perturbations and upslope flow over a heated, isolated mountain. *Mon. Wea. Rev.*, **136**, 4272–4288.

Vergeiner, I., and E. Dreiseitl, 1987: Valley winds and slope winds: observations and elementary thoughts, *Meteorol. Atmos. Phys.*, **36**, 264–268.

Whiteman, C. D., 2000: *Mountain Meteorology: Fundamentals and Applications.* Oxford University Press, 376 pp.

INVESTIGATION OF OROGRAPHIC VENTING OF ATMOSPHERIC BOUNDARY LAYER AIR USING OBSERVATIONS AND THE WRF-CHEM MODEL

Jian-Wen Bao[1], Sara A. Michelson[2], Evelyn D. Grell[2], Georg A. Grell[2]

[1] NOAA/Earth System Research Laboratory/Physical Sciences Division, Boulder, Colorado, USA
E-mail: *Jian-Wen.Wao@noaa.gov*
[2] NOAA/Earth System Research Laboratory and CIRES/University of Colorado, Boulder, Colorado, USA

Abstract: Three-dimensional air-mass transport under fair weather conditions in California's Central Valley between the atmospheric boundary layer (ABL) to the free troposphere (FT) is investigated with a case study using the observations from the Central California Ozone Study (CCOS) 2000 field experiment and the WRF-Chem model.

Keywords: *CCOS, WRF-Chem, atmospheric boundary layer, pollution transport, orographic ventilation and recirculation*

1 INTRODUCTION

Orographic ventilation and recirculation of pollution in the Atmospheric Boundary Layer (ABL) have been recognized as important mesoscale transport processes in the formation of poor air quality in areas surrounded by complex topography (see, e.g., Henne et al. 2004). One such area is the Central Valley (CV) of California. Although state-of-the-art mesoscale models are capable of simulating the transport processes, it is not clear how accurate the simulated processes are, given the inevitable uncertainties in the physics and input parameters of the models. In addition, the conditions necessary for initiating and maintaining the processes are not well understood in terms of mesoscale and micrometeorological dynamics. These two issues need to be addressed in order to improve model-based air quality forecasts and control planning in the CV. In a pilot research effort, a combined field and modeling investigation is conducted to address these issues by taking observations within the ABL and the transition layer between the ABL and the free troposphere in the CV, and applying a numerical model to simulate and analyze the observed properties of the transport processes. In this investigation, orographic ventilation and recirculation processes taking place along both the Coast Range and the Sierra Nevada slopes are simulated and compared with observations.

2 MODEL SETUP AND OBSERVATIONS

The WRF-Chem model (Grell 2004) is used in this study. The results shown are from simulations on a 4-km domain that encompasses the Central California Ozone Study (CCOS) 2000 field study area, extending from the Pacific Ocean in the west to the Sierra Nevada in the east, and from north of Redding, CA, south to the Mojave Desert. The case highlighted here is the 29 July to 3 August 2000 high-ozone episode, which is one of the poor air quality events that occurred during the CCOS field experiment. The RACM-KPP chemical mechanism is used in the WRF-Chem simulations along with the physics configuration including the Mellor-Yamada-Janjic ABL and the Monin-Obukhov (Janjic) surface layer schemes, the NOAH land surface model, the Goddard short-wave, RRTM long-wave radiation schemes and the WSM 5-class microphysics parameterization. Brief descriptions of the physics parameterization schemes in the WRF model can be found in (Skamarock et al. 2005). There are 50 vertically stretched levels with 30 levels within the lowest 2 km and the lowest model layer is about 24 m thick. The initial and boundary conditions are generated using the 6-hourly 40-km National Center for Environmental Prediction (NCEP) Eta analysis.

The CCOS observations are used to evaluate the skills of the WRF-Chem meteorological model in reproducing the overall pattern of the observed low-level flows. The observational datasets used for the meteorological comparison include a network of 24 915-MHz wind profilers and one 449-MHz wind profiler along with the surface data at these sites. The wind profilers provide hourly averages of wind speed and direction, typically to heights of 3000 m AGL. In addition to winds, the profilers measure the vertical profile of virtual temperature up to 1000 m AGL using the Radio Acoustic Sounding System (RASS) technique.

3 MESOCALE CIRCULATION ASSOCIATED WITH THE VENTOLATION

Mesoscale circulation components are important in the orographic ventilation and recirculation of the ABL pollution in the CV. These components are dynamically complex because they interact with each other. Previous observational and modeling studies reveal the distinct features of these components (Bao et al. 2008; Michelson and Bao 2008). First, the low-level winds in the Sacramento Valley (SV) are characterized by the

diurnal variation of the up-valley flow and the down-valley flow. Second, the central CV is characterized by the splitting of the incoming flow from the San Francisco Bay area. Third, the flow in the San Francisco Bay area is characterized by the diurnal variation of the strength of the incoming flow from the Pacific Ocean that moves through the Carquinez Strait. Fourth, the flow in the San Joaquin Valley (SJV) is characterized by the incoming flow that moves towards the south, where a low-level jet typically develops at night and interacts with the downslope flows along the foothills of the eastern side of the SJV to form the Fresno Eddy. In addition to the Fresno Eddy, interaction between the northward inflow and the nocturnal down-valley flow in the SV often leads to the formation of a counterclockwise local eddy to the north or northwest of Sacramento, known as the Shultz Eddy during the night. It remains a question as to whether or not these two eddies play a significant role in local pollution recirculation.

As documented in (Bao et al. 2008), comparisons of the observations and the simulation indicate that the WRF-Chem meteorological model captures the major characteristics of the observed low-level winds in the CV, but quantitative differences are noticeable. These differences can, in theory, be attributed to the errors in the simulated topographically induced local forcing (largely due the errors in the atmospheric boundary layer physics) and the simulated interaction between the upper-level winds and the aforementioned low-level flows.

4 SUMMARY AND CONCLUSIONS

Three-dimensional air-mass transport under fair weather conditions in California's CV between the atmospheric boundary layer to the free troposphere is investigated with a case study using the observations from the CCOS 2000 field experiment and the WRF-Chem model. First, the comparisons of the observations and the model simulation are carried out to show that the WRF-Chem model simulates the meteorological processes of this case well. Then, the movement of the tracers simulated by the WRF-Chem model is analyzed to reveal the characteristics of the three-dimensional transport. Our results indicate that the three-dimensional air-mass transport is very complex under fair weather conditions in the CV. During the day, the development of the convective ABL acts as an efficient "air pump" that transports pollutants upward as the ABL grows. However, the slope wind system around the CV plays an important role in redistributing pollutants vertically as well as horizontally. The tracer movement indicts that once lifted to the FT, the pollutants that originate in the ABL are vertically recirculated downward toward the ABL and horizontally transported by the synoptic flow. During the night, as the two major horizontal mesoscale low-level eddies (i.e., the Schultz and Fresno Eddies) are formed, the remnants of the pollution in the ABL converge horizontally and are recirculated along the foothills, where they remain at low-levels until sunrise and are then vertically redistributed as the daytime ABL develops. Under typical fair weather conditions in summer, there are two major lower tropospheric pathways for the ABL air masses to move out the CV: eastward over the Sierra Nevada and southward through the Tehachapi Pass.

REFERENCES

Bao, J.-W., S. A. Michelson, P. O. G. Persson, I. V. Djalalova, and J. M. Wilczak, 2008: Observed and WRF-Simulated Low-Level Winds in a High-Ozone Episode during the Central California Ozone Study. *J. App. Meteor. and Climat.*, **47,** 2372–2394.

Gell, G. A., S. E. Peckham, R. Schmitz, S. A. McKeen, G. Frost, W. C. Skamarock, and B. Eder, 2005: Fully Coupled Online Chemistry Within the WRF Model. *Atmos Environ.*, **39**, 6957-6975.

Henne, S., M. Furger, S. Nyeki, M. Steinbacher, B. Neininger, S. F. J. deWekker, J. Dommen, N. Spichtinger, A. Stohl, and A. S. H. Prévôt, 2004: Quantification of topographic venting of boundary layer air to the free troposphere. *Atmos. Chem. Phys.*, **4**, 497-509.

Michelson, S A and J.-W. Bao, 2008: Sensitivity of Low-Level Winds Simulated by the WRF Model in California's Central Valley to Uncertainties in the Large-Scale Forcing and Soil Initialization. *J. App. Meteor. and Climat.*, **47**, 3131–3149.

Skamarock, W. C. , J. B. Klemp, J. Dudhia, D. O. Gill, D. M. Barker, W. Wang, and J. G. Powers, 2005: A description of the Advanced Research WRF Version 2. NCAR Tech Notes-468+STR. [Available from UCAR Communications, P.O. Box 3000, Boulder, CO 80307.]

ASSESSMENT OF AIR QUALITY AND MIXING-LAYER HEIGHT IN AN ALPINE VALLEY FROM MEASUREMENTS AND NUMERICAL MODELLING

Stefan Emeis[1], Klaus Schäfer[1], Renate Forkel[1] , Friedl Obleitner[2] , Peter Suppan[1]

[1] Institute for Meteorology and Climate Research – Atmospheric Environmental Research (IMK-IFU), Forschungszentrum Karlsruhe GmbH, Garmisch-Partenkirchen, Germany
E-mail: *Stefan.emeis@imk.fzk.de*
[2] Institute of Meteorology and Geophysics, University of Innsbruck, Innsbruck, Austria

Abstract: Due to their geometrical shape Alpine valleys are strongly vulnerable to high anthropogenic emissions. Within the project ALPNAP measurements and modelling efforts have been undertaken to analyse the air quality and noise situation in several valleys of the Alps through which major trans-European traffic routes (motorway and railway) are running. Here we will present results with respect to air quality from a section of the Inn Valley east of Innsbruck. In-situ observations at the valley floor and on the slope and from a tethered balloon together with horizontally path-averaging (DOAS) and vertical profiling (SODAR, ceilometer) remote sensing instruments during winter 2005/06 yielded meteorological and air pollution data for the valley atmosphere close to and further away from the motorway/railway lines running through this valley. The highest pollutant concentrations built up during a ten-day high pressure episode with permanent snow cover which was coined by a persistent multiple layer structure with inversions in the valley atmosphere which was not broken up neither by valley nor by slope winds. A mesoscale numerical model (MCCM), with a spatial resolution of 1 km in the inner nest, has been used to simulate the air quality in this part of the valley for January 2006. Measured data and model simulations together give a good basis for reliable mitigation strategies to reduce the air pollution effects on the health of the local population. The effects of changing climate could be estimated from future frequencies of snow cover occurring in such valleys.

Keywords: *air quality, mixing-layer height, Alpine valleys, in-situ measurements, remote sensing, numerical modelling*

1 INTRODUCTION

Due to their geometrical shape Alpine valleys are strongly vulnerable to high anthropogenic emissions. This is especially true for winter and early spring when nocturnal radiative cooling over snow surfaces leads to an extremely stable thermal stratification of the valley boundary layer and the formation of persistent inversions which allow for a high accumulation of air pollutants at the valley floor.

Within the European Union INTERREG IIIb project ALPNAP (Monitoring and Minimisation of Traffic-Induced Noise and Air Pollution Along Major Alpine Transport Routes) measurements and modelling efforts have been undertaken to analyse the air quality and noise situation in several valleys of the Alps through which major trans-European traffic routes (motorway and railway) are running. Main emphasis has been laid on wintry episodes during which the strongest adverse environmental impact on the local population is expected. The results presented here will focus on air quality. Apart from in-situ measurements two further tools (ground-based remote sensing and numerical modelling with a chemistry-transport model) have been employed and are evaluated here.

2 DATA AND MODEL SETUP

The in-situ observations at the valley floor and on the slopes comprised apart from classical meteorological and air quality measurements the operation of a tethered balloon in the valley centre and the retrieval of path-averaged pollution data with a DOAS across and away to the motorway A12.

Ground-based remote sensing yielding vertical wind and aerosol profiles with an acoustic (SODAR) and an optical device (ceilometer) were performed during winter 2005/06. Acoustic and optical backscatter intensities were processed to derive the mixing-layer height and the vertical structure of the valley atmosphere (Emeis et al. 2008).

The coupled mesoscale meteorology-chemistry model MCCM (Grell et al., 2000) has been used to simulate the air quality in this part of the valley for January 2006. The model contains several online-coupled tropospheric gas-phase modules, a photolysis module and a BVOC emission module. Aerosol processes are described with the modal MADE/SORGAM aerosol module. Three nested model domains were simulated with the innermost nest having a spatial resolution of 1 km.

3 RESULTS

The measurements yielded meteorological and air pollution data for the valley atmosphere close to and further away from the motorway/railway lines running through this valley (Emeis et al. 2007, Schäfer et al.

2008). The air quality data show a clear dependence on the thermal stratification of the valley atmosphere and on the occurrences of inversions within the wintry valley boundary layer. The highest pollutant concentrations built up during a ten-day high pressure episode in January 2006, which led to a persistent multiple layer structure with inversions in the valley atmosphere which was not broken up neither by valley nor by slope winds. Figure 1 shows an extreme example for the thermal structure of the valley atmosphere which can form over a longer-lasting snow cover.

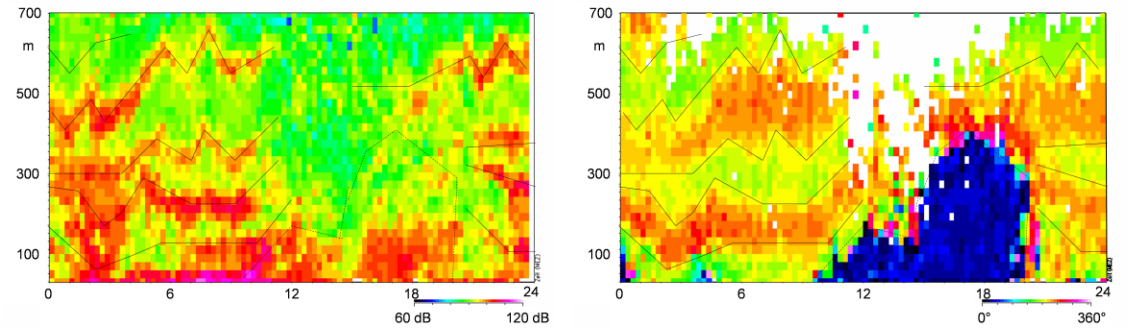

Figure 1. Acoustic backscatter intensity (left; purple and red: high, green: low) and wind direction (right; green: down-slope winds, red: down-valley winds, and blue: up-valley winds) from the SODAR measurements on January 29, 2006. The lines in the two Figures have been analysed from the wind direction changes in the right-hand frame (from: Emeis et al. 2007).

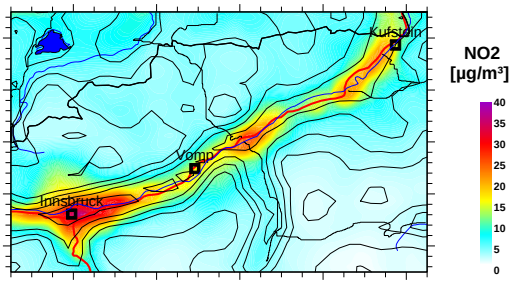

First results (Figure 2) of the mesoscale model MCCM show high concentrations of NO_2 at the valley ground and low concentrations on the mountain ridges. The high NO_2 concentrations are caused by the traffic of the highway at the valley floor, increasing by the medium and small cities as well as due to the mixing layer in which the air pollutants are trapped.

Figure 2. Simulated annual mean of NO_2 concentrations near the surface. Highest concentrations can be found at the valley floor along the highway route with peaks in and around cities. At higher altitude background concentrations of NO_2 are dominating.

4 CONCLUSIONS

Measured data and model simulations together give a good basis for the development of reliable mitigation strategies to reduce the air pollution effects on the health of the local population. As the snow cover was an important meteorological prerequisite for the formation of the extremely stable thermal stratification in the valley atmosphere, the effects of a changing climate on air quality in Alpine valleys could be estimated from future occurrence frequencies of a longer-lasting snow cover in such valleys. The possible corresponding long-term changes in atmospheric layering can influence the number of the exceedences of the EU threshold values of air pollutants as for NO_2 additionally to variances in the emission pattern and chemical processes.

Acknowledgements:
We thank the Austrian military for granting access to their Frundsberg barracks to place some of our remote sensing equipment there. The project ALPNAP (Monitoring and Minimisation of Traffic-Induced Noise and Air Pollution Along Major Alpine Transport Routes) has received European Regional Development Funding through the INTEREG IIIB Community Initiative.

REFERENCES

Emeis, S., C. Jahn, C. Münkel, C. Münsterer, K. Schäfer, 2007: Multiple atmospheric layering and mixing-layer height in the Inn valley observed by remote sensing. Meteorol. Z., **16**, 415-424.

Emeis, S., K. Schäfer, C. Münkel, 2008: Surface-based remote sensing of the mixing-layer height – a review. Meteorol. Z. **17**, 621-630.

Schäfer, K., J. Vergeiner, S. Emeis, J. Wittig, M. Hoffmann, F. Obleitner, P. Suppan, 2008: Atmospheric influences and local variability of air pollution close to a motorway in an Alpine valley during winter. Meteorol. Z., **17**, 297-309.

Grell, G. S. Emeis, W.R. Stockwell, T. Schoenemeyer, R. Forkel, J. Michalakes, R. Knoche, W. Seidl ,2000: Application of a Multiscale, Coupled MM5/Chemistry Model to the Complex Terrain of the VOTALP Valley Campaign. Atmospheric Environment, **34**, 1435-1453

COMPLEX VALLEY FLOWS AND THEIR IMPACT ON WATER VAPOUR TRANSPORT IN PRE-CONVECTIVE AND CONVECTIVE ENVIRONMENTS: A CASE STUDY

Cyrille Flamant[1], Cedric Champollion[2], Evelyne Richard[3], Laurent Labbouz[1], Frédéric Masson[4], J. Cuesta[5], P. Bosser[6], G. Pigeon[7]

[1] IPSL/LATMOS, CNRS and Université Pierre et Marie Curie, Paris, France
[2] Géosciences Montpellier, Université Montpellier II, CNRS, Montpellier, France
[3] Laboratoire d'Aérologie, CNRS et Université de Toulouse, Toulouse, France
[4] EOST, Institut de Physique du Globe de Strasbourg, Strasbourg, France
[5] IPSL/Laboratoire de Météorologie Dynamique, CNRS et Ecole Polytechnique, Palaiseau, France
[6] LOEMI/Institut Géographique National, Saint Mandé, France
[7] Centre National de Recherches Météorologiques, Météo-France and CNRS, Toulouse, France
E-mail: *cyrille.flamant@latmos.ipsl.fr*

Abstract: Complex valley flows in the Rhine Valley, as well as their impact on water vapour transport, are investigated in pre-convective and convective environments using airborne lidar data and GPS tomography, as well as high resolution numerical simulations. The analysis focuses on the 15 July case study during which an isolated convective storm was observed over the Black Forest. The reasons for null convective initiation over the Vosges are also investigated.

***K*eywords:** *Convection, airborne lidar, GPS tomography, mesoscale modelling*

1 INTRODUCTION

On 15 July 2007, an isolated convective storm was observed over the Black Forest in the framework of COPS (Convective and Orographically-induced Precipitation Study). Even though cumulus clouds were first observed to develop over the Vosges mountains (between 1130 and 1245 UTC), convective initiation (CI) was solely observed over the Black Forest on that day. Over the Black Forest, satellite imagery acquired every 15 min. show that shallow cumulii were first observed at 1145 UTC, and deep convection initiated shortly thereafter southeast of Freudenstadt (Kottmeier et al. 2008). The outputs from the European Centre for Medium-Range Weather Forecasts (ECMWF) model are broadly consistent with the satellite imagery and evidenced conditions favourable to CI over the Vosges in the 1200 UTC analysis, yet detrimental to CI in the 1500 UTC forecast issued from the 1200 UTC analysis. On the other hand, not so favourable conditions for CI were seen in the 1200 UTC analysis over the Black Forest, while the 1500 UTC forecast revealed favorable conditions for CI. The objective of this study is to understand the reason why CI did not occur over the Vosges on 15 June 2007.

2 DATA

In this study, we use a combination of high resolution observations from airborne lidar and Global Positioning System (GPS) tomography to analyse the water vapour variability in the region of the Rhine Valley associated with mountain flows. The airborne lidar LEANDRE 2 (Bruneau et al. 2001) was embarked on the SAFIRE Falcon 20 (F20). On 15 July 2007, the SAFIRE F20 performed two missions along a grid-type pattern (see Fig. 1) at an altitude of 5000 m above mean sea level (msl). The dynamics and thermodynamics at the meso-scale over the COPS domain are investigated using the mesocale model Meso-NH. Finally the synoptic situation is analysed using ECMWF analyses and forecasts.

3 THE ROLE OF DRY AIR MASSES WEST OF THE VOSGES

On this day, the synoptic situation was dominated by the presence of a deep eastern Atlantic trough and a ridge extending from the Mediterranean to Poland. In the low levels, the COPS region was under the influence of a strong southwesterly flow. In the morning, Meso-NH evidenced that a filament of dry air originating from the Mediterranean travelled northeastward reaching the Western part of the COPS domain, mostly to the West of and

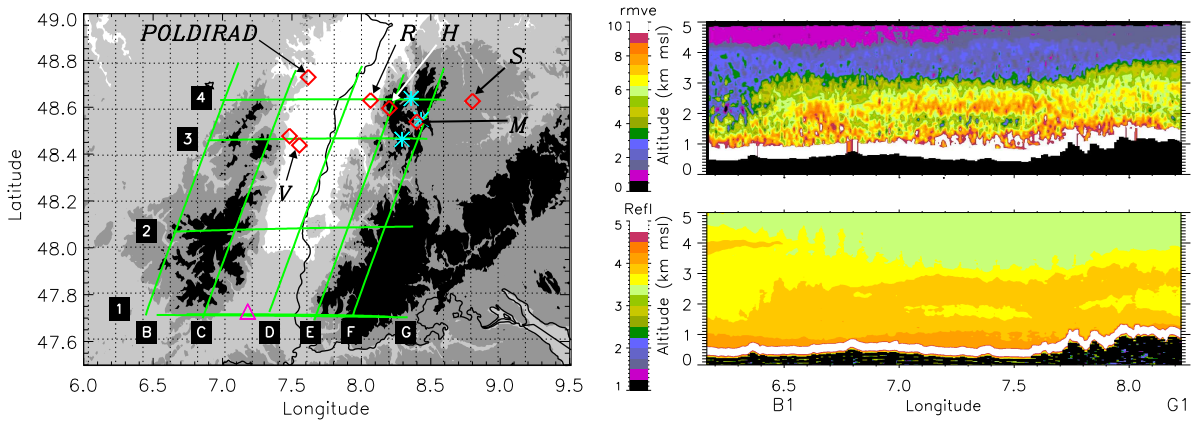

Figure 1: Left: Topography in the COPS domain. Overlain are the SAFIRE F20 flight track (green) and the location of the Supersites (red diamonds). Right: Atmopsheric reflectivity at 730 μm (bottom) and water vapour mixing ratio (top) issued from the airborne lidar LEANDRE 2 along leg B1-G1 between 0803 and 0830 UTC.

alongside the Vosges massif. This dry feature was observed in the morning by LEANDRE 2 (along leg G1-B1, West of B1, i.e. West of 6.4°E) between 2 and 3 km msl (Fig. 1). The Balloon soundings in Nancy revealed that this feature had the characteristics of a low-level jet and was present between 0000 and 1200 UTC (not shown). Airborne lidar measurements made in the afternoon (at times when CI was observed over the Black Forest) also show the presence of dry air masses West of the Vosges, and the accumulation of water vapour along the Eastern flank fo the Vosges (not shown). This was also corroborated by GPS tomography.

4 CONCLUSIONS

The variability of the water vapour field at the mesoscale investigated in pre-convective and convective environments using airborne lidar data and GPS tomography, as well as high resolution numerical simulations, suggest that the presence of a low-level jet transporting dry air masses from the Mediterranean region into the Western COPS region is mostly responsible for the absence of CI over the Vosges on 15 July 2007. The dry low-level jet feature appears to be responsible for preventing the moist air masses transported with the anabatic flow associated with the Rhine Valley-Vosges system from reaching the top of the Vosges. As a result, condistions detrimental to CI are observed over the Vosges.

Acknowledgements: *The authors wish to thank the SAFIRE (Service des Avions Français Instrumentés pour la Recherche en Environnement, www.safire.fr), the Institut Géographique National (IGN, www.ign.fr) and the Division Technique of the Institut National des Sciences de l'Univers (DT/INSU, www.dt.insu.cnrs.fr). The authors are grateful to D. Bruneau and P. Genau (LATMOS), F. Blouzon, A. Abchiche and N. Amarouche (DT/INSU) for re-fitting and operating the LEANDRE 2 system in the F/F20. Special thanks to A. Gribkoff, R. Cailloux and M. Laurens (SAFIRE) for operating the dropsonde system.*

REFERENCES

Bruneau, D., P. Quaglia, C. Flamant, M. Meissonnier, J. Pelon, 2001: The airborne lidar LEANDRE II for water-vapor profiling in the troposphere. I. System description. *Appl. Opt.*, **40**, 3450–3475.

Kottmeier, Ch., N. Kalthoff, U. Corsmeier, Ch. Barthlott, J. Van Baelen, A., Behrendt, R. Behrendt, A. Blyth, R. Coulter, S. Crewell, M. Dorninger, C., Flamant, Th. Foken, M. Hagen, C. Hauck, H. Höller, H. Konow, M. Kunz, H., Mahlke, S. Mobbs, E. Richard, R. Steinacker, T. Weckwerth, A. Wieser, and V. Wulfmeyer, 2008: Mechanisms initiating deep convection over complex terrain during COPS. *Meteorol. Z.*, **17**, 931–948.

DEVELOPMENT OF AN ALPINE LEE CYCLONE DURING MAP D-PHASE: FORCINGS FOR CYCLOGENESIS

Ron McTaggart-Cowan[1], T. J. Galarneau Jr.[2], L. F. Bosart[2] and J. A. Milbrandt[1]

[1]Environment Canada, Montreal, Canada
Email: ron.mctaggart-cowan@ec.gc.ca
[2]State University of New York at Albany, Albany, United States of America

Abstract: The development of a subsynoptic-scale cyclone in the Gulf of Genoa during the Mesoscale Alpine Project (MAP) Demonstration of Probabilistic Hydrological and Atmospheric Simulation of flood Events in the Alpine region (D-PHASE) project is investigated using analyses and model simulations. The cyclogenesis even, which led to the production of tropical storm force winds near the islands of Corsica and Sardinia, is shown to be related to the interaction between an upper-tropospheric short-wave disturbance and lower-level potential vorticity (PV) anomalies that occur as the flow in the Alpine region transitions from flow "over" to flow "around" the barrier. The role of the Alps in the initiation of these features is diagnosed using a set of model attribution tests involving modifications to the local orography. Moutain-scale PV banners and a lee-side warm anomaly are shown to combine to create a local environment conducive to sub-synoptic cyclogenesis, although the development pathway of the cyclone – as diagnosed by an eddy energy budget – depends strongly on the extent of the Alpine influence on the regional flow.

Keywords: ICAM, Alpine lee cyclogenesis, Genoa cyclones

1. INTRODUCTION

The rapid development of subsynoptic-scale cyclones in the Gulf of Genoa constitutes an important forecasting challenge for the western Mediterranean. One such event took place on 15 November 2007, during the Mesoscale Alpine Project (MAP) Demonstration of Probabilistic Hydrological and Atmospheric Simulation of flood Events in the Alpine region (D-PHASE) project Rotach and Coauthors (2009), and within 12~h led to the generation of tropical storm force winds near the islands of Corsica and Sardinia. This region is well known to favor the development of subsynoptic-scale cyclones (Buzzi and Tosi 1989), which generally occur as an upper-level trough over western Europe crosses the Alpine barrier [Pichler and Steinacker (1987) and others]. With dense coastal populations and numerous shipping lanes, such strong wind events in the western Mediterranean can have a large impact on the region despite their relatively small horizontal scale.

The present study presents a diagnosis of the key features that influence the development of the Genoa cyclone on 15 November 2007 and evaluates the ability of a set of control forecasts to simulate the evolution of the system. Section 2 briefly describes the datasets and model used for this investigation. A description of the cyclogenesis event and model simulations follows in Section 3.

2. DATA AND NUMERICAL MODEL

Two sources of analysis data form the basis for the analysis component of this study: the Canadian Meteorological Centre (CMC) global analysis (0.35° grid spacing) and the National Centers for Environmental Prediction final analysis (0.5° grid spacing). The latter data are used in calculations of air parcel trajectories and frontogenesis since the vertical motion field is not archived in the CMC analysis. A variety of observational platforms are used to both augment and evaluate the global analyses, including: an Italian radar composite for the D-PHASE project[1], Meteosat Second Generation visible and infrared satellite imagery, and QuikSCAT scatterometer data. Data from the World-Wide Lightning Location Network is used to evaluate the extent and intensity of deep convection associated with the GoG cyclone.

The GEM model is used for all simulations presented in this study. The nonhydrostatic model uses semi-implicit time-stepping and semi-Lagrangian advection (Cote et al. 1998). All simulations performed for this study are triply-nested, beginning with a global 0.35° forecast integrated from CMC analyses. A limited-area version of the GEM model (identified as CMCGEML during MAP D-PHASE) is launched simultaneously with a grid spacing of 0.135°, using the global model outputs as boundary conditions. A second nest (CMCGEMH/S) is started 6~h later with a grid spacing of 0.0225°. No convective parameterization is activated in integrations on the inner domain.

1Made available by the Agenzia Regionale Prevenzione e ambiente dell'Emilia-Romagna Servizio IdroMeteoClima (ARPA-SIM)

3. DIAGNOSIS OF FORCINGS FOR DEVELOPMENT

The development of an intense, subsynoptic cyclone in the Gulf of Genoa on 15-16 November 2007 has been analyzed, and a pair of forecast sequences have been evaluated. Three key components of the cyclogenesis event have been identified: 1) a long- ived upper-level CTD embedded in a synoptic-scale trough; 2) a lee-side surface thermal perturbation; and, 3) a primary orographic PV banner.

The passage of a short wave trough across the Alps leads to upwards-increasing PV advection and stability reduction over the Gulf of Genoa. The lower-level vortex develops along a lower-level horizontal shear line that forms in the confluence zone between easterly winds over the Gulf and the northerly Mistrals blowing off the coast of France. The influence of the Alps on the development of the GoG cyclone is highlighted by the transition of the flow from ”over” to “around” the Alpine barrier.The cold-frontal inversion near ridge-top and veering mid-level winds induce a transition to flow ``around'' the Alps on 15 November.

Before the transition, extensive precipitation occurred on the Alpine north side, and descent in the lee contributes – in conjunction with cold-frontal retardation – to the development of the lee-side warm anomaly. Following the flow transition, parcels curve cyclonically around the southwestern tip of the barrier, acquiring PV by differential friction and resulting in the formation of a primary PV banner. As shown in Fig. 1, the initiation of the cyclone in the model attribution tests occurred in a region of enhanced vorticity northwest of Sardinia that results from the superposition of these two PV features. This region is favoured for development since the ambient vorticity is readily streched by the extensive convection associated with the cold flow over the relatively warm Mediterranean waters. A noteworthy exception to this occurs in the COLD model simulation shown in Fig. 1. In this test the warm anomaly was removed, making the mountain-scale PV banner the primary feature in the Alpine lee. The upper-level disturbance couples with the banner in this case, leading to a development that occurs well to the west of the observed location (identified as Best Track in Fig. 1).

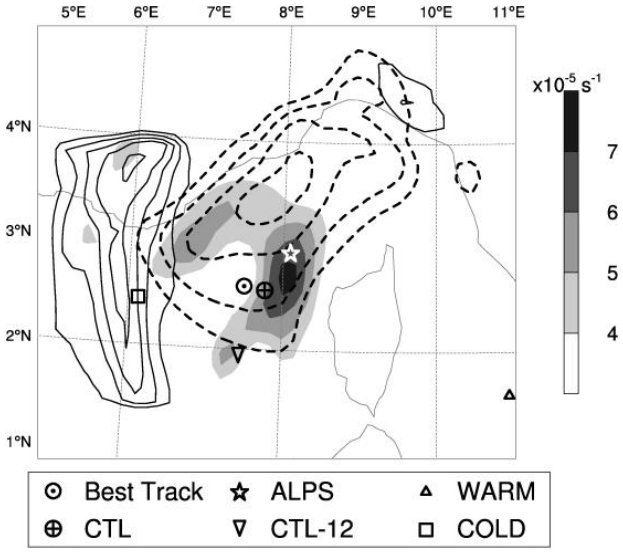

Figure 1: Relative vorticity (550-450 hPa) in shading as indicated on the greyscale bar, resulting from the combined inversion of the PV banner (solid lines show 950-600 hPa PV at 0.2 PVU intervals) and the lee-side warm anomaly (dashed ilnes show the surface potential temperature anomaly at 2 K intervals). The location of cyclogeneis in the attribution tests is shown with the symbols indicated in the legend.

The identification of the key components involved in this case of Gulf of Genoa cyclogenesis, and the interactions that occur between them during the flow transition, serve to illucidate the role of the Alps in rapid sub-synoptic scale development. A companion study investigates the sources of eddy energies associated with this event further illustrates the importance of the Alpine barrier in modulating the the development pathway (classical baroclinic versus convectively-driven) of the cyclone. These studies use modern models and high resolution datasets corroborate the findings of earlier studies and provide additional insight into the features and processes germante to Alpine lee cyclogenesis.

ACKNOWLEDGEMENTS

The authors would like to thank Kristen Corbosiero and Sergio Abarca who processed the WWLLN lighting used in this study, Mike Brennan who provided gridded QuikSCAT data, and Silvio Davolio who archived and granted us access to the ARPA-SIM radar composite.

REFERENCES

Buzzi, A. and E. Tosi, 1989: Statistical behaviour of transient eddies near mountains and implications for theories of lee cyclogenesis. *J. Atmos. Sci.,***43**, 2826-2837.

Pichler, H. and R. Steinacker, 1987: On the synoptics and dynamics of orographically induced cyclones in the Mediterranean. *Meteor. Atmos. Phys.*, **36**, 108-117.

Rotach, M. and Coauthors, 2009: MAP D-PHASE: Real time demonstration of weather forecast quality in the Alpine region. *Bull. Amer. Meteor. Soc.*, (in review).

Cote, J., S. Gravel, A. Method, A. Patoine, M. Roch and A. Staniforth, 1998: The operational CMC-MRB Global Environmental Multiscale (GEM) model. *Mon. Wea. Rev.*, **126**, 1373-1395.

A DYNAMICAL INFLUENCE OF THE HIMALAYAS ON THE WINTER MONSOON OVER SOUTHEASTERN ASIA

Sylvain Mailler[1,2], François Lott[1]

[1] Laboratoire de Météorologie dynamique, Paris, France
[2] Ecole Nationale des Ponts et Chaussées, Marne-La-Vallée, France
E-mail: *flott@lmd.ens.fr*

Abstract: Previous studies have shown (i) that the Tibetan plateau produces a significant fraction of the two components of the Equatorial Mountain Torque (EMT) in winter, (ii) that these torques are in part related to the East Asian cold surges, and (iii) that the cold surges affect the convection over the maritime continent. We show here that these relations are strong enough for the convection over the Equatorial South China Sea (ESCS) to be associated with significant signals on the two components of the EMT that can precede by a few days and more the convection. These signals are associated to surface pressure and temperature patterns that are strongly reminiscent of the East Asian cold surges. Our results therefore show that the Tibetan plateau couple dynamically the midlatitudes and the tropical region, and that the vectors of this dynamical coupling are the cold surges.

***K*eywords:** *Mountain torques, cold surges, tropical convection, winter monsoon*

1 INTRODUCTION

During the northern winter, the weather in eastern Asia, the South China Sea (SCS) and the maritime continent is dominated by the winter monsoon, where the active monsoon phase is characterized by northerly low-level winds along the East Asian coasts extending from Japan to the SCS and intense convective events over the SCS and Borneo (e.g. *Houze et al.*, 1981). As has been shown in earlier studies (e.g. *Chang et al.*, 2005), the Borneo vortex intensity and the East Asian cold surges are important in modulating this monsoon.

By showing that the convective events over the ESCS are often preceded by significant signals on the Equatorial Mountain Torque generated by the Tibetan plateau, we establish that the dynamical forcing of the Tibetan plateau on the East Asian winter monsoon is strong enough to have a direct impact on convection over this major monsoon variability center. We also verify that the vectors of this relationship between the Tibetan plateau and the monsoon convection are the cold surges.

2 DATA AND METHODS

The surface pressure and low-level temperature values are from the NCEP/NCAR reanalysis. After removing the annual and interannual variations, the resulting series will be noted $\widetilde{T}_{50m}$ and $\widetilde{P}_S$. The index $\widetilde{I}_C$ of the convective activity over the ESCS is the opposite of the average of the NOAA interpolated OLR over the sector $[105°\text{E};120°\text{E}]\times[0°\text{N};15°\text{N}]$. With this definition, positive values of $\widetilde{I}_C$ correspond to low OLR and active convection over the ESCS.

The two components $\widetilde{T}_{M,1}$ (along the Greenwich axis) and $\widetilde{T}_{M,2}$ (along the $90°$E equatorial axis) of the EMT due to the Tibetan plateau are computed following *Feldstein* (2006). A positive $\widetilde{T}_{M,1}$ results from a positive South-North pressure gradient over the topography while a negative $\widetilde{T}_{M,2}$ is associated to a West-East positive pressure gradient, as described in *Egger and Hoinka* (2008). Positive West-East pressure gradients also produce a positive polar torque $\widetilde{T}_{M,3}$ (*Lott et al.* (2004)).

The composite maps and series of Fig.1 are built using the 20 strongest positive peaks and the 20 strongest negative peaks of $\widetilde{I}_C$ from November through March (NDJFM) during the 1979-2007 period. A Student t-test is used to evaluate the confidence levels.

3 RESULTS

The composites of $\widetilde{T}_{M,1}$ and $\widetilde{T}_{M,2}$ keyed on $\widetilde{I}_C$ are shown in Fig.1a. In it we can see that there is a significant positive anomaly in $\widetilde{T}_{M,1}$ from D-6 to D-2 which peaks at D-5. After this peak in $\widetilde{T}_{M,1}$, Fig.1a shows that $\widetilde{T}_{M,2}$ becomes negative, and this lasts from D-4 to D0. To extract the intraseasonal variations that are visible on Fig.1a (periods around 20 days), we filter the series with the *Blackmon* (1976) low-pass filter that isolates signals with periods of 10 days and more.

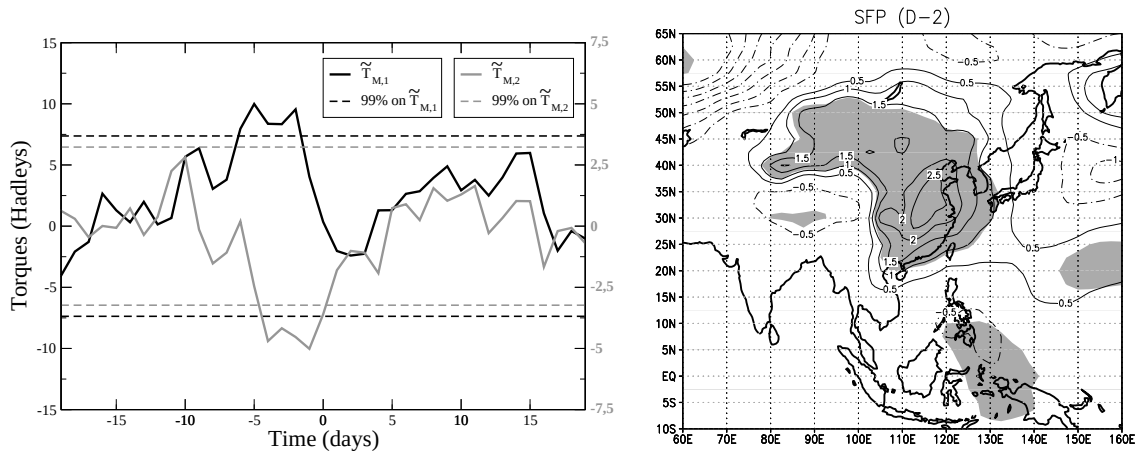

Figure 1: (a) Composite series of $\widetilde{T}_{M,1}$ (black solid) and $\widetilde{T}_{M,2}$ (gray solid) keyed on $\widetilde{I}_C$. Units for the torques are in Hadley: $1\,\mathrm{H} = 10^{18}\ \mathrm{kg\ m^2\ s^{-2}}$. The dotted lines correspond to the 99% significance level for $\widetilde{T}_{M,1}$ (black) and $\widetilde{T}_{M,2}$ (gray). (b) Composite of the IS $\widetilde{P}_S$ (hPa) two days before a peak of $\widetilde{I}_C$. Contour interval: $0.5\ \mathrm{hPa}$; positive values, light solid; negative values, light dotted; zero-contour omitted; 99% confidence, shaded.

Figure 1b shows that, two days before the convection peaks, there is a significant intraseasonal high pressure anomaly over East Asia. This signal is associated to a negative temperature anomaly, in a way that is typical of the East Asian cold surges (see *Mailler and Lott*, 2009). It is this surface pressure signal that produces the negative $\widetilde{T}_{M,2}$ at that time (Fig.1a).

4 CONCLUSIONS

The analyzes presented here reveal that the winter monsoon convective events over the ESCS are often preceded by large signals in both components of the EMT due to the Tibetan plateau. A detailed study of the surface pressure and surface temperature patterns associated to these EMT signals has been carried out by *Mailler and Lott* (2009). These authors show that the signals we described here on the two components of the EMT are associated with high surface pressure anomalies travelling from southern Siberia to the SCS within a week together with low temperature anomalies, and that this anomalies are closely linked to the East Asian cold surges.

Our results suggest that the EMT affects the onset and the break of the winter monsoon active phases. They have some predictive interest in the sense that the signals on the torques precede by a few days and more these on the convection. From a more theoretical point of view, our results are related to the fact that the orography triggers anticyclones. As there is a large body of theoretical literature in mountain meteorology related to the development of lee cyclones (see for instance *Smith* (1979)), we will need to check if these theories can be adapted to our cases in order to understand our statistical results from a theoretical point of view.

References

Blackmon, M. L. (1976), A climatological study of the 500 mb geopotential height of the Northern Hemisphere, *J. Atmos. Sci.*, *33*, 1607–1623.

Chang, C.-P., P. A. Harr, and H.-J. Chen (2005), Synoptic disturbances over the equatorial South China Sea and western Maritime Continent during boreal winter, *Mon. Weather Rev*, *133*, 489–503, doi:10.1175/MWR-2868.1.

Egger, J., and K.-P. Hoinka (2008), Mountain torque events at the Tibetan Plateau, *Mon. Weather Rev*, *136*, 389–404, doi: 10.1175/2007MWR2126.1.

Feldstein, S. B. (2006), Dynamical processes of equatorial atmospheric angular momentum, *J. Atmos. Sci.*, *63*, 565–581, doi: 10.1175/JAS3586.1.

Houze, R. A., S. G. Geotis, F. D. Marks, and A. K. West (1981), Winter monsoon convection in the vicinity of North Borneo. part I: Structure and time variation of the clouds and precipitation, *Mon. Weather Rev*, *109*, 1595–1614.

Lott, F., A. W. Robertson, and M. Ghil (2004), Mountain torques and northern hemisphere low-frequency variability. Part I: Hemispheric aspects, *J. Atmos. Sci.*, *61*, 1259–1271.

Mailler, S., and F. Lott (2009), Dynamical influence of the Tibetan Plateau on winter monsoon convection over southeast Asia, *Geophys. Res. Lett.*, *36*, L06708, doi:10.1029/2008GL036952.

Smith, R. B. (1979), Some aspects of the quasi-geostrophic flow over mountains, *J. Atmos. Sci.*, *36*, 2385–2392.

Dynamics on Vortex with Heavy Rainfall in East to Tibetan Plateau

Sixiong ZHAO[1] Shenming FU[1,2]

[1] Institute of Atmospheric Physics，Chinese Academy of Sciences, Beijing，100029, China

Email: *zhaosx @ mail.iap.ac.cn*

[2] Graduate University of Chinese Academy of Sciences，Beijing，100049, China

Abstract

Some vortexes form usually in east to Tibetan Plateau, which are called as the Southwest Vortex (SWV) because they appear in Southwest China.The majority of them form, develop and disappear in original places, only a few of them can move eastward, sometimes cause the strong heavy rainfall and severe flooding in East China. The formation and development of this kind of vortexes are the key scientific problems because of its importance in improving the prediction of disastrous weather in China. Therefore, the relevant investigation regarding this kind of the vortexes has been conducted. In this study, the vortex case of June 2008 , with the severe heavy rainfall in South China, is studied by using the reanalysis data from NCEP/NCAR, one-hour interval surface observation, intensive rawinsonde data, Satellite TBB data from FY-2C and conventional observation data. The results are as follows:

(1). The Southwest vortexes was the direct influencing system for the heavy rainfall, it developed ahead the trough in westerlies at 500 hPa and the vortex was steered by the trough, to move eastwards. The rainy area moved from west to east accompanying with SWV. The cold air played very important role and there existed significant cold advection at 500 hPa.

(2). There was the structure of weak warm core in the vortexes in upper troposphere rather than that of the cold core in the extra-tropical cyclones. However, the warm core of the SWV is weaker than that of tropical cyclone.

(3). The diagnostic analysis shows that the maintenance and intensification of vorticity were mainly associated with divergence term in vorticity equation which indicates the friction impact existed in low troposphere, especially that in planetary boundary layer in east to the Plateau.

(4). Convective activities and precipitation were always at the central area of SWV and the right-front side of the track of SWV. Convective cloud clusters were active during the heavy rainfall. Some of them belonged the meso-α or meso-β-scale systems, respectively, with the one-hour maximum of precipitation amount of 90 mm, longest period about 17 hours, and moved at almost as same as the speed of SWV. There were about 11 meso-scale rainy clusters, they are quasi-stationary or moved slowly. The interaction between the cloud clusters and the vortexes can be found and its formation mechanism seemed to be also related with The Second Kind of Conditional Instability (CISK). The release of latent heating contributed very significantly to development of the vortexes.

(5). The intensive air sounding of Guilin station, South China indicates that, the relative humidity was rich at the low levels whereas poor at the upper levels, the stratification at middle -- lower troposphere was neutral, with thermal inversion. After the SWV moved out, wind at low levels changed significantly, the CAPE decreased.

(6). Tropical system, that is, the monsoon trough extending from India, Bangladesh, Indo-China peninsula to South China and monsoon surges, associated with the monsoon trough, influenced the SWV and make the latter to re-intensify, also re-initiating the heavy rainfalls. There existed the obvious interaction between middle and lower latitude systems.

(7). Sufficient water vapor played very important role in occurrence of heavy rainfall, the Bay of Bengal and South China Sea, probably, are main water vapor source places.

(8). During the heavy rainfalls in June 2008, the SWV moved eastwards, and re-intensify in South China; the long persistence of the short wave trough at 500 hPa was closely responsible to the heavy rainfalls.

(9). The vortexes have the obvious characteristics of subtropical weather systems. This kind of vortexes is quite different from the cyclones in east to Rocky Mountains, North America and in east to Alps, Europe and more comparison studies between them should be conducted in future.

(10). The trough moved eastward accompanying with the eastward retreatment of subtropical high pressure and also the rainy area moved eastward. The subtropical high pressure system in West Pacific also plays the very important role in occurrence and maintenance of heavy rainfalls, at first, the subtropical high extend westward and quasi-stationary, so the short wave trough at 500 hPa moved very slowly, then the subtropical high pressure retreated eastward, the rainy area shifted from South China to East China with the eastward movement of the trough. A new vortex developed in the original SWV and then, replaced the latter.

(11). Based on the mentioned-above, one kind of vortex typed heavy rainfalls in South China during pre-rainy season has been proposed.

CLIMATE VARIABILITY IN NORTH-WESTERN ITALY THROUGH THE USE OF RECONSTRUCTED AND HOMOGENIZED THERMO-PLUVIOMETRIC SERIES

Simona Fratianni[1], Fiorella Acquaotta[1]

[1] Department of Earth Science, University of Turin, Turin, Italy
E-mail: *simona.fratianni@unito.it*

Abstract: In order to properly study climate variations, homogeneous series are needed. We have therefore analysed thirteen meteorological stations of Piedmont owned by SIMN (Hydrographic and Mareographic National Service) in the 1951-2006 period. We have set up a monthly series for every station and then we have applied the Standard Normal Homogeneity Test for their homogenization. These methods allowed us to estimate the real trend for each series. On the other hand, the non-parametric Mann-Kendall test has been used to understand the statistical meaning of the trend for the thermal-pluviometric series. We have calculated climate indices (frost days, days with no thaw, tropical nights, summer days, thermal sum, rainy days, density of precipitations) over WMO 30-years periods (1951-80, 1961-90, 1971-2000) and over the whole period.

Keywords: *Piedmont, temperature, precipitation, homogenization, climate change, climate indices.*

1 INTRODUCTION

In this study were analyzed climatic changes occurred in Piedmont, over the last fifty-six years. We studded the maximum and minimum temperatures and precipitation series extracted from the meteorological database of the ex-SIMN (Hydrographic National Service) now ARPA (Regional Agency for Environmental Protection) – Piedmont.

2 DATA AND METHODS

In order to create a complete database, without missing data, we have reconstructed the gap in the series We have identified the monthly, seasonal and annual gaps and considered as a gap not only the period with the total absence of records but also the range that did not have at least 80% of the data (Klein Tank and Konnen, 2003). For the reconstruction we have used three methods of spatial interpolation (Eischeid et al. 1995). For each candidate series, we have selected a maximum of four neighbouring stations.

Unfortunately, most data show non–climatic factors that may hide the real changes. The SNHT allows to detect and estimate the single shift variations of the mean value of a candidate series compared with a homogeneous reference series (Alexandersson et al. 1997). We have used the ratio for the precipitation series and the difference for the temperatures. Once identified the discontinuous value, the period antecedent must be corrected by the correction factors estimated by the test (Stépànek, 2005).

The trends have been calculated on the seasonal and annual precipitation series, on the maximum and minimum temperatures series and on the series of seasonal and annual anomalies standardized of the variable considered. In order to estimate the consistency of the series, a level of significance of 5% has been imposed, and the trends have been calculated using the non-parametric Mann-Kendall test (Bohm et al. 2001).

We have analyzed the average monthly values of the maximum and minimum temperatures and precipitation to obtain an overview of some climate indices defined by CCL/CLIVAR (Zhang et Yang, 2004).

3 RESULTS

Trends have been calculated on the reconstructed and homogenized series (Tab.1). The series with standardized anomalies of annual and seasonal precipitation of the stations located at less than 500 m of height, show decreasing trends mainly in winter and summer, save for the Varallo Sesia station, where a growing trend is recorded in winter, spring and autumn. For the stations located at a higher altitude than 500 m a.s.l., these patterns show instead a growing trend in almost all the seasons, except for winter and autumn at Salbertrand, the summer season at Piedicavallo and Bardonecchia and the winter and summer season at Valprato Soana. Despite that, for most of the series, both at an annual and seasonal level, the results of the Mann-Kendall test did not allow for the assimilation of the estimated trend. Only the trends associated with the spring and summer seasons at Vercelli and Oropa are significant in statistical terms.

The standardized anomalies of maximum and minimum temperatures show growing trends and the significance test allow for the assimilation of results. For both variables, the largest increase was determined in winter, save for the Vercelli station where, for minimum temperatures, the largest increase was found in spring, and Varallo Sesia maximum temperatures show a larger increase in summer. Growing and statistically

acceptable trends have also been calculated for the annual temperatures series (Tab.2). At the Vercelli, Turin and Luserna S. G. stations, the largest increase is recorded within the minimum temperature series, at Varallo Sesia and Asti within maximum temperatures.

Stations	Latitude	Longitude	Elev.[m]	Winter	Spring	Summer	Autumn	Year
Vercelli	45°19'32"	08°23'26"	135	(-)	(-)	(-) p=0.01	(+)	(-)
Asti	44°53'09"	08°12'48"	152	/	/	/	/	(-)
Torino	45°04'49"	07°40'25"	270	(-)	(-)	(-)	(-)	(-)
Cumiana	44°57'53"	07°23'31"	327	(-)	(-)	(-)	(-)	(-)
Varallo Sesia	45°49'14"	08°16'30"	453	(+)	(+)	(-)	(+)	(-)
Luserna S. G.	44°48'50"	07°14'32"	476	(-)	(-)	(-)	(-)	(-)
Susa*	45°08'10"	07°05'33"	520	/	/	/	/	(-)
Salbertrand*	45°04'20"	06°53'42"	1010	(-)	(+)	(+)	(-)	(-)
Piedicavallo*	45°41'35"	07°57'26"	1040	(+)	(+)	(-)	(+)	(+)
Oropa	45°37'40"	07°58'56"	1180	(+)	(+) p=0.01	(+)	(+)	(+)
Bardonecchia*	45°04'33"	06°43'03"	1353	(+)	(+)	(-)	(+)	(-)
Piamprato*	45°33'28"	07°34'27"	1555	(-)	(+)	(-)	(+)	(+)
Ceresole Reale*	45°28'08"	07°08'25"	2260	(+)	(+)	(+)	(+)	(+)

Table 1. Geographical location of the meteorological stations during the period 1951-2006. * Stations that have measured only the precipitation variable. Pattern of seasonal and annual trends found for every station: (-) decreasing trend; (+) growing trend; / not calculated trend. For Vercelli and Oropa stations, the probability value associated with the Mann Kendall test ($p<0.05$) is also shown, indicating that the trend calculated is statistically acceptable.

Stations	Maximum temperatures (°C/yr)		Minimum temperatures (°C/yr)	
Vercelli	+0.03±0.01	p=0.01	+0.05±0.01	p=0.001
Asti	+0.03±0.01	p=0.01	+0.006±0.008	p=0.001
Torino	+0.03±0.01	p=0.003	+0.04±0.01	p=0.001
Luserna S. G.	+0.05±0.01	p=0.001	+0.060±0.004	p=0.001
Varallo Sesia	+0.04±0.01	p=0.001	+0.03±0.01	p=0.001
Oropa	+0.04±0.01	p=0.001	+0.04±0.01	p=0.001

Table 2. Maximum and minimum annual temperatures trends; p shows the significance of the Mann-Kendall test.

We have also selected three periods of 30-years defined by WMO (1951-1980, 1961-1990 and 1971-2000) and we have individualized that the minimum values of the precipitation, the number of rainy days and the density of rain are always found in the second period, 1961-1990. Besides the changes individualized over time in all stations have also been revealed in the pluviometric regimes. The main change was the shift from a subalpine regime, with its main maximum in autumn to a prealpine regime with its main maximum in spring.

We have also analyzed the average monthly values of the maximum and minimum temperatures and some climate indices calculated on the three period of 30-years. By comparing the first and last 30-years period of the minimum temperature series, a 0.7 °C increase is shown, while for maximum temperatures the difference corresponds to 0.5°C; as a result, the number of tropical days has also grown. A decrease in the number of days of frost (from 80 to 67) and days without thaw (from 11 to 6 days) can be instead observed.

In accordance with the national and international bibliography, the minimum temperatures series have showed an increase greater than the maximum temperatures series and this have caused a decrease, over the years, in the number of months classified cold.

Acknowledgements: *The authors wish to thank ARPA Piedmont and in particular Roberto Cremonini, Manuela Bassi and Barbara Cagnazzi for supplying data and the suggestions given in this study.*

REFERENCES

Alexandersson, H. and A. Moberg, 1997: Homogenization of Swedish temperature data. Part 1: Homogeneity test for linear trends. Int. J. Climatol. Volume **17**, 25-34.

Bohm, R., I. Auer, M. Brunetti, M. Maugeri, T. Nanni and W. Schoner, 2001: Regional temperature variability in the European Alps: 1760-1998 from homogenized instrumental time series, Int. J. Climatol., Volume **21**, 1779-1801.

Eischeid, J., C. Baker, T. Karl and H. Diaz, 1995: The quality control of long-term climatological data using objective data analysis, Journal of Applied Meteorology, Volume **34**, 2787-2795.

Klein Tank, A. and G. Konnen, 2003: Trends in indices of daily temperature and precipitation extremes in Europe, 1946-99, Amer. Meteorol. Soc. **16**, 3665-3680.

Stèpànek, P., 2005: AnClim, software for time series analysis, Dept. of Geography, Fac. of Natural Sciences, MU Brno.

Zhang, X. and F. Yang, 2004: RclimDex (1.0), User manual, 23 pp.

AN ALPINE CLIMATOLOGY OF EXTREME EVENTS

Sophie Fukutome, Mark Liniger, Chritoph Frei

Federal Office of Meteorology and Climatology MeteoSwiss, Zurich, Switzerland
E-mail: *sophie.fukutome@meteoswiss.ch*

Abstract:
A climatology of extreme weather events is presented for the part of the Alpine region located in Switzerland. The General Extreme Value (GEV) Theory is used to estimate the distribution of maxima and/or minima of various climatological parameters at the stations of the Swiss Meteorological Observation Network. These parameters include precipitation, temperature, wind gusts and wind speed, snow, and consecutive dry days.

Keywords: *Extremes, Alps, climatology*

1 INTRODUCTION

Understanding today's climate requires knowledge of extreme aspects of the climate and their frequency. Especially in the Alpine Region, events such as heat waves, droughts, or heavy precipitation can have dire consequences. Our purpose is to provide a climatology of return periods and/or return values of climatological parameters relevant to extreme weather in Switzerland, which covers a large part of the alpine region.

2 DATA AND METHOD

The data used in the present study stems were measured at the stations of the Swiss Meteorological Observation Network. The parameters chosen encompass precipitation, temperature, wind, fresh snow, and the number of consecutive dry days. For precipitation and snow, various levels of aggregation, such as sums over 1, 2, 3, 4, 5, or 10 days are also examined. For precipitation, seasonal analyses are performed as well. For temperature, minima are also analyzed.

The Block Maxima method of the classical Extreme Value theory (Coles, 2001) is applied, in which the General Extreme Value (GEV) distribution is fitted to the maxima or minima of blocks of data. The parameters of the distribution are estimated with the maximum likelihood method. Confidence bounds with respect to the best estimate are estimated with the profile log-likelihood method.

Because of the large number of stations, the process is entirely automatized. The Kolmogorov-Smirnov test is implemented with a randomization procedure to automatically discard stations at which the data is incompatible with the best estimate.

3 RESULTS AND CONCLUSIONS

Maps of the 1-day and 5-day precipitation return values for a 30-year return period reveal some of the characteristics of the climate in the alpine region. In the summer, thunder-storms bring heavy precipitation to the pre-Alps, or the Tessin (Fig. 1 and 2, left-hand panel). In winter, low-pressure systems bring about precipitation events that extend over several days, hence the low values over the Swiss Plateau (Fig. 1 and 2, right-hand panel). These lasting winter events are also responsible for the smaller difference between summer and winter values in the Swiss Plateau for 5-day precipitation return values (fig. 2). The pattern of the 5-day precipitation return values reveal the lack of extended periods of rain in the summer in the Rhone Valley.

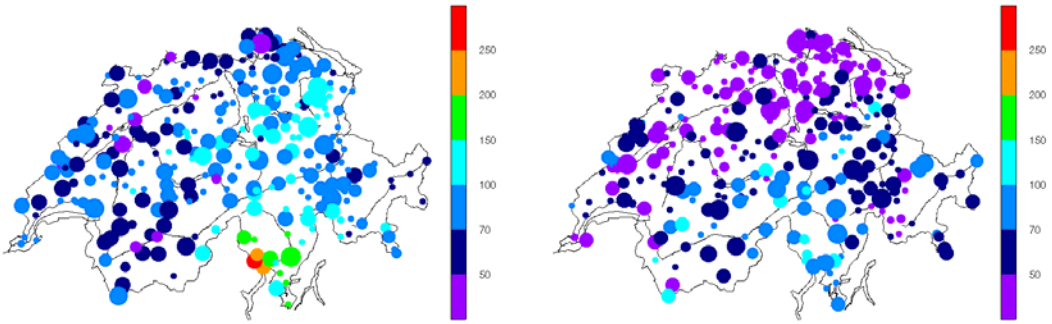

Figure 1. Return values of 1-day precipitation for a 30-year return period [mm]. Left: summer. Right: winter. The size of the dots is proportional to the length of the time series (longest: 1864-2008; shortest: 1964-2008).

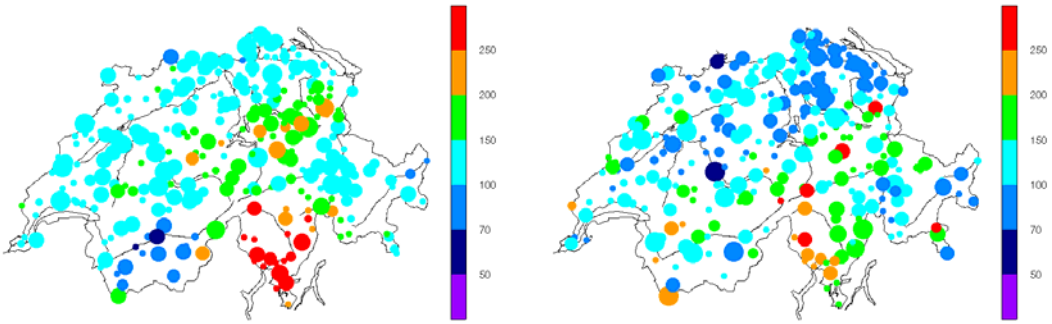

Figure 2. Return values of 5-day precipitation for a 30-year return period [mm]. Left: summer. Right: winter. The size of the dots is proportional to the length of the time series (longest: 1864-2008; shortest: 1964-2008).

Similar maps for fresh snow (not shown) show, as expected, an increase of the return values with altitude, but also highlight stations with particular extreme value behavior due to the topographical configuration. Valleys prone to Föhn can be recognized by the large return values of the mean wind speed.

In general, it can be said that the maps of return values for given return periods reflect the characteristics of the climate in the alpine region, and bring to light the areas liable to frequently suffer intense climatic events.

REFERENCES

Coles, S., 2001: An Introduction to Statistical Modeling of Extreme Values, 208 pp., Springer, New York.

Stephens, M. A., 1970: Use of the Kolmogorov-Smirnov, Cramer-von Mises and related statistics without extensive tables, J. Roy. Stat. Soc., **32B**, 115-122.

Winter storms with high loss potential in a changing climate: a regional perspective

Monika Rauthe[1], Michael Kunz[1], Susanna Mohr[1]

[1] Institute for Meteorology and Climate Research University Karlsruhe / Forschungszentrum Karlsruhe, Karlsruhe, Germany
E-mail: *monika.rauthe@imk.uka.de*

Abstract: In the RESTER (Strategien zur Reduzierung des Sturmschadenrisikos für Wälder) project the impacts of extreme storm events on the forests in Germany are analysed. The regional storm climate is quantified by means of wind gusts from regional climate models (REMO and CLM). Extreme value statistics are applied to estimate the gust wind speeds of a specific return period at every grid point. There is a systematic underestimation of the gust wind speeds in comparison to the observations (1971 – 2000), but the spatial patterns due to the orographic influences are well reproduced by the regional models. They are able to resolve partially the orographic amplifications on wind speeds, what is the big advantage over the coarse resolution of the global models. In the future (2021 – 2050) changes of the storm climate in Southern and Central Germany are not well-defined, while in Northern Germany an increase of the storm activity seems to be likely. Apart from the analysis of single model runs an ensemble composite of different models and scenarios is created to quantify the probability of the changes.

***K*eywords:** *winter storm, orography, climate change, RESTER*

1 INTRODUCTION

According to the recent publications of the IPCC, climate changes are unequivocal and changes in the global climate system will increase in the following decades (IPCC 2007). Concerning winter storms as reproduced by global climate models, an enhancement especially of severe cyclones over Europe is found (see review by Ulbrich et al. (2009) and references therein). Changes of the strength and/or occurrence of extreme natural hazards on the regional scale, however, are only partially known. Due to the low resolution of current global climate models, regional effects can be hardly estimated - especially for parameters like wind speed or precipitation, which are strongly amplified by local scale conditions (e.g. orographic effects). Because of the high loss potential of winter storms the knowledge about changes of the storm climate on a regional scale is very important. Our investigations are conducted in the framework of the research project "Herausforderung Klimawandel" funded by the federal state of Baden-Württemberg. Within the RESTER project, we characterises the changes in winter storm climate in Germany with a special focus on the region of Baden-Württemberg in the southwest of Germany.

2 DATA AND METHODS

This study is based on different data sets from regional climate models (REMO and CLM), which are are both forced by the global climate model ECHAM5. In contrast to ECHAM5 with a horizontal resolution of 2.5°, REMO and CLM have a resolution of about 10 and 18 km, respectively. For the projection period, the calculations include the IPCC emission scenarios A1B, A2 or B1 (IPCC 2007). Extreme value statistics are applied to quantify the storm climate. The analyses are based on the time series of wind gusts at each grid point. Using the method of independent storms with a minimum distance of 48 h for the hourly values and the peaks over threshold method, the maximum gusts of the 100 strongest events are fitted with the generalized Pareto distribution (Palutikof et al. 1999). The strength of storms of a specific return period is estimated from this distribution. This analysis is applied to every single grid point for both the control period (1971 – 2000) and the projection period (2021 – 2050).

3 RESULTS

To estimate the reliability of the regional climate models, they are evaluated for the control period against the so-called storm hazard map from CEDIM (Center for Disaster Management and Risk Reduction Technology) published by Heneka et al. (2006). Despite the systematic underestimation of the gust wind speeds the spatial patterns due to the underlying orography are well reproduced by the regional models. Altogether, the regional climate models are able to resolve the local amplifications of wind speeds, e.g. due to orography and land use. This is a big advantage over the coarse resolution of the global models. The underestimation of the gust speeds in the simulations is not relevant in the following, because only relative climate change signals are investigated.

Expected changes of the storm climate are analysed for the gust speeds of a 10-year return period. They vary in the different parts of Germany. The results of the single models show that the storm activity in Northern Germany will increase about 5 – 10% in the future. Also in Central and Southern Germany there is no clear trend, i.e. no

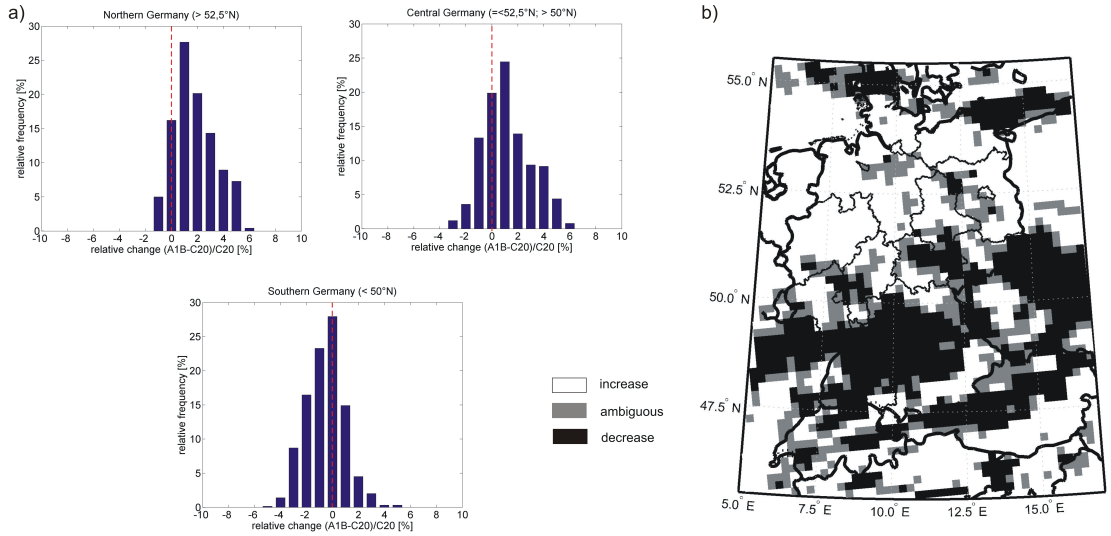

Figure 1: Relative gust wind speeds between the projection and control period relative to the control period for three parts of Germany of a 10-year return period. a) Ensemble mean of the seven regional climate simulations. b) Probable changes larger/smaller than $\pm 0.5\%$ predicted by the majority of the models.

strong changes of storm climate has to be expected. It has to be noted, though, that the changes of the storm climate in regional models greatly depend on the changes in the utilised global model. The ensemble, which is created by seven regional models runs on a uniform grid, confirm the result mentioned before. Figure 1a displays the histograms of relative changes of the gust wind speed for the ensemble mean in different parts of Germany. Furthermore, most likely changes of the storm climate can be identified by the ensemble composite (Fig. 1b). In Northern Germany, the increase of gusts is quite likely. In Central and Southern Germany the trends are indifferent and in some parts even a decrease of the storm activity seems to be possible. It has to be emphasised that such a differentiation between the regions is only possible by means of regional climate models.

4 OUTLOOK

Apart from the data presented here, CLM simulations with a resolution of ~ 7 km are available at our institute. First investigations show that the storm climate in Southern Germany exhibits no clear trend, but an influence of the orography is obvious. In the future, the CLM-7-km data will be also integrated in the ensemble approach.

In addition to the strength of the storms their horizontal extent is an important factor for the loss potential. A so-called storm index, which takes both the strength and horizontal extension of storms into account, is calculated following Della-Marta et al. (2009). First results show no large differences compared to the results of the grid-point analysis. In the future, these results will be linked with the economic losses by the storms.

Acknowledgements:
We thank the Max-Planck-Institute for Meteorology in Hamburg for conducting and providing the ECHAM5 and REMO model data. The REMO simulations were commissioned by the German Federal Environment Agency. The CLM simulations are part of the so-called "Konsortialläufe".

REFERENCES

Della-Marta, P. M., H. Mathis, C. Frei, M. A. Liniger, J. Kleinn and C. Appenzeller, 2009: The return period of wind storms over Europe, *Int. J. Climatol.*, **29**, 437 – 459, doi:10.1002/joc.1794.

Heneka, P., T. Hofherr, B. Ruck and C. Kottmeier, 2006: Winter storm risk of residential structures - model development and application to the German state of Baden-Württemberg, *Nat. Hazards Earth Syst. Sci.*, **6**(5), 721–733.

IPCC, 2007: *Climate Change 2007: the physical science basis: contribution of Working Group I to the Fourth Assessment Report of the Intergovernmental Panel on Climate Change*, [S. Solomon, D. Qin, M. Manning, Z. Chen, M. Marquis, K. B. Averyt, M. Tignor and H. L. Miller eds.], Cambridge University Press, 996 pp.

Palutikof, J. P., B. B. Brabson, D. H. Lister and S. T. Adcock, 1999: A review of methods to calculate extreme wind speeds, *Met. Appl.*, **6**, 119–132.

Ulbrich, U., G. C. Leckebusch and J. G. Pinto, 2009: Extra-tropical cyclones in the present and future climate: a review, *Theoret. and Appl. Climatology*, doi:10.1007/s00704-008-0083-8, published online.

SATELLITE-BASED RETRIEVAL OF GLOBAL RADIATION OVER COMPLEX TERRAIN: A CLIMATOLOGY FOR THE ALPS

Rebekka Posselt[1], Bruno Dürr[2], Reto Stöckli[1], Richard Müller[3], Mark Liniger[1]

[1] Federal Office for Meteorology and Climatology MeteoSwiss, Zürich, Switzerland
[2] Sunergy GmbH, Buchs, Switzerland
[3] Deutscher Wetterdienst DWD, Offenbach, Germany
E-mail: *rebekka.posselt@meteoswiss.ch*

Abstract: Meteosat second generation (MSG) satellite data is used to derive a climatology of surface incoming solar radiation (SIS) over the Alps. Monthly mean SIS maps, as well as the respective anomalies are made available over Switzerland from 2004 to the present. Comparisons with surface based station measurements and climatologies show a very good agreement.

Keywords: *ICAM, surface radiation, satellite,snow*

1 INTRODUCTION

The Satellite Application Facility on Climate Monitoring (CM-SAF, `www.cmsaf.eu`) is part of EUMETSAT's satellite data processing with a special emphasis on the retrieval of climate variables such as cloud parameters, radiative budget and water vapour. The MeteoSwiss contribution to CM-SAF is the validation and improvement of the standard surface incoming shortwave (SIS) radiation product especially over complex terrain such as the Alps. Special attention is drawn to the radiative influence of snow. For this purpose accurate retrieval of clouds over snow is required and the radiative properties of snow have to be considered.

2 DATA AND METHODS

Data from the Meteosat Second Generation (MSG) satellites (Meteosat 8 and 9, in operation since 2004) are used (Schmetz et al., 2002). They provide data in 12 channels covering the visible (VIS) and the infrared (IR) spectra on a horizontal resolution of 3km every 15 min. Additionally, there is a high resolution visible (HRV) channel with a spatial resolution of 1km.

Several IR and VIS channels are used to obtain information about the state of the atmosphere and the surface for each pixel. This information is then used to calculate the cloud index that accounts for radiation reflected from snow in addition to attenuated radiation due to clouds (Dürr and Zelenka, 2009). The SIS is then calculated by scaling the expected clear sky radiation with the cloud index. The clear sky radiation depends on the sun's elevation, surface elevation and the atmospheric turbidity. The latter describes the radiative impact of water vapour, atmospheric aerosols, ozone, etc. on the atmospheric transmission.

Figure 1 shows the monthly mean cloudindex (≤ 0: cloud free, ≥ 1: overcast) for December 2005. The original Heliosat algorithm (upper panel) (Beyer et al., 1996; Hammer et al., 2003) shows a very high cloud index over snowy regions (i.e., in the mountains) which is largely reduced by the new snow detection algorithm (lower panel).

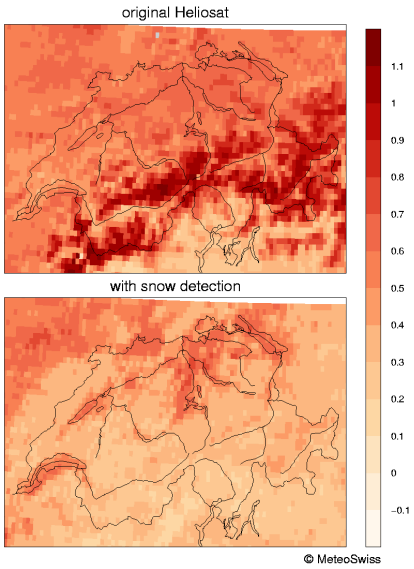

Figure 1: Monthly mean cloud index for Dec 2005 for the original Heliosat and for Heliosat with snow detection

3 RESULTS AND QUALITY ASSESSMENT

A complete 5-year dataset of SIS based on METEOSAT 8 and 9 data is derived. The derived SIS climatology is available as monthly mean SIS and corresponding monthly anomalies over Switzerland for the period 2004-2008. Figure 2 shows the overall mean SIS over Switzerland for the years 2004-2008. The usage of the HRV channel allows for a clear distinction of valleys and mountains. The mountainous regions receive larger amounts of shortwave radiation, amongst others due to snow effects and less foggy/cloudy days (than in the lowlands).

The satellite-retrieved SIS is validated with surface measurements from the Alpine Surface Radiation Budget (ASRB) network in Switzerland. Figure 3 displays two intercomparisons for the hourly mean SIS at the stations Payerne (lowlands) and Jungfraujoch (mountains) for March 2005. In general, the agreement is high with correlation coefficients of 0.94 for Payerne and 0.89 for Jungfraujoch. However, on some occasions the spread is rather large (marked with red points) which is more frequent at the mountainous station than at the lowland

station. The spread results partly from algorithm deficiencies in separating clouds from snow but also from the non-representiveness of comparing local station data to spatially integrated satellite measurements (Zelenka et al., 1999).

For specific climatological events, the physical consistency is further investigated using complementary high-resolution climate monitoring products inferred from surface observations over Switzerland. Figure 4 shows the anomalies of SIS, temperature and sunshine duration (last two: `www.meteoswiss.admin.ch/web/en/climate/climate_today/swiss_anomalies.html`), respectively, for April 2007. This month was characterised extremely high temperatures (more than $5\,^{\circ}\mathrm{C}$ higher than normal for Switzerland). Especially, the lowlands north of the Alps experienced additional radiative input of more than $45\,\mathrm{Wm}^{-2}$ which is consistent with strongly increased sunshine hours in that region.

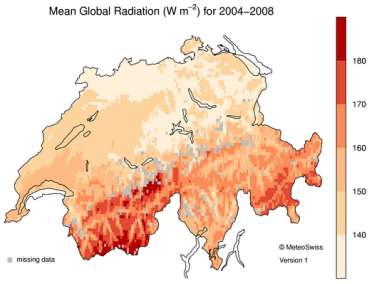

Figure 2: Mean SIS over Switzerland (2004-2008) [Wm^{-2}]

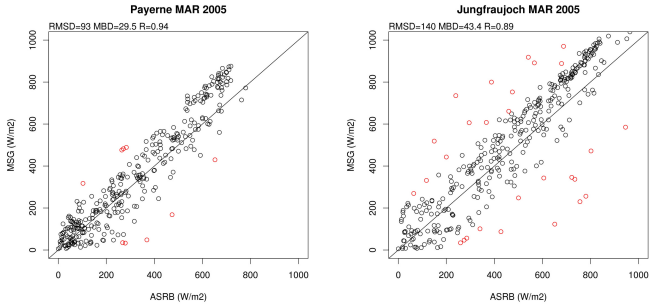

Figure 3: Comparison of SIS from ASRB Stations Payerne and Jungfraujoch to SIS retrieved from MSG satellites for March 2005

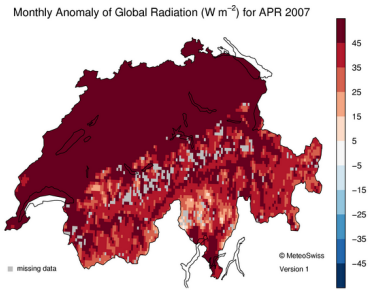

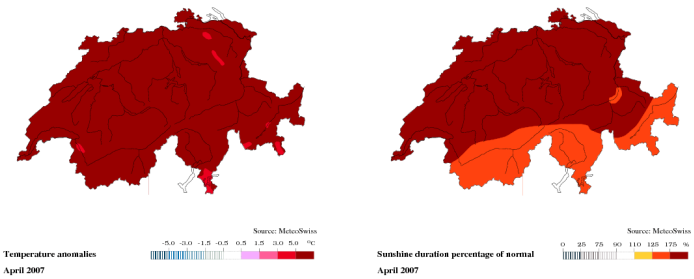

Figure 4: Monthly mean SIS anomaly, temperature anomaly and sunshine duration anomaly for Apr 2007

4 SUMMARY AND CONCLUSIONS

A 5-year climatology for satellite-derived SIS over Switzerland is presented. A new snow detection algorithm helps to distinguish clouds and snow in the alpine region which results in a more accurate estimation of SIS in that regions. There is a high agreement with radiation measurements at the surface, nevertheless, the cause for the partly large spread has still to be investigated. The presented satellite based SIS climatology complements the results and findings of climatologies derived from station based measurements. However, the satellite based climatology allows for a higher spatial resolution and provides information in regions that are not covered by measurement stations. The anomaly maps will be made available soon on `http://www.meteoswiss.admin.ch/web/en/climate/climate_today/swiss_anomalies.html`.

REFERENCES

Beyer, H. G., C. Costanzo, and D. Heinemann, 1996: Modifications of the Heliosat procedure for irradiance estimates from satellite images. *Solar Energy*, **56**, 207–212.

Dürr, B. and A. Zelenka, 2009: Deriving surface global irradiance over the Alpine region from METEOSAT Second Generation data by supplementing the HELIOSAT method. *Int. J. Rem. Sens.*, **(in press)**.

Hammer, A., D. Heinemann, C. Hoyer, R. Kuhlemann, E. Lorenz, R. Müller, and H. Beyer, 2003: Solar energy assessment using remote sensing technologies. *Remote Sens. Environ.*, **86 (3)**, 423–432.

Schmetz, J., P. Pili, S. Tjemkes, D. Just, J. Kerkmann, S. Rota, and A. Ratier, 2002: An Introduction to Meteosat Second Generation (MSG). *Bull. Amer. Meteor. Soc.*, **83 (7)**, 977–992.

Zelenka, A., R. Perez, R. Seals, and D. Renne, 1999: Effective Accuracy of Satellite-Derived Hourly Irradiances. *Theor. Appl. Climatol.*, **62**, 199–207.

Comparison of ground-based UV irradiance measurements with satellite-derived values and 1-D- and 3-D-radiative transfer model calculations in mountainous terrain

J.E. Wagner[1], A. Arola[2], M. Blumthaler[3], M. Fitzka[1], J.P. Gobbi[4], R. Kift[5], A. Kreuter[3], H. Rieder[6], S. Simic[1], A. Webb[5], P. Weihs[1]

[1] Institute for Meteorology, University of Natural Resources and Applied Life Sciences, Vienna, Austria
[2] Finnish Meteorological Institute, Kuopio, Finland
[3] Devision for Biomedical Physics, Innsbruck Medical University, Innsbruck, Austria
[4] Institute of Atmospheric Sciences and Climate, Aerosol Remote Sensing Group, Roma, Italy
[5] Devision for Earth, Atmospheric and Environmental Sciences, University of Manchester, Manchester, UK
[6] Institut for Atmospharic and Climate Science, ETH Zurich, Zurich, Switzerland
E-mail: *jochen.wagner@boku.ac.at*

Abstract: Results from three different calculation methods (satellite retrieval, 1-D- and 3-D-radiative transfer model) for UV radiation in terms of UV-Index, erythemally weighted daily doses and spectrally resolved UV-Irradiance at 305, 310, 324 and 380nm are presented and compared with ground-based high quality measurements. The real case study is performed in very inhomogenous terrain for cloudless situations. 1-D-simulations show the best agreement ($\pm 10\%$) with the measurements whereas 3-D-model simulations and satellite retrieved values often differ much more. Satellite retrieved values significantly underestimate radiation for most stations, while results from 3-D-model calculations mostly overestimate radiation.

***K*eywords:** *UV irradiance, albedo, radiative transfer model, OMI, Grimaldi, Disort*

1 MATERIAL AND METHODS

The ground-based measurements were performed during two measurement campaigns in late summer 2007 and late winter 2008 in Innsbruck and one measurement compaign in May 2008 at Sonnblick.

Satellite-derived UV-values were taken from Ozone Monitoring Instrument (OMI, see LEVELT ET AL. (2006)). For the 1-D-radiative transfer calculations we used the DISORT solver (see DAHLBACK and STAMNES (1991)). The 3-D-radiative transfer calculations were performed with the Monte Carlo Model GRIMALDI (see SCHEIRER and MACKE (2001) and SCHEIRER and MACKE (2003)).

Table 1: *Input parameter for the DISORT model are shown. The mountain stations are modeled as point above a surface with the mean elevation height of the digital elevation model used for the 3-D calculations. α and β stand for the aerosol Angstrom coefficients and sza is the solar zenith angle. The sza varies slightly from station to station (due to different geographic location) and from wavelength to wavelength (due to time differences in the order of one to three minutes of the measurements).*

Measurement site	surface	albedo	o_3	α	β	sza	date	time
Innsbruck	616m	0.01	265 DU	1.1	0.020	58.56°- 58.61	24.02.2008	12:31-12:32 UTC
Lans	833m	0.01	265 DU	1.1	0.016	58.50°- 58.66°	24.02.2008	12:31-12:33 UTC
Hafelekar	1386m	0.01	260 DU	1.1	0.004	58.55°- 58.71°	24.02.2008	12:31-12:33 UTC
Bodenhaus	1296m	0.01	349 DU	1.08	0.022	34.40°- 34.72°	09.05.2008	12:01-12:03 UTC
Kolm-Saigurn	1600m	0.01	349 DU	1.08	0.028	33.09°- 33.37°	09.05.2008	12:01-12:02 UTC
Sonnblick	2059m	0.01	345 DU	1.08	0.0008	34.35°- 34.67°	09.05.2008	12:01-12:03 UTC

2 RESULTS

To compare the results from satellite retrieval and 1-D- and 3-D-radiative transfer models we calculated ratios (measurement/model) shown in figure 1. Results from the 1-model show clearly the best agreement. The values agree always within 10%.

The 3-D-radiative transfer model agrees also very well for Sonnblick section, but there are huge differences at Innsbruck section. We investigate this behavior at the moment. One reason could be a wrong estimation of surface albedo for the Innsbruck section. Other effects, like aerosols, time differences and thus slighly inaccurate solar zenith angles due to the plan-parallel approximation, border effects (periodic border conditions are assumed) and the use of standard profiles for Rayleigh scattering and ozone absorption should contribute to the uncertainty by less than 5%.

Satellite retrieved values mostly underestimates the observed values significant (see figure 1). The agreement for the three stations of the Innsbruck measurement compaign is better than for the Sonnblick region. First of all

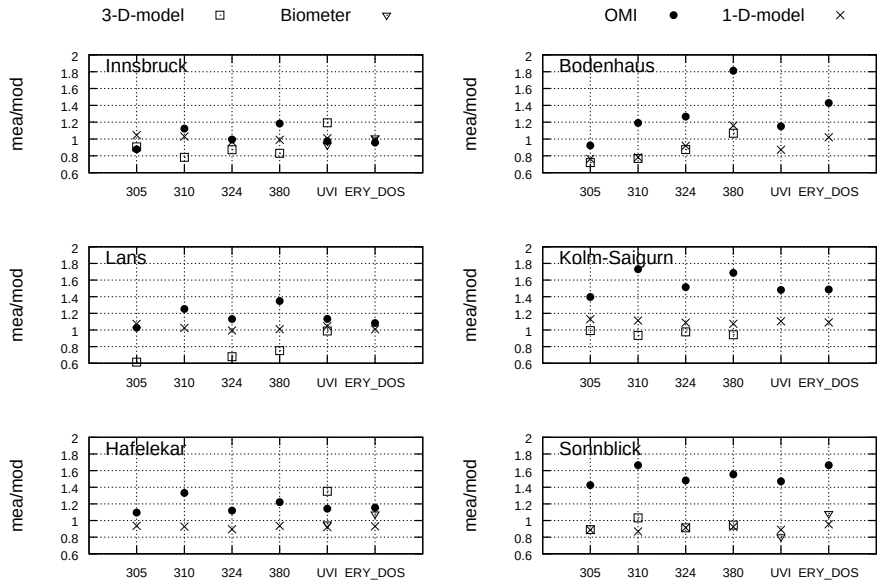

Figure 1: *The ratio of measured and calculated UV radiation (irradiance at 305nm, 310nm, 324nm, 380nm, UV-Index and erythemally weighted daily dose) is shown. Filled circles denote satellite-derived data, crosses denote 1-D-model and squares 3-D-model calculations. In addition triangles show the broadband measurements performed with Biometers. The left column shows results from February 24th 2008 12:30 UTC. The right column shows results from May 7th 2008 12:20 UTC.*

the altitude used in the satellite retrieval differs a lot from the real station height in our area of interest, due to the coarse resolution of the satellite data. Furthermore the cloud detection algorithm misinterprets snowcovered areas as clouds. In this areas the UV-radiation is scaled down.

3 CONCLUSIONS

One-dimensional radiation transfer models are able to reproduce ground-based irradiance measurements in mountainous regions very well. However the good agreement with measurements is very likely due to the compensation of significant effects (restriction of the horizon by the mountains and enhancing the radiation due to reflection at the (snow covered) ground and scattering in the air. To study such effects 3-D-radiative transfer models are indispensable. However the results from 3-D-model in this study are preliminary, since the number of "photons" used for the calculations (10^8) is too low to get the desired accuracy of about 5%. Model runs with 10^9 "photons" are already in preparation. With the current OMI-retrieval algorithm it is very difficult to get very accurate UV-values for ground stations in very mountainous terrain. To improve the algorithm for such areas, one should address issues like station height and cloud detection in (partly) snowcovered terrain.

Acknowledgements:
This work was mainly financed by the Austrian Science Fund (FWF) Projektnumber: P18780-N13.

References

DAHLBACK, A., STAMNES, K., 1991: A new spherical model for computing the radiation field available for photolysis and heating at twilight. Planetary and Space Science **39(5)**, 671–683.

LEVELT, P. F., VAN DEN OORD, G. H., DOBBER, M. R., MIÄLKKI, A., VISSER, H., DE VRIES, J., STAMMES, P., LUNDELL, J. O., SAARI, H., 2006: The Ozone Monitoring Instrument. IEEE Transactions on Geoscience and Remote Sensing **44(5)**, 1093–1101.

SCHEIRER, R., MACKE, A., 2001: On the accuracy of the independent column approximation in calculating the downward fluxes in the UVA, UVB and PAR spectral ranges. Jounal of geophysical Research **106(D13)**, 14,301–14,312.

SCHEIRER, R., MACKE, A., 2003: Cloud inhomogeneity and broadband solar flux. Jounal of geophysical Research **108(D19)**, doi:10.1029/2002JD003,321.

MAP D-PHASE: lessons learned and future developments

Mathias W Rotach[1], Marco Arpagaus[1], Manfred Dorninger[2], Christoph Hegg[3], Andrea Montani[4], Roberto Ranzi[5]

[1] Federal Office of Meteorology and Climatology, MeteoSwiss, Zurich, Switzerland
E-mail: *mathias.rotach@meteoswiss.ch*
[2] University of Vienna, Vienna, Austria
[3] WSL, Swiss Federal Institute for Forest Snow and Landscape Research Birmensdorf, Switzerland
[4] ARPA-SIMC, Bologna, Italy
[5] University of Brescia, Brescia, Italy

Abstract: MAP D-PHASE is a Forecast Demonstration Project of the World Weather Research Programme (WWRP) that is tied to the Mesoscale Alpine Programme (MAP). D-PHASE stands for **D**emonstration of **P**robabilistic **H**ydrological and **A**tmospheric **S**imulation of flooding **E**vents in the Alpine region. Its goal is to demonstrate the ability of reliably and operationally forecasting orographically influenced (determined) precipitation in the Alps and its consequences on the distribution of run-off characteristics. During the D-PHASE Operations Period (DOP) from June to November 2007 an end-to-end forecasting system was operated and a vast amount of data is currently being analysed and evaluated. The present contribution aims at briefly summarising the approach and components of D-PHASE. A number of lessons learned will be drawn from the outcomes. These include consequences concerning the optimal use of the D-PHASE/COPS joint data set as well as open questions and further directions.

Keywords: *Heavy precipitation, flash flood, forecast demonstration, WWRP, high-resolution numerical weather prediction, probabilistic forecast.*

1 INTRODUCTION

A Forecast Demonstration Project (FDP) of the World Weather Research Programme, quite generally, aims at demonstrating the advances an R&D activity has brought to operational atmospheric forecasting. Thus a FDP deals with the forecast of weather with international relevance (high impact weather); demonstrates a clear advance in forecasting capability; provides clear evaluation protocols and is characterized by an expectation of success. D-PHASE is the FDP in relation to the Mesoscale Alpine Programme (MAP, Bougeault et al. 2001) and aims at demonstrating an end-to-end warning system for flood events based on high resolution deterministic probabilistic hydrological and atmospheric modelling in the Alpine region. Some of the D-PHASE essentials are summarized in Table 1. The forecasting system's centre piece was a Visualization Platform (Fig. 1), on which warnings from atmospheric and hydrological models (both deterministic and probabilistic) and corresponding model fields were displayed in uniform and comparable formats. Also, meteograms, nowcasting information and end user communication was made available to all the forecasters, users and end users. From June to August 2007 the COPS (**C**onvective and **O**rographically induced **P**recipitation **S**tudy, Wulfmeyer et al. 2008) mission planning team was among the D-PHASE users. COPS provided high-resolution observational data for a sub-area of the D-PHASE domain that can – from a D-PHASE point of view - be employed for model verification and reliability assessment.

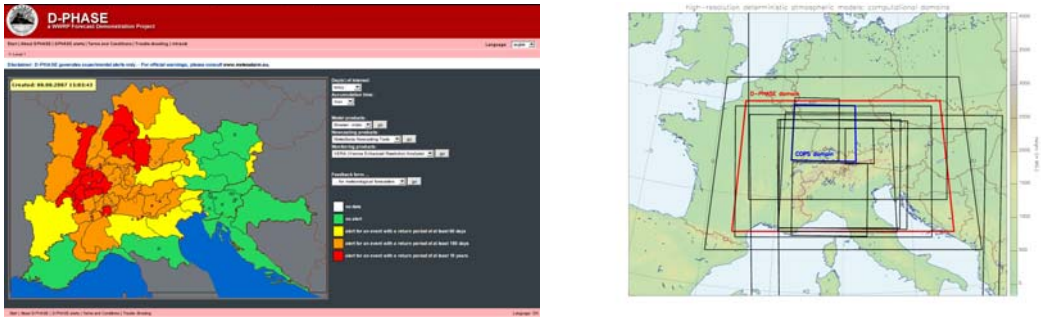

Figure 1. Left: Screenshot of the Visualization Platform (VP) for August 8 2007, level 1 (Alpine vide view); right: model domains for high-resolution atmospheric models including the D-PHASE (red) and COPS (blue) domains. Both from Rotach et al. (2009).

2 RESULTS

Details on D-PHASE, including background, organisation and scientific results can be found in Arpagaus et al. (2009) and Rotach et al. (2009). The more hydrological aspects are summarized in Zappa et al. (2008). Here we only focus on the main achievements and point to directions for further analysis. Just as MAP had proved

the feasibility of atmospheric/hydrological coupling, D-PHASE successfully demonstrated its operational use and extension to ensemble techniques. Judging from preliminary conclusions by atmospheric forecasters (Rotach et al. 2009) this is not only an advance in technical terms, but also helps both communities to take into account the respective other's sphere (hydrosphere vs. atmosphere) in order to improve the decisions and forecasts in one's own. This might be a 'lesson learned' that goes way beyond the present atmosphere-hydrosphere system and should be kept in mind for other applications of atmospheric modelling (such as air pollution dispersion or agro-meteorological applications).

D-PHASE Operations Period (DOP)	June-November 2007	COPS (Jun-to Aug) MAP (Sep-Nov)
D-PHASE area	> 40 catchments across the alps	
Participants	> 30 institutions	Hydro/Met Services Universities Research institutions
Target	Forecasting system for precipitation and flooding in the Alps	End-to-end
Instrument	Visualization Platform	Uniform formats
Approach	Numerical modelling, nowcasting → 30 atmospheric models → 7 different hydrological models → Radar, Satellite and analysis tools	Probabilistic & deterministic

Table 1. Summary of some D-PHASE facts.

Clearly, the single most important factor of success for D-PHASE was the interoperability of all the models: *common formats, common warning levels and common routines* to actually determine the warnings from the model outputs rendered the results comparable and therefore highly valuable. The possibility of comparing objective model verification (deterministic and probabilistic) for a substantial number of models and approaches with subjective evaluation of D-PHASE results (Rotach et al. 2009, for details) makes the D-PHASE data set quite unique.

This available data set together with detailed observations due to COPS will allow to

- systematically demonstrate the additional value of very high-resolution atmospheric modelling;
- investigate the properties and performance of Ensemble Predictions Systems both for atmospheric and hydrological models. Examples can be found in Arpagaus et al (2009) or Zappa et al. (2008).
- study predictability of convection processes and convective initiation using the present model results in connection with the observational results of COPS;
- benchmark models of all types by comparing them with a range of other models of the same category, or even other model types;
- systematically evaluate nowcasting tools such as the position forecast of convective systems in the Thunderstorms Radar Tracking (TRT) tool of MeteoSwiss using the available data, and possibly extend their functionality by introducing model products;
- judge the end user feedback on its own grounds, and compare it to the 'objective' verification results - thus learning even more concerning the improvement of the overall forecasting/warning system.

The D-PHASE data set, in conjunction with the observational data set due to COPS is now available as a testbed for atmospheric convection, in combination with orographic precipitation and coupled to hydrological modelling. The WWRP working group on Meso-scale Weather Forecast Research (WG-MWFR) has recently included the D-PHASE/COPS data set for this purpose in their strategic planning.

REFERENCES

Arpagaus M and 44 co-authors, 2009: MAP D-PHASE: Demonstrating forecast capabilities for flood events in the Alpine region. *Veröffentlichungen der MeteoSchweiz*, **78** (available from http://www.meteoschweiz.admin.ch/web/de/forschung/publikationen/meteoschweiz_publikationen/veroeffentlichungen.html).

Bougeault P, Binder P, Buzzi A, Dirks R, Houze R, Kuettner J, Smith RB, Steinacker R and Volkert H, 2001: The MAP Special Observing Period. *Bull. Amer. Meteor. Soc.*, **82**, 433-462.

Rotach MW and 38 co-authors, 2009: MAP D-PHASE: Real-time Demonstration of Weather Forecast Quality in the Alpine Region. *Bull. Amer. Meteor. Soc*., accepted.

Wulfmeyer V and 27 co-authors, 2008: The Convective and Orographically-induced Precipitation Study: A Research and Development Project of the World Weather Research Program for Improving Quantitative Precipitation Forecasting in Low-mountain Regions. *Bull. Amer. Meteor. Soc*., DOI 10.1175/2008BAMS2367.1.

Zappa M, Rotach MW, Arpagaus M, Dorninger M, Hegg C, Montani A, Ranzi R, Ament F, Germann U, Grossi G, Jaun S, Rossa A, Vogt S, Walser A, Wunram C, 2008: MAP D-PHASE: Real-time demonstration of hydrological ensemble prediction systems. *Atmos. Sci. Let.*, **2**, 80-87, **DOI:** 10.1002/asl.183.

Verification of precipitation forecasts of the D-PHASE data set

Tanja Weusthoff[1], Felix Ament[2], Marco Arpagaus[1], Mathias W. Rotach[1]

[1] MeteoSwiss, Zurich, Switzerland
[2] University of Hamburg, Hamburg, Germany
E-mail: *tanja.weusthoff@meteoswiss.ch*

Abstract: Precipitation forecasts from the Forecast and Demonstration Project D-PHASE are evaluated by means of different verification methods. Standard scores like (relative) bias and probability of detection are utilized for individual catchment regions based on Swiss radar data and the relative value for predefined warnlevels is determined (cost/loss analysis). The forecasts of selected models are additionally Fuzzy verified against Swiss radar data with a focus on a comparison of the performance of the two operational Swiss COSMO models with their different spatial (and temporal) resolutions. The results show a slight advantage for the higher resolution model on all spatial scales, especially at shorter accumulation times (e.g. 3 h).

Keywords: *D-PHASE, precipitation, verification*

1 INTRODUCTION

In the scope of D-PHASE a real-time end-to-end forecasting system for heavy precipitation and subsequent flood events in the Alpine region was set up. Based on probabilistic and deterministic atmospheric and hydrological models, warnings were issued for specific river catchments. The forecast data of the participating numerical models, including high resolution convection resolving models and models with parameterized convection, are stored in a central data archive at the World Data Center for Climate in Hamburg. These data are well suited to investigate the use of atmospheric/hydrological models for flood forecasting in mountainous regions. Various methods are applied to get an objective verification of the model forecasts.

2 VERIFICATION METHODS

2.1 Catchment Verification

The precipitation forecasts for individual catchment areas as shown in Fig. 1 as well as the alerts issued for predefined warning levels are verified against Swiss radar data (raw data and data calibrated by means of rain gauge measurements). The verification results for the full D-PHASE Operations Period (DOP, June - November 2007) will be presented with a focus on seasonal differences. The scores applied include the (relative) bias, probability of detection, temporal correlation, and relative value.

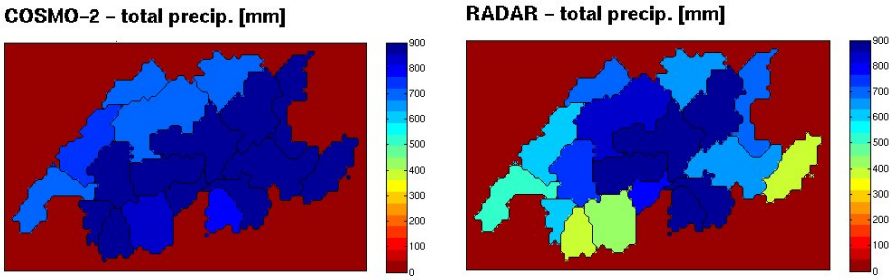

Figure 1: Catchment regions within Switzerland and parts of neighbouring countries. The plot shows total precipitation for each catchment for the whole DOP as forecast by COSMO-2 (left) and measured by radar (right).

2.2 Fuzzy verification

Selected models are additionally evaluated with reference to Swiss radar observations by means of Fuzzy verification methods. While standard verification methods require a point wise match of observation and forecast on the grid scale of the model, Fuzzy verification methods evaluate the forecast on increasing spatial scales by moving window domains of various sizes over the verification domain. An event is identified as e.g. the mean value over the respective window exceeding a given threshold (Upscaling) or the fraction of grid points in the

window exceeding the threshold (Fractions Skill Score). The verification is done on different spatial scales by varying the window sizes and for various thresholds defining an event. The scores are determined for 3 h and 24 h rain accumulations and are then aggregated on different time scales: days, months, and the whole period of 6 months. The robustness of the results is determined by means of a bootstrapping procedure. In addition, the sensitivity of the scores with respect to the rain amount and the dependency of the results on the weather type is investigated.

An example of the Fuzzy verification results for the whole DOP is given in Fig. 2. Each single box represents a specific spatial scale and a certain threshold, for which the respective scores are calculated. The skill of each of the two COSMO models increases with increasing spatial scale and decreases with increasing threshold. In order to compare the two models, the differences of the scores are calculated. The difference plot displayed on the right hand side gives a good impression on which scales the models are comparable and on which scales COSMO-2 outperforms COSMO-7.

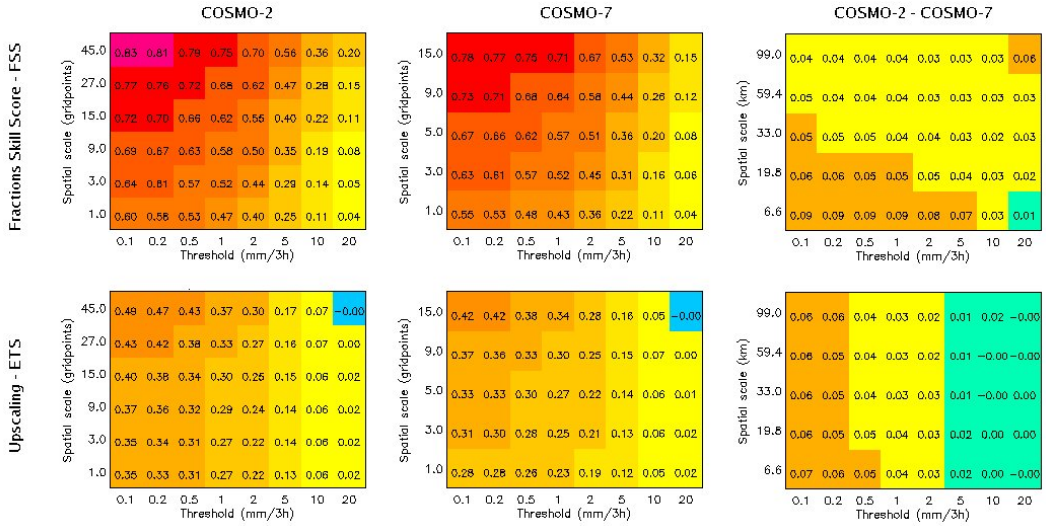

Figure 2: Results of fuzzy verification of COSMO-2 (left) and COSMO-7 (middle) for the whole DOP. Top panels show Fraction Skill Score, lower panels the Upscaling method. On the right hand side, the differences of COSMO-2 minus COSMO-7 are displayed. Positive numbers indicate a better skill of COSMO-2, negative values a better skill of COSMO-7, respectively.

3 RESULTS AND CONCLUSIONS

The data set produced during D-PHASE provides a good possibility to investigate the ability of different models to forecast precipitation for a well defined time period, including summer months with heavy convective rain and the autumn period with less precipitation in the region of interest.

The catchment verification shows no clear signal for a comparison between cloud resolving and convection parameterizing models. However, it reveals differences in the models performance for the two considered seasons. Generally, almost all models overestimate precipitation compared to radar. Adjusting radar data by means of rain gauge measurements results in a reduced overestimation by the models. The relative value calculated for the whole D-PHASE Operations Period on the other hand is larger for high resolution models, which indicates that these models were more useful than the coarser resolution models.

Concerning Fuzzy verification methods, COSMO-2 performs slightly better on all scales for 3 h precipitation accumulations, especially for low precipitation thresholds. In contrast, 24 h accumulations are comparable well forecast by both models in the considered period when using only 00 UTC runs for the comparison. The results show, amongst others, that high resolution convection resolving models generally reveal better skills, especially on shorter time scales and with respect to temporal correlation of precipitation. The statistical significance of the results is evaluated by means of a bootstrapping procedure.

REFERENCES

Arpagaus et al. (2009): MAP D-PHASE: Demonstrating forecast capabilities for flood events in the Alpine region. Report on the WWRP Forecast Demonstration Project D-PHASE submitted to the WWRP Joint Scientific Committee. Published as Veröffentlichung der MeteoSchweiz, 78, 2009, 68pp.

EVALUATION OF OPERATIONAL WEATHER FORECASTS: APPLICABILITY FOR FLOOD FORECASTING IN ALPINE BAVARIA

Uwe Ehret[1]

[1] TU München, Department of Hydrology, Munich, Germany
E-mail: *u.ehret@bv.tum.de*

Abstract: In this study, a range of both deterministic and ensemble rainfall forecast models are evaluated with respect to their applicability for operational flood forecasting in mesoscale alpine catchments in Bavaria. Both continuous and categorical performance measures are applied. In summary, the median of the Cosmo-Leps ensemble forecast outperformed all deterministic forecasts.

Keywords: *rainfall forecast, flood forecast, alpine, deterministic, ensemble, Cosmo-Leps*

1 INTRODUCTION

Flood forecasting in small, alpine head catchments is a difficult task: Due to their size and topographic setting, there are usually neither many upstream river gauges to base the forecast on, nor do forecasts based on river- and rain gauge observations provide lead times of sufficient length. Consequently, weather-, especially rainfall forecasts are needed and heavily influence flood forecast quality.

In this article, a wide range of operationally available rainfall forecasts, both deterministic and ensemble, are evaluated with respect to their quality and applicability for flood forecasting in a range of alpine river catchments in Bavaria. After the introduction, the available data, performance indices used and the set-up of the tests are described in section 2. Based on this, results are presented in section 3, followed by conclusions in section 4.

2 DATA & METHODS

2.1 Rainfall observations

Hourly rainfall observations from over 100 raingauges were used to calculate mean areal rainfall (linear interpolation) in seven (sub-) alpine catchments in and along the Bavarian alps, ranging from 221 km^2 to 1597 km^2. The time series extends from 01.08.2005 to 30.04.2008, excluding the snow-influenced winter months November through March. The time series includes a 300-year flood event in August 2005.

2.2 Rainfall forecasts

Rainfall forecasts were available from both deterministic and ensemble forecasting models (abbreviations in brackets): DWD GME (GME), DWD Cosmo-EU (LME), DWD Cosmo-DE (LMK), NCEP GFS (GFS), Aladin-Austria (ALA), modified MeteoSwiss Cosmo-7 (ALM) forecasts, operationally corrected by a MeteoSwiss meteorologist, Cosmo-Leps (CLE). Also, GME, LME and GFS forecasts were combined to a PEPS (PEP), and a median forecast series from CLE was calculated (CLM). CLE, GME and LME were available for the whole observation period, the others started 01.10.2006.

The forecasts were disaggregated to 1-hour sums (necessary for CLE, GFS and GME) and areal-averaged in the same manner as the rainfall observations. From all forecasts, only the 00:00 and 12:00 runs were used to assure a comparable data base for each forecast model.

2.3 Performance criteria

Continuous and categorical performance criteria were calculated to evaluate the deterministic forecasts: Root Mean Square Error (RMSE), Skill Score (SKSC), Threat Score (THSC) and Heidke Skill Score (HSKS), with the latter two being based on contingency tables. Ensemble forecasts were evaluated by the Briar Score (BRSC).

2.4 Test setup

As not all forecast data were available for the whole period, the performance criteria were calculated for two periods: 01.04.2005-30.04.2008 (only CLE, GME, LME) and 01.10.2006-30.04.2008 (all forecasts).

To account for the increasing forecast uncertainty, rainfall observations and forecasts were aggregated with increasing lead time. This is in accordance with the requirements on weather forecasts in flood forecasting: The

need for high resolution forecasts decreases with increasing lead time. 1/6/12-hour aggregations were used for the forecast ranges 1-9/12-18/24-72 hours, respectively.

To exclude times of no or low rainfall, performance measures were only calculated for areal rainfall observations in the time series exceeding an aggregation-dependent lower limit of 0.1/0.6/1.2 mm/h for 1/6/12-hour aggregations, respectively.

Thresholds for the contingency tables were set specific to each catchment according to the following rule: From all rainfall observations beyond the lower limit take the value with 5% exceedence probability. This was considered an acceptable trade-off between the opposing demands for low thresholds ensuring large enough class occupancies and high thresholds to consider only strong, flood-relevant rainfall events. In the 1-hour aggregation, thresholds were in a range from 1.7 to 3.1 mm/h. This is well below the warning threshold for strong rainfall by the German Weather Service (25 mm/h), which is probably due to the areal averaging.

Calculating 5 performance measures for 7 catchments, 2 period, 9 forecasts, 11 lead times and 3 aggregations led to a huge number of results. In order to condense this amount of information, two approaches were used: Firstly, forecast model performance was ranked for each calculation and averaged over all catchments. The advantage of the rank score is that it is a sharp discriminator and emphasizes even small differences in performance. Secondly, the performance scores were also averaged over all catchments to gain insight in the absolute score values. Investigating the results revealed that, for evaluation, a simple distinction in short- and long-term forecast depths (above or below 12-hours) was sufficient.

Based on the above results, the overall performance evaluation and intercomparison of the different forecasts was based on the manual analysis of condensed score space.

3 RESULTS

Analysing the performance measures in the manner described above, some interesting and surprising results were obtained:

With respect to the overall performance expressed by RMSE, the median of the Cosmo-Leps forecast, which basically is an artificial forecast, clearly outperformed the other models. This was the case for both periods investigated and both rank scores and absolute values. GFS won second place. It seems that the averaging effect of the median smoothes gross over- or underestimations which may occur for single-valued deterministic forecasts.

Results are a less obvious in the case of the threat score THSC, however it is noteworthy that LMK was never among the winners. This is against the assumption that LMK, with short update cycles and lead times should, at least in the short run, outperform the other models but it is in clear accordance with the experience of the flood forecasters of the alpine catchments of rivers Iller and Lech.

Comparing the forecasts to a simple persistence forecast, as expressed by the skill score SKSC and Heidke skill score HSKS again revealed a clear advantage of CLM compared to the other forecasts. Here, too, LMK was always found on the last places. With respect to absolute performance, SKSC of all models was sometimes negative for lead times up to 6 hours, for HSKS only for 1-hour forecasts. This means that in the very short range, a persistence forecast outperforms the others.

From a comprehensive view of all performance measures, some conclusions regarding the quality of the forecast models in the alpine spaces investigated could be drawn: The LMK model showed clear weaknesses. In other parts of Bavaria, however, this was not the case (unpublished study by the author). This indicates that LMK has problems with rainfall processes related to alpine settings. It should be noted, however, that the new version of Cosmo-DE might have overcome this problem.

Further, Aladin-Austria (ALA) performed consistently worse than most of the other models and might therefore be excluded from operational use for flood forecasting.

Apart from the deterministic models, Cosmo-Leps and the self-made PEPS from GME, LME, GFS were compared by means of the Briar score. It should be noted that for both cases, scores were usually quite low (i.e. good), which may indicate domination by large numbers of correct negatives. However, performance differences between the two were obvious and in favour of CLM.

4 CONCLUSIONS

In this study, a range of both deterministic and ensemble rainfall forecast models were evaluated with respect to performance in mesoscale alpine catchments in Bavaria. In summary, the median of the Cosmo-Leps ensemble outperformed all other forecasts. However, it should be investigated whether this artificial forecast exhibits a realistic temporal evolution or whether a single member placed in the centre of the ensemble, would provide similar performance scores plus 'realistic looks'.

Acknowledgements:
The author expresses his gratitude to the Bavarian Environment Agency (LfU) for supplying the data for this work.

A MULTI-MODEL INTERCOMPARISON STUDY FOR QUANTITATIVE PRECIPITATION FORECAST USING THE 6-MONTH MAP D-PHASE DATASET

Stefano Mariani[1], Marco Casaioli[1], Alexandre Lanciani[1], Barbara Lastoria[1], Christophe Accadia[2], Nazario Tartaglione[3]

[1] Institute for Environmental Protection and Research (ISPRA), Rome, Italy
[2] European Organisation for the Exploitation of Meteorological Satellites (EUMETSAT), Darmstadt, Germany
[3] Meteorology and Climate Centre, School of Mathematical Sciences, University College Dublin, Dublin, Ireland
E-mail: *stefano.mariani@isprambiente.it*

Abstract: Demonstrating the benefits in forecasting heavy precipitation and related flooding events in the Alpine region using high-resolution numerical weather prediction (NWP) models, ensemble prediction systems (EPSs), atmospheric-hydrological coupled systems, and real-time nowcasting tools is the purpose of MAP D-PHASE, a Forecast Demonstration Project launched in 2007 in the framework of the WMO WWRP Programme. The present work, performed within the MAP D-PHASE Working Group Verification (WG VER), aims at assessing and quantifying the performance of several NWP models during the entire D-PHASE Operations Period (DOP, from June to November 20007). This intercomparison study is performed by verifying on a daily basis quantitative precipitation forecasts (QPFs) against observational analyses using a multi-method approach based on multi-scale, objective and subjective methods. The combination of different deterministic forecasts, by means of multi-model poor man's ensemble (PME) approaches, is also taken into account for providing multi-model forecasts to be compared against the single deterministic models.

***K*eywords:** *MAP D-PHASE, QPF, multi-model poor man's ensemble, Barnes precipitation analysis, remapping, model intercomparison, verification, categorical scores, object-oriented technique, power spectrum analysis, subjective verification*

1 INTRODUCTION

European institution participating to the MAP D-PHASE project provided during the D-PHASE Operation Period (DOP, from June to November 2007), meteorological simulations modelled by numerical weather prediction (NWP) models and ensemble prediction systems (EPSs) over the D-PHASE and the Convective and Orographically-induced Precipitation Study (COPS) domains. Aim of this work, performed in the framework of MAP D-PHASE Working Group Verification (WG VER), is to evaluate the performance of several deterministic models during DOP and to understand the strengths and weaknesses of these models in forecasting precipitation events over a complex area, such as the Alpine region. Poor man's ensemble (PME) forecasts, obtained by combining the compared deterministic models, are considered within this verification study, as well.

2 FORECAST AND OBSERVED DATA

Several meteorological centers consider the quality of quantitative precipitation forecasts (QPFs) to be a general indicator of the capability of a NWP model to produce a good forecast, because precipitation strongly depends on atmospheric motion, moisture content, and physical processes. For this reason, this verification study is based on a daily intercomparison of QPF data against rainfall analyses, which are obtained by means of non-GTS rain gauge data (see Fig. 1) collected within WG VER from several meteorological services and environmental agencies.

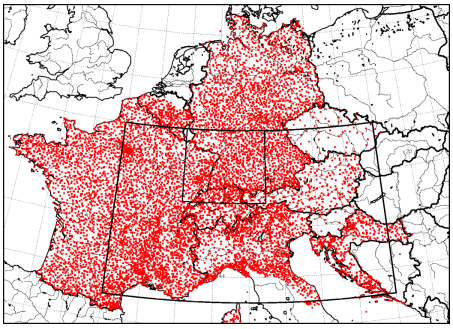

Figure 1: Status of non-GTS data during DOP, with indication of the MAP D-PHASE (large box) and COPS (small box) domains. Courtesy of Theresa Gorgas and Manfred Dorninger (University of Vienna, Austria).

More precisely, since rain gauges provide the more accurate, although localized, estimate of the observed weather, and NWP forecasts should be instead considered, in general, as areal mean quantities, the representativeness of the fields compared need to be addressed before applying any kind of verification method. Consequently, it has been decided to make a selection of the NWP models to be included into this verification work (see Table 1)

Very High Resolution (grid size $\sim$ 2–3 km)	High Resolution (grid size $\sim$ 7–10 km)
	ALADAT (ZAMG)
AROME (Météo France)	ALADFR (Météo France)
COSMOCH2 (Meteo Swiss)	COSMOCH7 (Meteo Swiss)
LAMI28 (ARPA SIM)	LAMI7 (ARPA SIM)
LMK (DWD)	LME (DWD)
LMITA (CNMCA)	LMEURO (CNMCA)
ISACMOL2 (ISAC-CNR)	MESONH8 (Univ. Paul Sabatier)
	QBOLAM11 (ISPRA, ex-APAT)

Table 1: List of the deterministic models selected for the verification study, categorized with respect to the grid size of the native grid. Acronyms and forecast providers as reported in the MAP D-PHASE Implementation Plan.

and to "optimally interpolate" both observations and forecasts at the same scales by means of the Barnes (1964) procedure and remapping (Accadia et al., 2003).

As reported in Table 1, models have been subdivided into two quasi-homogeneous categories, namely the **Very High Resolution**, in which models have a grid horizontal spacing of about 2–3 km, and the **High Resolution**, in which models have instead a grid spacing of about 7–10 km. Each one of these sub-groups can be also considered as a sort of "poor man's ensemble" group. So, according to the PME procedures presented by Ebert (2001), four deterministic forecasts can been obtained: the simple arithmetic ensemble forecast mean (AVE); the ensemble median precipitation forecast (MED); the probability matched forecast based on AVE (PAV); and the probability matched forecast based on MED (PMD).

3 VERIFICATION METHODOLOGY

A verification area, centred over the MAP D-PHASE domain and obtained as intersection of all the selected models' domains, has been considered for the implementation of a multi-method approach based on multi-scale (power spectrum analysis), objective (categorical scores and object-oriented techniques) and subjective methods. Multi-scale methods are a methodological requirement since traditional categorical scores, which measure point-to-point match, are sensitive to small displacement errors. Higher order moments should be studied to evaluate whether the fields to be compared are defined on grids with the same real resolution and whether they have the same amount of small-scale details. Furthermore, objective techniques can provide a quantitative basis to subjective verification, which in turn can suggest physical interpretations to the objective verification findings. Details about this verification methodology can be found in Mariani et al. (2009b).

4 CONCLUSIONS

Some of the verification findings will be illustrated during ICAM 2009, with particular emphasis on the impact of model resolution on the precipitation forecast quality at different scales, the suitability of the PME approaches to provide better forecasts than the single deterministic models, and finally, the helpfulness of the multi-method approach in order to better understand the verification results.

Acknowledgements:
Authors thank MAP D-PHASE partners, which provided NWP data during DOP, and meteorological services and environmental agencies, both at national and at regional level, which have made available non-GTS data for the verification tasks. Our thanks also go to WG VER members for their suggestions and support.

REFERENCES

Accadia, C., S. Mariani, M. Casaioli, A. Lavagnini, and A. Speranza, 2003: Sensitivity of precipitation forecast skill scores to bilinear interpolation and a simple nearest-neighbor average method on high-resolution verification grids. *Wea. Forecasting*, **18**, 918–932.

Barnes, S. L., 1964: A technique for maximizing details in numerical weather map analysis. *J. Appl. Meteor.*, **3**, 396–409.

Ebert, E. E., 2001: Ability of a Poor Man's Ensemble to predict the probability and distribution of precipitation. *Mon. Wea. Rev.*, **129**, 2461–2480.

Mariani, S., A. Lanciani, M. Casaioli, C. Accadia, and N. Tartaglione, 2009: A multi-method approach for quantitative precipitation forecast verification within the MAP D-PHASE project. *Proc. Joint MAP D-PHASE Scientific Meeting – COST 731 mid-term seminar*, Bologna, Italy, 107–115.

USING COPS DATA FOR THE VALIDATION OF THE HIGH-RESOLUTION NWP MODEL COSMO-DE

Kathrin Wapler[1], Axel Seifert[1], Bodo Ritter[1]

[1] Deutscher Wetterdienst (DWD), Offenbach, Germany
E-mail: *kathrin.wapler@dwd.de*

Abstract: The convective and orographically induced precipitation study had the aim to advance the quality of forecasts of orographically induced convective precipitation in complex terrain. The COPS observations, measured at different locations in the Black Forest and Vosges Mountains by a variety of instruments, give information of the boundary layer characteristics and convective initiation. The COPS data set is used for the validation of high-resolution convective-scale NWP simulations of the COSMO-DE model. Comparisons with radar, lidar, radiosonde and surface meteorological observations are performed to study the accuracy of the model in simulating the convective boundary layer.

Keywords: *high-resolution NWP, COSMO-DE, COPS*

1 INTRODUCTION

The convective and orographically induced precipitation study (COPS, Wulfmeyer 2008) took place in the Black Forest and Vosges Mountains from 1 June to 31 August 2007. The aim of this experiment was to advance the quality of forecasts of orographically induced convective precipitation by extensive observations and modelling of its life cycle, thereby identifying the physical and chemical processes responsible for deficiencies in quantitative precipitation forecasts over low mountain regions.

The 35 IOPs during COPS can be distinguished into forced convection, weakly forced convection and high-pressure convection including a variety of conditions, from severe precipitation events to cloud-free days. A variety of observation systems were operated in the area of interest at different locations in valleys as well as on mountain tops. The measurement instruments included radiosondes, Doppler lidar, aerosol Raman lidar, water vapour differential absorption lidar, microwave radiometer, cloud radar, C-Band polarization radar, energy balance stations, GPS receiver as wells as a fleet of research aircraft. The combination of the measurements by these instruments gives information of the boundary layer characteristics and convective initiation. Thus COPS aims to provide a useful data set for the evaluation of numerical models.

Convection initiation is often not adequately reproduced in state-of-the-art NWP models. This results in poor quantitative precipitation forecasts, both in terms of the spatial distribution as well as the temporal evolution of precipitation. An example is shown in Fig. 1. The figure shows the spatial distribution of observed and simulated 24 h accumulated precipitation in the COPS area as well as the diurnal cycle for IOP-1d. Scattered surface-based diurnally induced showers occurred over the Vosges and Black Forest as observed by radar. The precipitation is poorly represented in the operational high-resolution COSMO-DE simulation.

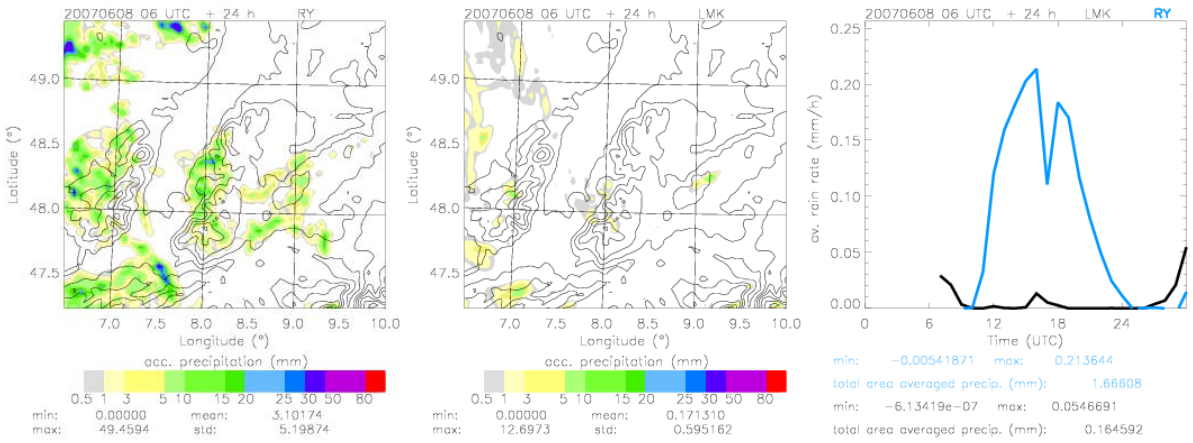

Figure 1. Spatial distribution of 24 h accumulated precipitation in the COPS area for IOP-1d (08.06.2007) from radar observations (left) and operational COSMO-DE simulations (middle); temporal evolution of observed (blue) and simulated (black) area averaged precipitation.

2 MODEL SET-UP

At the German Weather Service (DWD, Deutscher Wetterdienst) a 2.8 km version of the COSMO model, called COSMO-DE (Steppeler et al. 2003, Schättler et al. 2005), formerly known as LMK, is running operationally. Its domain covers Germany, Switzerland, Austria, The Netherlands, Belgium, and most of the Alps. Boundary conditions for the COSMO-DE come from the 7 km COSMO-EU which itself is nested in the global model GME (Majewski et al. 2002), running at a resolution of 40 km.

3 RESULTS

As an example of the evaluation of COSMO-DE using COPS data, comparisons with radiosondes are shown. These have been performed to evaluate the temporal evolution of the boundary layer. Figure 2 (left and middle panel) shows time-height cross-sections of the relative humidity measured by radiosondes launched at supersite R (Rhine Valley, near Achern) during IOP-1c and simulated profiles at the nearest grid point. On this day a few deep surface-based convective showers developed across the southern Black Forest that were not forecasted by the model. The gross features are simulated correctly however the model can't reproduce sharp gradients of relative humidity, e.g. the dry layer at about 3 km, and is too moist near the surface in the evening. The right panel in Fig. 2 shows the difference of simulated and measured temperature. Especially in the afternoon the model is too cold in the lowest 1.5 km and too warm above, thus it is to stable, prohibiting the initiation of convection.

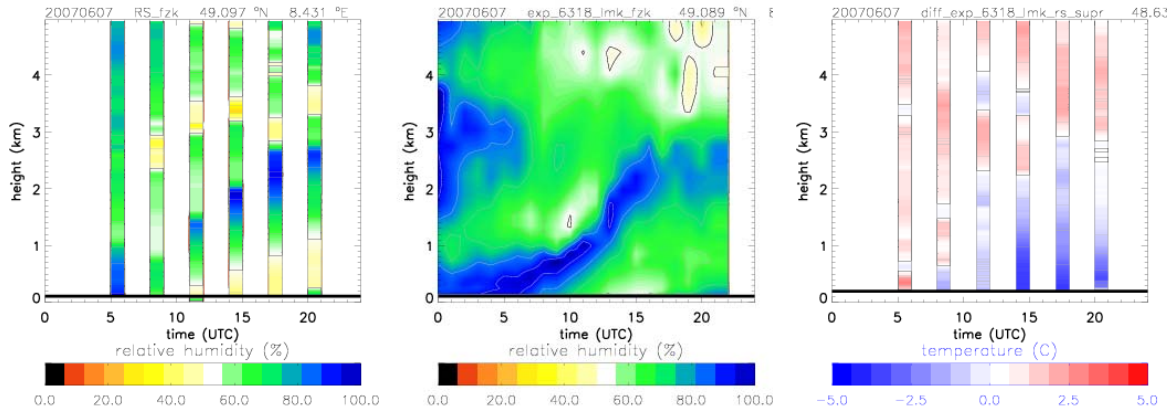

Figure 2. Time-height cross-sections of relative humidity during IOP-1c (07.06.2008) as observed by radiosondes at supersite R (left) and simulated with COSMO-DE at the closest grid-point. Time-height cross-section of the difference between observed and simulated temperatures (right).

4 CONCLUSIONS

High-resolution convective-scale NWP simulations of the COSMO-DE model are evaluated with the COPS data set. The model has shown its ability to forecast deep convection, especially forced convection, e.g. convection that is associated with frontal systems. However, problems occur in the forecast of moist convection in weakly forced conditions, e.g. small-scale orographically-induced deep convection or summertime airmass convection. In these situations explicit convection is often missing in the simulations. This is related to a too stable or too cold boundary layer.

REFERENCES

Majewski, D., D. Liermann, P. Prohl, B. Ritter, M. Buchhold, T. Hanisch, G. Paul, W. Wergen, and J. Baumgartner, 2002: The operational global icosahedral-hexagonal gridpoint model GME: Description and high-resolution test. J. Atmos. Sci. **139** , 319-338.

Schättler, U., G. Doms, and C. Schraff, 2005: A description of the nonhydrostatic regional model LM, Part VII: User's guide. Consortium for Small-Scale Modelling.

Steppeler, C., G. Doms, U. Schättler, H.W. Bitzer, A. Gassmann, U. Damrath, and G. Gregoric, 2005: Meso-gamma scale forecasts using the nonhydrostatic model LM. Meteorol. Atmos. Phys. **82** , 75–96.

Wulfmeyer, V., A. Behrendt, H.-S. Bauer, C. Kottmeier, U. Corsmeier, A. Blyth, G. Craig, U. Schumann, M. Hagen, S. Crewell, P. Di Girolamo, C. Flamant, M. Miller, A. Montani, S. Mobbs, E. Richard, M.W. Rotach, M. Arpagaus, H. Russchenberg, P. Schlüssel, M. König,, V. Gärtner, R. Steinacker, M. Dorninger, D.D. Turner, T. Weckwerth, A. Hense, and C. Simmer, 2008: The convective and orographically induced precipitation study. Bull. Amer. Meteorol. Soc. **89** , 1477–1486.

ASSIMILATION OF WEATHER RADAR REFLECTIVITY IN THE AROME MODEL FOR THE COPS-IOP9

Olivier Caumont[1], Éric Wattrelot[1], Geneviève Jaubert[1], Véronique Ducrocq[1]

[1] CNRM/GAME (Météo-France/CNRS), Toulouse, France
E-mail: *olivier.caumont@meteo.fr*

Abstract: The impact of the 1D+3DVar assimilation of reflectivity data from the French radar network on Arome analyses and forecasts at 2.5 km horizontal resolution is investigated for the Convective and Orographically induced Precipitation Study (COPS) Intense Observation Period (IOP) 9c (20 July 2007). For that, reflectivity data are assimilated in addition to conventional data, and the resulting forecasts are compared with those from a reference experiment assimilating conventional data only. Results show that the assimilation of reflectivity is beneficial, especially for intense precipitation.

Keywords: *radar, reflectivity, data assimilation, COPS*

1 INTRODUCTION

The Arome model is now running operationally at Météo-France since December 2008 at the horizontal resolution of 2.5 km. Within the Arome project, a novel 1D+3DVar assimilation method has been devised to assimilate reflectivity data (Caumont et al. 2008). It is currently heavily tested with a development version (Wattrelot et al. 2008) in order to include it in the next operational release. The present study is part of this series of tests.

The case chosen for this study is that of 20 July 2007, which corresponds to the IOP9c of the COPS campaign (Wulfmeyer et al. 2008). During the morning, pre-frontal convection occurs over central France in a southwesterly flow. Cells are advected and merge to form a squall line that passes over Germany during the afternoon. In the afternoon, precipitation affects France only sparsely, and we therefore focus our study on the morning.

2 EXPERIMENTAL SETUP

In this study, all experiments start at 0000 UTC 20 July 2007 from the latest three-hour 3DVar Rapid Update Cycle (RUC) forecast from the pre-operational Arome system (Brousseau et al. 2008), that assimilates conventional data, i.e., data from radio-sounding, screen-level stations, wind profilers, buoys, ships, aircrafts, satellites, but without radar reflectivity, Doppler velocity, nor Global Positioning System (GPS) data. In experiment 0RAD, only these data are assimilated at 0000 UTC. In 1RAD, reflectivity data from the Sembadel radar, which covers the Massif Central, are assimilated in addition to conventional data. The Sembadel radar was chosen because convective cells that merge into a squall line later in the morning are present over the Massif Central at 0000 UTC. In 11RAD, reflectivity data from all 11 French Metropolitan radars available for assimilation at that time are assimilated in addition to conventional data. In this study, 24-hour simulations with the Arome forecast system are launched from the respective analyses.

3 RESULTS

The 0RAD forecast predicts most convection patterns for the whole day, as shown for instance at 0900 UTC in Fig. 1, but a careful study reveals differences with observations in localized features in terms of intensity and location. Also, the forecast is overall lagging behind observations (compare the location of the leading edge of the mesoscale convective system (MCS) in Fig. 1). The 1RAD forecast is closer to that of 0RAD than to observations. Noticeable differences can be seen, though. For instance, the forecast is not lagging behind observations as much as in 0RAD (see Fig. 1). For 11RAD, the differences with 0RAD are more pronounced and some improvements can be seen in places. In particular, the timing seems to be even better in this simulation (compare the location of the MCS in Fig. 1).

The comparison of observed and predicted 12-hour accumulated precipitation between 0300 UTC and 1500 UTC (Fig. 2) shows that the large band crossing France from southwest to northeast is present in both observations and simulations. It is hard to tell which forecast is best from Fig. 2 only. That is why objective skill scores against raingauges have been computed for the same period (Tab. 1). All scores are improved when reflectivity data from one radar are assimilated, and even more when 11 radars are taken into account. Categorical skill scores for the same period (not shown) prove that most benefits from assimilating reflectivity data are gained for high precipitation thresholds (above 15 mm) in terms of false alarm rate and probability of detection. For lower thresholds, results are rather neutral for 1RAD and slightly positive for 11RAD.

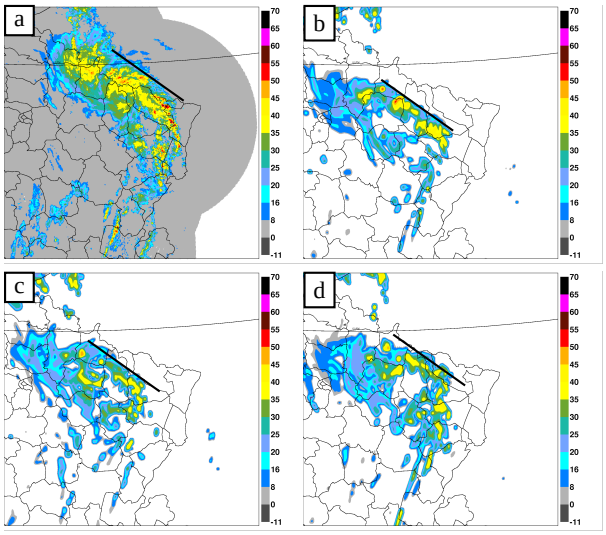

Figure 1: (a) Observed reflectivity (dBZ) composite at 0900 UTC; and simulated reflectivity (dBZ) at 700 hPa for (b) 0RAD, (c) 1RAD, and (d) 11RAD, at the same time. The solid, black line denotes the leading edge of the MCS.

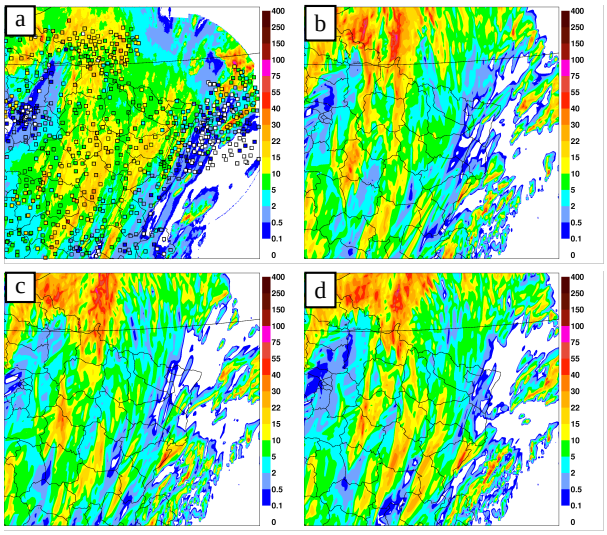

Figure 2: 12-hour accumulated precipitation (mm) between 0300 UTC and 1500 UTC (a) observed by raingauges superimposed on the composite radar estimate (Parent du Châtelet et al. 2006); and predicted by (b) 0RAD, (c) 1RAD, and (d) 11RAD.

Experiment	bias (mm)	RMSE (mm)	R
0RAD	0.21	7.15	0.46
1RAD	−0.09	6.66	0.49
11RAD	−0.05	6.22	0.58

Table 1: Bias, root mean square error (RMSE) and correlation coefficient (R) for accumulated precipitation between 0300 UTC and 1500 UTC (raingauge observations as reference). Data are first averaged over 0.2 °×0.2 ° squares.

4 CONCLUSIONS AND OUTLOOK

This sudy has shown, for a COPS case, that the 1D+3DVar assimilation of reflectivity data into the Arome numerical weather prediction system improved quantitative precipitation forecast over reference forecasts that were already very good. Improvements (e.g., better timing) were noticeable with the assimilation of data from one radar only, and even more with 11 radars. The largest improvements concern intense precipitation.

We plan to carry out the same experiments for the other days of IOP9, and also to study the impact of a rapid update cycle assimilating reflectivity and/or Doppler velocity data.

Acknowledgements: *The COPS campaign and this study benefited from support from the ANR (Agence Nationale pour la Recherche) and the CNRS/INSU (Institut National des Sciences de l'Univers).*

REFERENCES

Brousseau, P. *et al.*, 2008: A prototype convective-scale data assimilation system for operation: the Arome-RUC. *HIRLAM Tech. Rep.*, **68**, 23–30.

Caumont, O., S. Pradier-Vabre, G. Jaubert, and V. Ducrocq, 2008: 1D+3DVar assimilation of radar reflectivities for short-term high-resolution quantitative precipitation forecasts. *International Symposium on Weather Radar and Hydrology (WRaH2008)*, Grenoble and Autrans, France. Abstract no. 02-018.

Parent du Châtelet, J., P. Tabary, C. Gueguen, and B. Fradon, 2006: The Météo-France single-radar and composite QPE operational products. *Proc. 4th European Conf. on Radar in Meteorol. and Hydrol. (Erad 2006)*, Barcelona, Spain. Abstract no. 5.2.

Wattrelot, É., O. Caumont, S. Pradier-Vabre, M. Jurasek, and G. Haase, 2008: 1D+3DVar assimilation of radar reflectivities in the pre-operational AROME model at Météo-France. *Preprints, 5th European Conf. on Radar in Meteorology and Hydrology (ERAD2008)*, Helsinki, Finland.

Wulfmeyer, V. *et al.*, 2008: The convective and orographically-induced precipitation study: A research and development project of the World Weather Research Program for improving quantitative precipitation forecasting in low-mountain regions. *Bull. Amer. Meteor. Soc.*, **89**, 1477–1486.

IMPACT OF GPS DATA ASSIMILATION ON THE CONVECTIVE SCALE PREDICTION OF COPS IOP9

Geneviève JAUBERT [1] , Xin YAN [1], Véronique DUCROCQ [1], Pierre BROUSSEAU [1], Cédric CHAMPOLLION[2], Cyrille FLAMANT[3]

[1] GAME-CNRM, CNRS & Météo-France, 42 Avenue Coriolis, 31057 TOULOUSE Cedex 1, France
[2] UM2/CNRS,Place E.Bataillon, Montpellier, France
[3] LATMOS/IPSL, CNRS-UPMC, Boite 102, 4 Place Jussieu, 75252 Paris Cedex 05, France
E-mail: *genevieve.jaubert@meteo.fr*

Abstract: The impact of assimilating GPS delays in a convective scale NWP system has been studied for IOP9 (18-20 July 2007) of the COPS field campaign over the Black Forest and the Vosges region. The high-resolution temporary GPS receivers network deployed during the COPS campaign provides us a unique opportunity to evaluate the benefit of assimilating such high-spatial GPS data in addition to those from the operational European E-GVAP network. A clear positive impact on the AROME precipitation forecast has been found when the GPS delays are assimilated. The impact is more important on IOP9b (19 July). The comparison with other water vapour measurements performed during the COPS field campaign, such as those from additional soundings and water vapour LIDAR, shows that the tropospheric water vapour field is also improved.

Keywords: *Mesoscale Data Assimilation , GPS zenith delays , COPS*

1 INTRODUCTION

Recent works on the assimilation of high spatial and temporal resolution GPS Zenith Total Delay (ZTD) observations into mesoscale NWP systems suggest that better results can be obtained by increasing the model resolution. The availability of the GPS data from the field campaign COPS (Wulmeyer *et al.*, 2008), associated with the E-GVAP GPS data received operationally at Météo-France provide us an opportunity to verify the impact of GPS data assimilation at the convective scale. The new AROME system, a high-resolution data assimilation system based on non-hydrostatic resolving convection model, running operationally since December 2008 at Météo-France is used for that purpose. The impact has been evaluated on the COPS IOP9. During the three days of this IOP (18-20 July 2007), an elongated frontal zone developed upstream of the COPS region (the Vosges and Black Forest mountains in eastern France and southwestern Germany), associated with deep convection over the COPS region.

2 EXPERIMENTAL SETUP

AROME, the new convective-scale Numerical Weather Prediction system of Meteo-France (Seity et al. 2007), is running at 2.5-km resolution over a domain of 1600 km x 1250 km centred over France. A large part of the software of the AROME suite is common with the Météo-France ARPEGE and ALADIN NWP systems, and the ECMWF system IFS. The AROME dynamics is a non-hydrostatic extension of the limited-area NWP model ALADIN whereas the AROME physical package is extracted from the physical parameterizations of the Meso-NH research model. The AROME 3DVAR assimilation system is based on the ALADIN 3DVAR one.

The GPS ZTD data assimilation follows the ARPEGE and ALADIN GPS data assimilation implementation (Poli et al.,2007, Yan *et al.*, 2009), with slight differences due to higher resolution of the AROME system (Yan 2009). The GPS data which are assimilated come from the GPS network covering the COPS region with 76 stations and from the EUMETNET GPS water vapour program (E-GVAP, http://egvap.dmi.dk/) which provides near-real time GPS ZTD observations over Europe. A total of 316 GPS stations, from the E-GVAP and COPS networks, are included in the Arome domain.

Three AROME assimilation cycle experiments were running according to a 3-hour forward intermittent rapid update cycle: (i) without assimilating any GPS data (REF experiment), (ii) assimilating only the E-GVAP dataset (OPR experiment), and (iii) assimilating the COPS+E-GVAP dataset (COP experiment). In addition, the observations operationally used in the ALADIN-France model are assimilated in the three experiments: observations from radio-soundings, screen-level stations, buoy, ship and aircraft measurements, wind profilers, scatterometers, atmospheric motion vectors (AMS), and some satellites radiances, from METEOSAT/SEVIRI, and NOAA/ATOVS instruments. The REF and COP assimilation experiments start at 21 UTC, 5 July 2007 and the OPR experiment starts from the REF experiment at 00 UTC, 15 July 2007. 30-h AROME forecasts are launched at every 00 UTC on 18, 19 and 20 July from the REF, GPS and OPR analyses.

3 RESULTS

Figure 1a shows the ETS scores for the 12-h accumulated precipitation forecast from 03 to 15 UTC for the three days. The ETS values over the whole AROME domain (France domain) show that both COP and OPR experiments improve the precipitation forecast with respect to the REF one. When looking more specifically over the COPS region (SCOPS domain), the COP experiment performs better than the OPR one for weak precipitation, the both being better than the REF one. Assimilation of the high-spatial COPS GPS dataset in addition to the European E-GVAP dataset has thus a local positive impact.

The COPS data have been further exploited to evaluate the benefit of assimilating GPS ZTD observations on the water vapour field. First, a comparison has been carried out with the COPS additional Nancy soundings, not used in the assimilation cycle (Fig. 1b). This comparison shows that in overall the COP AROME forecasts perform better than the REF ones. This is particularly true for the the 18UTC radiosounding on July, 18: the 18-hour water vapour mixing ratio forecast fits very well with the observation .

The AROME forecasts have been also compared to the water vapour measurements from the airborne differential absorption lidar LEANDRE 2 on-board the French SAFIRE/F20 aircraft. Figure 1c shows the water vapor mixing ratio profiles averaged over the clear air columns along the 10 transects performed between 1224UTC and 1537 UTC during IOP9b for the AROME forecast of the three data assimilation cycle experiments. Three mean observed profiles are shown as observations have been averaged considering the same clear air columns as in the AROME forecast. Figure 1c shows that both COP and OPR runs perform better than the REF one, and that COP performs better than OPR.

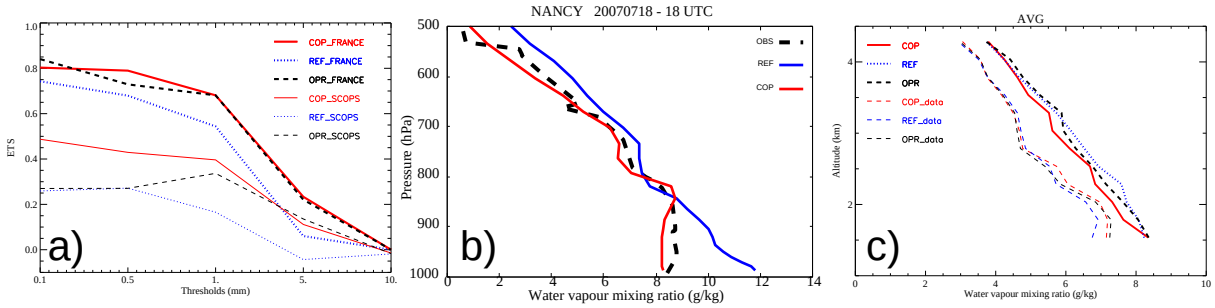

Figure 1: a) Equitable Threat Score (ETS) for 12-h accumulated precipitation forecast against raingauge observations from 03 UTC to 15 UTC, for 18,19 and 20 July 2007 over the FRANCE domain(bold lines) and the Smaller-COPS domain (SCOPS). b) Vertical profile of water vapour mixing ratio (g kg $^{-1}$) from the Nancy sounding at 18 UTC, 18 July 2007 (black dashed lines), and from the 18-h forecast REF (blue) and COPS (red) starting at 00 UTC, 18 July.c) Averaged profiles for the water vapour mixing ratio issued from the COP, OPR and REF AROME forecasts with respect to the LEANDRE 2 derived observations.

4 CONCLUSION

A clear positive impact of the assimilation of a large dataset of GPS ZTD observations in the AROME pre-operationnal suite has been obtained on the COPS IOP9 case study. Assimilation of GPS ZTD improves the short-range precipitation forecast as well as the forecast of the water vapour field. A large part of the impact can be attributed to the assimilation of the near-real time GPS ZTD dataset from E-GVAP. Assimilation of the high-resolution COPS GPS dataset in addition to the E-GVAP one leads to local positive impact on the weak precipitation.

Acknowledgements: *The COPS campaign and this study benefited from support from the ANR (Agence Nationale pour la Recherche) and the CNRS/INSU (Institut National des Sciences de l'Univers).*

REFERENCES

Poli P, Moll P, Rabier F, Desroziers G, Chapnik B, Berre L, Healy SB, Andersson E, EI Guelai FZ. 2007. Forecast impact studies of zenith total delay data from European near real-time GPS stations in Meteo France 4DVAR. *J. Geophys.Res.* **112**

Seity Y, Brousseau P, Malardel S, Masson, Bouttier, Hello 2007. Status of AROME developments, *Aladin Newsletter*, **33:**40-47

Wulfmeyer V *et al.* 2008. The convective and orographically-induced precipitation study: A research and development project of the WWRP for improving quantitative precipitation forecasting in low-mountain regions. *Bull. Amer. Meteor. Soc.* **89(10)**

Yan Xin 2009: Assimilation de donnes GPS pour la prévision de la convection profonde. *PhD*,P.Sabatier Univ. Toulouse France.

Yan X, Ducrocq V, Poli P, Hakam M, Jaubert G, Walpersdorf A. 2009a: Impact of GPS zenith delay assimilation on convective scale prediction of Mediterranean heavy rainfall.*J. Geophys.Res.*, Vol. 114

LONG-RANGE TRANSPORT OF SAHARAN DUST FROM CALIPSO, AIRBORNE AND GROUND-BASED LIDARS, AND A REGIONAL MODEL DURING COPS

J.-P. Chaboureau[1], E. Richard[1], J.-P. Pinty[1], P. Di Girolamo[2], C. Kiemle[3] and C. Flamant[4]

[1] Laboratoire d'Aérologie, Université de Toulouse and CNRS, Toulouse, France
[2] Dipartimento di Ingegneria e Fisica dell'Ambiente, Universita degli Studi della Basilicata, Potenza, Italy
[3] Institut für Physik der Atmosphäre, Deutsches Zentrum für Luft- und Raumfahrt, Oberpfaffenhofen, Germany
[4] Université Pierre et Marie Curie, Service d'Aéronomie/Institut Pierre-Simon Laplace, Paris, France
E-mail: *jean-pierre.chaboureau@aero.obs-mip.fr*

Abstract: A Saharan dust event affected the Rhine valley in southwestern Germany and eastern France on 1 August 2007 during the Convective and Orographically-induced Precipitation Study (COPS) experiment. Prior an episode of intense convection, a layer of dry and clean air capped by a warm and dusty layer was observed using Cloud-Aerosol Lidar and Infrared Pathfinder Satellite Observation (CALIPSO), airborne and ground-based lidar observations from North Africa to Western Europe. The origin of the different layers was investigated using a regional Meso-NH model simulation. Overall, the model reproduces the vertical structure of dust and water vapor. From the simulated Lagrangian back trajectories it is found that the dust was mobilized from Mauritania sources several days before while the dry layer subsided over the north Atlantic. Off Morocco, the dry layer fold down beneath the warm and dusty air and the two-layer structure was advected to the Rhine valley in about two days. As the dry layer can delay the triggering of convection for a few hours, such dusty episodes that occur prior to convective events might be of importance for quantitative precipitation forecasts.

Keywords: *COPS, precipitation, predictability, dust*

1 INTRODUCTION

Long-range transport of mineral dust in the free troposphere is important for many aspects including radiation and cloud microphysics. Such change in thermal structure can affect the skill in forecasts that do not predict dust routinely. For example, Chaboureau et al. (2007) showed an improvement in capturing the observed convective activity over West Africa at the 2-day range by the use of prognostic dust. However the impact on summertime precipitation over Western Europe has received little attention so far. On 1 August 2007 several ground-based lidars observed reaching the COPS area in the afternoon prior a convective event. The dust layer was also observed from airborne lidars in both the COPS area and upstream over the Iberian Peninsula and France. Some days before, CALIPSO observations shows the dust layer off the Moroccan coasts (Figure 1, top right). The long-range transport of dust is investigated using the mesoscale model Meso-NH (Lafore et al. 1998).

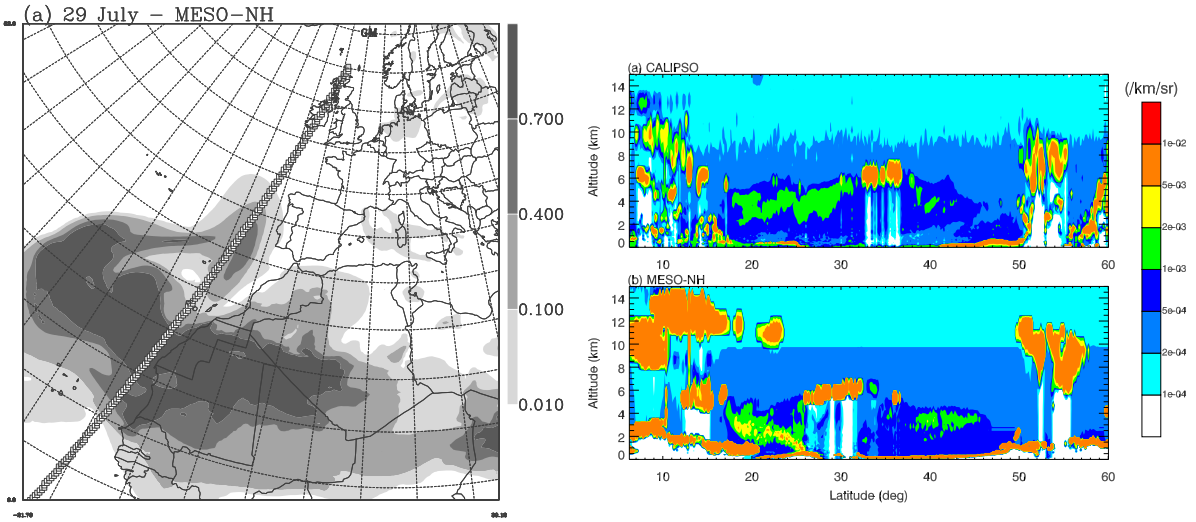

Figure 1: 0300 UTC 29 July 2007. (left) Total aerosol burden (g m^{-2}). The squares indicate the track of CALIPSO. (right) Vertical cross-section of 532-nm attenuated backscattering coefficient (km^{-1} sr^{-1}) along the line shown in left from (a) CALIPSO and (b) Meso-NH.

2 RESULTS

The case was simulated with triply nested models, with a horizontal grid spacing of 32, 8, and 2 km. The case was initialized on 26 July 2007 at 0000 UTC. In a first step it was integrated forward for 4 days using the outer grid only as model spinup for dust and cloud. For keeping the simulation close to the analyzed meteorological conditions, the simulation was nudged towards the ECMWF analyses. At 0000 UTC 1 August 2007 the case was then integrated for 24 hours using the three nested models without any nudging.

An overview of the dust event is given with a snapshot on 29 July (Figure 1). Dust with burden larger than 0.1 μmg was exported out of Africa and almost reached the coasts of the Iberian Peninsula. The good agreement achieved with the aerosol index (AI) obtained from the Ozone Monitoring Instrument (OMI, not shown) allows an assessment of the dust sources in Mauritania and northern Mali. The comparison with CALIPSO observations (Figure 1, right) shows that the model fairly well reproduced the vertical structure of the dust content.

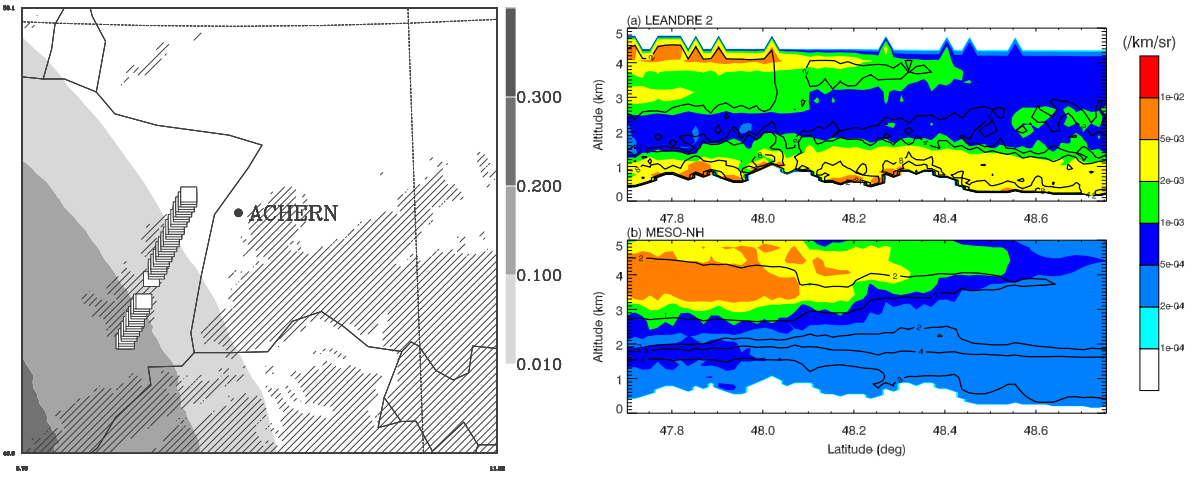

Figure 2: 1200 UTC 1 August 2007. (left) Total aerosol burden (g m^{-2}). The squares indicate the track of the SAFIRE Falcon. The hatch areas are topography above 500 m. (right) Vertical cross-section of 730-nm attenuated backscattering coefficient (shading, km^{-1} sr^{-1}) and water vapor mixing ratio (contours at 2, 4, 8 g kg^{-1}) at along the line shown in left from (a) LEANDRE 2 and (b) Meso-NH.

Another example is shown on 1200 UTC 1 August 2007 when the dust layer reached the COPS area (Figure 2). The LEANDRE-2 lidar sampled the dust layer between 3 and 5-km altitude. The Meso-NH simulation shows remarkable agreement with the observations in capturing the height and arrival time of the dust layer as well as the water vapor content. The lowest layer of high coefficient values is due to background aerosols not simulated by the model. Other comparisons with the DRL WALES airborne lidar and the BASIL Raman lidar operating from Achern confirm the ability of the model to reproduce the transport of dust from Africa to the COPS area.

3 CONCLUSIONS

The dust episode that affected the COPS area on 1 August 2007 is well reproduced by the Meso-NH model as seen with comparison with a set of lidar observations. Sensitivity studies on the predictibaility of precipitation to the dust content are under way.

Acknowledgements:
This study was funded by ANR (COPS France). The CALIPSO data were obtained from the ICARE center. Computer resources were allocated by IDRIS.

REFERENCES

[1] Chaboureau, J.-P., P. Tulet, and C. Mari, 2007: Diurnal cycle of dust and cirrus over West Africa as seen from Meteosat Second Generation satellite and a regional forecast model, *Geophys. Res. Lett.*, **34**, L02822, doi:10.1029/2006GL027771.

[2] Lafore, J.-P., et al., 1998: The Meso–NH Atmospheric Simulation System. Part I: adiabatic formulation and control simulations. Scientific objectives and experimental design, *Ann. Geophys.*, **16**, 90–109.

THE INFLUENCE OF AEROSOL PARTICLE NUMBER AND HYGROSCOPICITY ON THE EVOLUTION OF CONVECTION CLOUD SYSTEMS AND THEIR PRECIPITATION: A NUMERICAL STUDY BASED ON THE COPS OBSERVATIONS ON THE 12 AND 13 AUGUST 2007

Céline Planche, Andrea I. Flossmann, W. Wobrock

Laboratoire de Météorologie Physique, OPGC, CNRS-UBP, Clermont-Ferrand, France
E-mail: *C.Planche@opgc.univ-bpclermont.fr*

Abstract: A 3D cloud model with detailed microphysics for ice, water and aeosol particles (AP) is used to study the role of AP on the evolution of convective clouds and the subsequent precipitation. The model couples the dynamics of the NCAR Clark-Hall cloud scale model (Clark and Hall, 1991) with the detailed scavenging model (DESCAM) of Flossmann and Pruppacher (1988) and the ice phase module of Leroy et al. (2009). The microphysics follows the evolution of AP, drop, and ice crystal spectra. Aerosol mass in drops and ice crystals is also predicted.
The simulated cases are compared with radar observations on 12 and 13 August 2007 (LaMP X-band radar and Poldirad of DLR) over the northern Vosges mountains and the Rhine valley. In order to better understand the role of AP on cloud evolution and precipitation formation several sensitivity studies were performed by modifying not only aerosol number concentration but also their physico-chemical properties.

Keywords: *cloud modeling, detailed microphysics, aerosol particle impact, COPS*

1 INTRODUCTION

The impact of aerosol particles on precipitation formation is only partly understood. In this study we simulate with DESCAM 3D two convective cases observed during the COPS campaign and we examine the impact of the AP particles number and solubility on both the cloud evolution and precipitation formation.

This paper is divided into 4 parts. The model DESCAM 3D is briefly described in the section 2. The results with DESCAM 3D concerning the role of aerosol particles on cloud evolution and precipitation formation over the Vosges Mountains are discussed in section 3.

2 MODEL DESCRIPTION

The 3D model with detailed microphysics couples the 3D non-hydrostatic model of Clark and Hall (1991) with the Detailed Scavenging Model (DESCAM, Flossmann et al., 1988, Leroy et al., 2009) for the microphysical scheme. The microphysics model employs five distribution functions: three of them are number distribution functions for the wet AP, the drops and the ice crystals respectively and the remaining two are mass distributions of AP inside drops and ice particles. Aerosol particles cover the size range from nm to µm while drop and crystal sizes range from 2 µm to 1 cm.
The microphysical processes that have been implemented are: AP growth and activation/deactivation, condensation and evaporation of droplets, coalescance, homogeneous and heterogeneous nucleation, vapor deposition on ice crystals and riming. The model is described in detail in Leroy et al. (2009).

3 COPS CONVECTIVE CLOUD SYSTEMS

3.1 Model setup

The convective cloud systems observed on 12 and 13 August 2007 show quite different characteristics (Hagen et al., 2008) leading to different model setups in order to simulate both events.

For the 12 August case, the model domain covers 130 x 130 km in the horizontal and 16 km high in the vertical. The resolution is 1 km for the horizontal coordinates and 200 m for the vertical one. A second domain with a 250 m grid is nested for the area of interest. The dynamical time step is 3 seconds. The thermodynamic and dynamic conditions are given by the sounding of Nancy, 12 UTC for the 12 August. On 13 August a considerable western wind flow prevailed requiring the use of large scale initialization by means of the ECMWF reanalysis data at 6 UTC. Consequently the outer domain size increased to 384 x 256 km^2 with a horizontal grid of 4 km causing the nesting of two subdomains with 1 km and 0.25 km grid resolution. Figs. 1a and b give 3D views of the spatial location and structure of the convection for the innermost model domains. Convective clouds for both cases reach up to 5 km. On 12 August the precipitating cloud clusters form over the mountains and persists almost at the same place for about one hour. On 13 August, however, clouds and precipitation form on the eastern rime of the Vosges and cross during 1.5 h the entire Rhine valley.

To initialize the microphysics, the AP spectra follows Jaenicke (1988) for a continental air mass. In order to understand the role of AP concentration on cloud evolution and precipitation formation, the number of AP is increased and decreased for polluted and clean environment, respectively. Also, the solubility of AP is modified to understand its role on the rain formation.

a) **b)**

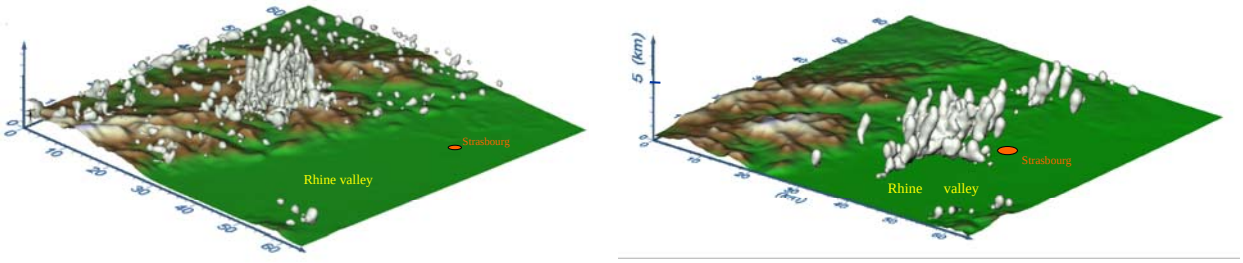

Figure 1. Field of cloud water for 12 August 2007 (a) and 13 August 2007 (b). The white envelope corresponds to 0.1 g/kg.

3.2 RESULTS

Table 1 gives the results of model simulations for the different aerosol number distributions and different particle solubility 60 min after cloud formation starts. Mean rain amount and rain maxima were taken at the surface while data for vertical wind; relative humidity and droplet number were taken at 2 km altitude.

Comparing the results obtained for the continental, clean and polluted cases we can see that the number of rain drops, the rain amount and the relative humidity are quite sensitive to the number of aerosol particles. However, the change of the AP solubility doesn't influence the dynamic or microphysical parameters.

Cases	mean rain amount (mm)	rain max. (mm)	N_{drops} (cm^{-3})	N_{drops} max (cm^{-3})	mean w (m/s)	RH (%)	RH max (%)
Continental	0.63	3.819	30.1	157.7	1.46	100.25	100.6
Clean	0.70	4.114	17.6	88.5	1.34	100.33	100.7
Polluted	0.57	3.264	59.4	405.9	1.40	100.12	100.3
50% soluble	0.63	3.820	30.2	157.6	1.46	100.26	100.6
5% soluble	0.63	3.822	30.1	157.2	1.47	100.25	100.6
$\alpha_c = 0.5$	0.64	3.856	25.8	129.8	1.47	100.22	100.5

Table 1: Rain amount, number of rain drops N_{drops}, vertical wind w and relative humidity RH average values and maxima for the continental, clean, polluted case. In these cases AP were chosen 100% soluble. For the 50 % and 5% soluble cases the continental AP distribution was used, just as for the last case where the sticking coefficient for water vapor was increased from 0.04 to $\alpha_c = 0.5$.

4 CONCLUSIONS

The simulation with our detailed cloud model show good agreement with the cloud and precipitation characteristics observed by our X band Radar and Poldirad of DLR. To understand the role of the AP on cloud evolution and precipitation formation several sensitivity studies were performed by modifying not only aerosol number concentration but also their physico-chemical properties. The numerical results show a strong influence of the aerosol number concentration on the precipitation intensity but little effect of the aerosol particle solubility on the rain formation can be found.

Acknowledgements:
The calculations for this study have been done on computer facilities of IDRIS, CNRS at Orsay and CINES in Montpellier, under the project 940180. The authors acknowledge with gratitude the hours of computer time and the support provided.

REFERENCES

Clark, T. L., and W. D. Hall, 1991: Multi-domain simulations of the time dependent Navier-Stokes equations : benchmark error analysis of some nesting procedure, *J. Comp. Phys.*, **92**, 456-481.

Flossmann, A. I. and. H. R. Pruppacher, 1988: A theoretical study of the wet removal of atmospheric pollutants. Part III : The uptake, redistribution, and deposition of (NH4)2SO4 particles by a convective cloud using a two-dimensional cloud dynamics model. J. Atmos. Sci., 45, 1857-1871.

Leroy, D., W. Wobrock and A. I. Flossmann, 2009: The role of boundary layer aerosol particles for the development of deep convective clouds: a high-resolution 3D model with detailed (bin) microphysics applied to CRYSTAL-FACE , Atmos. Res.; DOI: 10.1016/j.atmosres.2008.06.001

Jaenicke, R., 1988: Aerosol physics and chemistry. In Landolt-Börnstein: Zahlenwerte und Funktionen aus Naturwissenschaften und Technik, V 4b, G. Fischer Editor, Springer, 391-457.

Hagen M., J. VanBaelen and E. Richard, 2008: Orographic influence on life cycle of convection – observations during the COPS. ERAD conference, Helsinki, 2008

INVESTIGATIONS OF THE IMPACT OF AEROSOLS ON A HAILSTORM IN THE BLACK FOREST

Heike Noppel[1], Ulrich Blahak[1], Axel Seifert[2], Klaus D. Beheng[1]

[1] Institut für Meteorologie und Klimaforschung, Karlsruhe Institute of Technology, Germany
[2] German Weather Service, Offenbach, Germany
E-mail: *heike.noppel@kit.edu*

Abstract: Hail storms can cause significant damage to crops, buildings or cars. Therefore, it is of great interest to be able to predict them or to assess the potential to modify them by human activities either inadvertently by air pollution or by intended cloud seeding. To this aim a sophisticated two-moment cloud microphysical scheme has been implemented into the numerical weather prediction model COSMO. A hailstorm in the Black Forest that caused significant damage was simulated with this model system with a horizontal resolution of 1 km. COSMO forecasts with a coarser resolution and the standard one-moment microphysical scheme were used for initialization and boundary conditions. A severe hailstorm that resembles the observations quite well and produces realistic amounts of precipitation and hail at the ground develops with this model system, though some hours late. Sensitivity studies were conducted varying the concentration of cloud condensation nuclei (CCN) and the shape of the cloud droplet size distribution. Results show that both have a significant impact on hail accumulated at the ground and on the size of the hailstones. However, due to the complexity of the storm dynamics and microphysics, general statements whether an increase or decrease in CCN concentration invigorates a hailstorm can not be drawn.

***K*eywords:** *NWP model, hailstorm, aerososl effect, convective clouds, COSMO model*

1 INTRODUCTION

Recent studies of cloud interactions with particulate air pollution, performed mostly on a conceptual level, suggest that pollution aerosols can invigorate convection into severe storms by slowing down the conversion of cloud drops into precipitation. In pristine air rain formation is rather fast, invoking early downdrafts and preventing the lifting of much water to the supercooled levels, so that the cloud dies early with a moderate amount of rainfall. According to the hypothesis that should be tested within the ANTISTORM project, a high concentration of aerosol acting as cloud condensation nuclei (CCN) slows down rain formation and increases the amount of supercooled water in the mature stage of the cloud. This leads to enhanced riming, the production of hail, high precipitation rates and strong downdrafts.

The objectives of the ANTISTORM project were to test this hypothesis, study the impact of aerosols on convective storms in Europe, and "develop models that should help to improve forecasting and even suggest strategies for mitigating storms before disaster strikes" (http://antistorm.isac.cnr.it/).

The numerical model we used for our studies is the COSMO model combined with the 2-moment bulk microphysical scheme by Seifert and Beheng (2006). Some parameters and process descriptions of the 2-moment scheme have been altered to better represent "hail" particles (Blahak, 2008). In order to test the model and to investigate the impact of CCN, the case study described in the following section was chosen.

2 THE HAILSTORM OF JUNE, 28th 2006

On 28/06/2006 the small town of Villingen-Schwenningen (VS) situated in South-West Germany at the eastern edge of the Black Forest was hit by a strong hail storm. Due to the storm more than 100 people got injured and one man drowned. Additionally, many crops, cars and buildings were damaged, mainly by hailstones but also by flooding.

The synoptic situation was characterized by a strong vertical windshear, with northerly to easterly winds at the bottom and a strong wind from West to South-West at levels above 3000 m. According to radio soundings at Nancy and Stuttgart at 12 UTC, lifting condensation level was at about 800 m amsl and temperature at that level about 14 °C . Air temperature near the ground was about 19 °C with a high relative humidity.

In the late afternoon several convective cells could be observed in the vicinity of the Black Forest and the adjacent Rhine Valley. At about 17 UTC one of the cells split close to the crest of the Black Forest and the right cell moved almost perpendicular to the main wind in south-easterly direction. This right mover intensified, developing radar reflectivities of more than 65 dBZ, reached VS at about 17:30 UTC and passed it with the core of the cell situated slightly to the north of the town. After crossing the Swabian Alb, another nearby low montain ridge, the storm finally decayed.

3 MODEL SETUP

For the numerical simulations full orography was used and the model's initial state as well as the boundary values were adopted from operational COSMO-DE forecasts starting at 12 UTC on 28/06/2006. Integration time was 13 hours and the model domain 291 x 291 x 64 gridpoints with a horizontal resolution of 1 km. The COSMO-DE forecasts provided by the German Weather Service had been performed with the standard microphysical one-moment scheme. The output used as boundary conditions was available every hour.

For the nested grid, cloud microphysics was paramterized by an extended version of the two-moment scheme by Seifert and Beheng (2006). Besides modifications concerning hail by Blahak (2008) a new scheme for cloud droplet nucleation based on look-up tables by Segal and Khain (2006) as well as a shape parameter depending on mean diameter for sedimentation and evaporation of raindrops (Seifert, 2008) have been implemented. The scheme was validated for different CCN conditions by comparison to a spectral bin model (Noppel et al., 2008; Seifert et al., 2006).

Four different CCN concentrations leading to different typical maximum cloud droplet concentrations N_{drop} were assumed: (1) low CCN, N_{drop} = 100 cm^{-3}, (2) intermediate CCN, N_{drop} =350 cm^{-3}, (3) high CCN, N_{drop} = 1200 cm^{-3}, (4) very high CCN, N_{drop} = 2100 cm^{-3}. As CCN conditions may also change the size distribution of the nucleated droplets the parameters μ and ν of the assumed generalized gamma-distribution

$$f(x) = Ax^{\nu} \exp(\lambda x^{\mu}) \tag{1}$$

were also varied (x is particle mass). The two other parameters A and λ can be calculated from the predicted bulk mass and number densities (the 0th and 1st moment of the distribution). Three different cloud droplet size distributions (CDSD) were assumed: (a) ν=1/3, μ=2/3, (b) ν=1, μ=1, (c) ν=6, μ=1/3.

4 RESULTS

In all model runs, no convective cells at all develop in the vicinity of the Black Forest during the afternoon. Only at about 20 UTC first convective cells occur. At about 21:30 UTC a right mover occurs whose development is very similar to the observed hail storm. The simulated amount of accumulated precipitation as well in total (up to 51 mm) as for hail only (up to 14.9 mm) seems to be quite realistic and the model produces a significant number of large hailstones (at heights below 2 km amsl up to about 13 particles with more than 2.5 cm in diameter per 1000 m^3). In contrast, simulations with the standard one-moment scheme for microphysics fail to generate a right mover and produce much lower precipitation amounts.

When comparing the results for the different CCN scenarios it becomes evident that CCN concentration as well as the assumed CDSD do have a significant impact on the intensity, lifetime, and dynamics of a convective storm. For example, for scenario 4a (very high CCN concentration, CDSD (a)) the hailstorm is much weaker and passes VS about 15 km further to the North than for scenario 1a (low CCN concentration, CDSD (a)). The consideration of all storms that occur in the model domain shows that a variation in CCN concentration or CDSD may lead to a significant weakening of one hailstorm and at the same time to an invigoration of another one. As the temporal evolution is influenced by CCN concentration and CDSD, the impact of orographical structures also changes.

A closer examination of the dynamics and cloud microphysics of the right moving storm and the comparison of two of the CCN-scenarios reveals how complex the different processes and their interactions within such a storm may be and that it is is almost impossible to predict what will happen if certain microphysical conditions, like aerosol concentrations, change.

REFERENCES

Blahak, U., 2008: Towards a Better Representation of High Density Ice Particles in a State-of-the-Art Two-Moment Bulk Microphysical Scheme. *15th Intern. Conf. on Clouds and Precipitation*, July 7-11, 2008, Cancun, Mexico

Noppel, H., A. Khain, A. Pokrovsky, U. Blahak, K.D. Beheng, 2008: How well can a bulk scheme reproduce the microphysical processes within a convective storm? - Comparisons to a spectral bin model. *15th Intern. Conf. on Clouds and Precipitation*, July 7-11, 2008, Cancun, Mexico

Segal, Y. and Khain, A., 2006: Dependence of droplet concentration on aerosol conditions in different cloud types: Application to droplet concentration parameterization of aerosol conditions. *J. Geophys. Res.*, **111**, D15240, doi:10.1029/2005JD006561

Seifert, A., 2008: On the parameterization of evaporation of raindrops as simulated by a one-dimensional rainshaft model. *J. Atmos. Sci.*, **65**, 3608–3619

Seifert, A., K.D. Beheng, 2006: A two-moment cloud microphysics parameterization for mixed-phase clouds. Part 1: Model description. *M*eteorol. Atmos. Phys., **92**, 45–66.

Seifert, A., A. Khain, A. Pokrovsky and K.D. Beheng, 2006: A comparison of spectral bin and two-moment bulk mixed-phase cloud microphysics. *Atmos. Res.*, **80**, 46–66.

PRECIPITATION DOWNSCALING IN WESTERN NORWAY: TIME-STEP PRECIPITATION INTENSITY

I. Barstad[1], U. Heikkilä[1]and M. Mesquita[1].

[1] Bjerknes Centre for Climate Research, Bergen, Norway
E-mail: *Idar.Barstad@bjerknes.uib.no*

Abstract: High frequency observations from two field campaigns have been compared with time-step precipitation in a numerical model. The numerical model schemes seem not to fully reproduce the observed precipitation. The schemes produce too high level of wetness and the intensities are too low. Typical simulated intensities are about 9mm/hr, whereas the observed values are typically 15mm/hr.
Keywords: *ICAM, time-step precipitation, evaluation, wrf, STOPEX.*

1 INTRODUCTION

The resolution in mesoscale numerical models has increased in the last few years. This has produced higher levels of detail for atmospheric parameters such as precipitation. Evaluating the added improvement in the models is not straight forward. Many goodness measures (e.g. root-mean-square error and Pearson correlation) show reduced skills when the detail level is enhanced (Barstad and Smith, 2005). In this extended abstract we will show how two different microphysical numerical schemes perform at the time-scale of the model time-step.

2 EXPERIMENTS AND RESULTS

The island Stord on the west coast of Norway was chosen as an experimental site for orographic precipitation, STord Orographic Precipitation EXperiment (STOPEX 1; Reuder et al. (2007) and STOPEX 2). Stord has about 600m tall mountains, it is 20km long (north-south) and is 10km wide (west-east). See Figure 1 for geographical information. Southwesterly winds prevail in the area. During autumn 2005 (7 weeks) and 2006 (11 weeks), numerous rain gauges were deployed across the island, and several weather stations (AWS) surveyed the weather situation. The stations used in this study are shown in Figure 1.

The numerical model (WRFV3.0; www.wrf-model.org) was set up with two two-way nested domains (10km-3.3km) and the boundaries were orchestrated by the ECMWF-analysis. A standard set-up was used with 39 vertical layers. Two different microphysical schemes were tested: "mp3" - a simple 3-class scheme (Hong et al. 2004), and "mp10" - a more sophisticated multi-class scheme (Morrison and Pinto, 2006). The model time-step was 20s in the higher resolution domain. An fdda-nudging was used with 6-hour relaxation time outside the planetary boundary layer.

Table 1 shows the performance of the two schemes for 6 stations across the island, from west to east. 'Rain vs. no-rain' cases are shown in % for various accumulation periods and the total accumulated precipitation for Stopex 1 period is indicated. From the table, we find that the simulated 10min cases are too wet, particularly at the upwind flat land station (P1). The mp3-simulation is worse than the mp10 case. Longer accumulation periods camouflage this effect showing better results. The total precipitation amounts show too little simulated precipitation in elevated terrain, too much on the flat land and the mp3-simulation produces the highest values.

Station/measure	Wet (%) – 10min (mp3/mp10)	Wet (%)- 1hr (mp3/mp10)	Wet (%)- 3hr (mp3/mp10)	Wet (%) – 24hr (mp3/mp10)	Total accumulated (mm) (mp3/mp10/**obs**)
P1 upwind-flat land	525/443	285/254	195/183	119/119	787/729/**333**
P3 upwind-slope	360/311	219/203	160/152	110/108	927/766/**768**
P5 top	292/234	192/168	145/138	100/100	856/676/**1120**
P11 leeside-top	256/200	160/137	125/114	98/98	707/640/**1220**
P8 leeside-slope	331/265	208/182	163/154	111/113	804/634/**838**
P9 leeside-flat land	387/324	234/207	169/158	111/113	845/704/**640**

Table 1. Simulated precipitation across Stord island autumn 2005. Wet events (i.e. 100% means as observed) for various accumulation periods (column 2-5) and total accumulated amounts during the campaign (last column). "mp3" and "mp10" refer to two different microphysical schemes used. Underlined values indicate the ones with better skill. See Figure 1 for station locations.

In order to have a closer look at the intensities 'hidden' inside various accumulating periods (10min, 1hr etc.), we turn to tipping bucket measurements and to the comparison with the model time-step precipitation. Figure 2 shows the typical time between each tip (0.2mm amount) observed and simulated. The observed intensity is about 15mm/hr whereas the simulated is closer to 9mm/hr. The mp3-simulation, in particular, shows

too many weak intensity cases (200-400s in Fig.2). This fits with the general picture of a too wet model (Table 1).

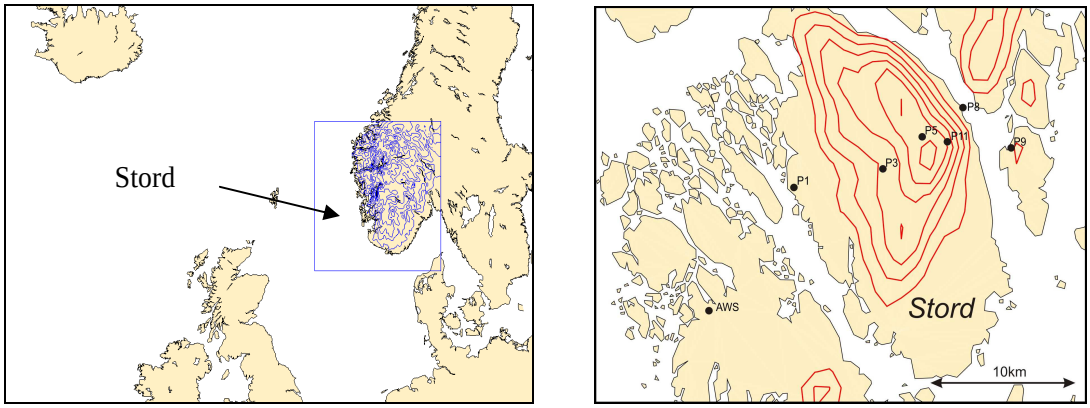

Figure 1. Left: The two nested model domains (10km-3.3km). Right: The terrain (every 100m starting at 100m elevation) is shown by 1km grid. Precipitation stations in Table 1 are indicated.

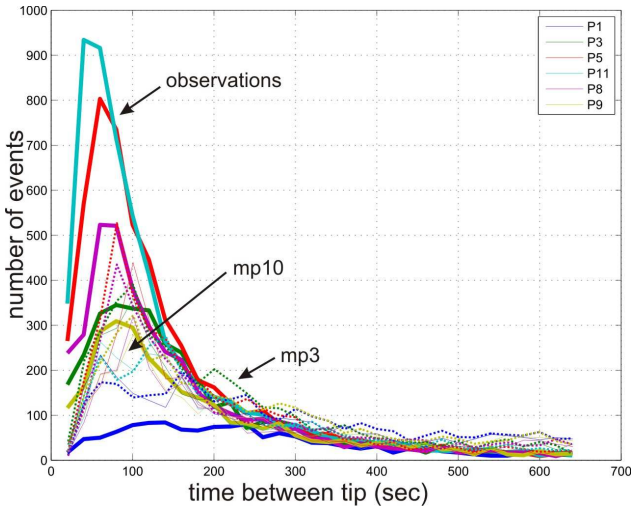

Figure 2. Tipping-bucket vs. modelled values for Stopex 1. 6 stations are shown, cf. Table 1. Heavy solid lines represent the observations, dotted lines the mp3-simulation, and the thin lines the mp10-simulation.

An important case is that of November 5th, 2006. The winds were steadily from the west throughout the day. Some of the rain gauges received as much as 100mm. Simulation of this case with a similar model set up as used in this report, but including an additional 1km nest, shows that the maximum precipitation intensity in a 1km grid was about 15-20% larger than in the 3km grid. This indicates that the precipitation results in the 3.3km grid should ideally be a bit lower than the observed values.

3 CONCLUSIONS

From this investigation, we find that simulation by a mesoscale model with 3.3km grid spacing, has similar problems as the standard problem for numerical models; it rains too often and too little. The simpler scheme used performs better than sophisticated ones in complex terrain, except on the flat land. A case study having higher resolution indicates that higher intensities (15-20% increase) are expected if a 1km grid is nested inside a 3km grid.

Acknowledgements:
Tor de Lange, Joachim Reuder, Geir Ottar Fagerlid, Marianne S. Andersen and Eli Anne Ersdal made valuable contributions in the acquisition of the observational data.

REFERENCES

Barstad, I. and R. B. Smith, 2005: Evaluation of an Orographic Precipitation Model. Journal of hydrometeorology **6**, 85-99.

Hong, S.-Y., J. Dudhia, and S.-H. Chen, 2004: A Revised Approach to Ice Microphysical Processes for the Bulk Parameterization of Clouds and Precipitation. Mon. Wea. Rev. **132**,103–120.

Morrison, H., and J. O. Pinto, 2006: Intercomparison of bulk microphysics schemes in mesoscale simulations of springtime Arctic mixed-phase stratiform clouds. Mon. Wea. Rev. **134**, 1880–1900.

Reuder, J., I. Barstad, G.O. Fagerlid and A.D. Sandvik, 2007: Stord Orographic Precipitation Experiment (STOPEX): An overview of phase I. Hydrology and Earth System Sciences **10**, 17-23.

GRIDDING DAILY PRECIPITATION FROM A SPARSE SURFACE NETWORK IN COMPLEX TOPOGRAPHY — A REDUCED-SPACE OPTIMAL INTERPOLATION APPROACH

Mark A. Liniger, Reinhard Schiemann, Christoph Frei

Federal Office of Meteorology and Climatology MeteoSwiss, Zurich, Switzerland
E-mail: *mark.liniger@meteoswiss.ch*

Abstract: A feasibility study is presented testing the application of reduced-space optimal interpolation for gridding daily precipitation from a sparse gauge network. The results of the study are encouraging, the method clearly outperforms a simpler reference technique and lends itself to the application both in a near real-time and a climate reconstruction context. Including weather-type information does not substantially improve the gridded fields.

***K*eywords:** *ICAM, optimal interpolation, precipitation, gridding, mapping*

1 INTRODUCTION

Operational networks of rain-gauge stations offer dense information on the distribution of precipitation. Yet, only a rather small part of this information is based on automatic measurements available in real-time. Most of the observations are taken manually and are available only weeks to years after the event. Thus, a real-time description of mesoscale precipitation fields is a challenge, in particular in complex topography. In this study, we propose a method to derive quasi real-time fine-scale precipitation fields. The method exploits the statistical relationship between the coarse real-time and dense climatic information. It is rigorously evaluated for daily precipitation fields over Switzerland and it is tested if the inclusion of weather type information yields improved results.

The same method can also be employed to reconstruct precipitation fields in the past when the density of observations was low.

2 METHOD AND DATA

The proposed method is reduced-space optimal interpolation (RSOI; Kaplan et al. 1997). It is normally applied in the context of climate reconstruction and has been used, for example, for reconstructing monthly precipitation totals in the Alps (Schmidli et al. 2001).

RSOI consists of two parts. First, principal component analysis (PCA) is used to obtain a reduced-space description of high-resolution data available during a calibration period. Thereafter, coarse data (available both in the calibration and in a reconstruction period) are used to estimate the principal component scores in the reconstruction period. In this way, the method considers both the temporal evolution of the data in the reconstruction period and the spatial covariance structure known from the high-resolution data.

In the application presented here, the high-resolution data (referred to as "OBS" below) are from a gridded daily precipitation climatology (Frei and Schär 1998, Frei and Schmidli 2006). Figure 1a shows the dense gauge network that forms the observational basis for these grids (red dots) and Figure 1b shows their long-term mean. The coarse data are gauge observations from a sparse network (Figure 1a, blue circles). The calibration period is 1971–1980 and daily reconstructed fields ("RSOI") are derived throughout 2001–2007. As a reference, daily fields created by means of a simpler gridding technique ("SIMPLE") and based on the same sparse gauge network are also taken into account. The study area is Switzerland.

Additionally, RSOI is applied separately for each weather type of two weather type classifications. These classifications are called PCACA (5 types) and SANDRA (22 types), respectively, and are from version 1 of the classification catalogue provided by COST Action 733 (`http://www.cost733.org`).

3 RESULTS

PCA efficiently reduces the dimensionality of the OBS grids. About 93% of the variance in these data can be represented by as few as 10 principal components. Several examples show that RSOI clearly outperforms the simpler gridding technique (e.g., Figure 2abc). A systematic quantitative evaluation of the SIMPLE and RSOI grids through the reconstruction period corroborates this finding (not shown here). The benefit is particularly high in situations of large-scale precipitation. For situations with highly localized precipitation features (e.g., due to thunderstorms) both methods perform at a comparable skill and features not captured by the sparse network cannot be represented satisfactorily (e.g., Figure 2def). Finally, we find that the gain in RSOI reconstruction skill due to the inclusion of weather type information is at best moderate and depends strongly on the weather type.

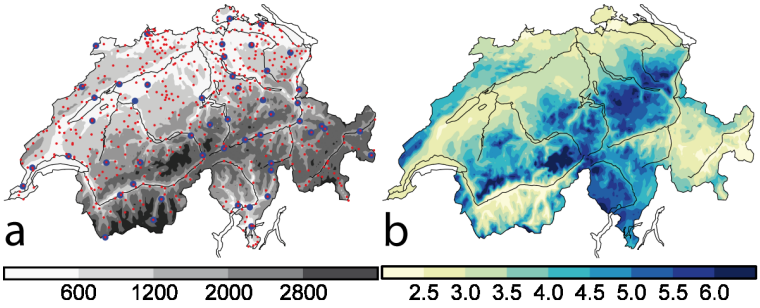

Figure 1: Overview of the study area. (a) Gauges of the sparse network (51 stations; blue circles), the dense network (typically 420 stations on individual days; red dots) and height of topography (shading). (b,c) Long-term mean of daily precipitation (mm d^{-1}).

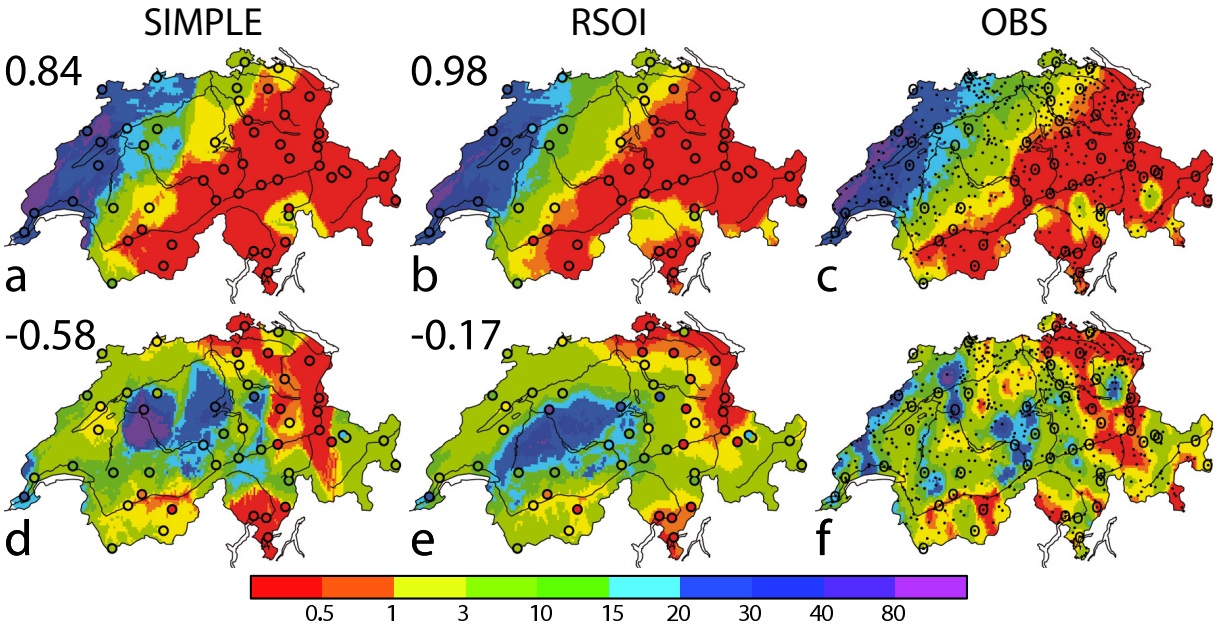

Figure 2: Examples of daily gridded fields (top: 2004-03-13, bottom: 2002-07-30). (a,d) reference method (SIMPLE), (b,e) RSOI, (c,f) high-resolution fields (OBS). Numbers show the mean-squared-error skill score quantifying interpolation quality.

4 CONCLUSION

RSOI is a promising candidate for real-time precipitation gridding. The method presented herein is entirely based on gauge measurements and does not use other sources of data such as radar observations. Therefore, it is attractive as a reference for methods using additional data sources, or in situations when no such additional observations are available. Apart from gridding in a near real-time context, the reconstruction of historical daily precipitation fields is a conceivable application of RSOI.

REFERENCES

Frei, C., and C. Schär, 1998: A precipitation climatology of the Alps from high-resolution rain-gauge observations. *Int. J. Climatol.*, **18**, 873–900.

Frei, C., and J. Schmidli, 2006 (in German): Das Niederschlagsklima der Alpen: Wo sich Extreme nahe kommen. *promet, meteorologische Fortbildung (Deutscher Wetterdienst)*, **32**, 61–67.

Kaplan, A., Y. Kushnir, M. A. Cane, and M. B. Blumenthal, 1997: Reduced space optimal analysis for historical datasets: 136 years of Atlantic sea surface temperatures. *J. Geophys. Res.*, **102**, 27835–27860.

Schmidli, J., C. Frei, and C. Schär, 2001: Reconstruction of Mesoscale Precipitation Fields from Sparse Observations in Complex Terrain. *J. Climate*, **14**, 3289–3306.

HIGH RESOLUTION ANALYSES BASED ON THE D-PHASE & COPS GTS –AND NON-GTS DATA SET

Theresa Gorgas, Manfred Dorninger, Reinhold Steinacker

Department of Meteorology and Geophysics, University of Vienna, Austria
E-mail: *theresa.gorgas@univie.ac.at*

Abstract: A high-resolution data set of surface observations which was set up for the whole year of 2007 in Central Europe is introduced and described. Also availability information for possible users is offered. For the same period and spatial domain an additional set of reanalyses based on the observation data is produced. Methods and examples are presented.

Keywords: *Surface observation data, reanalysis, VERA*

1 INTRODUCTION

In the framework of the programmes MAP D-PHASE and COPS the University of Vienna, collected GTS and Non-GTS data from the national and regional meteorological services for the year 2007 (GOP period) covering a greater Central Europe domain. All surface data are converted to a unique NetCDF format and the precipitation amounts accumulated to 1, 3, 6, 12 and 24 hour values. The data are uploaded to the WDCC (World Data Climate Centre) in Hamburg.

Based on the VERA (Vienna Enhanced Resolution Analysis) method, the GTS and Non-GTS data set is used to create a set of hourly reanalyses for 2007 over Central Europe with a grid-point distance of 8km.

2 THE COPS & D-PHASE GTS AND NON-GTS DATA SET

The MAP D-PHASE and COPS data set of GTS and Non-GTS surface stations involves about eleven thousand Non-GTS and more than thousand GTS stations. Several European national meteorological institutions where asked to provide data from regional operational observation networks, which are not included in the GTS system. As the data collection task concentrated only on operational data the data set does not include data produced during the field campaign of COPS. It is, thus, meant to extend the amount of data available for the COPS and D-PHASE intensive periods and to support continuative work on case studies in a larger area.

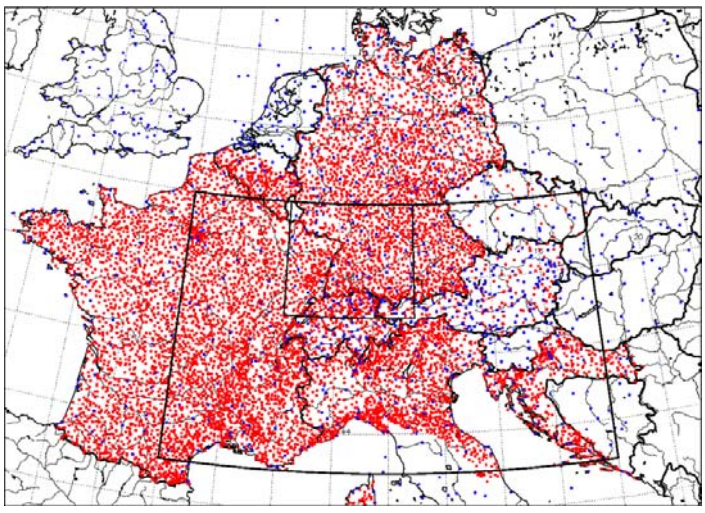

Figure 1. Distribution of all GTS (blue dots) and Non-GTS (red dots) stations. The majority of the latter are precipitation stations. The black frames define the COPS (smaller one) and D-PHASE (larger one) areas.

There is a wide range of parameters which are, if provided by the weather services involved in the data files: Additionally to the "main" parameters like wind, temperature, dew point, pressure and precipitation also other parameters like cloud coverage, present and past significant weather information, gusts, pressure tendency and maximum/minimum temperatures are collected. However, many of the regional observation networks only concentrate on few parameters.

It was always the highest temporal resolution available which was acquired from the providing institutions. Hence temporal resolutions of originally received data range from 5, 6 or 10 minutes to 1-hourly and 3-hourly and up to a maximum of 24-hourly measurements in the case of climatological stations. Especially in the case of precipitation values the variety of accumulation periods poses a problem for the reasonable application of the data.

In order to solve this problem the University of Hohenheim reprocessed the whole data set and produced additional sets, each for the accumulation periods of 1h, 3h, 6h, 12h and 24h. This step enables to the treat the data set as a whole for analysis purposes or other applications.

The data are saved in a unique NetCDF format and in annual files for each observing station, where each file includes all parameters measured by the station. The single files are available as packed files for country, data provider and network. Additional packages are available for each precipitation accumulation period.

3 VERA AND QUALITY CONTROL

VERA has been developed at the Department of Meteorology and Geophysics, University of Vienna. It has already been in use for operational 2D analyses in recent years. The calculation, based on a variational approach, is carried out on a regular 2D grid. Different resolutions (8km for the reanalysis data set, 16km for operational use) and arbitrary target areas can be chosen. For downscaling purposes VERA uses an a priori knowledge on small-scale physical processes over complex terrain, the so called "fingerprint technique", which transfers information from rich to data sparse regions. The hourly reanalyses are performed for following parameters: Equivalent potential and potential temperature, mean sea level pressure, wind and precipitation, the latter for 1h, 3h, 6h, 12h and 24h accumulation periods. In a post processing step also mixing ratio and moisture flux divergence are calculated.

In principle VERA could be defined as "model-independent", which means that it is not necessary to involve an NWP-model's first guess field in the analysis procedure. However, due to the large target area there are data lacking areas at the edge. Therefore grid values of analysis and forecast fields of the global GFS model are employed as bogus stations when there's no other surface observation station near a VERA grid point.

A very important element of the analysis system is the quality control scheme which corrects observational surface data before the analysis procedure. A variational scheme enables weighted correction recommendations for each station value. Wrong and unnatural values or simply stations with too large correction recommendations are sorted out. In the case of very high or highly variable station density - for example by performing analyses of the GTS and Non-GTS data set - partial clustering of stations is possible in order to avoid calculation difficulties.

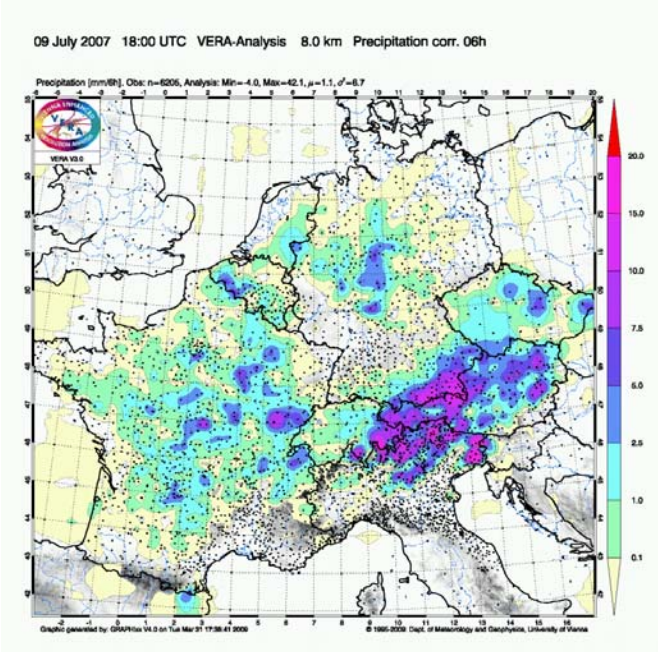

Figure 2. Example of a VERA analysis field for 6-hourly accumulated precipitation.

4 CONCLUSIONS & OUTLOOK

Like the observational data set also the re-analyses of 2007 shall be made available to all users at WDCC. It is intended to serve as a reference for ongoing studies in the framework of COPS and D-PHASE, for example as quick-look for case studies, as a basis for predictability studies or as reference data for verification activities. One of the next working steps concerning the analysis system will be the estimation of analysis errors, important additional information for all possible applications.

We thank all Central European data providers for their support and Thomas Schwitalla from the University of Hohenheim for his efforts concerning the accumulation of precipitation data.
The founding for our activities is provided by FWF (Austrian Science Fund) and DFG (German Research Foundation).

REFERENCES

Steinacker R., M. Ratheiser, B. Bica, B. Chimani, M. Dorninger, W. Gepp, C. Lotteraner, S. Schneider, S. Tschannett, 2006: A mesoscale data analysis and downscaling method over complex terrain. Mon. Wea. Rev., 134, 2758-2771.

Gorgas T. et al., 2008: The GTS and non-GTS data set for COPS and MAP D-PHASE, 7th COPS Workshop, October 27-29, Strasbourg. Presentation available at: https://www.uni-hohenheim.de/spp-iop/7th_COPS_WS/7th_COPS_workshop.html

Rotach, M.W and 38 co-authors, 2009: MAP D-PHASE: Real-time Demonstration of Weather Forecast Quality in the Alpine Region. Bull. Amer. Meteorol. Soc., accepted.

Wulfmeyer V and 27 co-authors, 2008: The Convective and Orographically-induced Precipitation Study: A Research and Development Project of the World Weather Research Program for Improving Quantitative Precipitation Forecasting in Low-mountain Regions. Bull. Amer. Meteor. Soc., DOI 10.1175/2008BAMS2367.1.

NOCTURNAL COLD AIR INTRUSIONS AT ARIZONA'S METEOR CRATER

C. David Whiteman, Sebastian W. Hoch, and Manuela Lehner

University of Utah, Salt Lake City, Utah, USA
E-mail: *dave.whiteman@utah.edu*

Abstract: A persistent nighttime near-isothermal atmosphere inside Arizona's Meteor Crater is produced by cold air inflow into the crater. A regional drainage flow builds up a layer of cold air on the upwind side of the crater and a shallow layer of cold air spills over the 30-60 m high rim and descends partway down the sidewall until reaching its buoyancy equilibrium level. Detrainment of cold air during its katabatic descent destabilizes the basin atmosphere, driving it towards isothermalcy.

Keywords: *ICAM, Meteor Crater, cold air intrusions, basins, katabatic flow, detrainment, atmospheric heat budget*

Arizona's Meteor Crater, 40 km east of Flagstaff, Arizona, is a uniform circular basin that is 1.2 km in diameter and 170 m in depth. The crater rim extends 30-60 m above the surrounding Colorado Plateau, a uniform plain that slopes gently downward from the Mogollon Rim towards the northeast to the Little Colorado River. An unusual nighttime temperature structure evolution occurs in the crater on synoptically undisturbed nights (Whiteman et al. 2008). To our knowledge, such a structure has not been previously reported in other basins. A 30-m-deep, intense inversion forms in the early evening on the crater floor. This is capped by a deep near-isothermal layer that extends to the crater's rim. This vertical temperature structure is maintained as the crater atmosphere continues to cool through the night. The processes responsible for the production and maintenance of the deep, persistent isothermal layer are the subject of this paper.

The isothermal layer was present on synoptically quiescent, clear nights in soundings from 3 tethersondes operated at the valley center, the lower west sidewall and the lower east sidewall. These soundings show that the bulk crater atmosphere is approximately horizontally homogeneous, with weak and variable winds (not shown).

Pseudo-vertical soundings from four lines of temperature data loggers running up the north, east, south and west sidewalls and out onto the adjacent plain were analyzed to visualize the temperatures and temperature gradients during the night in the near-surface layers. The temperature data were combined with wind data from the west, north and east rims and from a 10-m tower 2.5 km southwest of the crater center on the adjacent plain to produce Figure 1.

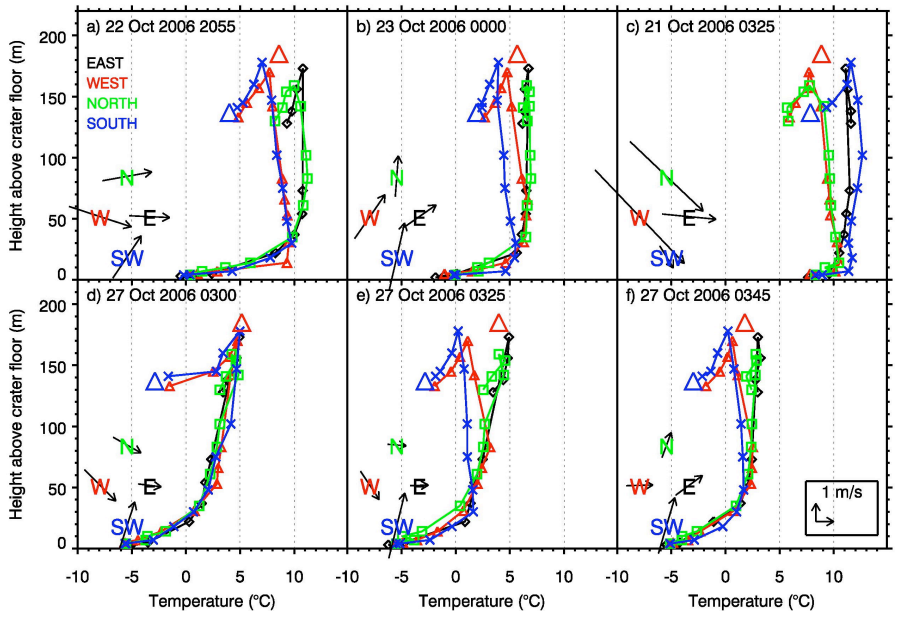

Figure 1. Pseudo-vertical temperature profiles from four lines of temperature data loggers running up the north (green squares), east (black diamonds), south (blue crosses) and west (red triangles) inner sidewalls of the crater to the rim level and out onto the adjacent plain. Vector winds from the 5-m level at the north and east rims, and from the 10-m level at the highest point on the west rim and at the Southwest site on the plain outside the crater are plotted schematically (not to scale) in the lower left part of each subfigure. The red and blue triangles indicate 2-m temperatures at the highest point on the west rim and at the Southwest tower site.

Pseudo-vertical soundings for 2055 MST on 22 Oct are shown in Figure 1a. Temperatures are colder on the south and west rim of the crater than on the north and east rim. Further, temperatures on the outer sidewall of the crater are colder to the south and west than over the plains to the north and east and are colder than temperatures inside the crater at the same height. These first two observations suggest that *cold air is advected to the crater during the night from the southwest*. It is already known (Savage 2008) that a regional-scale drainage or katabatic flow affects the Meteor Crater on undisturbed nights, producing peak winds of 2-4 m/s at heights at or below 50 m. Thirdly, the north and east soundings have an isothermal temperature gradient like that in the

tethersonde profiles, while the south and west lines exhibit a temperature lapse rate of about 15°C/km extending from the rim down into the crater. This observation suggests that *cold air coming over the rim flows down the south and west inner sidewalls of the crater*. The V shaped notch produced by the intersection of the south or west profiles with the north or east profiles occurs at about the same elevation in Figure 1a. But, there are many instances when the apex of the V-shaped notch varies in elevation between the south and west lines (e.g., Figure 1b). This fourth observation suggests that the *notch apex altitude represents the depth to which cold air coming over the rim can penetrate down the slope before reaching its level of buoyancy equilibrium*, where the katabatic current dissipates. When the flow at the Southwest site is predominantly from the south, the coldest air comes over the south rim and the deepest V notch forms on the south sidewall. When the flow is predominantly from the west, the deepest notch forms on the west sidewall (not shown). Thus, if the drainage flow approaching the crater changes direction, this is reflected in a movement of the V notch so that it is maintained on the upwind inner sidewall of the crater. The cold air inflows, which must detrain cold air into the ambient atmosphere as they flow down the sidewall, finally stop when they reach their buoyancy equilibrium level. The detrainment is stronger at higher elevations where steep slopes produce high speeds and where the inflow-ambient air temperature differences are a maximum. The detrainment of the cold air into the crater atmosphere destabilizes it, driving it towards isothermalcy. Figure 1c shows an event where cold air was advected to the crater from the northwest. In that case, the V notch formed on the west and north sidewalls of the crater, rather than on the south and west sidewalls. Finally, Figures 1d,e, and f show a transition from a stable lapse rate (22°C/km) in the crater at 0300 MST 27 Oct 2006 to a near-isothermal lapse rate (5°C/km) at 0345 MST associated with the initiation of a cold air inflow into the crater, as indicated by the formation of the V notches on the west and south sidewalls. Thus, the data support a hypothesis that *the isothermal atmosphere inside the crater is caused by the detrainment and horizontal mixing into the crater atmosphere of cold air that comes over the rim of the crater and flows down the inner sidewall of the crater.* This inflow hypothesis is illustrated in Figure 2.

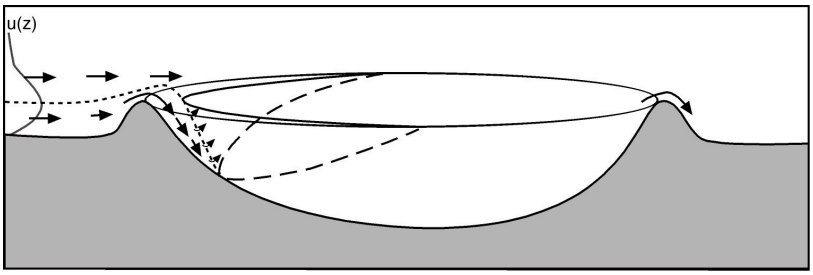

Figure 2. Illustration of the inflow hypothesis. The strongest inflow occurs on the upwind inner sidewall of the crater, with the inflows becomes weaker and penetrating to shallower depths with distance around the crater rim from the upwind direction.

CONCLUSIONS

A mesoscale drainage flow produces an inflow of cold air across the southwest rim of the Meteor Crater. This cold air descends the inner sidewall of the crater as a katabatic current. Detrained cold air from the katabatic current mixes horizontally, destabilizing the crater atmosphere. The horizontal mixing processes are not yet fully investigated, but breaking waves at the upper boundary of the katabatic current may play a role. In future research, a katabatic flow model will be used to simulate the inflow, and we will evaluate turbulence levels in the inflow layer, the effect of the inflow on the crater atmosphere heat budget and the role of the inflow on bulk atmospheric stability inside the crater.

Acknowledgements:
We thank the NCAR ISS and ISFF staff for providing equipment, field support and data processing. Barringer Crater Corporation and Meteor Crater Enterprises, Inc. provided access to the crater. Research was supported by the U. S. National Science Foundation Physical and Dynamic Meteorology Division through grants ATM-0444205 and 0837870 and Army Research Office grant 55900348. Author M .L. was supported by a Doktoratsstipendium aus der Nachwuchsförderung der Universität Innsbruck.

REFERENCES

Savage, L. C., III, S. Zhong, W. Yao, W. J. O. Brown, T. W. Horst, and C. D. Whiteman, 2008: An observational and numerical study of a regional-scale downslope flow in northern Arizona. *J. Geophys. Res.*, **113**, D14114, doi:10.1029/2007JD009623.

Whiteman, C. D., A. Muschinski, S. Zhong, D. Fritts, S. W. Hoch, M. Hahnenberger, W. Yao, V. Hohreiter, M. Behn, Y. Cheon, C. B. Clements, T. W. Horst, W. O. J. Brown, and S. P. Oncley, 2008: METCRAX 2006 – Meteorological experiments in Arizona's Meteor Crater. *Bull. Amer. Meteor. Soc*., **89**, 1665-1680.

ASPECTS OF COLD POOL LIFE CYCLE IN AUSTRIAN SINKHOLES

Manfred Dorninger

Department of Meteorology and Geophysics, University of Vienna, Vienna, Austria
E-mail: *manfred.dorninger@univie.ac.at*

Abstract: Many aspects of cold pool life cycle have been investigated in the recent decades. There have been some indications that the cold pool may oscillate under specific weather conditions. This and the quantification of the cold air outflow through the lowest pass have been addressed in an intense observing period which has been performed in the Gruenloch basin, Lower Austria from October, 19-21, 2008. The basin and the crest line have been equipped with 27 weather stations and one tethersonde at the basin floor. Up to 6 sondes have been operated simultaneously at different heights. Oscillating of the cold air pool is triggered by moderate to strong winds aloft and can only be detected with fast responsing sensors.

Keywords: *cold air pool, basin meteorology, extreme temperature minima, response time*

1 INTRODUCTION

Sinkholes represent an excellent natural laboratory to study formation, the maintenance, fluctuations and dissipation of temperature inversions during fair weather episodes with undisturbed radiative conditions (e.g., Whiteman,et al., 2004). One of the first meteorological observations in history in a basin were made at a place in the Northeastern Austrian limestone Alps, called Gstettner Alm or Gruenloch (Figure 1). It was known from that early observations, that the air temperature at the bottom of the sinkhole may decrease to values some 30 degrees (Centigrade) or more below the ambient temperature at the same level, leading to the lowest temperatures in Central Europe known so far (around –52 deg C, Aigner, 1952). Such extreme temperature minima can only occur when a snow cover is existing, which minimizes the surface heat flux.

Night-time temperature fluctuations at the basin floor during clear sky conditions observed in recent field campaigns indicate that the cold air pool oscillates, however the specific weather conditions have never been really investigated. This is also valid for the origin of the cold air outflow through the lowest saddle. In a field campaign conducted from October, 19-21, 2008, both aspects have been addressed. This paper concentrates on the oscillating aspect.

2 EXPERIMENTAL SET-UP

The station network (Figure 2) was designed to quantify the in- and/or outflow via the crest line including all

Figure 1. Gruenloch basin, view to the northeast from the Kleiner Huehnerkogel (1600 m). Basin floor at 1270 m, lowest saddle at 1320 m (to the left). Diameter at basin floor ~ 300 m, at crest height ~ 1000 m.

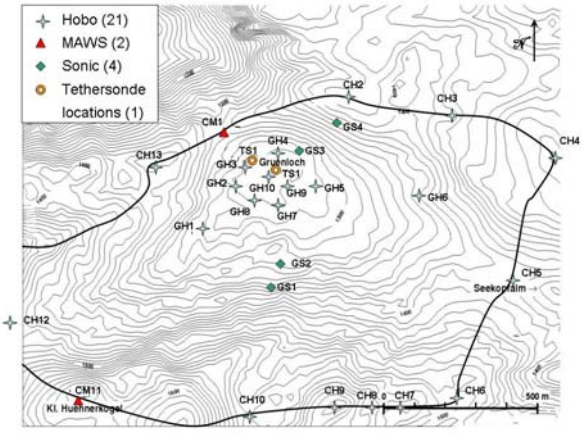

Figure 2. Experimental set-up. Locations of weather stations and tethersonde, 13 stations at the crest line and 14 stations at the basin floor, in operation from October, 19-21, 2008.

mountain peaks and passes and the wind and temperature field at the basin floor. Four weather stations equipped with 3D-sonic anemometers have been deployed at the slopes to investigate a possible cross circulation during daytime.

3 PRELIMINARY RESULTS

The intense observing period lasted from October, 19, 12:00 UTC to October, 21, 12:00 UTC. Figure 3 shows a typical temperature record for a undisturbed weather situation (left). However, during the first night from 19th to 20th a weak upper level short wave trough passed the region leading to moderate winds at crest height from the northwest. This triggered an oscillation of the cold pool indicated by the small temperature fluctuations. The second night was completely undisturbed and has a smoother temperature regime. Data are taken every five minutes which corresponds to the response time of the used temperature sensor in air moving at 1 m/s. On the right hand side the blow-up from the period October, 19, 21:30 to midnight, is depicted. One can recognize a drop in the temperature but hardly an oscillation.

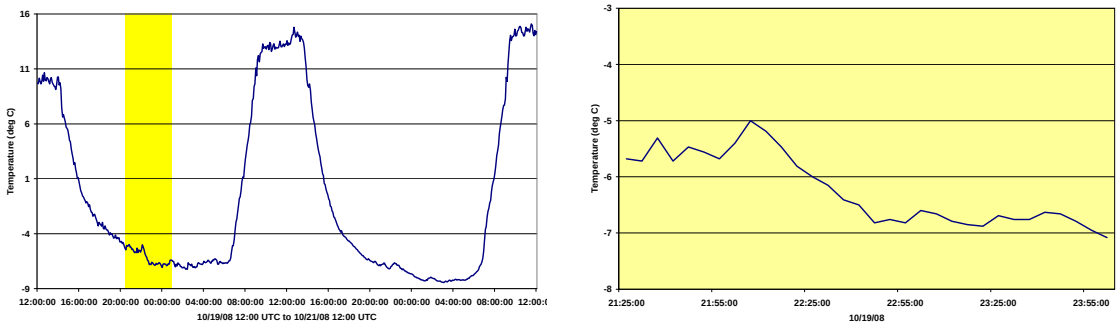

Figure 3. Left: Temperature record from station GH10 (see figure 2) at basin floor for undisturbed and clear sky from October, 19-21, 2008, yellow shaded box: time period, blown up on the right.

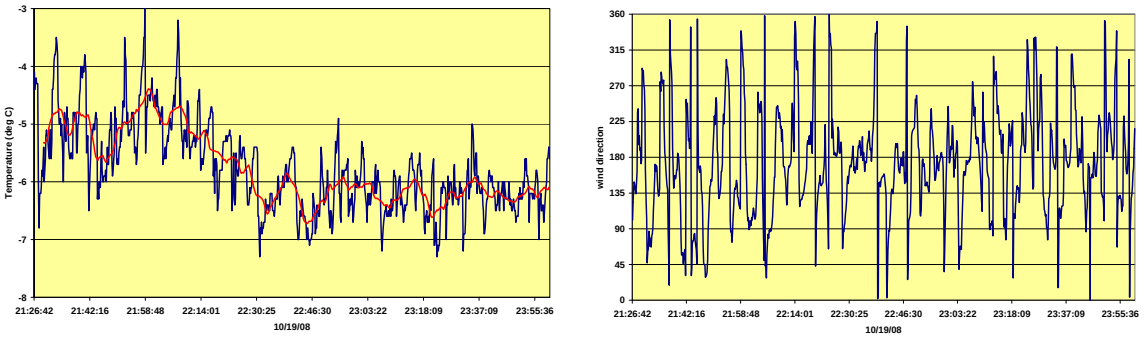

Figure 4. Left: Temperature record from lowest tethersonde for the same period as shown in figure 3, right. Red curve: 5 min gliding mean. Right: wind directions for the same time period.

During the "yellow" time period the height of the tethersonde was kept constant. The lowest sonde was located 1 m above basin floor. The response time of these probes is much faster than for the Hobo weather stations. Short term fluctuations of the temperature in the order of 2 to 3 deg C become evident as shown on figure 4, left hand side (Note: the same temperature scale is used as for figure 3, right, for comparison). These fluctuations are strongly connected to changes in the wind direction (figure 4, right). Wind speeds (not shown) are low with a maximum in the range of 1 m/s. Further evaluations are under way (e.g., characteristic frequency) to understand these fluctuations in detail.

Acknowledgements:
Many thanks due to the students from the University of Vienna for their contributions to the field campaign. Forstmeister P. Kupelwieser is thanked for providing access to the experimental area.

REFERENCES

Aigner, S., 1952: Die Temperaturminima im Gstettnerboden bei Lunz am See, Niederösterreich (The minimum temperatures in the Gstettner basin near Lunz, Lower Austria). *Wetter Leben*, Special Issue **1**, 34-37**.**

Whiteman, C. D., T. Haiden, B. Pospichal, S. Eisenbach, and R. Steinacker, 2004: Minimum temperatures, diurnal temperature ranges and temperature inversions in limestone sinkholes of different size and shape. *J. Appl. Meteor.*, **43**, 1224-1236.

THE ROLE OF SUBSIDENCE IN VALLEY AND BASIN WARMING

Thomas Haiden

Central Institute for Meteorology and Geodynamics, Vienna, Austria
E-mail: *thomas.haiden@zamg.ac.at*

Abstract: The role of thermally driven upslope flows and associated compensating subsidence in the diurnal warming of valley and basin atmospheres is re-investigated. Based on theoretical considerations and illustrated by a simulation of the morning transition during IOP5 of METCRAX it is discussed under what conditions and assumptions the redistribution of heat by the slope flow circulation produces a warming that is different from quasi-horizontal heat input.

Keywords: *valley warming, subsidence*

1 INTRODUCTION

Subsidence in valleys and basins due to thermally driven upslope flows is usually too weak to be measured directly. Its existence has been established by observational studies mostly through a sequence of vertical temperature profiles which show the downward motion of characteristic features, such as inversions. Theoretically, its existence derives from mass-conservation, since air transported upwards by upslope flows at the valley sidewalls must be replaced by downward motion in the valley interior. [Another way of closing the mass budget would be convergence of along-valley flow but observations show that this is not case. During the upslope, up-valley phase there is rather mass divergence along the main valley, mostly due to the branching out of tributary valleys which all develop up-valley flows (Freytag 1987).] The practical relevance of subsidence is that it can suppress mixed-layer growth in the valley and affect the dispersion of pollutants. In order to quantitatively estimate the strength of subsidence in a given topographic setting one needs an estimate of the upslope mass-flux at the valley sidewalls. An upper limit of this mass-flux can be computed based on the concept of 'equilibrium' slope flow.

2 EQUILIBRIUM SLOPE FLOW

The concept of equilibrium slope flow refers to a balance between diabatic heating and along-slope advection in the slope wind layer

$$\frac{\partial \theta_{SL}}{\partial t} = \frac{H}{c_p \rho D} - U \sin\alpha \frac{\partial \theta}{\partial z} \approx 0 , \tag{1}$$

where H is the sensible heat flux, D is the slope wind layer depth, U is the upslope flow speed, and α is the slope angle. From (1) the equilibrium upslope mass-flux is given by

$$\rho D U = \frac{H}{c_p} \left(\frac{\partial \theta}{\partial z} \sin\alpha \right)^{-1} . \tag{2}$$

If such equilibrium is present, it can be shown that the warming of the valley atmosphere due to subsidence corresponds to the sensible heat input at the same height

$$b c_p \rho \left(\frac{\partial \theta}{\partial t} \right)_{SUB} = \frac{H}{\sin\alpha} , \tag{3}$$

where b is half the width of the valley. In the real atmosphere, slope flows are closest to this kind of equilibrium if the slope is steep and homogenous, and the atmospheric stratification strong. If the slope flow strength is less than the equilibrium value by a factor f, where $0 \le f < 1$, then only a fraction fH of the sensible heat input will re-appear as subsidence warming, and the remaining fraction $(1-f)H$ is available for direct horizontal heat transport towards the valley interior. The resulting total valley warming is again the same as in the equilibrium flow case. This insensitivity of valley warming to the actual slope flow volume flux may explain why simple analytical models (Whiteman and McKee 1982, Haiden 1998) can reproduce the observed temperature evolution in valleys without actually modelling the details of the slope flow.

3 COMPARISON WITH METCRAX DATA

Results of a simple numerical model of horizontal heat input and dry-adiabatic adjustment are compared to observations of inversion break-up taken during the Meteor Crater field campaign (METCRAX) conducted in Arizona in 2006 (Whiteman et al. 2008). In real valleys the heat budget of a valley cross-section is influenced by along-valley temperature advection. Also, the mass budget of the upslope flow / subsidence circulation may not necessarily be closed within the two-dimensional cross-section. In closed basins the situation is much more constrained. The upward mass flux across any horizontal plane inside the basin *must* equal the downward mass flux. One has to be careful, however, that external influences such as cold air intrusions or intermittent mixing episodes can be ruled out, or quantified accordingly. During the IOP5 morning transition, the temperature evolution did not show disturbances of such kind.

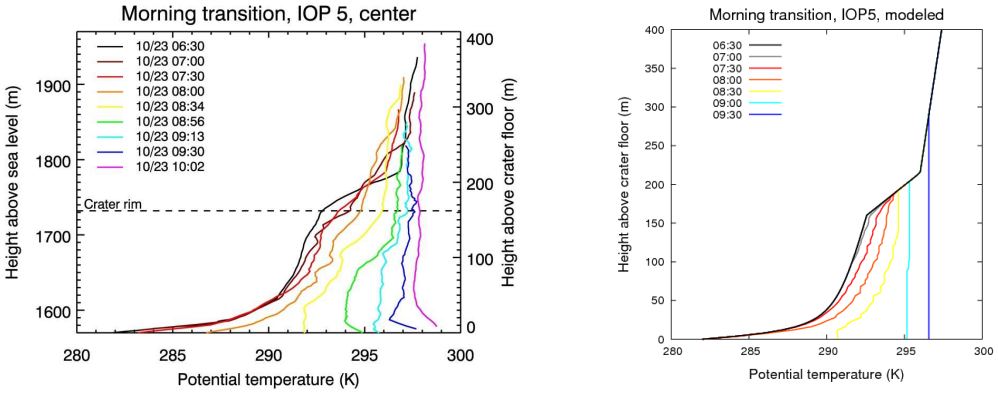

Figure 1. Evolution of potential temperature in and above the meteor crater during the morning transition of IOP5 of METCRAX. Left: observed, right: modelled.

As shown in Figure 1, the simple horizontal heat-input model with dry-adiabatic adjustment captures the main characteristics of the temperature evolution. In the observations, however, there appears to be a downward movement of the more stable layer near crater rim, especially between 07:00 and 08:56. This feature cannot be reproduced by the horizontal heat input method.

4 CONCLUSIONS

To a good approximation, the diurnal warming of valleys and basins can be modelled by horizontal heat transport from the sidewalls to the valley (basin) interior. This does not imply that there is in fact a horizontal transfer of air from the sidewalls towards the interior. It is the result of the organized overturning circulation comprised of upslope flow and subsidence motion. It applies to cases where the sidewalls are sufficiently steep so that the upslope mass-flux is close to its equilibrium value. An important practical consequence is that the warming in such cases can be modelled independently of the slope flows. On the other hand, observations which show a downward movement of stable layers in valley and basin atmospheres indicate deviations from equilibrium slope flow. According to (2) this is to be expected at heights where the stratification changes rapidly because the mass-flux cannot adapt to a different value over arbitrarily short vertical distances.

Acknowledgements:
I would like to thank Dave Whiteman and Sebastian Hoch for providing the METCRAX data and for many inspiring discussions.

REFERENCES

Haiden, T., 1998: Analytical aspects of mixed-layer growth in complex terrain. *Proceedings Eighth Conference on Mountain Meteorology*, Flagstaff, Arizona, 368-372.

Freytag, C., 1987: Results from the MERKUR Experiment: Mass budget and vertical motions in a large valley during mountain and valley wind. *Meteor. Atmos. Phys.*, **37,** 129-140.

Whiteman, C. D., and T. B. McKee, 1982: Breakup of temperature inversions in deep mountain valleys. Part II: Thermodynamic model. *J. Appl. Meteor.*, **21,** 290-302.

Whiteman, C. D., A. Muschinski, S. Zhong, D. Fritts, S. Hoch, M. Hahnenberger, W. Yao, V. Hohreiter, M. Behn, Y. Cheon, C.B. Clements, T. W. Horst, W. O. J. Brown, and S. P. Oncley, 2008: Metcrax 2006 – Meteorological experiments in Arizona's meteor crater. *Bull. Am. Met. Soc.*, **89,** 1665-1680.

ANALYSES OF NEWLY DIGITISED SNOW SERIES OVER THE LAST 100 YEARS+ IN SWITZERLAND

Wüthrich C.[1], Begert M.[1], Scherrer S.C.[1], Croci-Maspoli M.[1], Appenzeller C.[1], Weingartner R.[2]

[1] Federal Office of Meteorology and Climatology MeteoSwiss, Zurich, Switzerland
E-mail: *christian.wuethrich@meteoswiss.ch*
[2] Institute of Geography, University of Berne, Berne, Switzerland

Abstract: In this study a systematic analysis is conducted of 12 Swiss long-term snow series with newly digitised daily measurements since at least 1910. A single snow series even dates back to 1865 and hence belongs to one of the longest and continuous snow series. The 12 surface observation stations are situated in central and eastern Switzerland on altitudes between 450 and 2500 m asl. The trend analyses show an unprecedented decrease of new snow sum in the 1990s and a general reduction of the snow cover over the last 100 years.

Keywords: *Long-term snow series, Switzerland, trend analyses*

1 INTRODUCTION

Snow is on the one hand an important commercial factor especially in the Swiss Alpine region (tourism, hydro-electricity, drinking water) and on the other hand responsible for considerable hazards such as avalanches. In addition, snow can be used as an excellent indicator in detecting climate change. In this respect, high-quality and long-term snow series are crucial for reliable analyses. The objectives of this study are twofold.

In a first step, suitable long-term snow series have been selected, missing data digitised and the entire series quality checked. Therefore snow data from 12 different surface stations with daily measurements since at least 1910 have been selected (situated in central and eastern Switzerland at altitudes between 450 and 2500 m asl). Daily snow data between the beginning of the measurements in the early 20th / late 19th century and the 1940s have been digitised from historical MeteoSwiss paper data. The historically available parameters are a) new snow sum and b) snow depth. Since snow depth data are not available at every station, a reconstruction of this parameter has been undertaken using the method of Brown and Braaten (1998) by combining daily new snow, temperature, precipitation and a melting factor.

In a second step, the long-term snow series have been used for trend analyses over a time period >100 years.

2 LONG-TERM SNOW SERIES

The longest new snow series of Switzerland is dating back to 1865 and was measured in Segl-Maria (1798 m asl) in southeastern Switzerland. An example of the time series of days with snowfall ≥ 1 cm (Figure 1) in Arosa (1892-2008), Chur (1889-2008), Davos (1932-2008) and Segl-Maria (1865-2008) indicates an expected year to year variability and distinct decadal variability. In particular the period from 1940 to 1960 shows signs of fewer days with snowfall, in contrast to the 1970 and the 1980 with generally more days with snowfall. The last two decades mark again a period of fewer days with snowfall, which is in line with previous studies (e.g. Marty, 2008) and the current temperature increase in this region. A similar tendency as for days with snowfall can be indicated for the new snow sum (Figure 2).

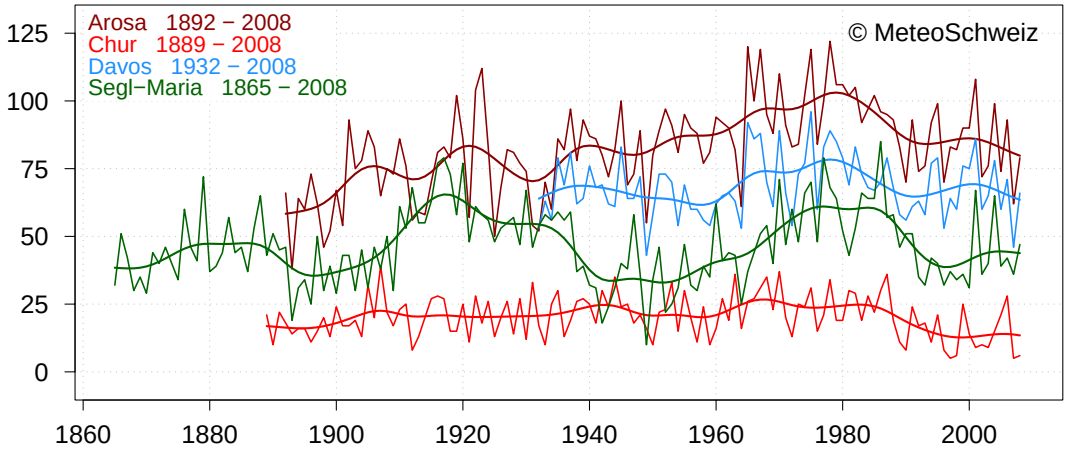

Figure 1. Time series of days with snowfall ≥ 1 cm for stations located in south-eastern Switzerland. Smooth lines indicate a 20-year Gauss filter.

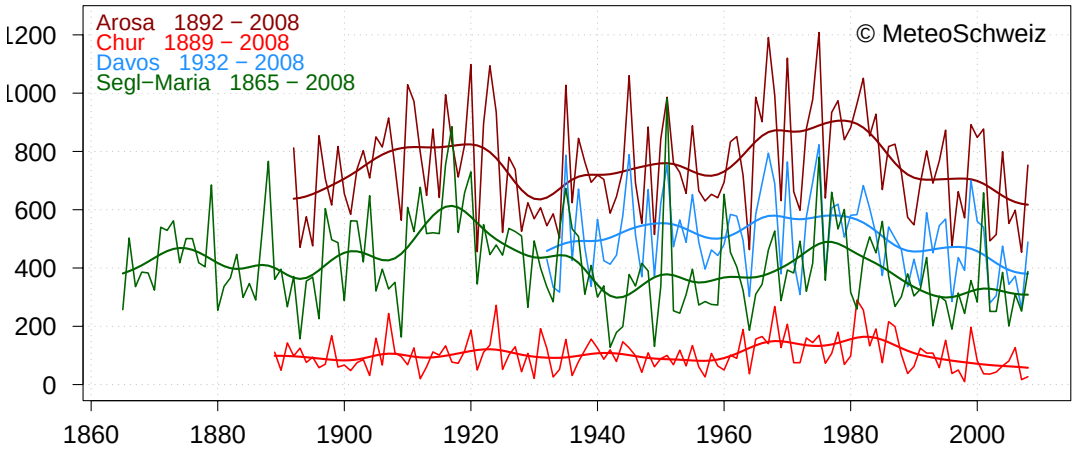

Figure 2. Time series of new snow sum in cm for stations located in south-eastern Switzerland. Smooth lines indicate a 20-year Gauss filter.

3 SNOW TRENDS

The 100 year trend analysis of days with snowfall ≥ 1 cm (not shown) reveals a significant decrease for stations below 800 m asl in the winter season (DJF) and for stations around 1800 m asl in the spring season (MAM). Similar results were found for seasonal new snow sums.

The analyses of the decadal new snow trends (not shown) during the last 100 years shows unprecedented low new snow sums in the winter seasons (DJF) of the 1990s on all highs, but on altitudes < 1500 m asl were already measured low new snow sum in the 1950s and the 1970s. In the spring season (MAM) the decadal snow trends shows as well a decreasing new snow sum in the 1990s. The 1960s shows in contrast to that a once only increasing of the new snow sum in the spring season (MAM) on all altitudes in the last 100 years.

4 CONCLUSIONS

The newly digitized and quality controlled long-term snow series back to the 19th century in Switzerland belongs to the longest continuous snow datasets available (except for very few missing weeks). These long-term snow series show that snow cover is varying substantially on seasonal and decadal time scales. Since snow data series of shorter periods have shown similar trends (e.g. Scherrer and Appenzeller, 2004; Laternser and Scheebli, 2003), our results can be used as a valuable extension. In addition long-term snow series act as useful indicator for climate change studies.

REFERENCES

Brown, R.; Braaten, R.; 1998: Spatial and Temporal Variability of Canadian Monthly Snow Depths (1946-1995); Atmosphere Ocean 36 (1), 37-54.

Laternser, M.; Schneebeli, M.; 2003: Long-term snow climate trends of the Swiss Alps (1931-99). International Journal of Climatology 23: 733 – 750.

Marty, C.; 2008: Regime shift of snow days in Switzerland. Geophy. Res. Lett., 35, L12501

Scherrer, S.C.; Appenzeller, C., 2004: Trends in Swiss Alpine snow days: The role of local- and large-scale climate variability. Geophy. Res. Lett., 31, L13215

DETERMINATION OF SNOW ACCUMULATION IN HIGH MOUNTAINS BASED ON DATA FROM CLIMATE STATIONS

Heidi Escher-Vetter[1], Markus Weber[1,2]

[1] Commission for Glaciology, Bavarian Academy of Sciences and Humanities, Munich, Germany
E-mail: *Heidi.Escher@kfg.badw.de*
[2] Institute of Meteorology and Geophysics, University of Innsbruck, Innsbruck, Austria

Abstract: Local measurements of precipitation are used to validate snow cover model results for Vernagtferner.

Keywords: *glaciers, winter precipitation, measurements and models*

1 INTRODUCTION

Snow accumulation S_a is an important quantity for modelling glacier mass balance and change. S_a is calculated e.g., by the model SURGES (**Su**bscale **R**egional **G**lacier **E**xtension **S**imulator), operated in the framework of the hydrological part of the grid-based DANUBIA system. It was designed to emulate the glacier retreat for global change scenarios runs. This model uses records of meteorological quantities from the operational climate network (ZAMG and DWD), such as air temperature and precipitation intensity p(t). A problem arises from the fact that the network does not extend into regions which are difficult to access. Therefore such series of precipitation event are extrapolated with the help of gradients derived from a cluster of records (Mauser and Bach, 2008). On this basis, the model is able to determine the water equivalent of the snow cover for the whole catchment. By definition, the algorithm enforces the reproduction of the actual records for the stations' locations. But in inaccessible areas a direct validation is not possible unless data are available from scarce storage gauges or snow height measurements, gathered for selected dates at the most. Under favourable conditions, these sparse informations can be used for an estimation of the validity of the model results.

2 PRECIPITATION DATA SOURCES

The basin of Vernagtferner, Oetztal Alps, is a well suited region for the model validation. Table 1 summarizes the usually used methods for measuring precipitation quantities at this site (Braun et al., 2004). The measurement of precipitation in strongly heterogeneous terrain is error prone, and various influences have to be considered. As precipitation can occur in form of rain or snow, not all devices are able to record all quantities. Unheated tipping buckets e.g., only record rainfall events correctly. The deposition of rain into the gauge is obstructed by heavy wind, and this is even worse in the case of snow. Sometimes the snow even covers the complete device. Evaporation and condensation effects are not the same for the devices as for natural surroundings, and misalignment of sonic rangers and stakes reduces the high instrumental accuracy. Only the model is capable to deliver both sums and time series of the water equivalent of the snow cover and of effective precipitation, but it is unable to consider snow redistribution by wind.

Method		**Instrumental Accuracy**	**p(t)**		**P**	
Device	Unit		Snow	Rain	Snow	Rain
Model	[mm w.eq.]	--	+	+	+	+
Tipping bucket	[mm w.eq.]	high		+		
Weighing gauge	[mm w.eq.]	medium	+	+	+	+
Storage gauge	[mm w.eq.]	high			+	+
Sonic ranger S_h	[m]	high	+		+	
Stake S_h	[m]	high			+	

Table 1. Precipitation methods available within the Vernagtbach basin; '+' indicates the capacity to record the quantities.

3 METHODOLOGY

Figure 1 shows the comparison of the modeled time series of water equivalent of the snow cover S_a and the measured snow height S_h. The general structure during the accumulation period is well met, but S_h depicts

additional details, which are caused by processes like settlement and potential redistribution, not considered by the model. The relationship between S_h and S_a is given by eq. 1.

$$S_a(t) = \rho \cdot S_h(t) \qquad \textbf{(1)}$$

The mean density **ρ** of the snow cover increases with time and is not known at this location.

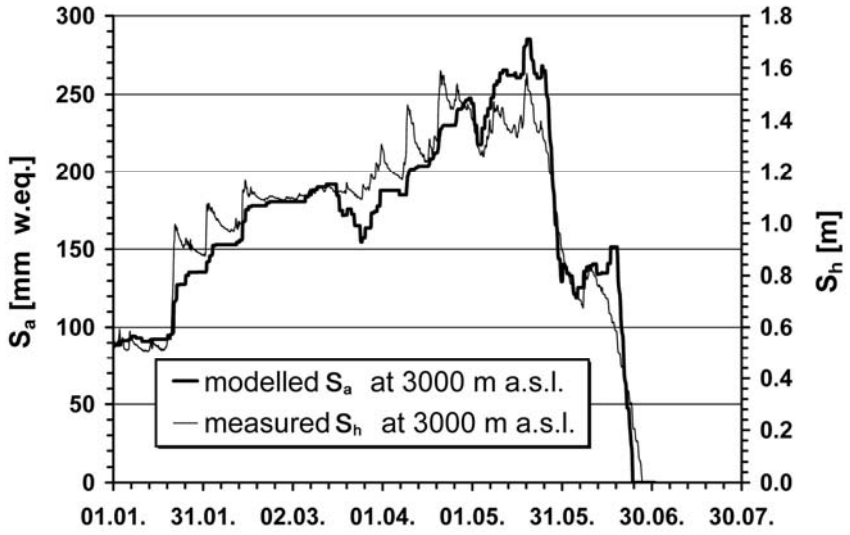

Figure 1. Time series of the recorded snow height of the Vernagtferner sonic ranger and the modelled water equivalent of the snow cover at the same location from 1 January to 31 July 2005.

Storage gauges provide only temporal sums P of the precipitation events over the time span t_0 to t (Eq. 2)

$$P(t) = \int_{t_0}^{t} p(t)dt \qquad \textbf{(2)}.$$

In general, snow height $S_h(t)$ can be calculated from an initial value $S_h(t_o)$ by equation (3)

$$S_h(t) = S_h(t_0) + \frac{r}{\rho} P(t) - M \quad \textbf{(3)},$$

if the local density of the snow cover and the mean portion r of snowfall to the entire precipitation is known, and melt losses M are considered. The records of the storage gauges P can be used in equation (3) for the calculation of S_h for the observation dates. During the winter period, r is close to one and M is negligible. As snow density is typically analyzed for only three to six sites, an average density has to be determined for the total glacier. At the spring survey of 2005, the average density was evaluated to 327 ± 17 kg/m³ (Escher-Vetter et al., 2009). A scale comparison of the series in Fig. 1 however results in a density of 170 kg/m³. This finding suggests that the extrapolated precipitation data have a bias of approx. 150 mm w.eq. to lower values in this case.

Acknowledgements:
Many colleagues helped in this study, and our special thanks go to Monika Prasch, Department of Geography, Ludwig-Maximilians-University, Munich, who provided the model results. Funding from the DFG, BMBF, the GLOWA-Danube project, the Academy Research Programme III.B.1 of the Fed. Rep. of Germany and the State of Bavaria is gratefully acknowledged.

REFERENCES

Braun, L.N.; Escher-Vetter, H.; Heucke, E.; Siebers, M. & Weber, M., 2004: "Experiences with the new ´Vernagtbach' hydro-meteorological station", *in Oerlemans & Tijm-Reijmer: Book of extended abstracts of presentation at the Workshop "Automatic Weather Stations on Glaciers", Pontresina, 28 to 31 March 2004, IMAU, 38 - 44.*

Escher-Vetter, H., M. Kuhn, and M. Weber, 2009: Four decades of winter mass balance of Vernagtferner and Hintereisferner, Austria: methodology and results. Annals of Glaciology 50, 87-95.

Mauser, W., Bach, H. 2008: „PROMET – a Physical Hydrological Model to Study the Impact of Climate Change on the Water Flows of Medium Sized, Mountain Watersheds“, *Submitted to Journal of Hydrology*

THE EXCEPTIONAL METEOROLOGICAL CONDITIONS OF THE DECEMBER 2008 IN THE TRENTINO AREA (NORTH EAST ITALY): SYNOPTIC AND NIVOLOGICAL ANALYSIS AT MESOSCALE

Roberto Barbiero[1], Massimiliano Fazzini[2], Mauro Gaddo[1]

[1]Provincia Autonoma di Trento – Dipartimento Protezione Civile e Infrastrutture.
2 University of Ferrara - Department of Earth Sciences –
Email massimiliano.fazzini@unife.it

Abstract: From the end of November, 2008 and for the whole month of December, 2008, the northern portion of the Mediterranean basin has been interested by a succession of synoptic situations that has brought perturbed weather also on the north east alpine sector of Italy**,** with persistent and snowy phenomenon often till in the Adige Valley. The nivometric data observed in the network of snow manuals fields - active with continuity from the winter season 1980-1981 - and in some automatic stations managed by the Civil Protection of the Autonomous Province of Trento, show "record" values at all the levels. If the analysis is extended to the other winter months, only in January 1986 and locally in December 1981, have been observed similar snow depth measures. The notable frequency of snowy episodes has determined serious and heavy repercussions on the human activities and particularly on the road and railway circulation. Over the 1500 meters of altitude, the heavy snowfalls and the strong winds have determined also the formation of wide frames of snow gust with consequent notable avalanche activity.

Keywords: *Trentino, heavy snowfall, return period, Genoa depression,*

1 INTRODUCTION

The Trentino territory belongs for its totality to the southern sector of the eastern chain of the Alps where the perturbed meteorological situations have origin from intense Mediterranean flows, very recurrent between the end of the autumn and the beginning of the winter. Also the recent winter season has been characterized by such evidence, since the end of the month of November, a succession of synoptic situations that has brought perturbed weather are occurred also in the days of Christmas and the New Year's Eve.

Two exceptionally perturbed phases can be distinguished in this period. The first one started on November 28 and it lasted up to December 1. After some days characterized by conditions of sunny weather for the presence of a high pressure field, on November 28 a centre of low pressure positioned on the upper Tyrrhenian Sea determines unstable flows from southwest on the Alps favouring diffused snowfalls beginning from the morning on the valleys with rains only in the southern valleys. Even if interested by a low centred on the Gulf of Biscaglia, in the following day of November 29 a suspension of the precipitations has been observed for the morning. After some irregular clearing up in the afternoon new precipitations followed in the night, snowy over the 500 - 600 meters about. On November 30 the transit of a front in phase of occlusion on the north Italy (Figure 1) determined moderate precipitations in the night, with snow over the 500 - 600 m. During the day intermittent precipitations still occurred, that have been becoming widespread and more intense from the evening. On the December 1, the transit of a new frontal system determines widespread precipitations, locally very strong, with limit of the snow that goes down until the valleys and then gradually increases up to 800-1200 m in the first morning; in the afternoon an attenuation of the phenomenon occurs with intermittent weak precipitations.

A second intense phase begins on December 10 and it ends on December 17, a week of consecutive precipitations. However the most intense phase interests the first two days. After a period characterized for stable and predominantly sunny weather, with north flows and a fall in minimum temperature values on December 9, from the night of December 10 the arrival of a perturbation (Figure 1) determines snowy precipitations up to low levels in the valleys, in intensification during the day. From the evening an attenuation of the phenomenon has been observed with gradual raising of the limit of the snow level due to the presence of warmer air. On December 11 conditions of perturbed weather persist, with weak or moderate rains in the valleys and with the snow's limit around 800-1000 m on the northern sectors, over the 1000 m on the southern sectors. A new intensification of the precipitations is observed from the evening. Again perturbed weather on December 12 with southeast flows that determine widespread precipitations up to the first afternoon. The limit of the snowfalls is very varying during the day between 1000 and 1500 m, more elevated on the south sectors, with limit decreasing to end of the event.

2. ANALISYS OF NIVOMETRIC DATA

The cumulated snowfall observed during the two phases of perturbed weather has reached exceptional values among 90 cm of the River Adige Valley and 350 cm at the higher levels of Val di Sole valley (Tonale Pass, 1880

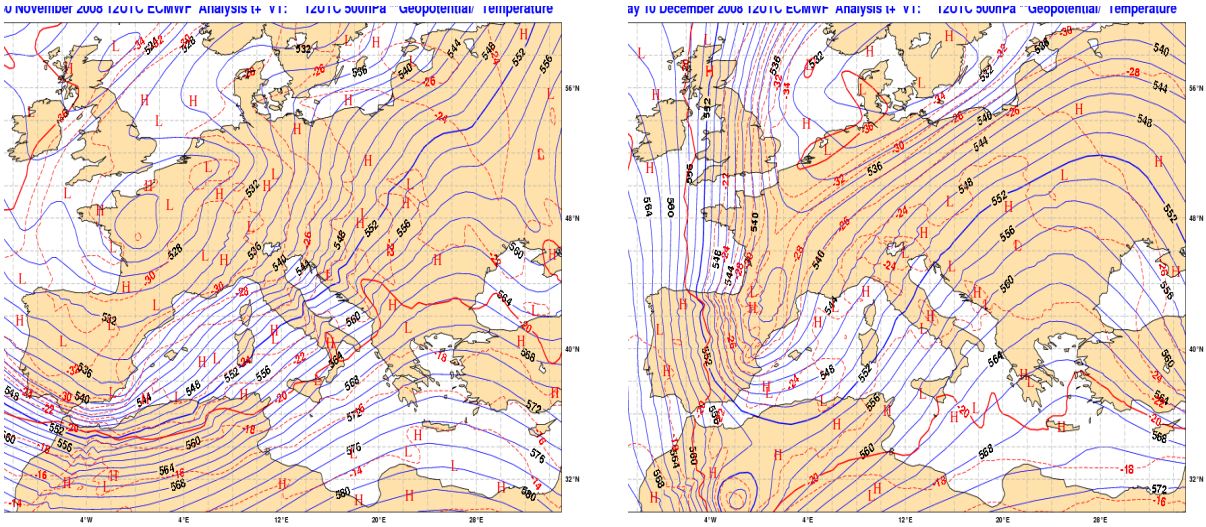

Figure 1 – Geopotential and temperature - 500 hPa – Analysis 30/11/2008 12 UTC (left) and 10/12/2008 12 UTC (right)

m). The monthly cumulated values are decidedly more elevated, considering all the events observed in the period, and vary, that average, from 250 cm at 1500 m level to 450 cm at 2000 m level.

Such values are everywhere double in comparison to the maximum ones observed in the period 1981-2007. Only for the station of Caoria (915 m), the observed data is lower than the maximum historical value of 147 cm recorded in December 1981. On the base of the available data, it has been possible to quantify in about 90 years the return period of a so intense snowfalls. If the analysis is extended to other winter months, it is observed that only in January 1986, in some stations of the Fassa Valley and the Non Valley, the cumulated snowfalls observed are comparable but however lower of about 15-20%.

Such exceptional cumulated snow depth data has been reached also thanks to the numerous other perturbed events observed that have brought weak to locally moderate snowfalls also in the days of Christmas and the New Year's Eve. A first analysis underlines that during and immediately after the two principal snowy events, the index of avalanches danger has reached the degree 4 - strong - on a scale of 5 levels and a number exceptionally high of avalanches have been observed, also of notable dimensions, around 300 events and primarily in the western area (Daone Valley, Giudicarie Valleys, Non Valley) - Meteotrentino, personal communication

3 CONCLUSIONS

The two phases of strongly perturbed weather that have interested the Trentino region derive from a synoptic circulation very recurrent and that determines the higher precipitations with that characterized by the presence of a dynamic depression on the gulf in Genoa (Fazzini et al, 2006, Fazzini 2007). If a cold layer has been formed in the preceding days due to a antyciclonic persistence, the advection of wet and warm air from the Mediterranean Sea determines snowfalls precipitations in the lower levels of the Adige Valley, above all if intensity is heavy (Barbiero et al,. 2007).

Acknowledgements: - *We thank all contributors for all meteorologist and nivologist of PAT - Dipartimento Protezione Civile e infrastrutture*

REFERENCES:

Roberto Barbiero, Massimiliano Fazzini, Mauro Gaddo & Carlo Bisci (2007): Analysis of recent meteorological configurations responsible for substantial snowfalls in the Trentine sector of the Adige valley bottom (eastern italian Alps) *Proc. 29th Intern. Conf. on Alpine Meteorology*, Chambery, France; 312-315

Massimiliano Fazzini, Alessandro Cecili, Alessandro Cinnirella, Mauro Gaddo e Paolo Bolli (2006): Une nouvelle méthode pour la réalisation d'une carte dynamique de l'enneigement du territoire du Trentino (Italie Nord -Orientale) » in Les risques liés au temps et au climat . *Proc. XIX Colloque International de Climatologie*, Gerard Beltrando, Malika Madelin et Hervé Quenol edit.– Epernay – 249-254

Massimiliano Fazzini (2007)**:** Applicazioni della climatologia al "rischio neve": la carta dinamica dell'innevamento della provincia di Trento *Proc. VII congresso di Meteorologia del Friuli Venezia Giulia***.** Regione Autonoma Friuli Venezia Giulia ed, 37-52.

ESTIMATING FOEHN DYNAMICS FROM TRAIN AND CABLE CAR ACCIDENTS

Hans Richner

Institute for Atmospheric and Climate Science, ETH Zurich, Zurich, Switzerland
E-mail: *hans.richner@ethz.ch*

Abstract: Two foehn-related accidents are described: A narrow gauge train was blown from the track and overturned, and a chairlift derailed and ultimately dropped to the ground. The first incident occurred during a strong foehn storm, the second during a moderate foehn. It must be assumed that - particularly in the second case - gustiness played a dominant role.

Keywords: *ICAM, foehn, societal impact, mountainous meteorology, weather-related accidents*

1 INTRODUCTION

Foehn situations can produce violent storms in the lee of mountain ranges. In recent years, in Switzerland, wind speeds in the range of 150 km/h and more were responsible for material damage to fixed structures (such as buildings, piers. etc.), boats, trains, and cable cars. They instigate significant financial losses because transportation systems were delayed or had to be shut down, and - worst of all - they were the cause for severe injuries and even casualties. The two most spectacular incidents happened both in the Jungfrau region: On November 11, 1996, a double motorcoach was used for evacuating a tourist group from the Jungfrau summit to Grindelwald. Despite the fact that the motorcoach was coupled to two heavy snowplows, it was blown from its track. Several passengers suffered light and medium injuries. On January 3, 2008, high winds during a foehnstorm "derailed" the cable of a double chair cable lift. First, the lift stopped, and the cable was caught in the cable catcher, but successive gusts threw the cable out of the catcher, the chairs dropped to the ground. One person died and several were severely wounded. The mean wind speed indicated by the mandatory wind monitoring system was just about at the alarm level.

After the first accidents mentioned here, a rather dense anemometer system was installed in the region, this in addition to the mandatory wind monitoring system required at each cable car. The fact that winds were below the alarm level when the accident happened raises several questions: (i) Are the alarm levels too high? (ii) Are the anemometers mounted at locations which deliver representative values? (iii) Is there sufficient wind information to recognize potentially dangerous situations?

2 OBJECTIVES FOR INVESTIGATIONS BASED ON ACCIDENT ANALYSES

By law, all major accidents with public transportation systems are investigated by an office within the Swiss Federal Department of the Environment, Transport, Energy and Communications (UVEK); the investigation reports are public. In the report of the later accident, the term "gust" appears several times, however, it is never directly dealt with. Quite obviously, neither the wind monitoring system nor the operation procedures deal with gusts in a quantitative manner. The only gust-related parameter which is observed is the peak wind speed.

Any aerial cable car installation is a structure capable to oscillate with many degrees of freedom, and a mathematical treatment of its dynamics is extremely complex. Somewhat simpler is a train on rails. Such a system can in first approximation be treated as a rigid object, in a second step, the rocking (due to the fact that the car is on shock-absorbing springs) can also be considered.

3 THE ANALYSES AND SOME QUALITATIVE CONCLUSIONS

Figure 1 shows the motor coach involved in the incident of November 11, 1996. If mass and dimensions of the car are known, the pressure can be calculated which is needed to balance the gravitational force for a given tilt angle. From this pressure value, the wind speed component perpendicular to the side of the car can be computed with reasonable accuracy.

Assuming stationarity (i.e., a constant, steady wind) a moment calculation (with respect to the downwind rail) should yield the wind speed which was determined as critical in a wind tunnel test. However, since foehn winds are turbulent in general, and even more so near the surface, one must assume that a particularly strong gust overturned the motor coach. The strength of such a gust can be estimated if a certain duration of said gust is assumed. Of course, for a given tilt angle, the strength (or speed) of such a gust would have to be larger than the speed of a steady air stream because it has to overcome the additional inertial force. [Quantitative information will be supplied in the conference presentation.]

Figure 1. The motor coach after being derailed by foehn winds. (© Minirex AG, Schweizerische Eisenbahn-Revue)

Figure 2. Chairlift accident. The cable was caught in the cable catcher, a subsequent gust threw it out. (Source: public UUS report)

As mentioned, the accident with the chair lift (Fig. 2) is much more difficult to treat theoretically. Nevertheless, from the sequence of incidents and from available observations, some conclusions can be made.

Tourists on the chairlift reported that first the cable "derailed". Such an incident causes an emergency stop of the installation. The cable catcher, a device designed to prevent the cable from dropping to the ground, caught the derailed cable. However, subsequent gusts jolted the cable out of the catcher, the cable and the attached chair dropped to the ground.

Because of the 1996 accident described above, the Jungfrau Rail Company installed a wind-monitoring network consisting of ten anemometer sites. From these, from the two anemometers installed at the chair lift, and from two stations run by MeteoSwiss, some wind data is available (the site anemometer data is not recorded). Wind speed was just about reaching the wind alarm level, however, it was not excessive (Fig. 3). Striking is the fact that at least one station exhibited a very regular oscillation of wind speed, however, compared to the natural frequency of the cable (which is in the second range) these oscillations were much slower (period was about 10 … 15 minutes). Hence this observation is most likely irrelevant for the accident. It must be assumed that gusts which were either synchronous to the swinging cable or extremely strong (as one passenger reported) caused the cable to drop. Due to the very steep topography, winds can have significant vertical components, however, because the anemometers measure only in the horizontal plane, these cannot be observed.

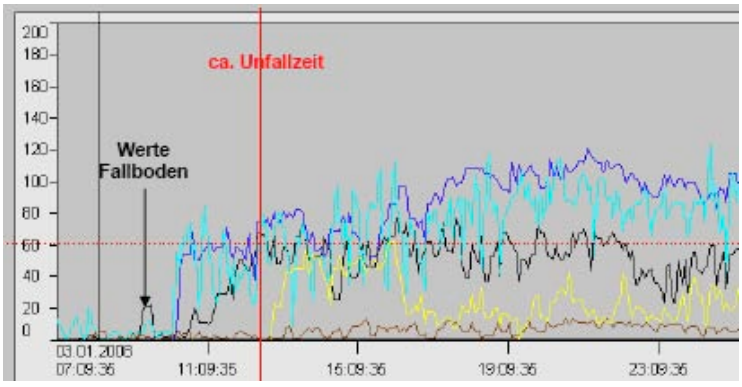

Figure 3: Wind speed recordings of stations in the accident area. The black trace is from the anemometer site closest to the disaster. Note the regular oscillation of the cyan trace. The horizontal red line represents the alarm level. (Source: public UUS report)

4 FINAL REMARK

The dynamics and the turbulent characteristics of strong winds near the surface can, of course, be investigated and analysed much easier with proper instrumentation. Nevertheless, using basic physical laws to investigate accidents as described here gives the numbers found in "scientific" observations immediately a new and also very practical meaning. In addition, a comparison of nearby instrumental measurements with estimations derived from the accidents themselves demonstrates dramatically the fact that it is extremely difficult to make representative observations over complex terrain and/or in turbulent conditions.

Acknowledgements:
The support by the "Unfalluntersuchungsstelle Bahnen und Schiffe" and by the "Jungfrau Railways" is gratefully acknowledged.

TRAPPED LEE WAVE INTERFERENCE IN PRESENCE OF SURFACE FRICTION

Ivana Stiperski[1], Vanda Grubišić[2]

[1] Meteorological and Hydrological Service, Zagreb, Croatia
E-mail: *stiperski@cirus.dhz.hr*
[2] University of Vienna, Vienna, Austria

Abstract: Lee-wave interference over twin peaks in the presence of a frictional boundary layer is investigated by means of idealized high-resolution two-dimensional simulations with the NRL COAMPS model. The interference is examined under linear to highly nonlinear flow regimes. The results show that the pattern of positive and negative interference, evident in the wave amplitude and rotor strength, is consistent with the predictions of linear interference theory. Interference is found to most significantly affect the flow in the lee of the downstream ridge, preventing boundary-layer separation there under conditions of destructive interference and amplifying rotor strength under constructive interference in different flow regimes. Only under strongly nonlinear conditions is the rotor strength amplified by constructive interference beyond that obtained in the lee of a single mountain.

Keywords: *boundary layer separation, critical mountain height, nonlinearity, rotors*

1 INTRODUCTION

Trapped lee waves form downwind of a mountain ridge under conditions conducive to wave energy confinement within the lower troposphere. The study of nonlinear lee-wave resonances over twin ridges under free slip conditions (Grubišić and Stiperski 2009) shows that the resonance is governed by the ratio of the intrinsic trapped lee wave wavelength λ_s and the ridge-separation distance V. The positive and negative interference patterns are evident in the wave amplitudes and total wave drag. In the presence of a frictional boundary layer, the adverse pressure gradients associated with nonlinear, trapped lee waves are expected to lead to boundary layer separation and formation of recirculating regions (or rotors) underneath lee wave crests (Doyle and Durran 2002). Here we investigate the effects of a frictional boundary layer on the lee wave resonance and rotor strength over twin peaks.

2 MODEL SETUP

Two-dimensional numerical simulations were carried out using the nonhydrostatic COAMPS model initialized with an idealized sounding. The surface wind speed is 10 m s^{-1}, vertical wind shear equal to 6 m s^{-1} km^{-1}, and the stability N=0.012 s^{-1} is constant within the troposphere (Fig. 1). Friction at the lower boundary is imposed via a partial-slip condition with surface roughness z_0=0.01m. A set of idealized simulations was conducted for single and double bell-shaped obstacles for mountain heights H=300-1500 m and valley widths V=30-65 km. The mountain half-width is 5 km. The simulations were run for 10 hours during which time a quasi-steady state was reached in the simulations.

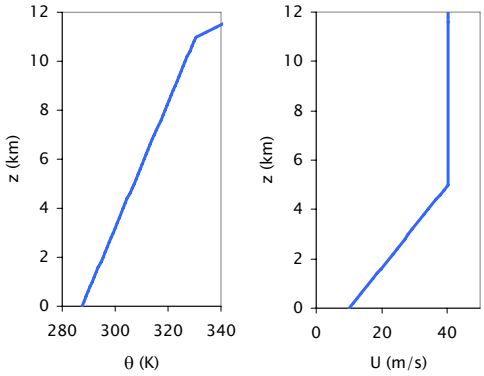

Figure 1. Initial upstream profile of potential temperature (K) and horizontal windspeed (m s^{-1})

3 RESULTS

3.1. Linear regime H< H_c=600 m

For twin peaks lower than H_c the wave interference pattern follows the linear interference theory predictions with constructive and destructive interference occurring, respectively, for V=n*λ_s, and V=(2n-1)/2* λ_s, where λ_s is the intrinsic horizontal wavelength downwind of a single obstacle for the given upstream profile (λ_s=21.8 km) and n>2 is an integer (Fig. 2). The positive and negative interferences are barely evident in the wave amplitudes and horizontal velocity perturbations in the lee of the first obstacle (A_1 and U_1 over the valley), but leave a clear imprint in the lee of the second obstacle, where the wave amplitude and horizontal velocity perturbation (A_2 and U_2) are enhanced or reduced relative to the value in the lee of a single mountain (A_s). The non-dimensional wavelengths cluster around integer values. The flow structure over the downstream obstacle is different under constructive and destructive interference (not shown). Whereas under constructive interference the flow resembles that over a single ridge, for destructive interference the potential temperature and horizontal wind speed are symmetric around the downstream peak. For H>H_s=370 m, the wave-induced adverse pressure

gradients are strong enough to cause boundary-layer separation and rotor formation in the lee of a single obstacle (U_s<0). Within the valley, the rotor strength (U_1) remains equal to U_s for all V, whereas downstream of the secondary obstacle the decrease in amplitude due to destructive interference is strong enough to prevent reversed flow formation, leading to large differences between the flows under constructive and destructive interference.

3.2. Nonlinear regime H_c<H<H_n=1000 m

For H>H_c=600 m the regime becomes nonlinear as the mountains are high enough for flow reversals to occur underneath the first lee wave crests, downstream of both obstacles irrespective of the interference pattern. In the weakly nonlinear regime, H_c<H<H_n=1000 m, the rotors over the valley remain unaffected by the second ridge. The rotors downstream of the second ridge do not attain velocities larger than those downwind of a single ridge, even under constructive interference (not shown).

3.3. Highly nonlinear regime H > H_n

For H≥H_n=1000 m, the nonlinearities start to affect the solutions significantly. Even though the interference still retains its linear pattern of occurrence, it is no longer evident in the variations of total drag (Fig.2), and the V/λ attains also non-integer values. The flow within the valley, unaffected by the secondary obstacle with the linear and weakly non-linear regimes, is weaker than in the lee of a single obstacle and exhibits some variation with V. Also, A_2>A_1 for all V. For H=1000 m constructive interference significantly enhances the rotors developing in the lee of the second ridge, while the rotors within the valley are weaker. For H=1500 m, the enhancement of the rotor circulation is somewhat weaker, possibly due to the nonlinear interaction between the wave field and the PBL flow.

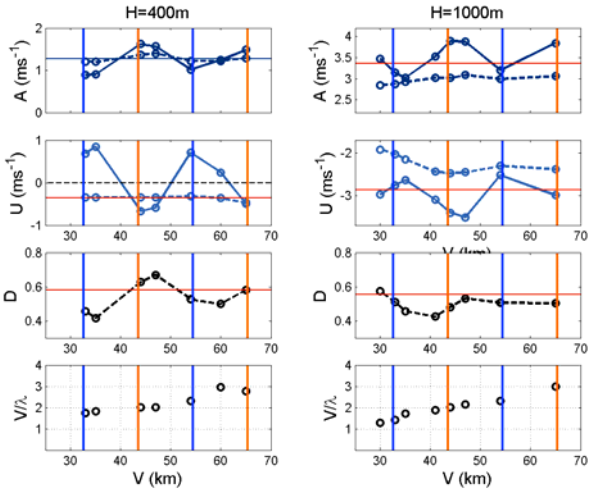

Figure 2. Amplitudes: A_2 (solid), A_1 (dashed); rotor strength U_2 (solid), U_1 (dashed); normalized wave drag (D); non-dimensional wavelength (V/λ), as function of valley width V for H=400 m (left) and H=1000 m (right). Solid red horizontal lines denote values downstream of a single ridge. Vertical lines denote V for which constructive (orange) and destructive (blue) interference is predicted by the linear interference theory.

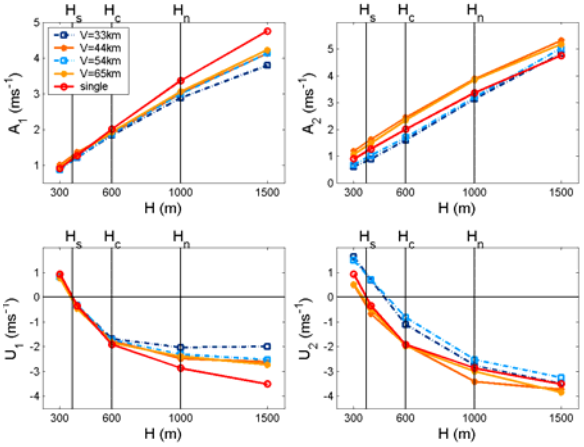

Figure 3. Amplitudes and rotor strength downstream of the first (A_1,U_1) and second (A_2,U_2) obstacle as function of mountain height H. Different V for which constructive (orange) and destructive (blue) interference occurs are indicated, with the values for single ridge in red. Vertical lines denote threshold mountain heights H_s=370 m, H_c=600 m, and H_n=1000 m.

4 CONCLUSIONS

Figure 3 summarizes the influence of mountain height and interference pattern on the wave amplitudes and rotor strength. The significance of the three threshold mountain heights (H_s, H_c and H_n) is best evident in the rotor strength diagrams. Rotors start to form (U_i<0, i=1,2) once the critical mountain height H_s for boundary layer separation is reached. Up to H_c = 600 m, the wave amplitudes and rotor strength increase linearly with H. Within the valley, the U and A values coincide with those for a single ridge, whereas downwind of the second obstacle a clear distinction between constructive and destructive interference is evident in both of these values. Weaker wave amplitudes under destructive interference require a higher critical mountain height for the rotor formation there. In the strongly nonlinear regime, for H>H_c, while the distinction between the interference patterns is becoming more apparent over the valley, where an indication of a limit to the rotor strength is also obtained, downstream of the second ridge the distinction is getting smaller and the rotor strength increases with H reduced.

REFERENCES

Doyle, J.D., and D.R. Durran, 2002: The dynamics of mountain-wave-induced rotors. *J. Atmos. Sci.*, **59**, 186–201.

Grubišić, V., and I. Stiperski, 2009: Lee wave resonances over double bell-shaped obstacles. *J. Atmos. Sci.*, In press.

A NUMERICAL STUDY OF THE COMBINED PROCESSES LEADING TO MEDITERRANEAN QUASI-STATIONARY MCS

Véronique Ducrocq[1], Céline de St. Aubin[1], Emilie Bresson[1], Olivier Nuissier[1], Didier Ricard[1]

[1] GAME-CNRM, Météo-France & CNRS, Toulouse, France
E-mail: *veronique.ducrocq@meteo.fr*

Keywords: *deep convection, heavy precipitation, quasi-stationary mesoscale convective systems*

1 INTRODUCTION

Northwestern Mediterranean regions are frequently affected by torrential rainfall associated with mesoscale convective systems. These systems can stay at the same location during several hours, focusing high-rate precipitation in a specific and limited region. Ingredients favouring the triggering of these events are relatively well-known now (Nuissier et al., 2008; Ducrocq et al., 2008). They include a slow-evolving synoptic environment, conditional convective instability, a low-level moist flow impinging the region, etc. But on the other hand, understanding how these ingredients combine and interact to produce more or less precipitation with different anchored locations is still an open question. The goal of the present study is to address this question based on idealised high-resolution modelling, following the study of Bresson et al. (2009).

2 MODEL SETUP

The effects of the mesoscale atmospheric conditions and of the terrain on the location and intensity of the quasi-stationary precipitating systems are investigated through 2.4-km MESO-NH simulations. Atmospheric conditions are idealized, but not the terrain as we wanted to keep in our simulations the strong topographic component of the region (e.g. sea surrounding by coastal mountain ranges). The idealized atmospheric conditions used as initial and boundary conditions contain the main characteristics of the flow observed during heavy precipitation events over the Cévennes region (Massif Central, see Fig. 2 for location). Indeed, these cases evidence a moist conditionally unstable South-Southeasterly flow over the Mediterranean Sea impinging on the Massif Central Southeastern foothills. With respect to the Bresson et al (2009) study, the simulation domain has been extended southwards and the initial wind fields is now vertically uniform in intensity and direction. Table 1 provides the description of the sensitivity experiments carried out.

Experiments	Max wind U_0	Moisture decrease α	Model terrain
CTRL	20 m s^{-1}	95%	real
WIN10, WIN30, WIN40	10, 30, 40 m s^{-1}	95%	real
ALPS, PYREN, MASC	20 m s^{-1}	95%	Remove the Alps, the Pyrenees, the Massif Central
HUM85, HUM90, HUM100	20 m s^{-1}	85%, 90%, 100 %	real

Table 1. Characteristics of the MESO-NH simulations.

3 RESULTS

The control experiment successes in simulating a quasi-stationary mesoscale convective system with large accumulated rain amounts. Whereas during the initial transition phase, the orographic forcing produces precipitation over the Massif Central foothills, a low-level cold pool progressively forms and pushes the convective system upwind (Fig. 1b). During the stationary phase, the orographic lifting is weaker as the cold pool and the convective system slow down the low-level flow. Two other triggering mechanisms operate. Upstream over the Sea, low-level wind convergence provides the necessary upward lifting for the triggering of new convective cells, whereas more downstream the cold pool facing the low-level moist flow supplies additional lifting. The deflection by the Alps of the flow (Fig. 2b) contributes to increase the both forcing mechanisms.

The set of experiments varying the basic flow speed from 10 to 40 m/s show that the flow speed influences both the location of the precipitating system (Fig. 1) and the occurrence of the cold pool. The weaker the flow speed is, the more upstream the precipitating system is located. Besides, with intense flow, evaporation from the Mediterranean Sea is increased, resulting in nearly saturated lower-levels for experiments with intense flow. Evaporation of falling precipitation is therefore restrained in these experiments and no significant cold pool is formed. The dominant forcing are therefore different according to the flow speed. With low-speed flow, new convective cells are mainly triggered by the low-level convergence over the Sea and by the cold pool. On the

opposite, flow-over regimes are favoured with intense and moist flows and the main mechanism to steadily trigger new cells is orographic lifting in the experiments with high-speed flow. These experiments produce the largest rainfall amounts (Fig. 1cd).

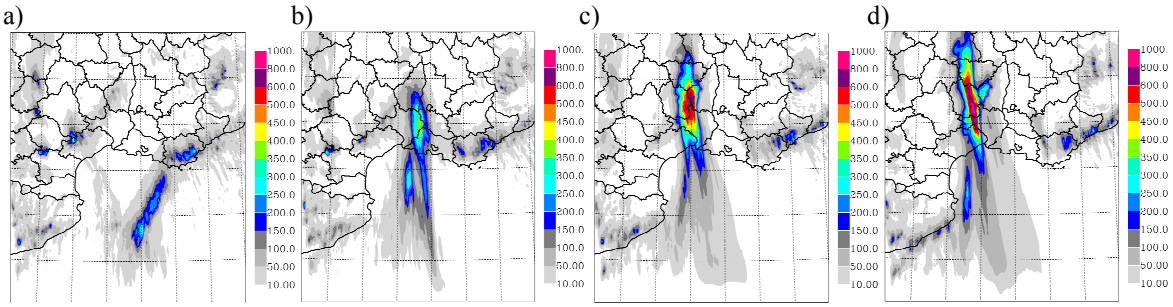

Figure 1. 24-h accumulated surface rainfall (mm) for day 2 of simulation for : a)WIN10; b) CTRL; c) WIN30; d) WIN40.

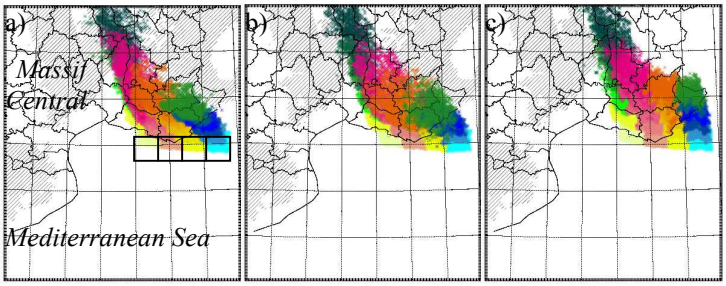

Figure 2. Plumes of Lagrangian parcels that are initially contained in 4 contiguous boxes of 0-500m depth from 42 to 48 h of simulation (by 1 h step) for: a) HUM85; b) CTRL and c) ALPS simulations. The initial parcel boxes are shown in a).

Then, the effects of the mountain ranges have been examined, by alternatively removing them. Even though the mountain ranges are removed, a quasi-stationary convective system is obtained for all the experiments. Removing the Alps helps to highlight the role of this mountain range in deflecting the low-level flow on the eastern side of the domain. The effect of the flow deflection by the Alps is to increase the low-level wind convergence (Fig. 2c). Such deflection of the flow is also evidenced for the Pyrenees although less important than for the Alps. Concerning the Massif Central, it clearly plays a role in blocking the cold pool in the Rhône valley, besides the orographic lifting effect already identified.

Finally, the sensitivity to the environment moisture distribution has been investigated by modulating the moisture apart the axis of maximum flow and humidity. Results of the experiments show that the environmental moisture influences both the location and intensity of the quasi-stationary precipitating system. Indeed, a dryer environment favours a more important deflection of the flow by the Alps as well as a more intense and wider cold pool, pushing the convective system more upstream. The cold pool exerts larger upward lifting, resulting in larger accumulated precipitation than the control experiment. On the opposite, a horizontally homogeneous moist environment reduces the evaporation of precipitation and therefore the cooling beneath the convective system, but supplies larger moisture to produce high precipitation amounts.

4 CONCLUSION

The synthesis of all the sensitivity experiments carried out shows that the location and intensity of the Mediterranean quasi-stationary mesoscale convective systems depend not only on a unique combination of characteristics of the mesoscale environment in which the systems form and evolve (flow speed and direction, moisture distribution, terrain of the region). As instance, the same location of the system can be obtained by varying either the flow speed or the moisture. However, the MESO-NH experiments evidence four main low-level mesoscale forcings which combine or compete to explain the intensity and the location of the system: cold pool forcing, orographic lifting, low-level wind convergence and flow deflection by neighbouring mountains. According to the characteristics of the environment, some of them could be dominant or absent.

REFERENCES

Ducrocq, V., O. Nuissier, D. Ricard, C. Lebeaupin et T. Thouvenin, 2008: A numerical study of three catastrophic precipitating events over southern France. II: Mesoscale triggering and stationarity factors, *Quarterly Journal of the Royal Meteorological Society*, **134**, 131-145.

Nuissier, O., V. Ducrocq, D. Ricard, C. Lebeaupin et S. Anquetin, 2008 : A numerical study of three catastrophic precipitating events over southern France. I: Numerical framework and synoptic ingredients, *Quarterly Journal of the Royal Meteorological Society,* **134**, 111-130.

Bresson, R., D. Ricard and V. Ducrocq, 2009: Idealized mesoscale numerical study of Mediterranean heavy precipitating convective systems, *Meteorology and Atmospheric Physics*, **103**, 45-56.

TOPOGRAPHIC AND DIURNAL EFFECTS ON TROPICAL AND SUBTROPICAL CONVECTION IN SOUTH AMERICA

Ulrike Romatschke[1,2], Socorro Medina[1], Robert A. Houze, Jr[1], Kristen Rasmussen[1]

[1] Department of Atmospheric Sciences, University of Washington, Seattle, USA
[2] Institute for Meteorology and Geophysics, University of Vienna, Vienna, Austria
E-mail: *ulli@atmos.washington.edu*

Abstract: Tropical Rainfall Measuring Mission (TRMM) Precipitation Radar (PR) and National Centers for Environmental Prediction (NCEP) reanalysis data are used to investigate the relation of convective precipitation systems to the topography of South America. Three types of convective radar echo structures are defined: *Deep convective cores* (convective 40 dBZ echo ≥ 10 km in height), *wide convective cores* (convective 40 dBZ echo area ≥ 1000 km²) and *broad stratiform regions* (stratiform echo area ≥ 50,000 km²). Their geographic distribution, diurnal cycles, and relation to the precipitation pattern are studied to gain insight into the mechanisms leading to convection in the vicinity of the Andes. Diurnal heating and capping of the low-level moist flow by dry air flowing over the Andes affects the evening formation of *deep* and *wide convective cores*. Nocturnal downslope flow influences the formation of *wide convective cores* in the early morning. *Broad stratiform regions* appear to be a later stage of mesoscale system development and their locations coincide with the areas of maximum rainfall. The South American low-level jet influences the location of maximum convective activity.

Keywords: *TRMM, South America, convection, diurnal cycle*

1 INTRODUCTION

Since precipitation in tropical and subtropical South America is mostly of convective origin, understanding the mechanisms leading to the development of convective systems is fundamental. Various studies have shown the significant roles of the topography (e.g. Lenters and Cook, 1995), the diurnal heating (e.g. Garreaud and Wallace, 1997), and the synoptic forcing (e.g. Nogués-Paegle and Mo, 1997) in the formation of convection. Data from the satellite-borne Tropical Rainfall Measuring Mission (TRMM) Precipitation Radar (PR) show the location, vertical and horizontal structure, intensity, and nature of convective systems in unprecedented detail. National Centers for Environmental Prediction (NCEP) reanalysis data provide the synoptic context.

In this study we use the summer months of ten years of TRMM PR data to identify three categories of convective radar echo structure: (1) *Deep convective cores* (convective 40 dBZ echo ≥ 10 km in height), which are associated with localized vigorous young convection and often with severe weather. (2) *Wide convective cores* (convective 40 dBZ echo ≥ 1000 km² in horizontal area), which are associated with mesoscale convective systems (MCSs) likely in an early stage of their life cycle. (3) *Broad stratiform regions* (stratiform echo ≥ 50,000 km² in horizontal area), which are associated with MCSs likely in a late stage of their life cycle. This classification allows us to clarify the different convective forcings.

2 DIURNAL HEATING, TOPOGRAPHIC AND SYNOPTIC FORCING OF CONVECTION

Deep convective cores are mainly observed in the subtropics near and to the east of the eastern Andean foothills (Fig. 1a). *Wide convective cores* occur over the same regions and also over the tropical eastern Andean foothills, the Amazon Basin, and the eastern part of the South Atlantic (Fig. 1b). *Broad stratiform regions* are most frequent in the same locations as the *wide convective cores,* however in the subtropical plains they occur to the east of the regions where the *deep* and *wide convective cores* are maximum (Fig. 1c). *Broad stratiform regions* prominently coincide with the regions of maximum surface precipitation (cf. Fig. 1c and d).

The focus of this study is on the eastern Andean foothills and the subtropical plains. In these regions, *deep convective cores* occur preferentially in the afternoon and evening in connection with solar heating. They are observed in an environment of strong directional wind shear where moist low-level easterlies are capped by dry westerlies aloft. This leads to a build-up of extreme instability which is released as the surface flow is lifted over the foothills, similarly to what is observed over the US Great Plains (Carlson et al., 1983) and near the Himalayas (Houze et al., 2007). *Wide convective cores* also peak in the afternoon due to similar mechanisms and also during the morning. Composites of NCEP reanalysis data suggest that the early morning maximum may be associated with nocturnal downslope flow along the foothills, which leads to convergence with the prevailing wind. *Broad stratiform regions* are most frequently observed in the late morning in the same regions as the morning *wide convective cores,* suggesting that they represent similar systems in a later stage of development.

The location of the convection is controlled by the strength of the South American low-level jet (SALLJ), a northerly flow that forms preferentially at night along the eastern Andean foothills. The SALLJ is strengthened as mid-latitude low pressure systems approach from the west. This leads to increased moisture transport from the Amazon Basin to the subtropics and enhanced wind convergence along the subtropical foothills and plains. Hence, the convective activity increases in these regions. As the low pressure systems move further east, anomalous southerly flow along the eastern Andean foothills counteracts the SALLJ and increases moisture and wind convergence to the north, enhancing convection and precipitation along the tropical foothills.

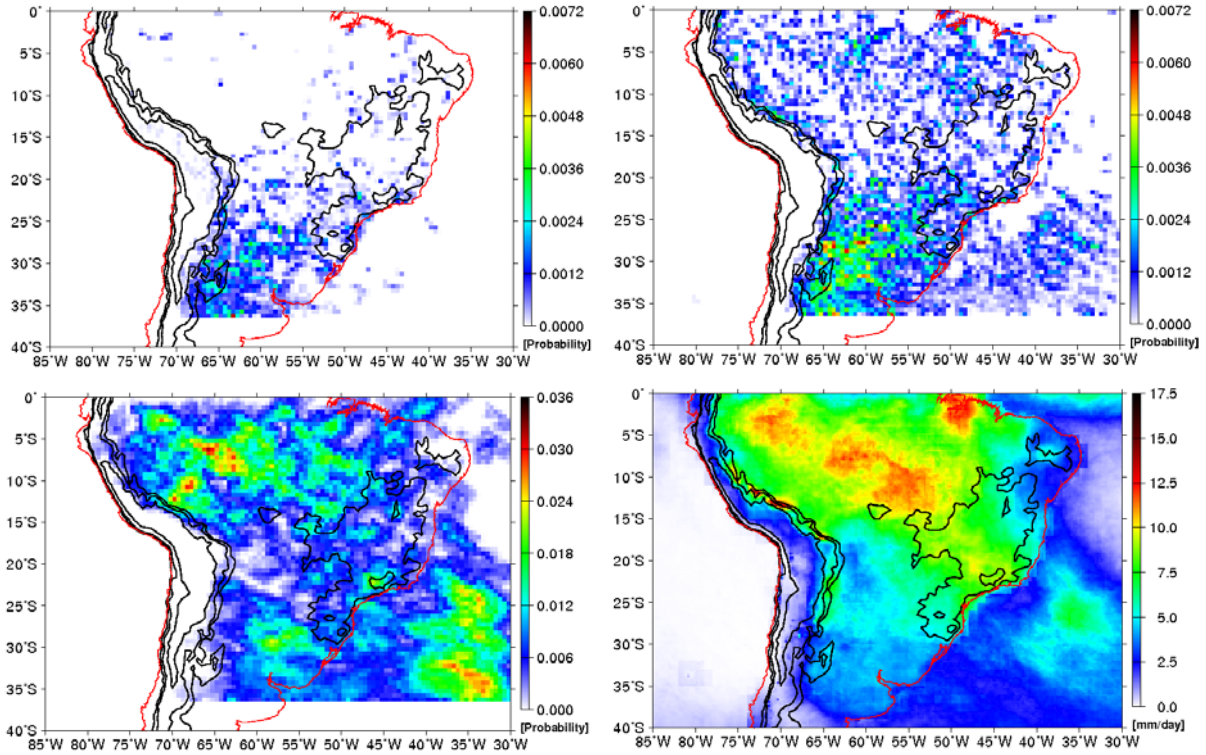

Figure 1. Distribution of the probability of finding (a) a *deep convective core*, (b) a *wide convective core*, and (c) a *broad stratiform region* during summer and (d) summer precipitation climatology from TRMM product 3B43. Orographic contours of 0.3 km, 1.5 km and 3 km are shown in black. Note the different color scales.

3 CONCLUSIONS

Analysis of different types of convective structure highlights how the diurnal heating, the topography and the synoptic forcing play together to develop the convective systems, which predominate in the vicinity of the Andes. Capping of the low-level moist flow by dry air aloft leads, in combination with topographic forcing and diurnal heating, to the formation of *deep* and *wide convective cores* in the evening. Nocturnal downslope flow influences the early morning formation of MCSs containing *wide convective cores* in an early stage and *broad stratiform regions* in a later stage of their life cycle. The locations of occurrence of *broad stratiform regions* coincide with the maximum climatological precipitation. The exact location of the region with maximum convective activity is controlled by the strength of the SALLJ.

Acknowledgements:
Stacy Brodzik and Carol Archambeault assisted in the data processing. This research was supported by the National Science Foundation (ATM-0505739/ATM-0820586) and the National Aeronautics and Space Administration (NNX07AD59G).

REFERENCES

Carlson, T. N., S. G. Benjamin, G. S. Forbes, and Y. Li, 1983: Elevated Mixed Layers in the Regional Severe Storm Environment: Conceptual Model and Case Studies. Mon. Weather Rev., **111**, 1453-1474.

Garreaud, R. D., and J. M. Wallace, 1997: The Diurnal March of Convective Cloudiness over the Americas. Mon. Weather Rev., **125**, 3157-3171.

Houze, R. A., D. C. Wilton, and B. F. Smull, 2007: Monsoon convection in the Himalayan region as seen by the TRMM Precipitation Radar. Q. J. R. Meteorol. Soc., **133**, 1389-1411.

Lenters, J. D., and K. H. Cook, 1995: Simulation and Diagnosis of the Regional Summertime Precipitation Climatology of South America. J. Clim., **8**, 2988-3005.

Nogués-Paegle, J., and K. C. Mo, 1997: Alternating Wet and Dry Conditions over South America during Summer. Mon. Weather Rev., **125**, 279-291.

STRUCTURE OF MID-LATITUDE CYCLONES CROSSING THE CALIFORNIA SIERRA NEVADA AS SEEN BY VERTICALLY POINTING RADAR

Socorro Medina[1], Robert A. Houze, Jr.[1], Christopher R. Willimas[2], and David E. Kingmill[2]

[1] Department of Atmospheric Sciences, University of Washington, Seattle, USA
E-mail: *socorro@atmos.washington.edu*
[2] University of Colorado, Cooperative Institute for Research in Environmental Sciences, and NOAA/Earth System Research Laboratory, Boulder, USA

Abstract: Previous work has shown that a layer of intermittent updraft cells, apparently turbulent in nature, develops as the middle sector of mid-latitude cyclones passes over the Oregon Cascades and that these cells likely contribute to the windward enhancement of precipitation. This study finds a similar layer of cells as the middle sector of extreme extratropical cyclones pass over the Sierra Nevada of California, providing evidence of the repeatability of the signal.

Keywords:, *vertical shear layer, turbulence, orographic precipitation enhancement*

1 INTRODUCTION

Most of the precipitation in the western United States falls during the winter months as mid-latitude cyclones from the Pacific Ocean move inland (Fig. 1, left and center). Previous studies have provided insight into how the precipitation varies from one sector of an extratropical cyclone to another (e.g., Nagle and Serebreny 1962). These studies have focused on the horizontal patterns of cloud and precipitation in the cyclones. However, when these weather systems move over mountainous terrain, the horizontal patterns are affected by the orography and become complex. High temporal and vertical resolution reflectivity and Doppler velocity profiles obtained by vertically pointing (VP) S-band radars (White et al. 2003) provide a better alternative to describe the precipitation processes in different sectors of extratropical cyclones passing over complex terrain. For example, Medina et al. (2007) analyzed the vertical structure of cyclone precipitation over the Oregon Cascades (mbo in Fig. 1), while Kingsmill et al. (2006) focused over the Northern California Coastal Mountains (czd in Fig. 1).

Medina et al. (2007) identified vertical structures that are apparently produced when moist flow impinges upon the terrain. When the middle sector of a storm, characterized by the transition from warm to cold advection, passes over the windward slope, scanning radar observations show that a shear layer often forms on the windward slope. Within the shear layer, the VP radial velocity shows intermittent updraft cells (> 0.5 m s^{-1}). These cells, which are apparently turbulent, are thought to be crucial for enhancing the growth of precipitation particles and for speeding up their fallout over the windward slope (Houze and Medina 2005). This study is part of an investigation aimed at understanding how the complex terrain of the western US modifies the structure of mid-latitude cyclones advancing from the Pacific Ocean. The specific objective of this study is to test the repeatability of the structures observed by Medina et al. (2007) in other west coast locations.

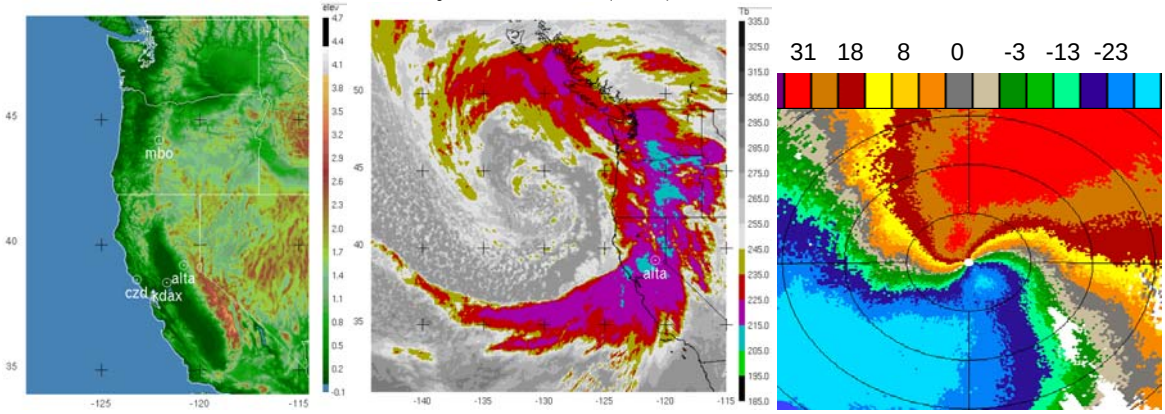

Figure 1. Left: Topography of western US (km) and relevant sites. Center: Infrared satellite temperature (K) during the passage of a mid-latitude cyclone over the area of study (1530 UTC 4 Jan 2008). Right: Radial velocity (m s^{-1}) at 2.4° elevation from the Sacramento radar (kdax, 1457 UTC 4 Jan 2008). Range ring spacing is 25 km. Positive (negative) values indicate flow away from (toward) the radar.

2 DATA

The main dataset for the study is the VP S-band radar data collected as winter storms moved over the western slopes of the California Sierra Nevada. The data was collected during the National Oceanic and Atmospheric

Administration (NOAA) Hydrometeorological Testbed (HMT, Ralph et al. 2005). The VP dataset was collected at Alta (Fig. 1) and Colfax (~17 km southwest of Alta) and it extends over three winter seasons. We use Weather Surveillance Radar (WSR-88D) data and infrared images from the Geostationary Operational Environmental Satellite (GOES) to obtain the larger context of the VP radar structures.

3 RESULTS

The passage of mid-latitude cyclones over the Sierra Nevada is separated by periods dominated by a high pressure offshore of California (i.e., blocking or omega pattern). When this pattern breaks, weather systems are able to penetrate into the region of interest. Preliminary analysis of the VP radar structure suggests that the extreme storms (either by amount of precipitation accumulated and/or by wind intensity) present a layer of intermittent cells in the perturbation radial velocity located above the radar bright band near 2 km (dBZ, left panel; RV', right panel in Fig. 2). RV' was calculated as the residual between the actual radial velocity and the 60 minutes running average radial velocity (Matrosov et al. 1994). The period in Fig. 2 corresponds to the infrared satellite image in the Fig. 1 (center), indicating that the occurrence of the cells coincides with the passage of the middle sector of a storm. The horizontal radial velocity pattern (Fig 1, right) illustrates the strong shear during this case, which was characterized by a south-southeasterly jet at low levels, along the central valley, and strong southwesterlies aloft.

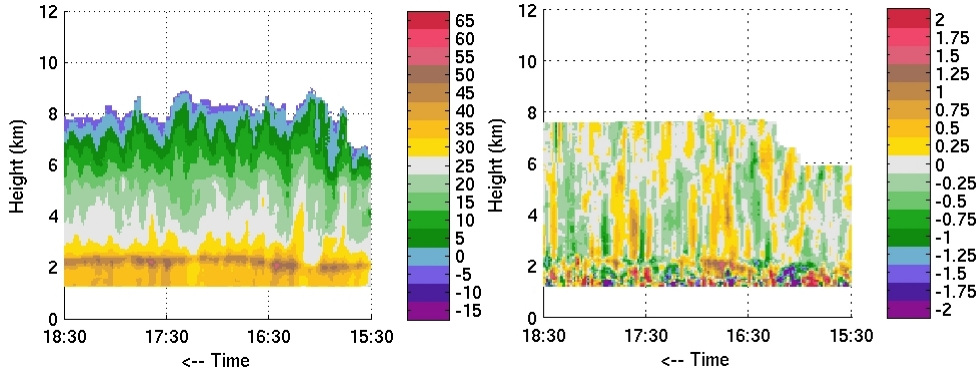

Figure 2. VP radar structure at Alta (4 Jan 2008). Left: reflectivity (dBZ). Right: perturbation radial velocity (RV', m s^{-1}). Positive (negative) values indicate RV' toward (away from) the radar.

4 CONCLUSIONS

This study finds a layer of updraft cells as the middle sector of extreme extratropical cyclones passes over the Sierra Nevada of California, mounting the evidence of the generality of this orographic precipitation signal.

Acknowledgements:
The first and second authors were supported by National Science Foundation grants ATM-0505739 and ATM-0820586. Martin Ralph is acknowledged for his suggestions regarding the analysis the VP radar data. The KDAX data was plotted using NOAA's weather and climate toolkit.

REFERENCES

Houze, R.A., and S. Medina, 2005: Turbulence as a Mechanism for Orographic Precipitation Enhancement. *J. Atmos. Sci.*, **62**, 3599–3623.

Kingsmill, D.E., P.J. Neiman, F.M. Ralph, and A.B. White, 2006: Synoptic and Topographic Variability of Northern California Precipitation Characteristics in Landfalling Winter Storms Observed during CALJET. *Mon. Wea. Rev.*, **134**, 2072–2094.

Matrosov, S.Y., B.W. Orr, R.A. Kropfli, and J.B. Snider, 1994: Retrieval of Vertical Profiles of Cirrus Cloud Microphysical Parameters from Doppler Radar and Infrared Radiometer Measurements. *J. Appl. Meteor.*, **33**, 617–626.

Medina, S., E. Sukovich, and R.A. Houze, 2007: Vertical Structures of Precipitation in Cyclones Crossing the Oregon Cascades. *Mon. Wea. Rev.*, **135**, 3565–3586.

Nagle, R.E., and S.M. Serebreny, 1962: Radar Precipitation Echo and Satellite Cloud Observations of a Maritime Cyclone. *J. Appl. Meteor.*, **1**, 279–295.

Ralph, F.M., R.M. Rauber, B.F. Jewett, D.E. Kingsmill, P. Pisano, P. Pugner, R.M. Rasmussen, D.W. Reynolds, T.W. Schlatter, R.E. Stewart, S. Tracton, and J.S. Waldstreicher, 2005: Improving Short-Term (0–48 h) Cool-Season Quantitative Precipitation Forecasting: Recommendations from a USWRP Workshop. *Bull. Amer. Meteor. Soc.*, **86**, 1619–1632.

White, A.B., P.J. Neiman, F.M. Ralph, D.E. Kingsmill, and P.O.G. Persson, 2003: Coastal Orographic Rainfall Processes Observed by Radar during the California Land-Falling Jets Experiment. *J. Hydrometeor.*, **4**, 264–282.

SOURCES OF UNCERTAINTY EXAMINED BY HIGH-RESOLUTION ENSEMBLE MODELING

Christian Keil and George C. Craig

Deutsches Zentrum für Luft- und Raumfahrt (DLR), Institut für Physik der Atmosphäre
Oberpfaffenhofen, Germany
E-mail: *christian.keil@dlr.de*

Abstract: Forecasts of the high resolution ensemble prediction system COSMO-DE-EPS of Deutscher Wetterdienst (DWD) are used to examine the dominant sources of uncertainty of convective precipitation. A validation with radar data using traditional as well as novel spatial verification measures highlights differences in precipitation forecast performance in differing weather regimes. When the forecast uncertainty can primarily be associated with local, small-scale processes individual members run with the same variation of the physical parameterisation driven by different global models outperform all other ensemble members. In contrast when the precipitation is governed by the large-scale flow all ensemble members perform similarly.

Keywords: *ICAM, predictability, precipitation, COPS*

1 INTRODUCTION

Predictability, or forecast uncertainty, of convective precipitation is influenced by all scales, but in different ways in different meteorological situations. Forced-frontal convective precipitation associated with synoptic weather patterns may be predictable for several days and is primarily governed by lateral boundary conditions in limited area models. Single convective cells developing during air-mass convection situations, which of themselves are predictable only for a matter of hours, are frequently triggered by local, small-scale processes enforced e.g. by mountain ridges and are anticipated to react sensitively to changes in the model physics.

2 TOOLS AND INGREDIENTS

In the *high resolution ensemble prediction system* COSMO-DE-EPS an ensemble of forecasts is generated by combining initial and lateral boundary conditions of four different global models with five variations of physical parameterizations using the COSMO-DE model (dx=2.8km). Forecast quality of all 20 ensemble members is validated using hourly instantaneous *Radar data of the European Composite*. Here the conventional *bias score* is used to provide an integral estimate of the model's behaviour in over- or underpredicting rainfall and the spatial verification measure *DAS* (Keil and Craig, 2009) combining displacement and amplitude errors is applied.

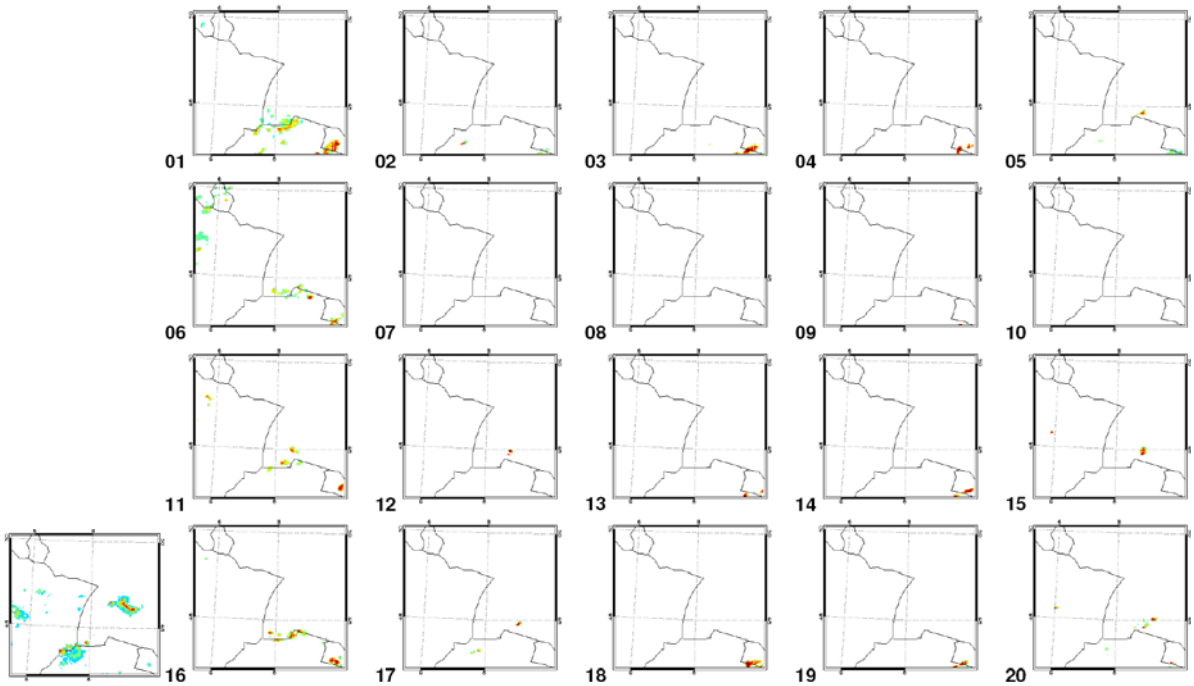

Figure 1. Radar observation (bottom left) and stamp map of forecast synthetic radar imagery displaying all 20 members of COSMO-DE-EPS on 12 August 2007 at 17.15 UTC.

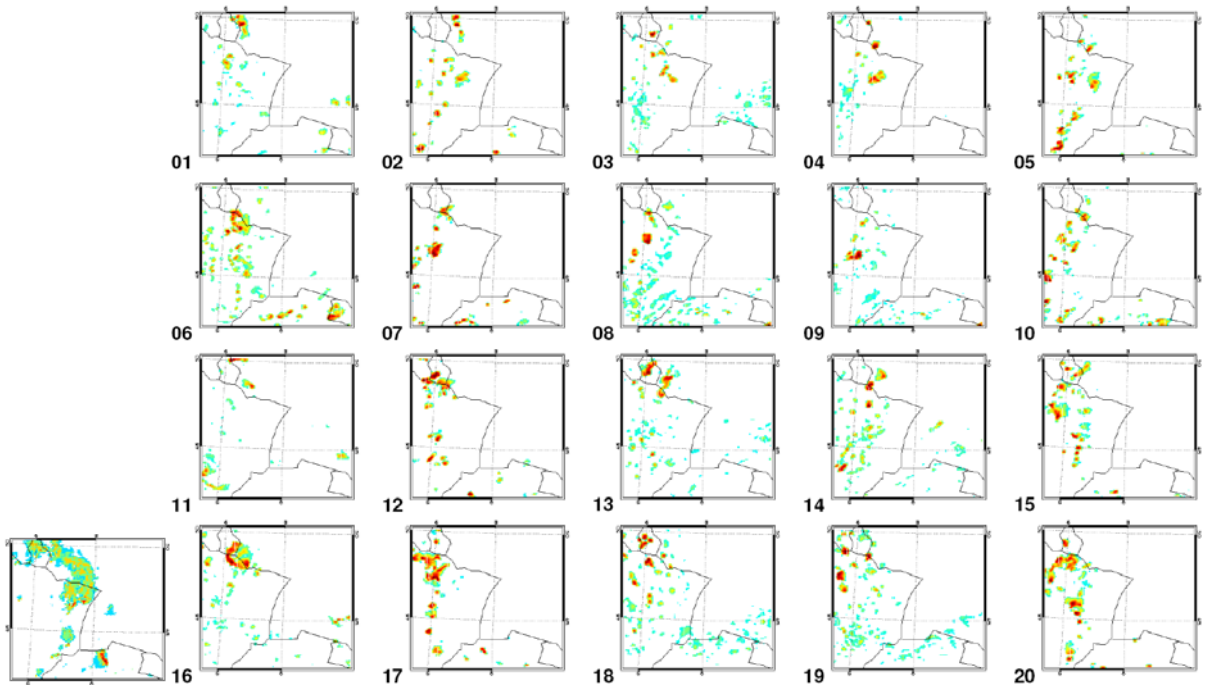

Figure 2. Same as Fig.1 but at 23.15 UTC.

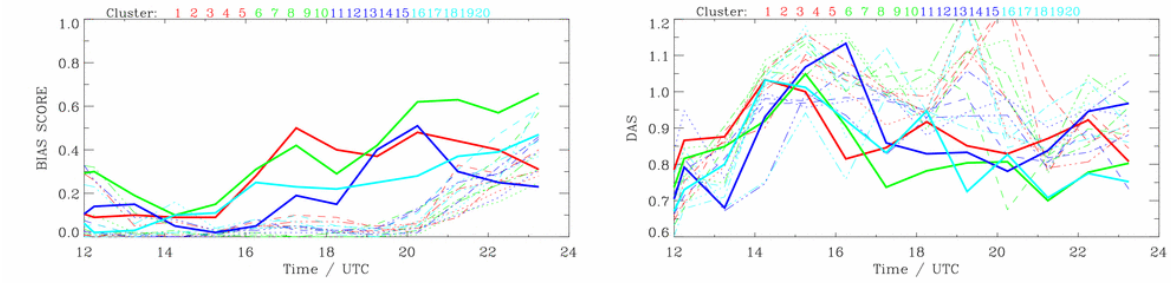

Figure 3. Bias score (left) and DAS (right) for all ensemble members applying a threshold of 19 dBZ on 12 August 2007. Different colours depict different driving global models, solid lines members 1, 6, 11 and 16 with changed entrainment rate.

3 RESULTS

Forecasts of COSMO-DE-EPS are continuously available from 8 to 16 August 2007 covering various meteorological situations during the COPS field experiment. One of the largest spread in bias score occurs during IOP15 on 12/13 August 2007. In the afternoon of 12 August local convection triggered by orography occurred in the COPS region. Members 1, 6, 11 and 16 of the ensemble system outperform the other members generating some convective precipitation along the Swiss-German border at 17.15 UTC (Fig.1). These 4 members are driven by different global models but are run with a modified entrainment rate. In contrast, precipitation along a cold front affects the region at 23.15 UTC. This synoptically forced precipitation is forecast by all members (Fig. 2; not at the correct position, however!) indicating a lower forecast uncertainty, i.e. a higher predictability. Both, the bias score and DAS show the good performance of these 4 individual members and the smaller spread at night when the front enters the COPS region (Fig.3).

4 OUTLOOK

The concept of convective timescale (Craig et al. 2009) will be applied in order to distinguish between different predictability regimes.

REFERENCES

Craig, G. C., C. Keil, and D. Leuenberger, 2009: Constraints on the Impact of Radar Rainfall Data Assimilation on Forecasts of Cumulus Convection**.** Submitted to QJ

Keil, C. and G .C .Craig, 2009: A displacement and amplitude score employing an optical flow technique. WaF, in press.

PROBABILISTIC FORECASTING OF THUNDERSTORMS THROUGH COMBINING NOWCASTING METHODS WITH NWP

Kirstin Kober, George Craig, Christian Keil, Arnold Tafferner

Deutsches Zentrum für Luft- und Raumfahrt, Institut für Physik der Atmosphäre, Oberpfaffenhofen, Germany
E-mail: *kirstin.kober@dlr.de*

Abstract: Short term forecasting of thunderstorms or convective precipitation is an ongoing challenge in atmospheric research. In this work the two different approaches nowcasting and numerical weather prediction (NWP) are applied probabilistically.

Keywords: *probabilistic, thunderstorms, nowcasting, NWP*

1 INTRODUCTION

Nowcasting and NWP are two different methods to address the unsolved problem of short term forecasting of convective precipitation. It is known that nowcasting methods which are based on extrapolation of observations in time perform quite well for very short term prediction (0-1 hour) as in this timeframe the motion of thunderstorms can adequately be described by advection. Physics are included at best very simply and therefore processes like growth and decay are not well described. Hence for longer lead times the skill of the forecasts based on nowcasting decreases quite rapidly. High-resolution NWP is in some cases able to simulate thunderstorms. NWP in general gains skill in forecasting convective precipitation after a certain spin-up time. The inherent uncertainty of the methods and of the meteorological situations requires a probabilistic view to evaluate the skill of the forecasts.

2 DERIVATION OF PROBABILITIES FROM RAD-TRAM AND COSMO-DE-EPS

For the advection based forecasts the radar tracker Rad-TRAM (Kober and Tafferner 2009) is used. Rad-TRAM is upgraded to produce probabilistic forecasts up to 4 hours using the Local Lagrangian method (Germann and Zawadzki 2004). Every 15 minutes a nowcast is provided which forecasts the probability that the threshold of 37dBZ is exceeded (Fig.1).

a) 15 min nowcast for 1700 UTC b) 60 min nowcast for 1700 UTC c) 120 min nowcast for 1700 UTC

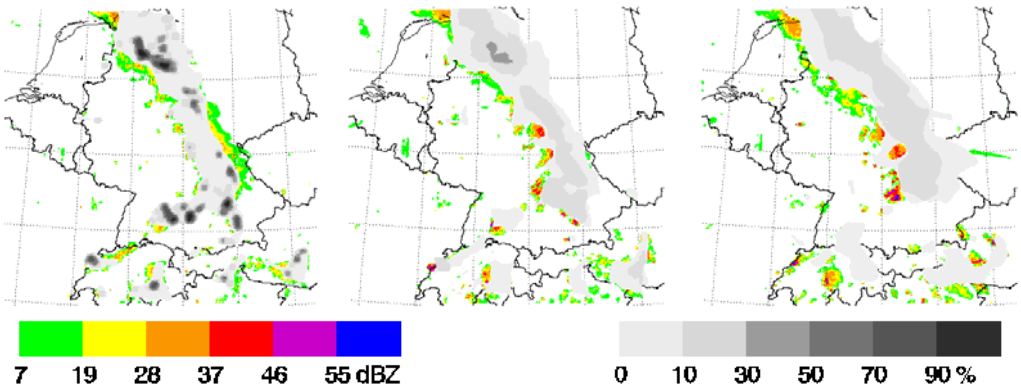

Figure 1: Probabilistic nowcasts with Rad-TRAM-prob for 29.07.2008 at 1700 UTC (a) 15min, b) 60min, c) 120 min). In the background colour-shaded the reflectivities of the European composite at the started time step and grey-shaded the nowcasted probabilities (coloured: www.pa.op.dlr.de/icam2009/extabs).

For the numerical forecasts the experimental, not yet operational, high resolution (2.8km) ensemble of Deutscher Wetterdienst (DWD) is used. Synthetic radar reflectivities are used to forecast the probability that 37dBZ is exceeded. This probability can be derived from the ensemble by two different methods. First, every member can be treated as a deterministic solution and the probability is derived similar to the spatial neighbourhood method (Theis et al. 2005). Second, the entire ensemble is used to derive at each gridpoint the fraction of the members that exceed the threshold. An example for both methods is shown in Figure 2.

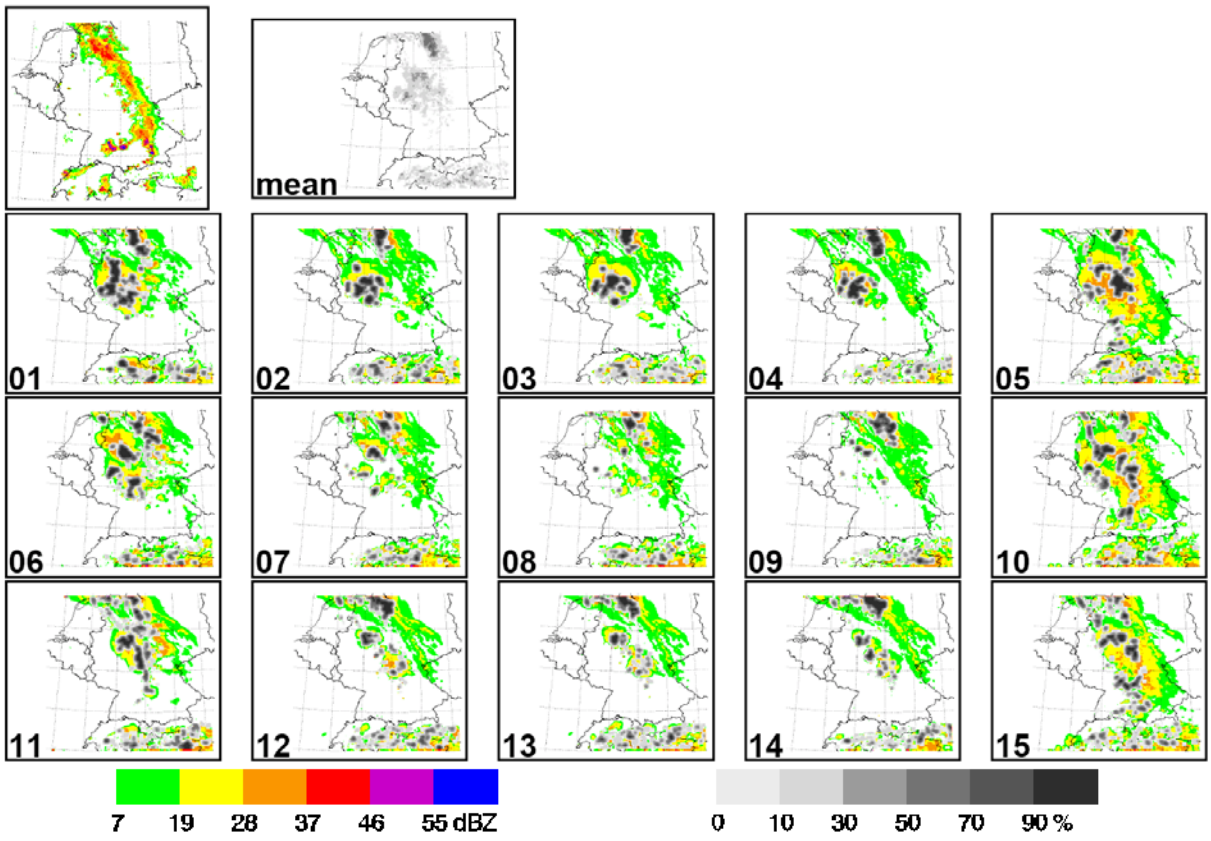

Figure 2: Stamp map of probabilistic COSMO-DE-EPS forecasts showing 15 members and their average (top right) (grey-shaded) for 29.07.2008 at 1700 UTC. In the background the synthetic radar reflectivities and the observed radar reflectivity (top left) is colour shaded (coloured: www.pa.op.dlr.de/icam2009/extabs).

3 FORECAST QUALITY

The forecast skill of Rad-TRAM and COSMO-DE-EPS probabilistic forecasts is calculated with the standard quality measures for the verification of probabilistic forecasts of dichotomous predictands: the Brier Score and its decomposition, reliability diagrams, and ROC curves (Wilks 2006). Furthermore the Conditional square root of ranked probability score (CSRR) is calculated (Germann and Zawazdki 2004). With these scores the development of quality with lead time and on average is calculated for both forecast sources for selected episodes (not shown). First results show that especially short nowcasts have more reliability and resolution than the NWP forecasts.

4 FUTURE

The next step will be to calculate to development of forecast skill in different synoptic situations. With this knowledge methods to combine the two forecast sources can be investigated. Weighting functions for example could be the probabilistic step to be included into the system 'Wx-FUSION' (Weather Forecast User oriented System Including Object Nowcasting) currently under development at DLR. Wx-FUSION will generate forecasts of different weather hazards relevant for applications in airport environments.

REFERENCES

Germann, U., I. Zawadzki, 2004: Scale dependence of the Predictability of Precipitation from Continental Radar Images. Part II: Probability Forecasts. *J. Appl. Meteor*. **43**, 74 - 89.

Kober, K., A. Tafferner, 2009: Tracking and nowcasting of convective cells using remote sensing data from radar and satellite. *Meteorol. Z.* **1**, 75-84.

Theis, S. E., A. Hense, U. Damrath, 2005: Probabilistic precipitation forecasts from a deterministic model: a pragmatic approach. *Meteorol. Appl*. **12**, 257-268.

Wilks, D.S., 2006: Statistical Methods in the Atmospheric Sciences. San Diego, London: Academic Press, 282pp.

ENSEMBLE METEOROLOGICAL FORECAST FOR THE UPPER RHONE RIVER BASIN

Javier Garcia Hernandez[1], Paul Sirvent Gimenez[1], Frédéric Jordan[2], Jean-Louis Boillat[1], Anton Schleiss[1]

[1] Laboratoire de Constructions Hydrauliques (LCH), Ecole Polytechnique Fédérale de Lausanne.
EPFL-ENAC-ICARE-LCH Station 18, CH-1015 Lausanne, Switzerland,
E-mail: javier.garciahernandez@epfl.ch
[2] e-dric.ch eau énergie environnement ingénieurs conseils,
Grand-Chemin 73, CH-1066 Epalinges, Switzerland

Abstract
A semi-distributed hydrological model was developed for the Upper Rhone River basin in Switzerland. It is currently operational for a real-time flood forecast in the Rhone Valley. It simulates the snow and glacier melt, soil infiltration and run-off processes, flood routing in rivers as well as hydropower scheme operations.

For the computation of flood prediction, the numerical meteorological forecasts COSMO-LEPS, COSMO-7 and COSMO-2, provided by MeteoSwiss, have been assimilated. The forecast errors are analyzed by comparing the performance on different time periods, regarding the observed and the predicted rainfall and temperature over the entire catchment area as well as in punctual locations. The influence of the lead time is described with the aim of providing an estimation of the forecast error. A performance evaluation is achieved considering indexes like Brier Score and Relative Operating Characteristic.

Keywords: *Deterministic and ensemble meteorological forecast, Brier Score, Relative Operating Characteristic*

1 INTRODUCTION

Forecasting precipitation is a complex task because the formation of precipitation involves interactions between many different types of processes related to synoptic-scale, mesoscale dynamics, boundary conditions, etc. Further complexity occurs in mountainous regions where the topography influences in an important way the cloud dynamics and the precipitation microphysics.

Ensemble prediction system (EPS) is a feasible way to complete deterministic forecasts with an associated occurrence (Buizza & al., 2005). The existing uncertainty about the current state of the atmosphere is taken into account by calculating different forecast scenarios with an associated probability. EPS constitutes one of the most promising avenues in the meteorological research (Demeritt & al., 2007).

COSMO-LEPS is the limited-area EPS (Ensemble Prediction System) developed within the COSMO consortium (Consortium for Small-scale Modeling) since 2002. This system combines the benefits of the ensemble approach with the high-resolution of the limited-area model integrations. The COSMO-LEPS system provides daily ensemble forecasts with high resolution (horizontal mesh-size of 10 km) based on a 16-member ensemble for central and southern Europe with a lead time of 132 hours. Initial and boundary conditions are representative members of the global ECMWF (European Centre for Medium-Range Weather Forecasts) ensemble. The purpose of COSMO-LEPS is the improvement of the early and medium-range predictability of extreme and localized weather events, particularly when orographic and mesoscale-related processes play a crucial role (Marsigli & al., 2007).

Deterministic forecasts COSMO-7 and COSMO-2 are complementary to COSMO-LEPS. The regional COSMO-7 is driven by the global model of ECMWF and covers most of western and central Europe. It is calculated twice daily for 72 hours lead time on a grid spacing of about 6.6 km. The local COSMO-2, driven by COSMO-7, covers the Alpine region with Switzerland at the center and is computed on a grid spacing of about 2.2 km. It is provided 8 times daily for 24 hours lead time. Both COSMO-2 and COSMO-7 offer the benefit of the nowcasting and short range forecasting.

Meteorological predictions are finally used as input for the hydrological model, created with Routing System (García & al., 2007), producing hydrological ensemble forecasts as well as deterministic forecasts for the flood prediction in the Upper Rhone River basin (Jordan, 2007).

2 METEOROLOGICAL INDEXES

Indexes like the intensity or temperature bias and volume or average temperature bias for different time periods as well as indexes commonly used in meteorology such as the Brier Score (BS) and the Relative Operating Characteristic (ROC) are used to evaluate the forecast performance.

The bias represents the report between the predicted and observed values. The BS allows comparing the forecast probability of an event and its occurrence (Brier, 1950). It depends on three factors: reliability, resolution and uncertainty. The ROC curve defines the ability of a probabilistic forecast system to distinguish between situations predicting the occurrence and the non-occurrence of an event (Mason & Graham, 1999). It is frequently applied to assess the ability of ensemble forecast systems to discriminate between the occurrence and non-occurrence of precipitation accumulations over a specific threshold.

3 RESULTS

The proposed indexes allow the comparison of deterministic COSMO-7 (C7) and COSMO-2 (C2) and probabilistic COSMO-LEPS (CL) forecasts for different time periods.

Bias indicators show a big dispersion in the precipitation intensity for the deterministic forecasts as well as for the weighted average of the probabilistic one. Besides, an overestimation of the precipitation is in general produced which increases by a long way the forecast period.

Temperatures are usually rather well predicted and similar in all the forecasts. The hourly error is around 2.5°C and the daily average error around 2°C.

BS commonly show values smaller than 0.4 for all studied forecasts (Figure 2, left). Forecasts are generally better than the persistence (prolongation of the first day measured observation). However, a severe assessment is necessary for higher rain intensities. This will be possible as soon the re-simulations of past events (September 1993 and October 2000) from MeteoSwiss will be achieved.

The ROC index proves that the probabilistic forecast is better for the prediction of an event exceeding a threshold (Figure 2, right). Thresholds of 5 to 50 mm/24h have been studied, being the performance of the probabilistic forecasts higher for smaller thresholds, as well as for deterministic meteorological forecasts. Although, re-simulations will also be required for heavier precipitation data. Regarding the Correct Alarm Ratio and the Miss Ratio (Mason & Graham, 1999), probabilistic forecasts provide also better results.

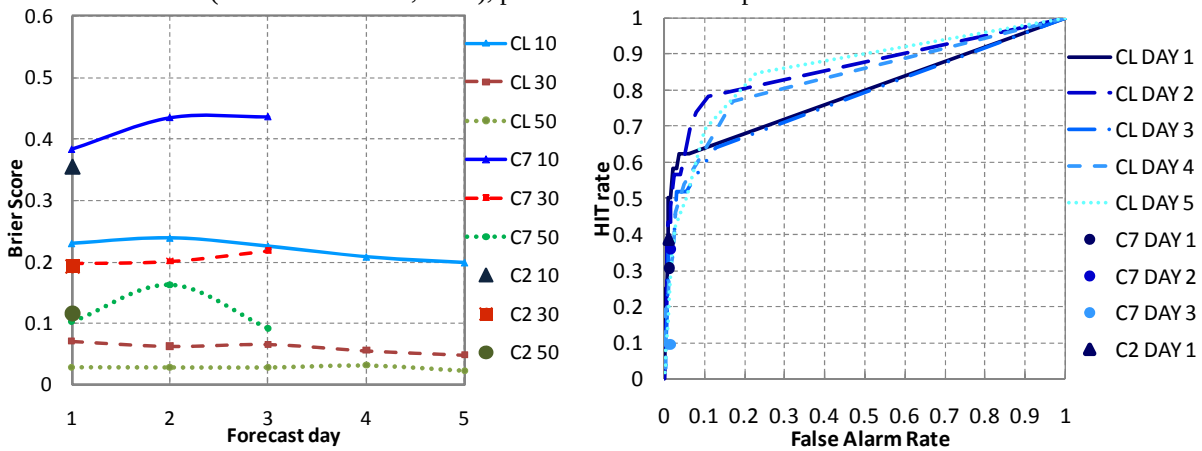

Figure 1: Left: Brier Score for different thresholds (10, 30 and 50 mm/24h), forecasts from 01.07.2008 to 02.28.2009. Right: ROC for the 30mm /24h threshold, forecasts from 01.07.2008 to 02.28.2009.

4 CONCLUSIONS

The indexes used to evaluate the forecast performance show the improvements of the EPS in the meteorological area. The results provided decrease the uncertainty in the flood forecasting domain, where the methods of risk analysis have taken more importance during the last years, allowing the decision-makers to know the rationality of their decisions.

More events of extreme precipitations are necessary for the assessment of high thresholds in order to have a large sample providing representative results. That is the motivation of events re-simulations by MeteoSwiss.

Acknowledgements:

The present research is part of the MINERVE project, funded by the Swiss Federal Office for Environment (FOEV), the Canton of Valais and the Canton of Vaud. Meteorological data are provided by the Swiss Weather Services (MeteoSwiss).

REFERENCES

Brier, G. W. (1950). Verification of forecasts expressed in terms of probability. *Monthly Weather Review*, Vol. 78, 1, 1-3.

Buizza, R., Houtekamer, P.L., Toth, Z., Pellerin, G., Wei, M. and Zhu, Y. (2005). A comparison of the ECMWF, MSC and NCEP global ensemble prediction systems. *Monthly Weather Review* Vol. 133, 1076–1097.

Demeritt, D., Cloke, H., Pappenberger, F., Thielen, J., Bartholmes, J. and Ramos, M.H. (2007). Ensemble predictions and perceptions of risk, uncertainty and error in flood forecasting. Environmental Hazards 7, 115-127.

García Hernández, J., Jordan, F., Dubois, J., Boillat, J.-L. & Schleiss, A. (2007). Routing System II: Flow modelling in hydraulic systems, *Communication du Laboratoire de Constructions Hydrauliques N°32*, ed. A. Schleiss, EPFL, Lausanne.

Jordan, F. (2007). Modèle de prévision et de gestion des crues - optimisation des opérations des aménagements hydroélectriques à accumulation pour la réduction des débits de crue. PhD Thesis N°3711, Ecole Polytechnique Fédérale de Lausanne.

Marsigli, C., Montani, A. and Paccangnella, T. (2007). Ensemble activities at ARPA-SIM: the COSMO-LEPS and COSMO-SREPS systems. *Proceedings, 29th International Conference on Alpine Meteorology*, 4.-8. June 2007, Chambéry.

Mason, S.J. and Graham, N.E. (1999): Conditional probabilities, relative operating characteristics, and relative operating levels. *Weather Forecasting*, Vol 14, Issue 5, 713-725.

THE CANADIAN HIGH-RESOLUTION NWP SYSTEM FOR THE 2010 WINTER OLYMPICS

Jason Milbrandt[1], Ron McTaggart-Cowan[1] and Jocelyn Mailhot[1]

[1] Numerical Weather Prediction Research Section, Environment Canada, Montreal, Canada
E-mail: *Jason.Milbrandt@ec.gc.ca*

1 INTRODUCTION

The 2010 Winter Olympics and Paralympics will be held near Whistler/Vancouver, Canada during January-March, 2010. In support of the operational forecasting during the events and as a testbed for NWP systems in Canada, Environment Canada will be running a high-resolution limited-area mesoscale model, twice daily. The main objectives are to improve the forecast of precipitation quantities and types, winds, and temperatures in this coastal region of complex orography. The influence of steep terrain surrounding the venues is clearly one of the greatest challenges associated with numerical modelling in the Whistler/Vancouver region. This complexity is enhanced by the presence of the Burrard Inlet, the Strait of Georgia, and the Pacific "data void" in the vicinity of the forecast region. In order to provide accurate forecasts in a region so strongly influenced by forcings on the broad range of scales from cyclones in the Gulf of Alaska, through frontal windstorms, to terrain-induced flows, the high-resolution modelling system will use a triply-nested model grid, with horizontal spacings of 15 km, 2.5 km and 1 km. The inner nest is shown to be capable of resolving many of the orographic features in the Whistler/Vancouver area and of producing realistic simulations of channelled and orographically-perturbed flows.

One important component of a cloud-resolving atmospheric model is the cloud microphysics parameterization. A cloud scheme affects the model dynamics through latent heat release due to phase changes of water as well through changes to buoyancy; it interacts with the radiation scheme through its production of hydrometeor fields; and it is responsible for the prediction of precipitation phase, type, and quantity. In the Canadian high-resolution forecast system, a detailed six-hydrometeor-category double-moment bulk scheme will be used. To our knowledge, this will be the first time that a fully double-moment bulk scheme will be used for an operational forecast system such as this one. In addition to optimizing the scheme for operational use, a new approach to explicitly forecasting the solid-to-liquid ratio of precipitating snow using information provided by the microphysics scheme is being explored.

2 PROGNOSTIC SNOW DENSITY FROM THE MICROPHYSICS SCHEME

The microphysics parameterization is a modified version of the multi-moment bulk scheme described in Milbrandt and Yau (2005). The scheme was originally designed as a research tool for cloud-resolving models. It has since been adapted for operational purposes. The single-moment version of the scheme has been running in the quasi-operational Canadian 2.5-km limited-area model since April 2008 with the double-moment version being tested in the current (2009) prototype of the 2010 Winter Olympics high-resolution forecast system. Several of the modifications made to the original scheme pertain to the treatment of the snow category. To reflect a modern understanding of the proper representation of ice crystal categories, the exponent in the mass diameter relation for snow has been changed from 3 to 2, with corresponding changes to the coefficients (e.g. Mitchell, 1996). A physical implication of this is that the bulk density of snow is not longer a prescribed constant as with the previous representation of snow, as spherical particles with a constant density, but rather the density is inversely proportional to the maximum particle dimension. This is consistent with ground-based distrometer measurements (Brandes et al., 2007).

For the quantitative prediction of the depth of accumulated snowfall, most NWP systems predict the liquid-equivalent solid precipitation and then multiply it by an assumed solid-to-liquid ratio. In the current microphysics scheme, we exploit the new aspect of the representation of snow that its bulk density is a variable function of size to provide an estimate of the instantaneous solid-to-liquid ratio of precipitating snow. This quantity is equal to the ratio of the volume flux to the mass flux at the surface. With a constant bulk snow density, the fluxes are simply proportional to each other by a factor of the assumed density. Thus, for a snow density of 0.1 g cm^{-3}, for example, the solid-to-liquid ratio will be exactly 10-to-1. With a variable density, on the other hand, the ratio increases with the mean-mass diameter of the snow distribution. Thus, we are exploiting

both the variable density with the new mass-diameter relation plus the fact that a double-moment scheme can provide a better estimate of the mean-mass diameter than a single-moment scheme, since it can explicitly include processes such as aggregation and size-sorting. Estimates of the densification of snow during melting are made. For the calculation of the instantaneous solid-to-liquid ratio, we also apply the precipitation flux ratio for graupel, mass-weighted with that of snow. The effect of this is that the solid-to-liquid ratio can change with the environmental conditions. For example, if riming becomes important during a snowfall event, which is often the case in the mountainous coastal regions of the Vancouver area, there will be a shift from snow to graupel in the model which will be reflected by a decrease in the instantaneous solid-to-liquid ratio.

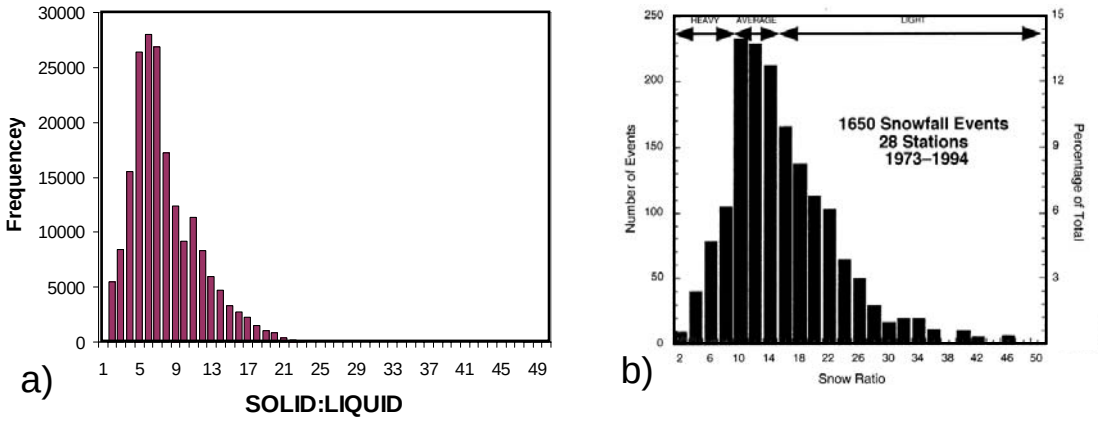

Figure 1. a) Frequency of the grid-point values of the solid-to-liquid ratio of the accumulated 12-h solid precipitation for a 2.5-km simulation of a heavy snowfall even in eastern Canada. b) Histogram of the number of observed values of a given solid-to-liquid ratio for 1650 snowfall events over 28 stations in the north-east United States during 1973-94. Reproduced from Roebber et al. (2003).

Although this work is preliminary and more comparison to observations is required to evaluate the method, the proposed approach for the prognostic solid-to-liquid ratio appears to produces a realistic range of values. For example, for a heavy snowfall even in eastern Canada, Fig. 1a shows the number of grid points with specific values of the solid-to-liquid ratio for the accumulated snowfall. For a qualitative comparison only, Fig. 1b shows the frequency of values for 21 year period over the north-east United States. Note that such observations vary with geographical location. Modification to the scheme have been made since the above simulation, such as imposing a lower limit on the slope of the snow size distribution, and the method now generally produces higher values than shown in Fig. 1a.

3 CONCLUSION

An overview of the Canadian high-resolution forecast system for the 2010 Winter Olympics will be presented along with some results from the 2009 winter practicum. This season has shown that there is indeed added value to the forecast with the high-resolution (2.5-km and 1-km) grids. The new approach for the prognostic solid-to-liquid ratio produces a realistic range of values. Comparisons of specific cases to observations will be presented.

REFERENCES

Brandes, E. A., K Ikeda, G. Zhang, M. Schonhuber, R. M. Rasmussen, 2007: A statistical and physical description of hydrometeor distributions in Colorado snowstorms using a video distrometer. *J. Applied Meteor. and Climatology.* **46**, 634-650.

Milbrandt, J. A. and M. K. Yau, 2005: A multimoment bulk microphysics parameterization. Part II: A proposed three-moment closure and scheme description. *J. Atmos. Sci.*, **62**, 3065-3081.

Mitchell, D. L., 1996: Use of mas- and area-dimensinoal power laws for determining precipitation particle terminal velocities. *J. Atmos. Sci.*, **53**, 1710-1723.

Roebber, P. J., S. L. Bruening, D. M. Schultz, and J. V. Cortinas Jr., 2003: Improving snowfall forecasting by diagnosing snow density. *Wea. and Forecasting*, **18**, 264-287.